UNIVERSITY OF SOUTHAMPTON

FACULTY OF PHYSICAL SCIENCES AND ENGINEERING

Electronics and Computer Science

Screen-Printed Low Temperature Piezoelectric Thick Films for Energy Harvesting on Fabrics

by

Ahmed Almusallam

Thesis for the degree of Doctor of Philosophy

April 2016

UNIVERSITY OF SOUTHAMPTON

FACULTY OF PHYSICAL SCIENCES AND ENGINEERING

Electronics and Computer Science

Screen-Printed Low Temperature Piezoelectric Thick Films for Energy Harvesting on Fabrics

by

Ahmed Almusallam

Jurys:

Dr Jack Hale

Dr Nick Harris

Supervisors:

Prof. Steve Beeby

Dr. Russel Torah

Dr. John Tudor

Thesis for the degree of Doctor of Philosophy

April 2016

UNIVERSITY OF SOUTHAMPTON

ABSTRACT

FACULTY OF PHYSICAL SCIENCES AND ENGINEERING

Doctor of Philosophy

SCREEN-PRINTED LOW TEMPEATURE PIEZOELECTRIC THICK FILMS FOR ENERGY HARVESTING ON FABRICS

By Ahmed Almusallam

This thesis details the improvement in the dielectric, piezoelectric and mechanical (such as flexibility) properties of screen-printed flexible low-temperature PZT-polymer composite films on woven-fabrics. These improvements have been achieved by optimising the composite formulation and the post processing procedures. The polymeric binders were evaluated to find the optimum PZT-binder composite. The optimum PZT-binder composite with weight ratio 2.57:1 (denoted ECS-PolyPZT 6a) provided a relative dielectric constant of 146 and a d_{33} value of 22.8 pC/N at initial poling conditions measured on alumina. The PZT phase was a mixture of PZT particle sizes 2 and 0.8 μm with weight ratio of 4:1. Applying optimum poling conditions improved the d_{33} values to 36, 40 and 70 pC/N when the material screen-printed on alumina, Kapton and Polyester-cotton. The difference in the d_{33} coefficients on the different substrates is due to the clamping effect and in each case the free-standing d_{33fs} value was calculated to be 80 pC/N. Applying cold isostatic pressing (CIP) at 250 MPa for 2 minutes improved the d_{33} values to 76.6 pC/N on Polyester-cotton. Adding 0.2% silver-nano particles by weight to the material improved the d_{33} to 76 pC/N on Polyester-cotton with no CIP. Combining these two measures yields a d_{33} value of 83 pC/N. The final optimised d_{33fs} was 98 pC/N compared with the original value of 49 pC/N.

When evaluating these films for use in energy harvesting applications, it was found that when applying compressive and tensile forces, the output mainly depends on the compliance of the substrate. The optimum PZT-binder composite printed on 1 × 1 cm^2 woven-fabric Kermel, which has a higher compliance than Polyester-cotton and Cotton fabrics, provided output energy of 0.2 and 0.018 μJ/cycle when connected to a 30 and 1 MΩ resistive load in compression and tension, respectively. However, when applying a bending force to the sample, the output voltage increases

with reducing compliance and increasing thicknesses of the substrate. Cotton substrates with lower compliances and higher thickness gave the highest energy output of 0.192 μJ per bending cycle into 70 MΩ when applying a bending curvature of 5 mm radius. Therefore, careful selection of the substrates is important to maximise the performance in sensing or energy harvesting application.

Table of Contents

List of figures

List of tables

DECLARATION OF AUTHORSHIP

I, Ahmed Almusallam declare that the thesis entitled *Screen-Printed Low Temperature Piezoelectric Thick Films for Energy Harvesting on Fabrics* and the work presented in it are my own and has been generated by me as the result of my own original research.

I confirm that:

1. This work was done wholly or mainly while in candidature for a research degree at this University;
2. Where any part of this thesis has previously been submitted for a degree or any other qualification at this University or any other institution, this has been clearly stated;
3. Where I have consulted the published work of others, this is always clearly attributed;
4. Where I have quoted from the work of others, the source is always given. With the exception of such quotations, this thesis is entirely my own work;
5. I have acknowledged all main sources of help;
6. Where the thesis is based on work done by myself jointly with others, I have made clear exactly what was done by others and what I have contributed myself;
7. Parts of this work have been published as: [1], [2], [3], [4] and [5]

Signed:.....

Date: .....

Acknowledgements

I would like to express my sincere gratitude to my supervisors, Prof. Steve Beeby, Dr. Russel Torah and Dr. John Tudor for their constant guidance, support and motivation during the years of this research and the year before in my master degree.

I would like to thank all of the researchers in Printing Electronics Laboratory Group for their support and inspiration. In particular, I would like to sincerely thank Dr.Dibin Zhu for the constant support and help during this research and also in my master degree. I also would like to thank Dr. Kai Yang for the help in Chemistry during the development of the materials. Also, I would like to thank Dr. Zhenhua Luo for the help and advice in analysis and the evaluation of the proposed devices.

I would like to acknowledge Ministry of Education of Saudi Arabia and Saudi Arabian Cultural bureau in the United Kingdom (UKSACB) for the sponsorship and the financial support during this research and my master degree.

Last but not least, I have to thank my great parents for their support and encouragement throughout my life without whom I would never have been able to progress as far as I have. The endless love that they have provided me over the years was the energy of my success. Also, many wholehearted thanks to my amazing brothers Mohamed, Khaled and Yasser.

To my parents for their infinite love, inspiration and support

List of Symbols

$\mathbf{P_{CIP}}$	Cold isostatic pressing pressure
$\mathbf{t_{CIP}}$	Cold isostatic pressing time
ε_r	Relative dielectric constant
d_{33}	Longitudinal piezoelectric coefficient
d_{33clp}	Clamped longitudinal piezoelectric coefficient
d_{31clp}	Clamped transverse piezoelectric coefficient
d_{33fs}	Free standing longitudinal piezoelectric coefficient
d_{31fs}	Free standing transverse piezoelectric coefficient
E	Poling electric field
E_{eff}	Effective electric field on the particles
t	Poling time
T	Poling temperature
ν_s	Poisson ratio of the substrate
ν_p	Poisson ratio of the piezoelectric film
Y_s	Young's modulus of the substrate
Y_p	Young's modulus of the piezoelectric film
C_s	Mechanical compliance of the substrate
T_3	Stress at the 3-direction
$T_{1,2}$	Stress at the 1-2 plane
S_1, S_2	Strain at the 1-2 plane
t_s	Thickness of the substrate
t_p	Thickness of the piezoelectric film
C_p	Capacitance of the piezoelectric film
R_c	Radius of curvature when bending
C_n	Maximum number of complete bending cycles
d_{SFP}	Diameter of the PZT filler
C_f	Complete bending cycle at which cracks were observed
R_v	Volume resistivity

Glossary of Terms

PZT	Lead Zirconate Titanate
DCP	Direct-contact poling
CDP	Corona-discharge poling
CIP	Cold Isostatic Pressing
SFP	Single-filler particle
MFP	Multi-filler particle
PVDF	Polyvinylidene fluoride
SAW	Scanning Electron Microscope
PVC	Polyvinyl chloride
PDMS	Polydimethylsiloxane

Chapter 1: Introduction

1.1 General Overview

Undoubtedly, with the advancement in microelectronics, prodigious attention has been paid to improving and inventing new methods for powering such systems. Nowadays the use of wireless sensor nodes, mobile phones and MP3s are widespread and the need to power these systems is increasing daily. The traditional methodology, as represented by batteries, is not suitable for many applications since they require effort to replace, even more so in places geographically difficult to reach.

Energy harvesting techniques can increase the life time of the battery. The wasted mechanical energy which is related to structural vibration, deformation, and stretching can be exploited by piezoelectric materials which are capable of generating electric power from such movements. This has given a rise to a significant interest in using piezoelectric materials to supply the energy for low-power micro-electronic and wireless systems. Fabrics were originally developed to protect man from the elements, such as wind and rain, but were later developed for use in furniture coverings, carpets and household applications. The idea that fabrics could be exploited to power micro-electric systems such as mobile phones and MP3s is relatively new. This requires an investigation into flexible piezoelectric materials that have the desired output power and can be easily fabricated and therefore industrialised.

This project is concerned about printing thick film piezoelectric composite materials on flexible substrates, such as woven-fabrics and applying these materials as energy harvesters to exploit the kinetic energy of human movement and the displacement of the fabric. The material should possess higher piezoelectric properties than PVDF, be flexible and suitable for low temperature curing to be compatible with fabric applications.

Piezoelectricity was discovered by the two brothers Jacques and Pierre Curie in 1880 [6] and since then, researchers have been using this method in many applications [7]. When a mechanical stress is applied causing a consequent mechanical strain to certain classes of materials, they generate an electric charge which is accumulated at the surface of the material [8], this is known as the direct piezoelectric effect. However, when the opposite procedure is adopted in which an external electric field is applied, a deformation occurs in the material, called the piezoelectric inverse effect. It was discovered by Lippmann in 1881 [9]. Piezoelectricity is currently being employed in applications such as sensors, detectors, actuators, motors (e.g. piezoelectric motors) and energy harvesters.

The piezoelectric properties of the material are identified by parameters called piezoelectric coefficients. These coefficients reflect how piezoelectric a material is, and the higher the piezoelectric property, the higher electrical power that could be harvested. The most commonly cited coefficient is the piezoelectric charge coefficient (d) which is defined as the electric charge generated per unit area when a force is applied (C/N) [10]. It can also be defined as the resultant strain when an electric field is applied. A second piezoelectric coefficient is the piezoelectric voltage coefficient (g). It is defined as the open circuit electric field generated when a mechanical stress (N/m^2) is applied. These coefficients are described in more detail in Chapter 2: [10].

Nowadays, a plethora of materials possess piezoelectric properties which are naturally existed (e.g. quartz) or chemically synthesised piezoelectrics (e.g. lead zirconate titanate, PZT). PZT is a ferroelectric material and requires polarisation to become piezoelectric. Ferroelectric materials have a crystal structure and can be found in ceramic or polymer forms (some other forms will be discussed later). The first piezoelectric materials considered were quartz and Rochelle that are a natural single piezoelectric crystal. However, the first ferroelectric material barium titanate ($BaTiO_3$) ceramic was found by Waigner and Salomon in the early 1940s which has a Curie temperature of between 9-200°C and a d_{33} of 50-100 pC/N. In 1954, Jaffe et al. [11] developed a new piezo-ceramic, PZT, to improve the thermal stability and piezoelectric properties (d_{33} of 150-600 pC/N) of piezoelectric ceramics. Most of these materials are commercially processed initially in a powder form that is then pressed and fired to form hard and rigid ceramics. In general, piezoelectric ceramics are mechanically inflexible (stiff) but can provide excellent piezoelectric properties, good coupling coefficients and are cheap. Printable PZT films were first demonstrated by mixing the PZT powder with a suitable liquid phase material (vehicle) and glass powder in order to form a material phase that can be printed onto a solid structure (substrate), before drying and sintering. These films are typically processed at very high temperatures that may not be suitable for very low temperature applications such as those using flexible plastic or fabric substrates.

Piezoelectric polymers have been discovered, such as poly vinylidene fluoride or PVDF by Kawai [12]. This material is a homopolymer and subsequently, its copolymer and terpolymer counterparts such as P(VDF-TrFE) and P(VDF-TrFE-CFE) were discovered. Piezoelectric polymers are mechanically flexible and possess piezoelectric properties that are lower than piezoelectric ceramics (e.g. PVDF can give a d_{33} of 20-30 pC/N) [13]. However, they are not as cheap as piezoelectric ceramics but they are mechanically flexible and can be cured at low temperatures (100-250°C).

Mixing piezoelectric ceramic powder with a liquid polymeric binder at a suitable ceramic/polymer weight ratio has the potential advantage of combining the positive features of

the ceramics (such as high piezoelectric coefficients d_{33}, relative dielectric constants ε_r and electromechanical coupling coefficients) and the polymer (flexibility and low temperature curing). This type of formulation is called a piezoelectric composite, which can be produced in many forms. The type investigated in this work has 0-3 connectivity, i.e. it is a three dimensional polymeric matrix loaded with piezoelectric ceramic powder mixed. These piezoelectric composites can be used for sensing, actuating and energy harvesting systems especially in flexible applications given its improved mechanical flexibility compared with piezoelectric ceramics.

These materials can be deposited by a printing process which gives high throughput and production flexibility, thereby reducing the cost of the device. Printing is a technique which has been employed by ancient civilisations such as Egyptians who used stencilling art for printing their great designs and shapes. Screen-printing is an inexpensive technique for producing thick films (1 μm up to 200 μm) on a variety of substrates. Screen-printing enables the printing materials with predefined patterns which are achieved by the patterned emulsion layer on the screen. This is advantageous as this technique can be used in a wide range of applications compared than other traditional techniques, such as extrusion and pressing.

Kinetic energy harvesters have been used for exploiting vibration energy from the surroundings such as fridges [14], microwaves [15] and car vibrations, supplying power to fixed-placed wireless sensor nodes. Kinetic energy sources are not just limited to vibrations. The dynamic movements of humans have also been the focus of researchers to gain electrical energy from human motion and supply electronic systems such as mobile phones and MP3 players. Flexible piezoelectric materials could potentially provide an effective contribution in converting the human-body movement into electrical power.

This thesis presents an investigation into new screen-printed, flexible and low temperature PZT-polymer composites with improved piezoelectric coefficients d_{33}, relative dielectric constants ε_r and mechanical flexibility. The work includes optimisation of PZT-polymer weight ratios in the composite, as well as an optimisation of different particle size ratios of PZT to gain the highest piezoelectric properties with these composite materials. The poling process was investigated to maximise the piezoelectric properties of the printed piezoelectric films. The change in piezoelectric responses caused by the variation in the boundary conditions of different substrates (such as alumina, Kapton and woven polyester-cotton woven fabric) is also explored. The influence of air voids of the films and the addition of silver nano particles to the materials are also investigated. The polymer composites were also screen-printed on different types of fabrics and output voltage and power were evaluated in terms of load resistance for different types of forces such as compression, tension and bending.

1.2 Objectives of the Thesis

- Maximizing the d_{33} value of the composite material screen-printed on fabrics. Increasing the piezoelectric properties (represented by d_{33} coefficient) of active material typically leads to a production of a higher output power.
- To develop a piezoelectric film which is mechanically flexible and can withstand (i.e. without cracks or wrinkles on the surface) at the minimum radius of curvature the human body joint can bend (9 mm for thumb finger [16]).
- To thermally cure the material below 200°C as increasing the curing temperature limits the selectivity of fabrics.
- Screen-printing the optimum materials on different types of fabrics and evaluation of the output voltage and power.

1.3 Statement of Novelty

The production of thick-film piezoelectric composites is novel as follows:

- Investigating and improving the properties (e.g. flexibility, film adhesion, low temperature curing dielectric and piezoelectric properties) of the screen-printed piezoelectric composites for fabric substrates by investigating the types of the binder mixed with the ceramics.
- Investigation and comparison between poling techniques for low temperature piezoelectric composites films.
- Producing screen-printed low temperature flexible piezoelectric composites for flexible electronics applications. The free-standing unconstrained films can provide as high d_{33} as 98 pC/N and cured and poled at temperatures (90°C) that are suitable for smart-fabric applications. The PZT-polymer films can withstand bending with a curvature less than 9 mm radius.
- Investigation of the PZT particle sizes and PZT-polymer weight ratios on the piezoelectric properties of the screen-printed low temperature piezoelectric composites.
- Exploration of the mechanical boundary conditions of flexible substrates on the mechanical and piezoelectric performances of the low temperature flexible piezoelectric films.
- Improving the dielectric and piezoelectric properties by compressing the film printed on Kapton and polyester-cotton, using cold isostatic pressing (CIP).

- Improving the dielectric and piezoelectric properties by inserting metal particles in the screen printed low-temperature piezoelectric films.
- A study and evaluation of the output voltage and power, and energy of the optimum formulations when screen-printed on different types of fabrics and compressive, tensile and bending forces are applied.

1.4 Structure of the Thesis

Chapter 2: This chapter provides a general description of the theory of piezoelectricity and piezoelectric materials. It also categorises the types of piezoelectric materials and states some examples. Material formulations, processing, fabrication and curing are reviewed in this chapter. As a poling process is required to activate the piezoelectric properties of the ferroelectric materials, the poling process and different poling techniques were reviewed.

Chapter 3: It explores the screen-printability of the piezoelectric paste and the best type of poling technique that can be used to provide the best piezoelectric properties, ease of use, good mass production and suitability to fabric applications. This chapter also describes in detail the screen-printing and poling processes that will be applied to the whole piezoelectric devices in this study.

Chapter 4: It presents the influence of the polymer (especially its dielectric properties) on the dielectric and piezoelectric properties of the composite as a whole. Different types of polymers were tested when they were mixed separately with PZT powders. The tests involved screen-printability, adhesion on the substrates and the best d_{33} values they can provide. Optimum materials were chosen. Also, the effect of PZT weight loading on the dielectric, piezoelectric and mechanical properties of the printed films was studied. Optimum PZT weight loading were obtained for this investigation for every composite.

Chapter 5: It investigates the clamping effect caused by the boundary conditions of the substrates on the d_{33} values. It shows the actual and the effective d_{33} values of the optimum material on different substrates such as alumina, Kapton and Polyester-cotton. Also, poling process optimisation of the direct contact poling was given to the optimum material.

Chapter 6: Introduces the effect of the PZT (large and fillers) sizes on the piezoelectric behaviour of the low temperature piezoelectric composites. Also, it also presents the effect of adding filler powders to the composite. The main and filler PZT particle sizes and weight ratios were calculated. Optimum main to filler PZT particles weight ratio was provided.

Chapter 7: Air voids existence inside the piezoelectric composites is one of the great challenges that affect the dielectric, piezoelectric and mechanical properties of the film. This chapter discusses the elimination of the air voids by using cold isostatic pressing (CIP) which led to an increase in the dielectric and piezoelectric properties of the film.

Chapter 8: This chapter is dedicated to further improving the piezoelectric properties of the screen-printed piezoelectric composites by inserting metal nanoparticles inside the mixture prior to screen-printing. The CIP process was reapplied to the new material and dielectric, piezoelectric and resistive properties of the samples measured.

Chapter 9: This chapter discusses the experimental results of the produced output voltage, power and energy from the piezoelectric composite when it was screen-printed onto different types of woven fabrics. The generated outputs were studied under compressive, tensile and bending forces.

Chapter 10: This chapter provides a final conclusion and summary of the achievements of the thesis and also suggests future work that may improve the performance of the screen-printed low temperature piezoelectric composite material.

Chapter 2: Piezoelectric Theory and Devices Processing

2.1 Introduction

The discovery of piezoelectricity has led researchers to employ it in applications such as sensing, actuating and energy harvesting. This chapter presents the physical principles of piezoelectricity and the developments in the field of piezoelectric materials. This chapter also covered the following areas

- The difference between piezoelectricity and ferroelectricity.
- Piezoelectric properties and their definitions.
- A further description of piezoelectric materials and their categories.
- Piezoelectric composites, processing and their state of the art.
- Piezoelectric materials deposition techniques.
- Methods of poling the piezoelectric materials.

2.2 Piezoelectric Concept

The piezoelectric effect is fundamentally the accumulation of charge when a mechanical strain is applied to certain materials [7, 8]. This action is called the direct piezoelectric effect and was discovered by the two Curie brothers. However, the Curie brothers did not discover the inverse effect, when the opposite process is achieved by applying an external electric field and a mechanical strain is consequently produced. This is called the inverse piezoelectric effect and was discovered by Lippmann in 1881 [9]. Ever since, piezoelectricity has been employed in a broad range of applications (e.g. sensing, actuating, and energy harvesting).

Polar materials are those crystals that exhibit a certain degree of polarisation when an external effect is applied, such as an external electric field or temperature gradient. As a member of the polar materials family, ferroelectrics are a special case showing a spontaneous polarisation P_s when an external electric field is applied. The spontaneous polarisation vector can be switched between two orientations according to the direction of the applied electric field. In this case, ferroelectrics can show piezoelectric activity if an external force is applied and an electric charge is produced. Nowadays, most piezoelectric materials are ferroelectrics (e.g. barium titanate $BaTiO_3$ and lead zirconate titanate PZT) except quartz. Quartz possesses a natural spontaneous polarisation without applying an external electric field [17].

For a ferroelectric material, the dipoles of the molecules are aligned in the direction of the applied electric field and a net polarisation is generated [18]. Figure 2-1 schematically illustrates the orientation of the dipoles before, during and after poling process. The dipoles are typically oriented in the piezoelectric material. Several methods are used for poling ferroelectrics, such as direct and corona poling, these are described in section 2.9 on page 43.

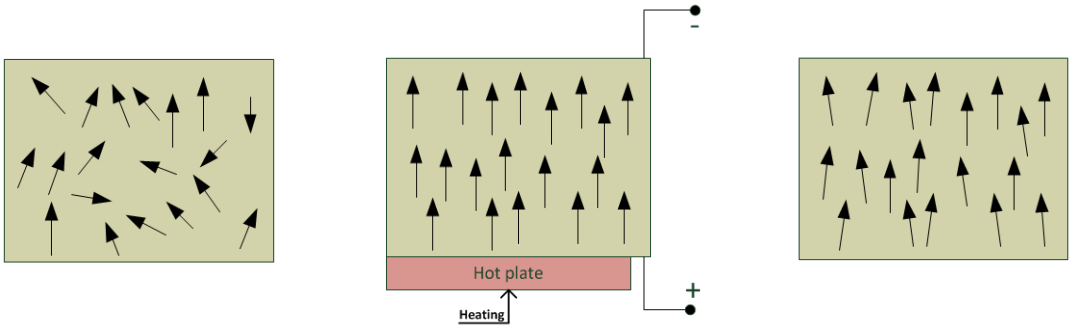

(a) Prior Poling (b) During Poling (c) After poling

Figure 2-1: The effect of poling on the dipoles of a ferroelectric material

The direction of the external electric field, polarization, force applied on the element and charge extractions are all interrelated parameters and can be described using the piezoelectric coefficient. The relations between them can be summarised when measuring the piezoelectric coefficient reflecting the piezoelectric activity of the piezoelectric element. These parameters are discussed in the following section.

2.2.1 Piezoelectric Coefficients

The electric response of a piezoelectric material can be measured by considering the amount of charge generated , or by the voltage generated across the film when an external force is applied [19]. From an electromechanical consideration, the electrical signal is dependent on the mechanical stress (T) applied to the piezoelectric material. Accordingly, this procedure introduces the most common two mathematical expressions, known as piezoelectric constants [19]. Figure 2-2 shows the X, Y, Z and their corresponding vectors (from 1-6) which are used to describe the directions of polarisation, applied force and charge extraction.

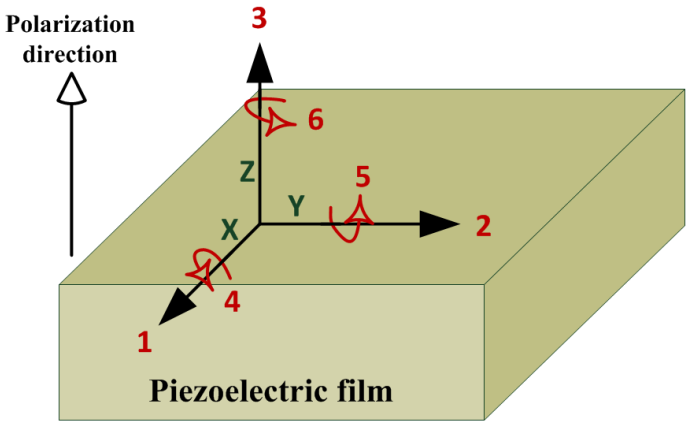

Figure 2-2: Directions of mechanical and electrical vectors 1 to 6

Piezoelectric materials have interrelated mechanical and electrical properties; hence the piezoelectric coefficients have a double subscript which relates to both the mechanical and piezoelectric directions. The first subscript shows the direction of the externally applied electrical field and the second subscript shows the direction of the mechanical stress applied to the material. The longitudinal piezoelectric charge coefficient d_{33} is used when the applied force and the generated charge are in the same direction of the polarisation, which is the 3-direction as shown in Figure 2-3(a). The transverse piezoelectric charge coefficient d_{31} is used when the force is applied at a 90º angle (1-direction) from the direction of polarisation and generated charge.

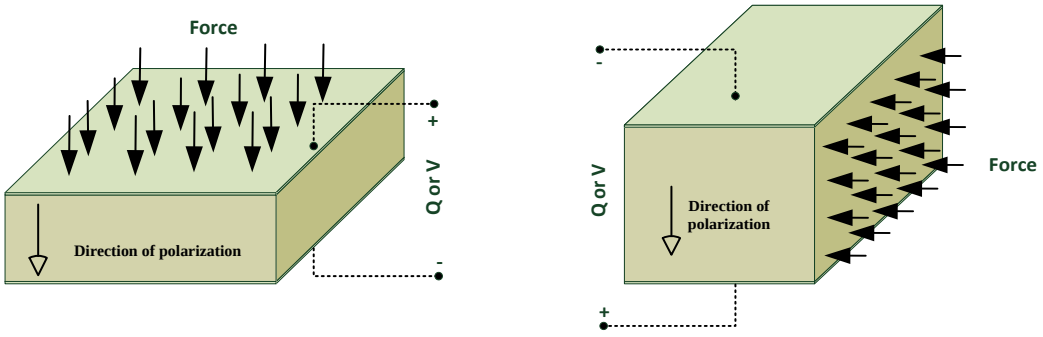

(a) d_{33} mode (b) d_{31} mode

Figure 2-3: Examples of two commonly used directions of electrical and mechanical vectors [10]. (a) d_{33} mode. (b) d_{31} mode

The most commonly used coefficient used to describe piezoelectric activity is d_{33}. This measurement is more applicable because the direction of the applied force and charge extraction are in the same direction. For the direct piezoelectric effect (see Figure 2-4), the piezoelectric charge coefficient is a measure of the amount of generated charge (Q) when 1 N of force is applied to the piezoelectric element.

$$d_{ik} = \frac{C/m^2}{N/m^2} = C/N \tag{2-1}$$

The subscripts in equation (2-1) represent the tensor notation shown in Figure 2-2 and they can have the following values. K, l = 1, 2,…, 6 and i, j = 1, 2, 3. Some of these notations will be also used later in some relations.

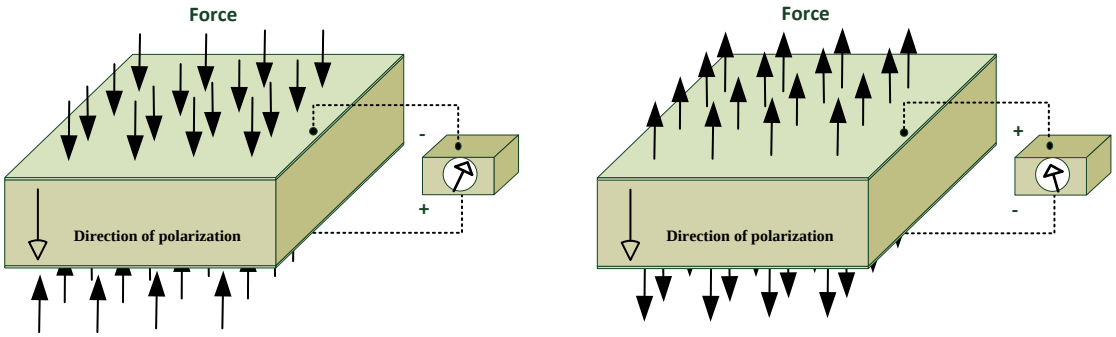

Figure 2-4: The applied force and charge for the direct effect

However, for the inverse piezoelectric effect (see Figure 2-5), the piezoelectric charge coefficient is a measure of the displacement (m) achieved when 1 V is applied.

$$d_{ik} = \frac{m/m}{V/m} = m/V \tag{2-2}$$

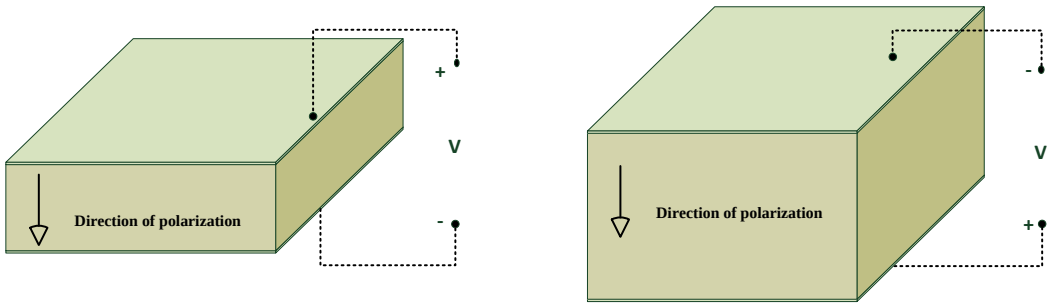

Figure 2-5: The applied voltage and the deformation

The following equations describe in detail the relationship between the properties parameters of the piezoelectric element. These equations are known as constitutive equations [20].

$$S_{kl} = s_{kl}^{E}\, T_l + d_{ik} E_i \tag{2-3}$$

$$D_i = d_{ik} T_k + \varepsilon_{ij}^{T} E_j \tag{2-4}$$

Where S is the strain, T is the stress (N/m^2), E is the electric field (V/m) and D is the electric displacement (C/m^2). s is the compliance (m^2/N), d is the piezoelectric coefficient (C/m) and ε is

the dielectric constant (F/m). Also, the subscripts T and E show a constant stress and electric field, respectively.

2.2.2 Ferroelectric Domains

Some crystalline materials naturally show piezoelectric response such as Quartz. The atomic structure of the crystalline piezoelectric material does not show a centre of symmetry unlike the crystalline ones. This non-symmetrical structure introduces a dipole moment in the unit cell. Some other poly-crystalline ceramics which are known as ferroelectric ceramics can induce the piezoelectric effect if poled by an external electric field such as PZT and $BTiO_3$. The perovskite crystal structure of PZT is shown in Figure 2-6. Such atomic structures contain three different ions ABO_3 [21]. A lattice of lead Pb or barium Ba (A) and oxygen atoms (O) surround a tetravalent atom such as titanium Ti or Zirconium (B).

This atomic structure changes with varying temperature. Above a specific temperature known as Curie temperature, the atomic structure becomes symmetrical cubic as shown in Figure 2-6(a). At this point, the ionic charges in the structure reach equilibrium and accordingly the electric dipole moment is removed. The piezoelectric activity is dependent on the electric dipole. However, below Curie temperature, the atomic structure shows non-symmetry as shown in Figure 2-6b and accordingly, the dipole moment exists.

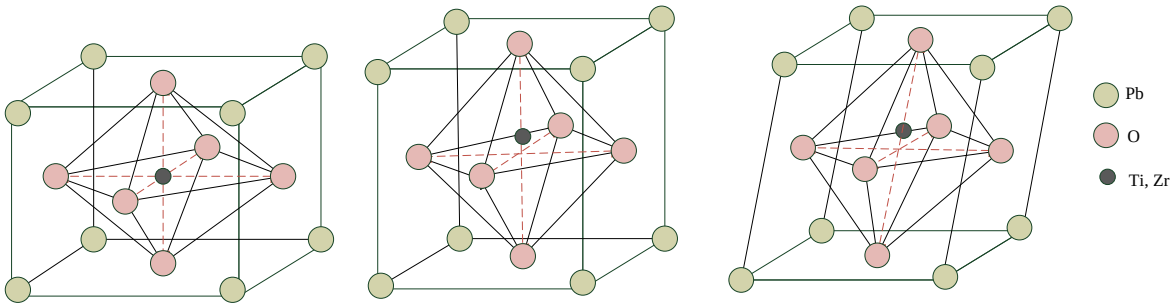

Figure 2-6: Perovskite crystal for PZT [17]. (a) Paraelectric cubic state. (b) Ferroelectric tetragonal state. (c) Rhombohedral state

The ferroelectric domain is defined as the region of the crystals where spontaneous polarisations are uniformly oriented. A domain wall refers to the region between two domains. Domains are separated by walls with opposite oriented polarisation (180º walls) and those which separate domains with vertical polarisation are called 90º walls [17]. The domain has a dipole. In crystals, these dipoles are randomly spread in the piezoelectric material. Polycrystalline materials consist of fragmented distribution of tiny domains which are randomly oriented. As they are randomly oriented, the sample is piezoelectrically neutral because the dipoles cancel each other.

Ferroelectric materials are transformed into polar states under the application of an electric field at raised temperatures. This process is known as poling, which reorientates the dipole moments within the ferroelectric material.

2.3 Measurements of the Piezoelectric Coefficients

The most commonly used metric for piezoelectric behaviour in energy harvesting applications is the piezoelectric coefficient d (C/N). To obtain reliable measurements of the piezoelectric properties, the devices should be fabricated using a robust and repeatable method. Therefore, the easiest way to measure these properties is by applying the force and the extraction of the produced charge in the same direction (3-direction). The charge extraction is achieved with the aid of electrodes in the plane perpendicular to the applied electric field and charge extraction (1-2 plane). This leads to easy and reliable measurements of the piezoelectric coefficient d_{33}. Most of the applications use the capacitive structure either for measuring the piezoelectric properties or for producing transducers (sensing or energy harvesting).

There are a lot of methods for measuring the piezoelectric coefficients, but the most commonly used amongst them are the direct, indirect and Berlincourt methods. The direct method is applied when a known force is applied to the piezoelectric sample and the charge produced is measured. To find the value of d_{33}, equation (2-1) is used. Figure 2-4 on page 11 illustrates the relation between the force applied and the generated voltage. It shows that applying a compression in the same direction of the poling axis generates a voltage with the same polarity of the piezoelectric element, however if a tensile force is applied to the piezoelectric element, a voltage of an opposite polarity is generated. Most of the contributions use this method because it has simple setup and the produced voltage can be measured with normal equipment. A typical set up is commonly used by connecting the piezoelectric sample to a charge amplifier and then when the force is applied, the generated charge is measured.

The indirect method uses the inverse piezoelectric effect for measuring the piezoelectric coefficient d_{33}. The voltage is applied to the piezoelectric element which is deformed and the displacement is measured. The measurement of the piezoelectric coefficient is achieved by equation (2-2). Figure 2-5 on page 11 shows the relation between the applied voltage and the generated displacement. It shows that the applied voltage of the same polarity will produce an expansion in the piezoelectric material along the direction of poling and the voltage of opposite polarity will produce a compression in the same direction of poling. This method is employed in acoustic devices with a generated A.C. field. Indirect method is rarely used because of the

difficulty in measuring small displacements (few nanometres) when the piezoelectric element is deformed.

The most common method that is used for piezoelectric coefficient is the Berlincourt method. It is fundamentally a dynamic technique with a varying load [22]. Figure 2-7 illustrates the basic Berlincourt d_{33} measurement setup. The piezoelectric capacitive structure sample is clamped between two probes. The bottom probe applies a low-frequency oscillating force on the sample. The charge produced is collected via the two probes and compared to a built-in reference sample, producing a d_{33} reading.

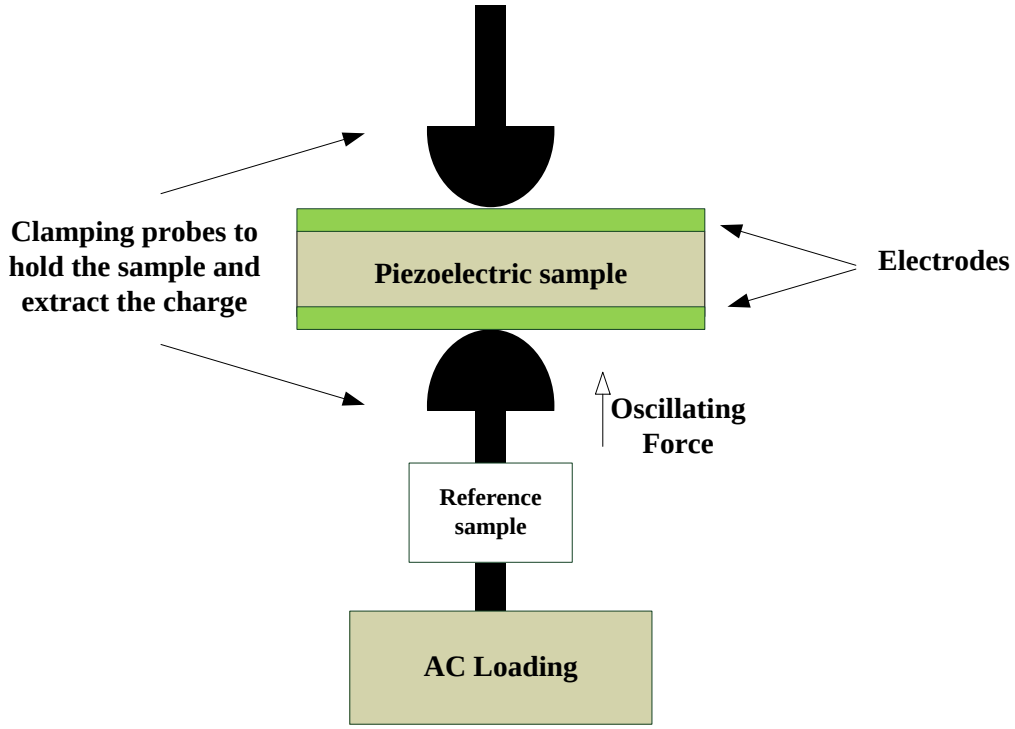

Figure 2-7: A schematic showing the Berlincourt measurement system

2.4 Piezoelectric Materials

Most of the crystal materials are categorised into 32 classes [23]. Twenty one out of the 32 classes of crystal structure are piezoelectric materials which are non-centrosymmetric [24]. The materials, in which all dipoles are oriented, produce a surface charge density and show spontaneous polarization P_s, are called pyroelectric materials. Ten classes out of the 21 for the piezoelectric materials are pyroelectric. Furthermore, pyroelectrics are polar materials. Ferroelectrics are a special case in polar or pyroelectric materials [17]. In terms of polarisation, ferroelectrics have spontaneous polarization P_s that shows at least two equilibrium states and the

spontaneous polarisation vector that can be switched between these two states by an external electric field. Figure 2-8 shows the relationship between piezoelectric, pyroelectric and ferroelectric materials.

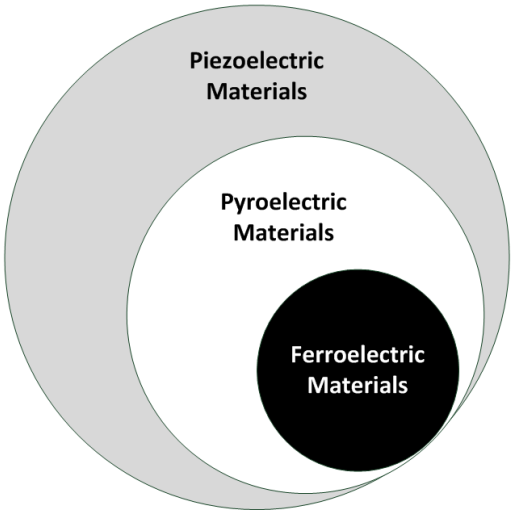

Figure 2-8: Piezoelectric, pyroelectric and ferroelectric materials relationship [25-27]

Piezoelectric materials are categorised in three groups: inorganic, organic and composite piezoelectric materials. The description of these materials is provided in subsections 2.4.1, 2.4.2 and 2.4.3. Table 2-1 shows the typical values of some of the piezoelectric coefficients and Young's modulus of some common piezoelectric materials, which are described and discussed in the following subsections.

Material Name	d_{33} (pC/N)	Y (GPa)	Material Category
Quartz	2.33 [28]	76.5 [29]	Single crystal
PZT-5H	650 [30]	61[31]	Ceramic
PMN-PT	1500-2600 [30]	38 [32]	Single crystal
PZN-PT	1400-2700 [30]	15 [31]	Single crystal
PVDF	25.8 [33]	3 [33]	mono-polymer
P(VDF-TrFE) 25 mol%	33.5 [33]	1-3 [33]	copolymers
P(VDF-TrFE-CTFE)	Unknown	0.4 [8]	terpolymer

Table 2-1: Typical values of piezoelectric coefficient and Young's modulus of some of some of the piezoelectric materials

Finding the commercial active piezoelectric material that has high piezoelectric properties d_{33} and is suitable for 0-3 connectivity type composites (discussed later in section 2.4.3) was essential at this stage. In this study, the target is not to produce or develop any of these active piezoelectric materials that mentioned in Table 2-1 as material processing of such materials need separate investigation to maximise their properties which is beyond the scope of this study. This decision was made because of two reasons:

1. To fully concentrate on studying the effect of the mixing polymeric binders with active piezoelectric materials such as PZT ceramic and their effect on the poling conditions and therefore piezoelectric activity.
2. Producing single-crystal piezoelectric materials such PMN-PT is challenging although they gave higher d_{33} values. This is because the proper material composition needs a special investigation for maximizing the piezoelectric activity of the film, which is beyond the scope of this study. Also, finding commercial single crystal piezoelectric (e.g. PMN-PT) in a powder form was difficult in the market.

2.4.1 Inorganic Piezoelectric Materials

The inorganic piezoelectric materials are represented in some of the solid single crystals (e.g. Lead Magnesium Niobate / Lead Titanate PMN-PT) and ceramic materials (e.g. Lead zirconium titanate PZT and lead lanthanum zirconium titanate PLZT). Most of the inorganic piezoelectric (or ferroelectric) ceramics have the Perovskite structure shown in Figure 2-6 on page 12. The ceramic itself contains crystallites which consist of a domain in which the unit cells' polar direction are arranged. The processing of such materials to be deposited on substrates is later described in section 2.5 on page 30.

Piezoelectric ceramics show advantageous features, such as high piezoelectric and pyroelectric coefficients, a large range of possible dielectric permittivity, low mechanical and dielectric loss, and high electromechanical coupling coefficients [8]. However, these materials are also mechanically inflexible and sensitive to ageing. Moreover, they are not suitable for smart fabric applications because of their high temperature processing. Therefore, to exploit their beneficial features and exclude their drawbacks when used in flexible application, they need to be processed in a form of composite material, discussed in section 2.4.3.

2.4.1.1 Hard and Soft Piezoelectric Ceramics

Piezoelectric ceramics can be categorised into two types: hard and soft ceramics. They can be produced both by inserting a dopant into an inert PZT material. The dopant can be an acceptor (e.g. niobium) or a donor (e.g. nickel) that are employed to produce hard and soft PZT ceramic, respectively. Table 2-2 shows a comparison between soft and hard piezoceramics. The comparison shows greater piezoelectric coefficients (d_{33}); mechanical Q factor and dielectric constants can be provided by soft piezoceramics which are required to give efficient low power energy harvesters and also sensitive sensing devices. Soft piezoceramics devices can be easily poled compared to its hard piezoceramics counterpart. Higher piezoelectric activity, dielectric

property and ease in poling process are the factors needed to create energy harvesters with higher electric power rates.

Comparing parameter	Soft Piezoceramics	Hard Piezoceramics
Fabrication	Produced by inserting a DONOR dopant (e.g. nickel) into a standard piezoceramic (e.g. PZT)	Produced by inserting an ACCEPTOR dopant (e.g. niobium) into a standard piezoceramic (e.g. PZT)
Piezoelectric coefficient d_{31} [34]	High piezoelectric coefficients (e.g. PZT 5H of -274 pC/N)	Low piezoelectric coefficients (e.g. PZT-8 of -97 pC/N)
Dielectric constant [34]	High dielectric constants (e.g. PZT-5H of 3400)	Low dielectric constants (e.g. PZT-8 of 1000)
Applications	Mainly exploited in low power applications such as low power energy harvesting and high sensitive sensing	Mainly exploited in high power applications such as sonar

Table 2-2: Comparison between soft and hard piezoceramics

From the general comparison shown in Table 2-2, soft piezoceramics are more suitable for energy harvesting in low power electronics applications. Their higher d_{33} values are significant factors to be exploited in energy harvesting applications. Soft piezoceramics, such as PZT-5H, provide a good option to be used as a main active constituent in piezoelectric composites and can be exploited in flexible electronics applications, instead of piezoelectric polymers which typically have lower piezoelectric performance.

From Table 2-3, PZT-5H can obviously provide higher piezoelectric and dielectric properties compared to its counterparts. In view of these promising properties, PZT-5H can be used as the main active piezoelectric material that can be mixed with polymeric binder or epoxy resin.

Property	Symbol	Dimension	PZT material Type			
			PT2 [35]	**PZT-5H [36]**	**PZT-4D [36]**	**PZT-27 [36]**
Commercial name			-	PZ29, Ferroperm	PZ62	PZ24, Ferroperm
Piezoelectric coefficients	d_{33}	pC/N	67	575	300	425
	d_{31}	pC/N	-3	-240	-130	-170
Dielectric constant (@ 1kHz)	K_{33}^{T}	1	218	2900	1300	1850
Coupling factors	k_p	1	0.03	0.07	0.58	0.65
	k_t	1	0.510	0.40	0.47	0.49
Curie Temperature	T_C	°C	238	235	300	350

Table 2-3: Typical properties of some of PZT materials

2.4.2 Organic Piezoelectric Materials

Piezoelectric polymers represent the organic piezoelectric materials. These piezoelectric polymers are part of a group of electroactive polymers. Generally, all the polymers that are able to change their dimensions and shapes by electrical stimulus are called electroactive polymers. Piezoelectric polymers have overcome some of the challenges that piezoelectric ceramics represent, especially if depositing on flexible substrates is desired (e.g. plastic substrates or fabrics). However, they suffer from lower dielectric constant, piezoelectric coefficient, electromechanical coupling, breakdown voltages and surface energy, compared to their ceramic counterparts [8, 37].

Piezoelectric polymers (e.g. PVDF) are those materials which have a permanent dipole moment experiencing a linear relation between the electric field applied and the stress. Finally, electroactive papers (e.g. cellulose sandwiched between two metallic electrodes) are materials which look like a paper, consisting of some entangled fibres acting as piezoelectric materials [8]. The electroactive polymers categories are summarised in Figure 2-9 showing the three types that show piezoelectric activity (coloured in blue). They show spontaneous polarisation under the application of external electric field and produce electrical charge under mechanical stress.

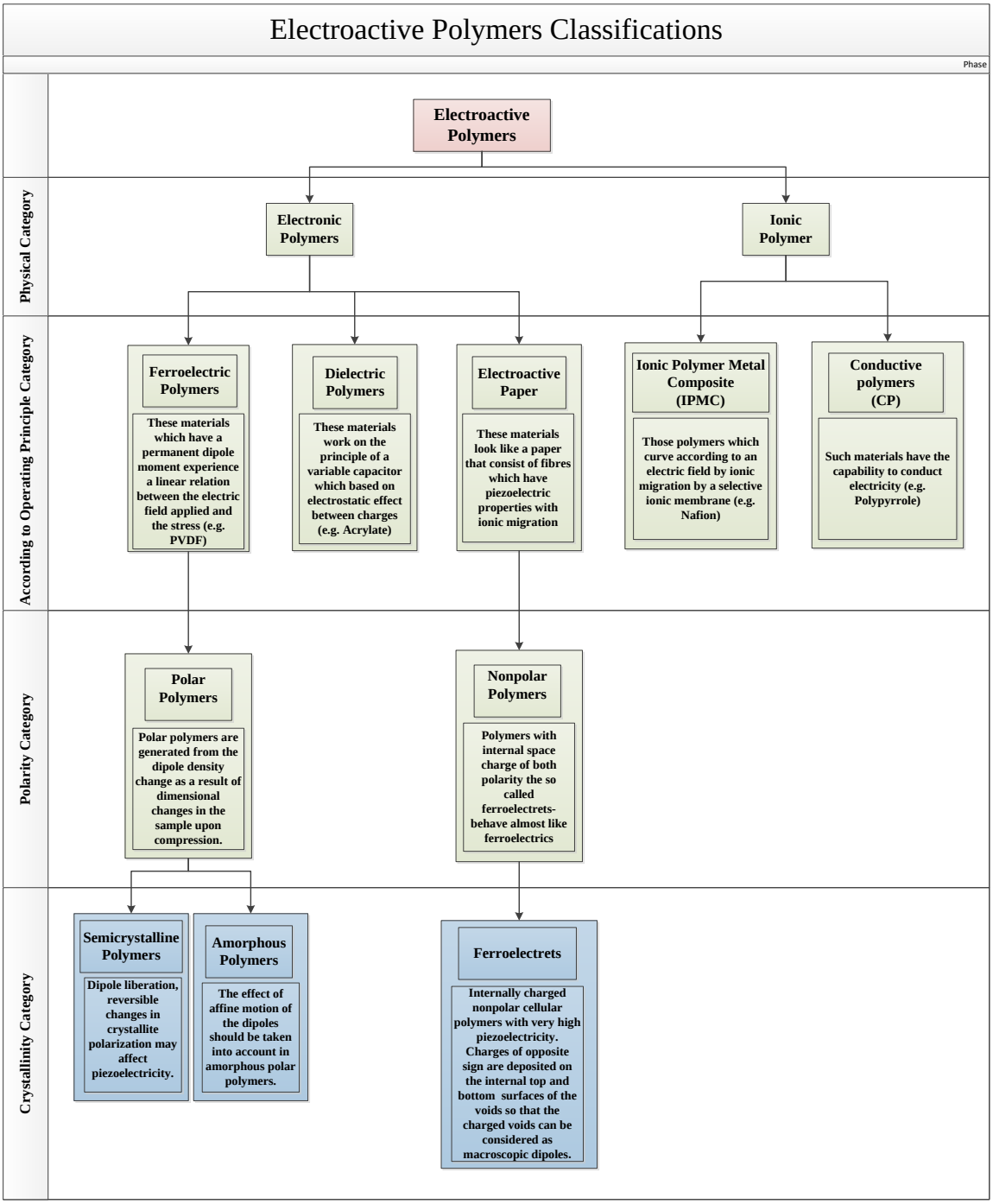

Figure 2-9: Electroactive Polymers classifications [8, 38, 39]

2.4.2.1 Amorphous Ferroelectric Polymers

In amorphous ferroelectric polymers, the molecules are randomly oriented and interlaced with each other. They usually produce lower piezoelectric properties than semi-crystalline polymers. In semi-crystalline polymers, the crystalline phase keeps the alignment of the dipoles when the electric field is removed, which does not happen in amorphous piezoelectric polymers [19, 40]. To activate their piezoelectric properties, they are polled by applying a strong electric field at a

raised temperature that is enough to enable mobility of the dipoles. The polarisation and subsequent piezoelectric properties are partially kept when the temperature is reduced below the glass transition at fixed electric field [41]. In 1980, Miyata et al. [42] discovered piezoelectric properties in vinylidene cyanide copolymer (VDCN) and vinyl acetate (VAc) that are entirely amorphous polymers. After poling at 150°C, close to glass transition temperature (T_g = 170 °C), and subsequently cooling down under the same electric field, the transverse piezoelectric coefficient was measured; d_{31} = 10 pC/N. This type of organic piezoelectric polymer is still in the early stages of investigation, while initial results of the previous contributions show very low longitudinal and transverse piezoelectric coefficients.

2.4.2.2 Semi-Crystalline Piezoelectric Polymers

These are polymers comprised of crystallites dispersed in the amorphous region, as shown in Figure 2-10 [43]. The charges are placed at the interfaces among the crystallites while the amorphous regions support the ferroelectric polarisation [38]. Semi-crystalline piezoelectric polymers are classified into three groups according to the type of polymerisation. These three common types are piezoelectric homopolymers, piezoelectric copolymers and piezoelectric terpolymers.

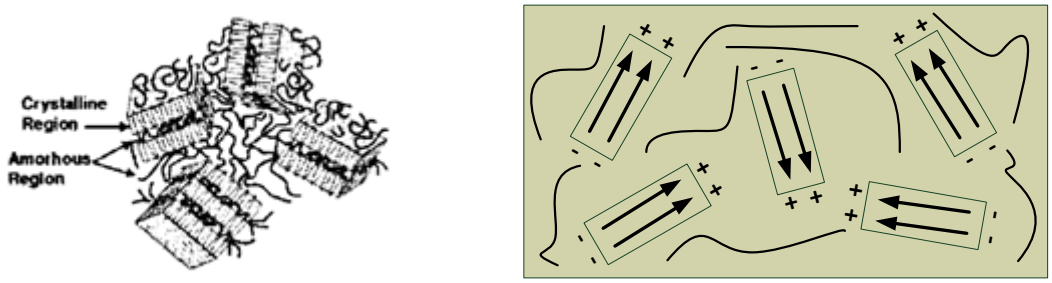

(a) (b)

Figure 2-10: Semi-crystalline polymers. (a) Molecular structure [43]. (b) Schematic of Semi-crystalline polymers

Semicrystalline piezoelectric polymers show spontaneous, permanent electric polarisation, similar to the ferromagnetism that provides permanent, spontaneous magnetisation. They also have spontaneous polarisation which is reversed on the presence of an external electric field [44]. Therefore, they have the hysteresis phenomena as it occurs in ferroelectric ceramics.

When an elevated temperature is applied to such materials, normal dielectric behaviour is observed but at certain critical temperature; Curie temperature and in the presence of even a small electric field, major polarisation occurs. This means spontaneous polarisation appears on the ferroelectric materials below the Curie point. The phase transition at the Curie point is dependent on the variation of lattice symmetry of the material [44]. Piezoelectric behaviour can be obtained

below the Curie temperature because of the fact that the non-polarised crystals have the centre of symmetry. However, piezoelectricity disappears above Curie temperature [45].

2.4.2.2.1 Semi-Crystalline Piezoelectric Homopolymers

In 1969, Kawai discovered the piezoelectric activity in Poly(vinylidene fluoride) polymer (PVF_2 or PVDF [12]. The condensed structure formula of PVF_2 (PVDF) is $(CF_2CH_2)_2$ and has a degree of polarisation. The degree of polymerization is the number of monomeric units in a polymer *n*. Moreover, PVDF is a semi-crystalline polymer with approximately half of its molecules in the amorphous non-crystalline state and the remaining half in crystalline state.

Polyvinylidene fluoride (PVDF) is a semi-crystal homopolymer and its crystallinity varies from 40-60%. There are four crystal phases: α, β, γ and δ [12, 46]. The α-phase is the one that is thermodynamically very stable and is not actually polar. The β-phase is actually polar and is responsible for high piezoelectric activity of the polymeric material. Phase transition operation is one of the solutions for increasing the piezoelectric activity of the piezoelectric polymeric materials. Phase transition from α to β phase can be applied by stretching the films or subjecting these materials to a high electric field (>3.5 MV/cm). γ–phase is in the middle between the α-phase and β-phase and is formed at crystallisation temperature between 160-170°C [47, 48]. Finally, the δ-phase is polar and can be obtained by achieving an electric field greater than 12 kV/cm [46].

Stretching a semi-crystalline piezoelectric polymer is important to orient the amorphous matrix in the piezoelectric layer, as shown in Figure 2-11(a). This helps the rotation of the crystallites by the external electric field, as shown in Figure 2-11(b). To eliminate the mechanical stress on the piezoelectric material caused by stretching and to increase its crystallinity, the material can be annealed in two steps one for treatment and another for increasing the crystallinity [49]. Stretching is not a preferable process as it limits the substrates types and, accordingly, applications of the material.

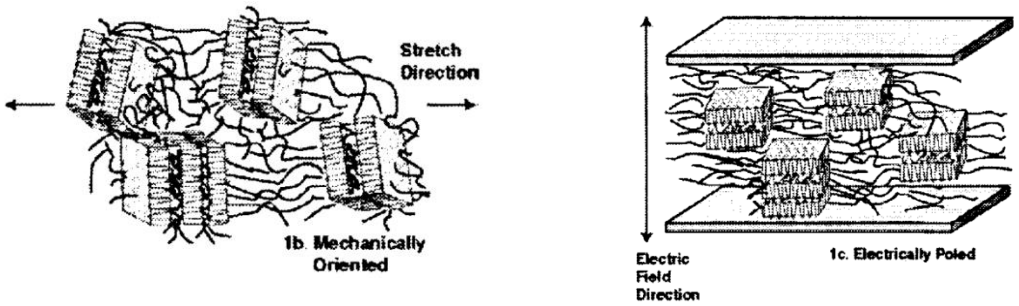

(a) (b)

Figure 2-11: Poling of piezoelectric polymers [43]. (a) Stretching the polymer. (b) Applying electric field

2.4.2.2.2 Semi-Crystalline Piezoelectric Copolymers

Unlike piezoelectric homopolymers, the piezoelectric copolymer is a piezoelectric polymer that is derived from two (or more) monomeric species [37]. The most common piezoelectric copolymers are: poly[(vinylidenefluoride-co-trifluoroethylene] P(VDF-TrFE); poly [(vinylidenefluoride-tetrafluoroethylene] P(VDF-TFE); and Poly(vinylidene fluoride-hexafluoropropylene) P(VDF-HFP). For semi-crystalline piezoelectric homopolymers, activating the piezoelectric properties requires stretching, as described previously. The application of stretching is not suitable for producing microfabrication devices [50]. In piezoelectric copolymers, the piezoelectric, electromechanical and dielectric properties of the material such as $P(VDF_xTrFE_{(1-x)})$ depends on the molecular weight molarity/ratio of the VDF portion in the piezoelectric copolymer [51]. Copolymerisation forces the polymer in a complete polar crystalline phase that consequently reduces the need for stretching piezoelectric material [43]. The crystallites of the copolymer (e.g. PVDF-TrFE) are larger compared to homopolymers (e.g. PVDF) (up to 90% crystalline). This leads to greater remnant polarisation, a lower coercive field and eliminate the hysteresis loop [43].

2.4.2.3 Ferroelectric Polymer Electrets (Ferroelectrets)

Ferroelectrets are non-polar polymers which have piezo- and pyroelectric properties. To activate their piezoelectric properties, opposite polarity charges are produced in the dielectric barrier discharge (DBD) and trapped at the internal surfaces of the voids when an external electric field is applied [38]. These trapped charges are illustrated in Figure 2-12. These voids are dipoles which, in terms of the elastic properties of the piezoelectric materials, activate the functional properties of the ferroelectret material [38]. Ferroelectret polymers are not ferroelectrics, but they behave like ferroelectric materials. Their ferroelectric behaviour comes from the final film formation (polymer with air voids) not because of the molecular arrangement such as that of ferroelectrics [52]. The incoming electric charge is only dependent on the number and size of the voids inside the polymer, not on the crystal structure of the lattice. These ferroelectrets exhibit higher piezoelectric coefficients compared with piezoceramics and piezoelectric polymers. The most common ferroelectrets are Teflon (PTFE), Polypropylene (PP), Polyethylene terephthalate (PET) and Cyclo-olefin copolymers (COC).

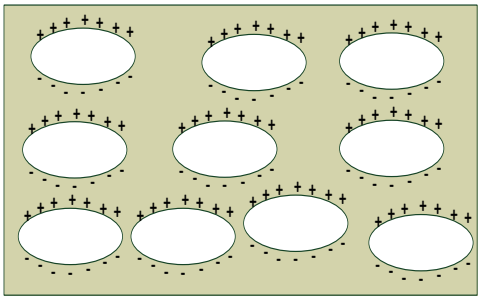

Figure 2-12: A schematic of charged voids inside the ferroelectrets

2.4.2.4 State of the Art of Piezoelectric Polymers

This section discusses the most resent contributions of the piezoelectric polymers types discussed before. The discussion involves the deposition technique used, the piezoelectric and dielectric properties and mechanical properties, the substrate used and finally the poling process to activate the piezoelectric properties of the materials. Table 2-4 lists the most recent contributions of the piezoelectric polymers, with the solvent mixed with fabrication type, the substrate they are deposited on and their piezoelectric coefficient d_{33} values. Most of the dielectric constant lay below 20 and the Young's modulus were mostly not specified. None of the materials have been used or associated with smart-fabric technology. Despite the good mechanical flexibility that is one of their features, they suffer from relatively low piezoelectric coefficients and low dielectric constants (<20) than their piezoelectric composites counterparts (discussed in the following sections).

Ferroelectrets actually offer both high piezoelectric coefficients d_{33} and mechanical flexibility, as shown in the second part of Table 2-4. However, the difficulty in fabricating voids and the complex fabrication technique have made depositing ferroelectrets polymer in one easy step a challenge, one which may lower the mass-production and raise the price of the devices. In addition, printing such materials would be challenging due to the requirement to create voids in the final film.

Ref.	Year	Piezo polymer-solvent	Deposition	Substrate	d_{33} (pC/N)	Comments
[53]	2004	Amorphous polyimide (b-CN)APB/ODPA	Casting	Glass plate	16.5	It was cured relatively at higher temperature (240°C), low d_{33} and dielectric constant (5).
[54]	2011	P(VDF-TrFE)-g-butyrolactone	Screen-printing	PET Sheet (175 µm)	-32 (±6)	The d_{33} values were measured without considering the clamping effect of the substrate and the poling method was not specified.
[55]	2011	Parylene-C	CVD	Not specified	0.1-2	High processing temperature process step (690°C) therefore cannot be adopted for fabric applications low d_{33}.
[56]	2012	PVDF-MEK	Casting	Polypropylene	-20	AC sinusoidal poling (75 MV/m @ 0.01 Hz), the d_{33} measured without substrate (no clamping effect).
[57]	2014	P(VDF-TrFE)	Screen-printing	poly(ethylene imine) (PEI)	*	The d_{33} measurements of the films were not specified.
[58]	2012	Cellular PP sheets	-	Not specified	200	Poling process was not specified, poled at room temperature, not screen-printable.
[59]	2012	Cellular PP films (40% voids)	-	Not specified	270	Annealed for treating at 70 °C for 151 h and the film was not screen-printable.
[60]	2012	FEP multilayers	Pattering FEP and fusion bond	Without substrate	1000	Poled at 18 MV/m at room temperature, complicated fabrication process.
[61]	2013	Cellular PDMS	Casting	Without substrate	1148	Poled at 35 MV/m at 90 °C, voids were creased with 3 PDMS layers, complicated fabrication process, not suitable for good mass production.

*Unknown

Table 2-4: State of the art of the ferroelectric polymers and ferroelectrets. The dielectric constants and Young's modulus were not specified for most of the proposed films

2.4.3 Piezoelectric Composites

Sections 2.4.1 and 2.4.2 discussed the prominent single-phase piezoelectric materials: piezoelectric ceramics and polymers and ferroelectret. They can be processed according to the type and the form of the piezoelectric material and the deposition process, which depend on the design and the size of the device. However, the use of these materials as single-phases is not

preferred because of low piezoelectric coefficients, the high cost of piezoelectric polymers and the incompatibility of ceramics for low temperature (below 200°C) and flexible applications. Therefore, an intermediate compromise is achieved by using piezoelectric composites.

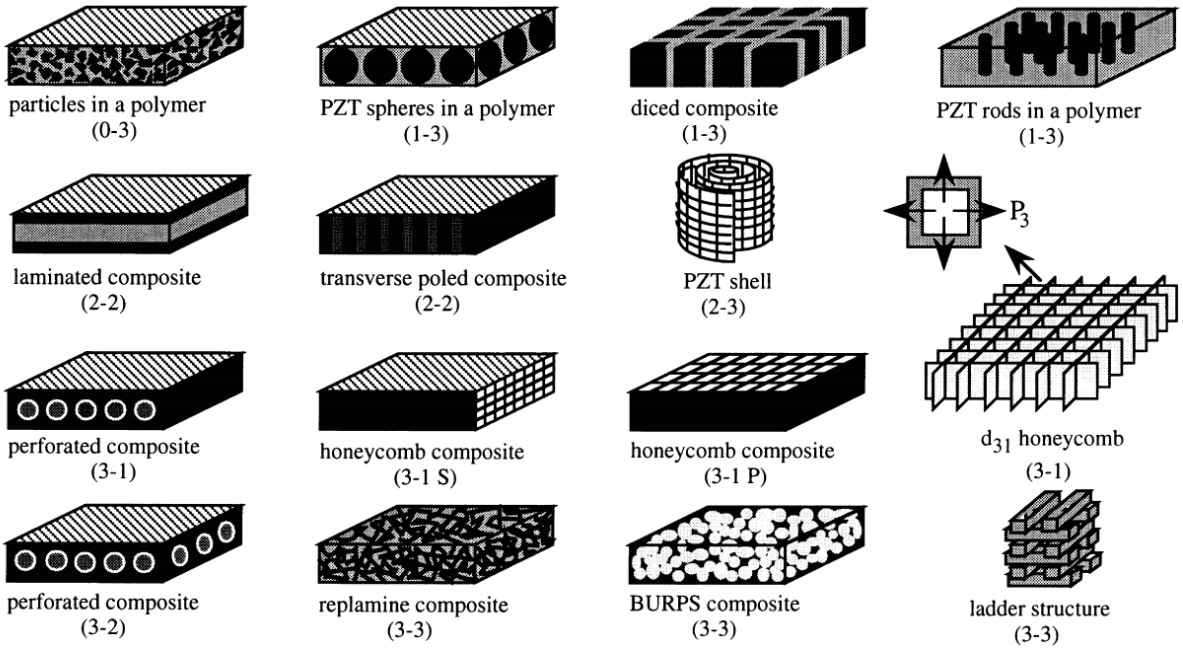

Figure 2-13: Schematic of piezoelectric composites with different types of connectivity [62]

The piezoelectric composite is a mixture of at least two basic materials; typically a piezoelectric material and a binder. There are several types of piezoelectric composites, as shown in Figure 2-13. The most common types are with (1-3), (3-2) and (2-3). The PZT block is etched making holes or patterns on the side (1-3) or both sides (3-2) vertical to the direction of the poling electric field. The polymer fills these holes or patterns creating the piezoelectric composite. This type of piezoelectric composite requires micromachining process which may not be suitable for smart-fabric applications.

The (0-3) piezoelectric composites provide the best option for this work as it can be fabricated straightforwardly by mixing a piezoceramic (e.g. PZT) with a polymeric binder. The 0-3 connectivity type piezoelectric composite can contain two active materials (e.g. PZT and PVDF are added together) that show relative active properties. Any material added to the mixture will dilute the optimum performance properties of both materials but with the correct formulation can provide a suitable compromise depending on the application. For example, if a polymer is added to piezoelectric ceramic (e.g. PZT), then the flexibility of the material can be improved but at the expense of the overall piezoelectricity of the material due to the reduced active material content and more difficult to realign the dipoles during poling.

The polymeric binder might have piezoelectric properties, such as PVDF and its copolymer, or any other type of polymer. A non-piezoelectric polymer can be used instead, such as a polymeric binder or epoxy. These types of composites have attractive properties ; for instance, their d_{33} is comparable to their piezoelectric polymers counterparts (discussed in section 2.4.3.2) but are easier to fabricate, flexible and processed at lower temperature ranges (100-250 °C) thus broadening their applications.

Finally, the formulation of the ceramic-polymer composites is a straightforward process with simple mixing techniques. Ceramic-polymer composites are processed depending on their usage and the type of fabrication of the desired device. They can be simply formulated by mixing the polymer with a solvent to form a liquid phase binder which is later mixed with the ceramic powder. The solvent phase can be more than one solvent with different weight loadings in the composite to tailor the formulation to the desired deposition technique.

2.4.3.1 The Effect of Piezoelectric Ceramic Particle Size

Piezoelectric ceramic particle size in the composite affects the piezoelectric property d_{33} of the whole composite. The piezoelectric properties increase alongside the increase of the particle size of the piezoelectric ceramic, without concern for the piezoceramic to polymer ratio.

Lower piezoelectric properties d_{33} are provided by smaller piezoelectric ceramic particle sizes in the piezoelectric ceramic-polymer composites. This is because the particles are homogeneously distributed and separated by the polymer matrix inside the piezoelectric-polymer composites, but with reduced opportunities for the particles to contact with each other. In addition, smaller size particles tend to be more spherical while irregular shape particles give them opportunities to contact each other; therefore, piezoelectric interaction occurs. However, large particle sizes of piezoelectric ceramics ordinarily have irregular shapes and sizes, while their large size in the polymer increases the probability of the particles being in contact and consequently increasing piezoelectric properties. Figure 2-14(a) [63] shows a schematic of piezoceramic particles inside the polymer matrix, where phases 1 (ceramic) and 2 (polymer) are, respectively, piezoceramic particles and polymer binder.

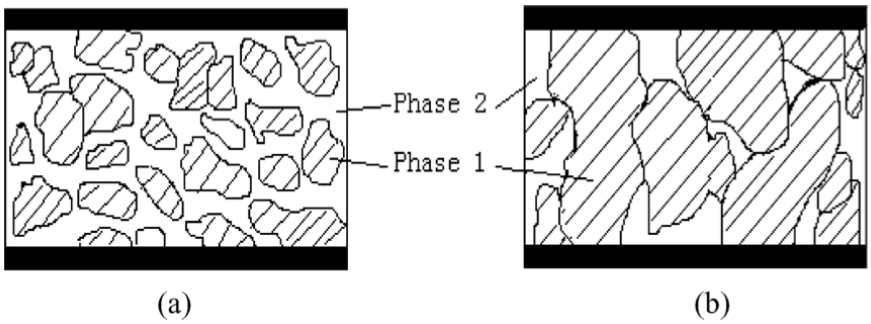

Figure 2-14: Piezoceramic particles inside polymer for both (a) small particle and (b) large particle [63]

Table 2-5 shows the contributions that confirm that reducing the particle size of the ceramic in the composite reduces the piezoelectric properties of the composite whatever the polymer phase weight loading is.

Ref.	Particle Size (µm) From-To	Composite	Deposition	d_{33} (pC/N) From-To	Comments
[64]	2-130	($BaTiO_3$)-Phenolic Powder resin	Unknown	9-30	Cured at high temperature (310 °C for 15 min) and flexibility is not reported.
[65]	5-95	$PZT_{30\%wt.}$-Nylon 57	Hot pressed	11-28	
[63]	1.45-294.07	PLN-white cement	Pressed into disks	7-27	Piezoelectric properties are increased by the grain size and flexibility is not reported.
[66]	3-482	$PZT_{50\%}$-$PE50_{50\%}$	Pressing	2-22	
[67]	34-316	$PZT_{50\%}$-$PE50_{50\%}$	*	6-20	
[68]	5-125	$PZT_{67\%}$-Eccogel 1365-80 polymer	Molding	21-28	

*Unknown

Table 2-5: Contributions regarding the effect of particle size on the piezoelectric and dielectric properties

2.4.3.2 State of the Art of Piezoelectric-polymer Composites

There is a plethora of piezoelectric composites in the field, but there are limited contributions from the literature on screen printable ones. Table 2-6 shows some of the piezoelectric composites with different fabrication techniques without reporting their flexibility. Most of these contributions are a mixture of piezoelectric powder (e.g. PZT) with piezoelectric polymer (e.g. PVDF). When mixing piezoelectric ceramic and polymer, each component has opposite remnant polarisation after poling, are which most likely to cancel each other and reduce the overall remnant polarisation of the whole film and therefore the subsequent piezoelectric coefficient d_{33}. This issue can be solved if the piezoceramic phase (PZT) and the piezopolymer phase were poled in antiparallel directions as stated by [69]. However, this method requires the piezoelectric film to

be poled twice which may degrade the mass production of the devices. Also, it is only useful for high piezopolymer weight loading (70%) otherwise the effect of this poling method on the d_{33} value will be insignificant and only printing piezoelectric polymer is desired (using one step of poling). Moreover, the authors did not mention the measurement method of obtaining the d_{33} values of the materials which is highly dependent on the mechanical boundary conditions of the substrate on which the piezoelectric film is printed (discussed in details on Chapter 5:). None of the piezoelectric composites presented have been investigated on woven-fabric.

Ref.	Composite	Deposition technique	Curing T (ºC)	Substrate	d_{33} (pC/N)	ε_r	Comments
[65]	**$PZT_{30\%wt.}$-Nylon**	Hot pressed	*	*	28	73	Piezoelectric properties are increased by the grain size. Also, flexibility was not tested.
[70, 71]	**PZT-PTF**	Screen-printed	*	Mylar	15	*	This is the only screen-printed contribution mixing piezoceramic with non-piezoelectric polymer. Also, flexibility was not tested and low d_{33} values were obtained.
[72]	**PZT-Acrylic paint**	Spray	*	*	10-30	*	It is a mixture of piezoelectric ceramic and non-piezoelectric polymer.
[69]	**$PZT_{27\%vol.}$-PVDF-$TrFE_{73\%}$**	Compression molding	220	*	20	*	This investigation solved poling the piezoceramic-piezopolymer composite films of different signs d_{33} by poling the polymer and the PZT in antiparallel directions.
[73]	**$PZT_{30\%wt.}$-PVDF-$TrFE_{70\%}$**	Screen-printed	*	Glass	~10	71	Mixing piezoceramic with a PVDF piezopolymer decreases d_{33} as they have opposite polarity and cancel out. Also, flexibility was not tested and low d_{33} values obtained.
[74]	**$PZT_{70\%wt.}$-PVDF**	Screen-printed		ITO/PET	24	88	Flexibility was not tested.
[75]	**$PZT_{67\%}$-PVDF**	Hot-pressed	200	Without	48	150	Processed at unsuitably high temperature. Higher d_{33} as there is no effect of substrate clamping. Poling method was not specified.
[76]	**$PZT_{60\%}$-epoxy**	Poured into a mould	55	Teflon Spacer	16	40	Low d_{33} and ε_r values and flexibility was not mentioned.

*Unknown

Table 2-6: Remarkable contributions towards the piezoelectric composites (*Continued*)

Ref.	Composite	Deposition technique	Curing T (°C)	Substrate	d_{33} (pC/N)	ε_r	Comments
[77]	**PiezoPaint PP-50B (PZT-polymer)**	Screen-printing	120	Aluminium	45	125	This printed film is not flexible.
[78]	**ZnO-(SU-8)**	Spin coating	90	Free-standing	8	*	The investigation discussed vibration energy harvesters. Spin coating is not suitable for fabric applications.

*Unknown

Table 2-6: Remarkable contributions towards the piezoelectric composites

2.5 Processing of Piezoelectric Materials

The processing of piezoelectric materials depends on the type of piezoelectric material (e.g. piezoelectric polymer, ceramic or a composite) and the method of deposition (screen or inkjet printing). When the type of material and the deposition method are specified, processing parameters (such as viscosity, vapour pressure of the solvent added or even the size of the grains) can be identified and also quantified. The mixing of piezoelectric materials is desirable for combining properties. For example, PZT material, which has higher piezoelectric coefficient, is not suitable for lower temperature applications such as printing on textiles. To solve this problem, PZT material can be mixed with low temperature binders, which can be cured at lower temperatures that are suitable for textiles. By this procedure, two features have been combined: piezoelectric performance and curing at lower temperatures.

2.5.1 Polymer-based Piezoelectric Materials

As stated before, the processing of polymer-based materials, such as PVDF and P(VDF-TrFE), depends on the deposition method. The printing or deposition requires the material to be in a liquid phase [79]. This is achieved by mixing the pure polymer with a solvent that can be evaporated later. Choosing a suitable solvent is essential because some polymers are not easily dissolved to achieve a homogenous mixture with some solvents. Li et al. [80] investigated the effect of the type and the content of the solvent on the membrane structure and performance of PVDF polymer. Also, Chen et al. [81] have reported that the solvent itself can have an influence on the piezoelectric material. There is a critical quantity that can be added to the piezoelectric composites that determines the properties of the film.

2.5.2 Ceramic-based Piezoelectric Materials

There are some factors affecting the processing of ceramic-based materials. These factors include the size of the particles, gaps between these particles and viscosity of the mixture and porosity of the film. Mostly, three components are used to formulate the thick film piezoelectric paste; the active material (piezoelectric material), the binder and the solvent [82]. Most of the piezoelectric ceramics come in solid phase (powders) which needs to be transformed to the liquid phase in order to easily and smoothly deposit/print them [79]. The solvent was required to help liquidize the mixture.

Large particles of the material increase the gaps between particles (the larger the particles the greater the gaps between particles). These gaps are undesired because the mechanical properties of the printed layer are reduced. Therefore, filler (usually from the same material) with smaller size particles can be added to fill the gaps between the larger grains. Many reported contributions in particle size optimisation give maximum mechanical and piezoelectric properties [83, 84]. They have reported an optimisation of particle size in piezoelectric and mechanical properties of the piezoelectric composites. The produced formulation was screen-printed on alumina substrates and the piezoelectric properties were tested.

2.5.3 Drying and Curing of the Materials

2.5.3.1 Piezoelectric Composites

While printing, the drying process is essential when further prints are desired to increase the thickness of the film or to preserve the printed layer from contamination (e.g. dusts). Drying solidifies the film so that a further print cannot affect the thickness of the previous prints. Moreover, the dust cannot contaminate the material when the liquid phase is partially removed from the material. Drying can be applied in an oven under a low temperature (e.g. <120 °C).

For high temperature piezoelectric composite, materials that use for example glass frit as a binder, sintering is required. The sintering process is necessary to make the binding material melt around the PZT powder and produce a strong bonding between the constituents. As a result, the porosity of the material is reduced and the mechanical properties are therefore improved. Furthermore, the application of pressure decreases sintering time and the porosity between the particles [79, 85]. Sintering is carried out in a furnace which has three zones: the preheat zone, sintering zone and cooling zone [86]. The preheat zone is responsible for removing any organic materials and solvents. The sintering zone is for the actual sintering process when the particles are

fused or the binder is sintered with the surrounding particles. The cooling zone is responsible for cooling down the material after it is sintered.

However, for low temperature piezoelectric composites that use polymers or epoxies as a binding system, a curing process is required. This curing process is mainly achieved to convert the material from its liquid form into a solid form by removing the solvent phase within the material. The curing process for low temperature piezoelectric materials is typically achieved either thermally or by UV-irradiation. In the case of thermal curing, the piezoelectric ceramic is mixed with polymeric binder which are typically cured in a temperature range of 150-200°C [82]. For UV-curing, the UV-curable ceramic-based materials (e.g. PZT) are prepared by mixing the milled PZT powder with a UV curable monomer and a photoinitiator [87]. The photoinitiator is responsible for absorbing the UV photons generating reactive radicals and transferring the photons energy into the curing material and the monomer enhances the bonding between particles [88]. Two important factors are considered to activate the photoinitiator with UV light, wavelength and intensity. The photoinitiator can be activated properly by the correct wavelength and sufficient intensity; if not the chemical reaction will not or will only partly occur. This curing method employs the ultraviolet light in wavelength of 200-400 nm. The monomer improves the cross linking within the curing material.

2.6 Deposition of Piezoelectric Materials

Material deposition can be divided into two categories depending on the thickness of the deposited layers; that is, thin or thick depositions. Thick film deposition can produce films with typical thickness between 1-200 µm [89, 90]. In general, thick film technology is a deposition method that is capable of depositing/printing films with greater thickness in one deposit/print. This can increase the mass production and density of the printed film and also reduce the time and the cost of the printed devices. In addition, thick film technology is compatible with the fabric industry and depositing films that have low temperature processing. These features gave thick-film technology the advantage of incorporating these features to produce thick and dense piezoelectric composite films with high mass production. One of the methods for depositing materials on a substrate is printing. There are several types of printing materials, some of which are described below.

2.6.1 Thick-Film Screen Printing

Screen-printing is a technique of depositing materials by forcing inks with different compositions and rheological characteristics through a pre-patterned screen onto a substrate

surface using a squeegee [91]. Screen printing has widespread use in graphics art production, especially in fabrics (e.g. T-shirts and graphics on clothes). This technology is also employed for printed electronics technology, such as fabricating sensors, thick film hybrid circuits and energy harvesters [7]. Screen printing typically produces print thicknesses of 1-200 µm per layer [90]. Accordingly, screen-printing has proved itself in micro-electronics and is already considered suitable for fabric production. If screen-printing is used for depositing piezoelectric films on fabric, then it will combine two features:

- Deposition technique that has been used for centuries in fabric production.
- Deposition technique that has proven itself in high mass-production micro-electronics circuitry and devices.

Although screen-printing of images on fabric is widespread, yet it has not been used to produce piezoelectric layers on fabrics. It will offer the compatibility of both fabric production and the piezoelectric composites as discussed in this section and section 2.4.3.2. The screen is typically comprised of an aluminium frame and a wire mesh coated with an ultraviolet sensitive emulsion. The aluminium frame is used for mounting the mesh under tension before coating the emulsion layer. The mesh is made of silk, nylon, polyester or stainless-steel [92]. The high mesh counts and the thread's small diameter can be adopted for screens that are dedicated to fine print definition [92, 93]. To transfer the pattern into the screen, the ultraviolet sensitive emulsion can be exposed to the UV light through a patterned mask. The transferred pattern is left as open spaces in the screen and the unexposed areas of the emulsion layer are dissolved [92].

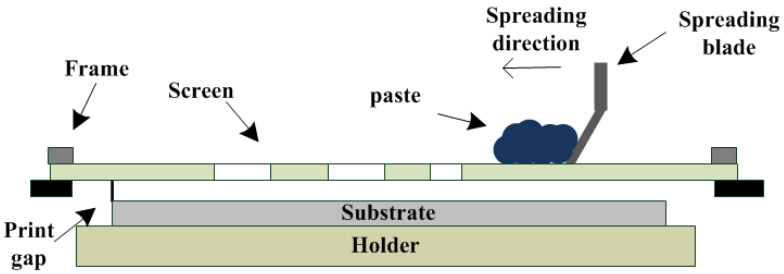

(a)

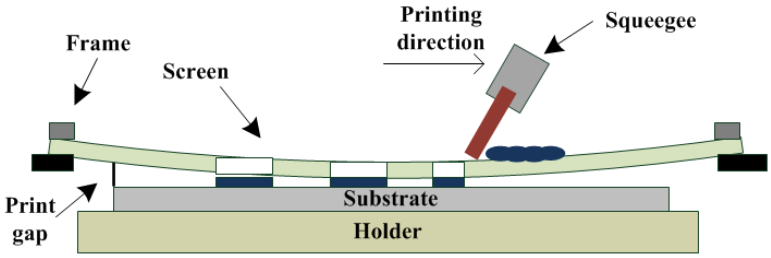

(b)

Figure 2-15: Schematic of screen printing process. (a) Flood stroke. (b) Print stroke

As shown in Figure 2-15, the screen printing process is divided into two stages: flood and print strokes. For the flood stroke, the paste is spread over the top surface of the screen but with no downward pressure as depicted in Figure 2-15(a). As a result, the spread paste fills the openings in the screen. In Figure 2-15(b) the squeegee pressurises the paste through the openings and conveys it to the substrate [92]. Some parameters need to be considered before starting the printing process, such as squeegee velocity and pressure during printing and the printing gap.

There are many contributions in the literature which use screen-printing to produce piezoelectric films for sensing, actuating (piezoelectric inverse effect) and energy harvesting (piezoelectric direct effect). These contributions can be categorised in terms of the processing temperature of screen-printed piezoelectric materials. Most of the contributions of screen-printed piezoelectric materials were done using high temperature materials in which piezoelectric ceramic-based vibration energy harvesters and sensors (e.g. accelerometers) are produced.

Many high temperature piezoelectric devices were screen-printed. In 2001, Glynne-Jones et al. [94] reported a tapered piezoelectric electric energy harvester screen printed on to stainless steel. The piezoelectric material (PZT) is sandwiched between two electrodes deposited on a dielectric layer to avoid short circuiting because the substrate is stainless steel. The piezoelectric composition used as a paste was PZT-5H powder mixed with Corning 7575 glass and a thick film vehicle. This device can produce an output power of 2.1 μW at a resonance frequency of 80.1Hz and an optimum resistance 333 kΩ.

Zhu et al. [95] report a bimorph piezoelectric vibration energy harvester that includes multiple PZT layers. Three devices were fabricated with different numbers of PZT layers: single, double, and triple PZT layer bimorphs. The overall thickness for each side of the bimorph for each device did not exceed 150μm thickness. This means that the thickness of the PZT layer for single, double and triple PZT layer device was 150, 75 and 50 μm respectively on each side. The simulation and experimental results were close to each other. A single PZT layer device produces a maximum power of 69.18 μW at an optimum load of 158 kΩ and at resonance frequency of 64.5 Hz. The double PZT device generates a maximum output power of 97.9 μW at an optimum load of 37 kΩ and a resonance frequency of 64.5 Hz [95]. The triple PZT layer device produces a maximum output power of 82.61 μW at an optimum output load of 17 kΩ and a resonance frequency of 64.2 Hz. The results show that the double PZT layer device generates higher power more than single and triple PZT layers devices [95]. Figure 2-16 shows the screen-printed devices and, schematically, the design of the multi-layer bimorph generators.

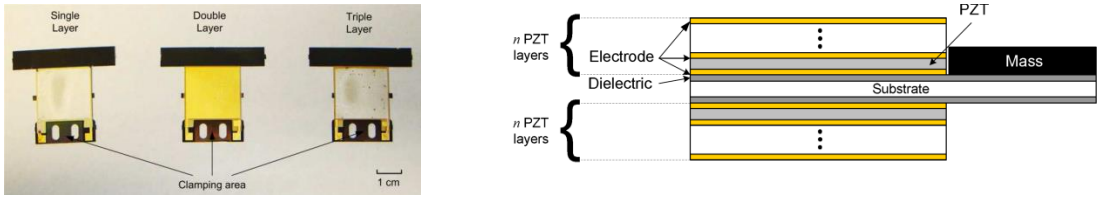

(a) (b)

Figure 2-16: Multi-layer piezoelectric energy harvesters [95]. (a) The actual devices and (b) the schematic of the multi-layer piezoelectric harvester

Some other contributions regarding screen-printing piezoelectric materials have been listed in Table 2-7. None of these applications of screen-printed piezoelectric materials was printed on fabric. The screen-printed films were associated with energy harvesting, transducing or sensing. Most of the contributions used high temperature curing material. However, the screen-printed low-temperature piezoelectric composites were either single-phase piezoelectric polymers or composites with a phase of piezoelectric polymer. Only two composites from Piezoceramic-piezopolymer were used. The first contribution [70] showed low d_{33} values (15 pC/N) compared to PVDF polymer films. The second one showed high d_{33} but the flexibility of the produced films was not suitable for fabric applications. In most of the other contributions, the formulations were screen-printed on stiff or inflexible substrates such as glass or stainless steel.

Material type	Mixture	Substrate	Application	Comments	Ref.
Composite	**PZT-PTF**	Mylar	*	• PZT-5H (<6µm grain size) mixed with PTF dielectric paste • The printed material showed very low d_{33} value although it was printed on flexible substrate.	[70, 71]
Composite	**PZT-lead borosilicate glass**	Alumina	*	• The sintering temperature was over 800°C, therefore it is not suitable for fabric applications • The printed film was stiff and not flexible.	[96]
Composite	**$PZT_{70\%wt.}$-PVDF**	ITO/PET	Film speaker	• The film was printed on ITO that was placed on PET. • Maximum d_{33} of 24 pC/N.	[74]
Composite	**$PZT_{30\%wt.}$-PVDF-$TrFE_{70\%}$**	ITO/glass	*	• The film was printed on a layer of ITO which is deposited on a glass substrate. • The d_{33} value reached 10 pC/N.	[73]
Composite	**PZT-lead borosilicate glass**	Stainless steel sheets	Vibration energy harvesting	• The curing temperature was over 800°C and not suitable for fabric applications. • The printed film was stiff and not suitable for fabric applications.	[95]
Single-phase polymer	**P(VDF-TrFE)- g-butyrolactone**	PET Sheet (175 µm)	Matrix sensor array	• The maximum d_{33} achieved was 32pC/N.	[54]
Single-phase polymer	**P(VDF-TrFE)-**	Polyethyleneimine (PEI)	Ultrasonic transducer	• d_{33} values were not mentioned. • The mixture constituents were not mentioned.	[97]

*Unknown

Table 2-7: State of the art of the screen-printed piezoelectric materials (*continued*)

Material type	Mixture	Substrate	Application	Comments	Ref.
Composite	**PiezoPaint PP-50B (PZT-polymer)**	Alumina	Sensor array for impact detection	• The printed material was not flexible and not suitable for flexible electronics applications.	[77]
Composite	**PZT-borosilicate glass**	Free-standing cantilever	*	• High temperature cured material. • The screen-printing deposition was associated with sacrificial layer method to create the free-standing cantilever	[98]

*Unknown

Table 2-7: State of the art of the screen-printed piezoelectric materials

Choosing a suitable screen-printed piezoelectric polymer to be used as a binder can have the following problems:

- Electric field cancelation during poling process (i.e. piezoelectric ceramic and polymer polarisation interaction during poling).
- Suitability for fabric application (e.g. low-temperature cured (<200 °C) and screen-printability).

Flexibility in material processing: For example, there is always a concern about the type of solvent added to the PVDF or its copolymers; that is, when processed as the type of the solvent can affect its piezoelectric activity. This may lower the overall piezoelectric coefficient of the composite. However, by using none of the piezoelectric polymers this concern is eliminated. Combing piezoelectric composite with thick film screen-printing technology can help increase the mass-production of the devices; raise the piezoelectric coefficient d_{33} and the dielectric constants; and increase mechanical flexibility in designing the devices. This will increase varieties of devices with different patterns. Moreover, this technique will grow the varieties of fabrics used. Using such piezoelectric composite with screen-printing will not restrict the type of fabric used.

2.6.2 Inkjet printing

Inkjet printing has attracted researchers and manufacturer due to some advantages, such as low temperature processing, non-contact printing, printing without patterned mask, suitability for different substrates and less ink waste [99]. However, this method suffers from issues such as clogging and blockage of nozzles and print heads during printing [100].

Inkjet printers have two modes of operations; continuous and drop-on-demand (DOD) [101]. For continuous mode, the ink continuously jets out of the nozzle as shown in Figure 2-17(a). Individual jetted droplets are then electrically charged by the charging electrodes [102]. The charge cannot penetrate the volume of the droplet and is placed on its surface. The polarity of the electrode is then switched to charge the following droplet produced from the nozzle. Depending on its charge, the droplet is deflected by the field plates. The uncharged droplets are caught by the catcher for later re-use. The charged droplets are oriented onto the substrate and the charge level determines the place at which they land [102].

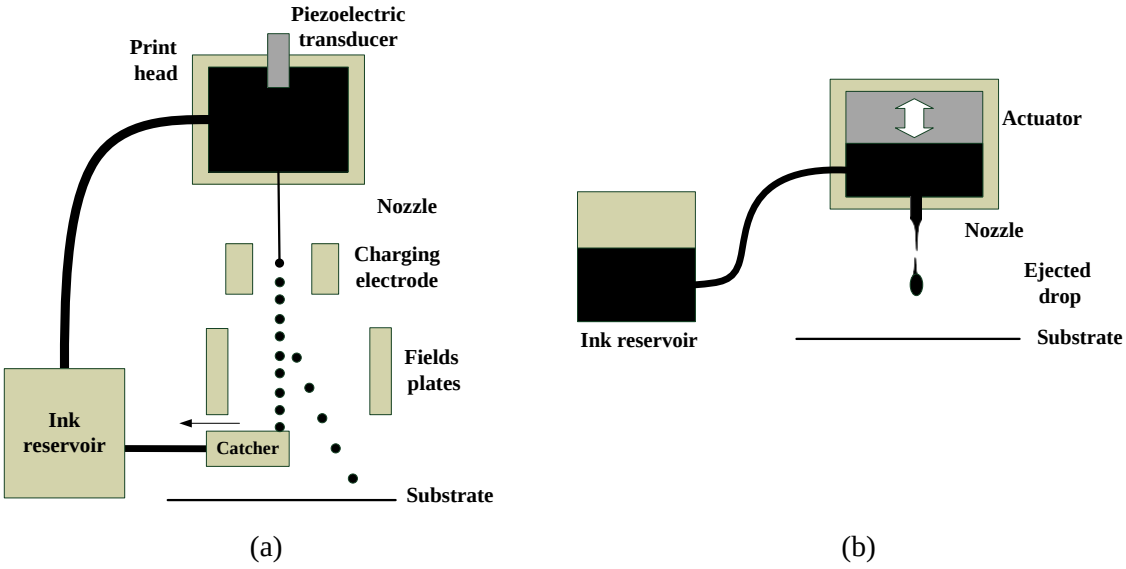

Figure 2-17: Schematics of the main types of Inkjet printer [102]. (a) Continuous Inkjet printer. (b) Drop on Demand (DOD) printer

The second type of inkjet printing technique is drop-on-demand (DOD). The DOD printers have a print head with an array of nozzles. When needed, the drops are jetted from these nozzles to form the desired printed pattern [102]. Figure 2-17(b) illustrates the nozzle function schematically. The ink is placed in a reservoir and is pumped to an ink cavity for printing. An actuator produces a change in the cavity volume which, when activated, causes a force to produce an ejected drop. From this operation, the size of the drop is affected by the wave propagation of the ink and the volume of the cavity. The pulse can be generated thermally or piezoelectrically. In the thermal DOD (bubble-jet), the ink is subjected to a sudden temperature rise to form vapour bubbles which are used to eject the drops [101]. As bubble-jet employs water as a solvent, this technique is limited to polymers that are soluble in water [101]. The piezoelectric DOD uses a piezoelectric transducer which causes a volume change in the cavity when the piezoelectric material is actuated by an external electrical excitation. Piezoelectric DOD is suitable for most solvents. Inkjet printing method offers great fingerprints in printing piezoelectric films on top of different varieties of substrates without using a mask. Many contributions were proposed in

inkjet-printing PZT layers on the top of different substrates. Some of these contributions are listed in Table 2-8.

Printer	Nozzle Diameter (µm)	Ceramic Type	Particle Sizes (nm)	Additions	Ref.
IBM model 3852/2 'Colorjet'	65	TiO_2	*	• Acrylic polymer and polyvinylbutyral • A mixture of ethanol and propan-2-ol for dilution. • Ceramic percentage in the mixture 50%	[103]
DOD Hewlett Packard Deskjet 500 with 60 nozzles	50	3Y-TZP	100-200	• A mixture of low molecular weight of polyethylene glycol (PEG) with water was used as a dispersant. • Ceramic percentage in the mixture was 60%.	[104]
Epson Stylus 500	40-100	PZT	199	• The PZT nanoparticles were dispersed in Dispex HDN (Allied Colloids, UK) dispersant and PVA binding system.	[100]
The Biodot Continuous Inkjet printer	60	PZT	*	• A mixture of Methyl ethyl ketone and absolute ethanol was used for room temperature printing. • Wax was employed for high temperature printing. • For both cases phospholan PE182 (Akros Chemicals Ltd., UK) was used as a dispersant. • Ceramic percentage was 20%.	[105]

*Unknown

Table 2-8: Some contributions of inkjet-printed PZT layers

None of the previous contributions mentioned the piezoelectric properties of the printed films. In 2012, Machida et al. [106] combined inkjet printing, chemical solution deposition and a surface energy controlling technology. The inkjet-printed PZT film had a 2 µm thickness. The printed film gave a dielectric constant of 1700 and a remnant polarisation of 10 $\mu C/m^2$. The estimated piezoelectric coefficient was 77 pm/V which was low compared to high temperature piezoelectric composites that were deposited by other printing techniques, such as screen-printing. In this contribution, the PZT particle size ratio to the head diameter was not mentioned. Prim alcohol was also added to the solvent to improve the ejection stability of the droplet.

There is no contribution on inkjet printing for flexible piezoelectric composite which requires a polymer phase in the printed ink. As mentioned before in section 2.4.3.1 on page 26, the greater the particle size, the higher the piezoelectric properties of the printed piezoelectric film. However, ink-jet printing suffers from the limitation of the size of ceramic particles because the diameter of

the nozzle head is typically small (see Table 2-8) which cannot help create piezoelectric films for energy harvesting because the d_{33} values will be very low. Moreover, the viscosity of the printed film should be very low to guarantee the stability of the ejected droplets from the head of the inject printer. To achieve this, a higher weight percentages of solvents will be required on account of the PZT particles which can affect the density of the printed film and also the dielectric and piezoelectric properties.

2.7 Piezoelectric Materials and Smart-fabric Applications

Some of the contributions mentioned on the state of the art of piezoelectric polymers, ferroelectrets and composites were only dedicated for depositing these materials on flexible substrates, but not on fabrics. However, there are some other contributions that have exploited the piezoelectric concept on fabric and flexible substrates for energy harvesting or sensing.

Description	**V_{OC} (mV)**	**Current (pA)**	***f*** **(Hz)**	**Charge Density ($\mu C/m^2$)**	**Power density (mW/m^2)**	**Energy density (mJ/m^3)**	**Vol. (mm^3)**	**Ref.**
Coated PZT fibres embedded in a piece of woven fabric	480	*	4.6	*	*	3425	146	[107]
Piezoelectric Nanowires grown on fibre	1-3	5	1.33	*	20-80 for a bundle of fibres	*	*	[108]
Piezoelectric ribbons printed onto rubber	*	*	320	800	*	*	*	[109]
Enhanced piezoelectric printed onto rubber	*	5 ribbons (30) 10 ribbons (62)	*	*	*	*	*	[110]

*Unknown

Table 2-9: Contributions over wearable and flexible applications

Some of the most important over-wearable, smart-fabric and flexible electronics applications are summarised and listed in Table 2-9. Guillot et al. [107] embedded PZT fibres (coated with jacket) in a piece of woven fabric. Two electrodes sandwiched the fabric-PZT fibre composite. The authors did not explain the mechanism of extracting the produced charge; there were air gaps between the piezoelectric fibre and the electrodes. This increases the possibility of losing charge. Moreover, the d_{33} measurements and flexibility of the devices were not clarified in the study. The other contributions showed complicated micromachining technology which made the mass-

production quite challenging. In addition, they did not specify the piezoelectric or dielectric properties of the produced materials. However, there are some other contributions of flexible piezoelectric composites for energy harvesting applications on fabrics listed in Table 2-10. These composites were also listed according to the force type that was used to harvest electrical energy.

Material	Force Type	Area (cm^2)	Current (μA)	Voltage (V)	Comments	Ref.
$BaTiO_3$-(SW/MW-CNTs)-RGO films deposited using solution-casting	Bending	5×6	0.35	3.2	• The film consists of $BaTiO_3$ nano particles; Single and Multi-walled carbon nano tubes (SW/MW-CNTs) and reduced graphene oxide (RGO). • The d_{33} values were not investigated.	[111]
PMN-PT nanowires-PDMS composite film deposited by spin-casting	compressive	1×0.5	2.29	7.8	• The material was deposited on Ti/Au (10/100 nm) coated polyimide film. • Using spin casting for depositing such materials is challenging on woven-fabrics. • Nanowires may show some difficulties in fabrication (e.g. flat surface) and in mixing.	[112]
$LiNbO_3$ nanowire-PDMS composite film deposited by spin-coating	Compressive	*	0.09	0.46	• The film was deposited on Kapton which was attached to polyester film. • These outputs were produced at calculated strain of 0.0168.	[113]
$(Na_{0.5},K_{0.5})NbO_3$ nanoparticles embedded in P(VDF-TrFE) nanofibers	Bending	*	0.78	0.98	• The NKN-P(VDF-TrFE) nanofibers layer was placed between PET films coated with indium tin oxide (ITO). • They used complicated fabrication process to produce this nanocomposite film.	[114]

*Unknown

Table 2-10: Recent contributions of the piezoelectric composite devices with its investigated force type

2.8 Power Consumption and Wearable Electronics Applications

Flexible piezoelectric films can be exploited as a smart-material for energy harvesting of human body movement. Piezoelectric energy harvester on woven-fabrics for exploiting human movements is typically used for powering human body sensing systems particularly in health monitoring and biometric systems (which includes sensors, data managements represented by microcontrollers and data transmission such as Bluetooth) [115] and also for powering electronic

devices (e.g. LEDs) [111]. Figure 2-18 shows basic piezoelectric power generator system for wearable electronic systems.

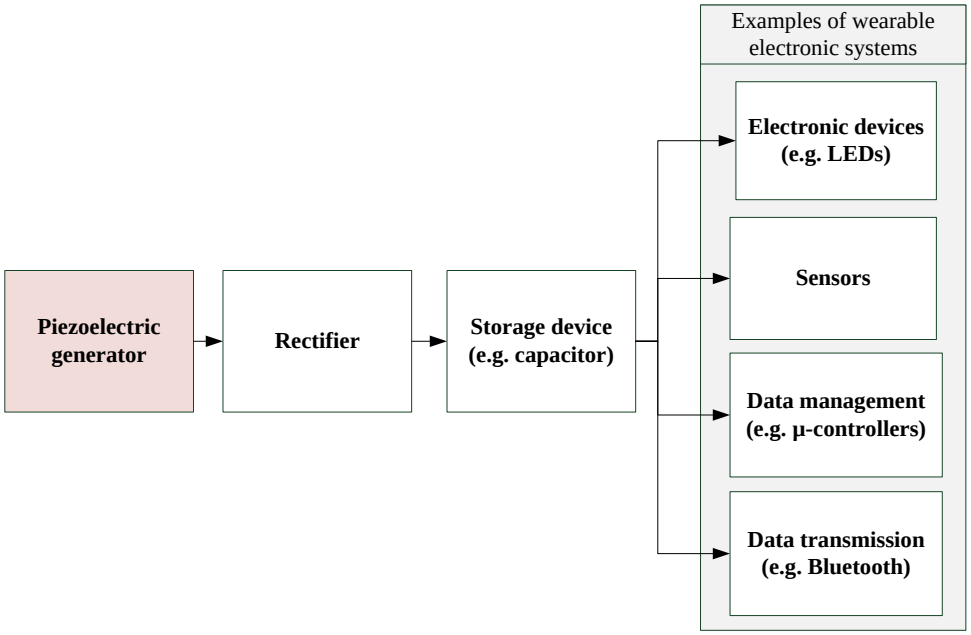

Figure 2-18: Basic wearable electronic systems that can be powered by piezoelectric generators that exploit body movements

Table 2-11 shows some examples of the systems that can be used for body-worn and wearable electronic systems and their corresponding power consumptions. The proposed piezoelectric composite film needs to satisfy the energy required for one duty cycle for at least one of the systems shown in the Table 2-11 with respect to its power consumption conditions. Some applications such as body monitoring include more than one of these systems in Table 2-11. Using such smart materials for energy harvesting is application-dependent. Therefore, the proposed piezoelectric film has to meet the minimum requirements to satisfy energy of one duty cycle. This duty cycle must be wisely designed according to the application.

Application	Electronic system	Operating voltage (V)	Power/energy consumption	Comments
Sensors	ADXL330 Accelerometer, ANALOG	2	400 µW	This system can be used as a body worn accelerometer
Data control	PIC16F676, Microcontroller, MICROCHIP	2	Operating mode=17 µW Sleeping mode = 2 nW	They are used for data management and can be implanted in the shoe or the fabrics.
	Apollo-ultra-low power microcontroller, ambiqmicro	1.8-3.8	Operating mode=54 µW Sleeping mode = 180 nW	
Transmitting systems	Bluetooth [116]	3.3	10 µJ/byte for 0.2 seconds	They are used for transmitting the data received from the data control system and can be implanted in the shoe or the fabrics
	802.15.4/ZigBee CC2480 [117]	2.2	73 µJ in 1.2 seconds duration for 8 byte transmission	
	AM-RT4-433, RF Transmitter		Operating mode=8 mW Sleeping mode = 100 nW	

Table 2-11: Examples of applications that can be used for human biometric measurements and health care monitoring systems with their estimated power consumption. Note, the power consumption was estimated according to the electronic system's data sheet

2.9 Methods of Poling Ferroelectric Materials

To activate the piezoelectric properties of the ferroelectric material, a poling process is essential. The poling process cannot be carried out above the Curie temperature. Above the Curie temperature, the central ion is placed on average in the plane of the structural ions. However, below the Curie temperature, the central ion is placed out of the plane and, accordingly, the charges are no longer in equilibrium state and provide a dipole. When the net dipole of the material is oriented, piezoelectric properties are activated. This net dipole can be oriented by applying an electric field to the piezoelectric material with elevating temperature. High poling temperatures have to be carefully considered for some of the active material and fabric substrates. For piezoelectric polymers, polarisation does not just depend on the applied electric field. It also depends on the available crystallinity, the fraction of crystals which are polar and the molecular chains' orientation of the material [19].

2.9.1 Direct-Contact Poling (DCP)

This method of poling is typically achieved by applying a voltage across the electrodes that sandwich the piezoelectric material [38]. The applied electric field depends on the thickness of the material and the applied DC voltage as equation $E = V/t_p$ (where t_p is the thickness of the piezoelectric layer) describes [118]. This is achieved under an elevated temperature. Heating up is essential in the poling process to enable the molecules inside the piezoelectric material to move freely. After heating reaches the desired temperature, the piezoelectric material is left for a certain time under the same electric field and temperature [96]. The piezoelectric material is then cooled down whilst maintaining the same applied voltage. Once the piezoelectric material temperature reaches room temperature, the applied voltage is turned off. At this point, the poling process is complete and the d_{33} values of the material may be obtained. Figure 2-19 illustrates schematically the apparatus of the contact poling process.

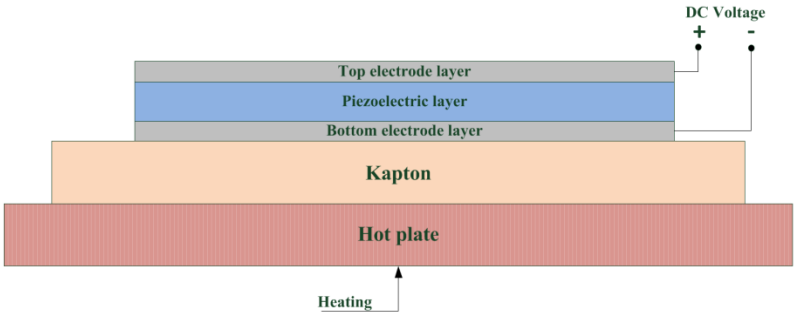

Figure 2-19: Schematic showing an example of Direct Contact Poling (DCP). The Kapton substrate is only an example

The setup of this method is simple and ideally provides the distribution of the electric field across the piezoelectric element between electrodes areas. Therefore, the size of the sample is not a problem with this method. In addition, the integrity of the electric field can be controlled by the applied voltage as long as it is below the maximum dielectric strength voltage of the deposited piezoelectric element.

2.9.2 Corona Discharge Poling (CDP)

Researchers started to utilise corona discharge in dielectrics as they had been invented for electrophotographic system in the 1940s. A corona is an electrical discharge that occurs when a voltage difference is observed between asymmetric electrodes [119]. These electrodes can be a wire, point, tip (top electrode), plate or cylinder [120]. Corona discharge has two distinct regions. The first region is close to the cathode where ions are generated. This leads to a gas movement because of the collisions amongst the excited particles and neutral molecules. The other is called

the drift region which appears between the cathode and the anode [120]. At a certain electric field, charge density increase in the drift region to the point where an electrical path is created between the cathode and the anode causes a dielectric breakdown in the medium (e.g. air). The path produces a fine blue line of light called a Corona. A potential difference is also generated between the cathode and the anode.

Normally, the printed ferroelectric or the ferroelectret materials are polarised or charged with corona discharge method by applying an electric field before the dielectric breakdown of the material [18]. When a corona discharge is used for poling the piezoelectric material, it oxidises the surface of the top layer (this layer could be electrode or the active layers) as CO_3^- and $(H_2O)_nH^+$ ions are produced for positive and negative coronas respectively [120]. The two methods of corona poling are shown in Figure 2-20: normal corona and triode-corona poling. The only difference between the two methods is that a metal grid is placed between the sample and the needle for triode-corona poling. This grid is used for homogenising the corona field which is generated via the needle over the sample and also for controlling the voltage applied on the sample by V_g.

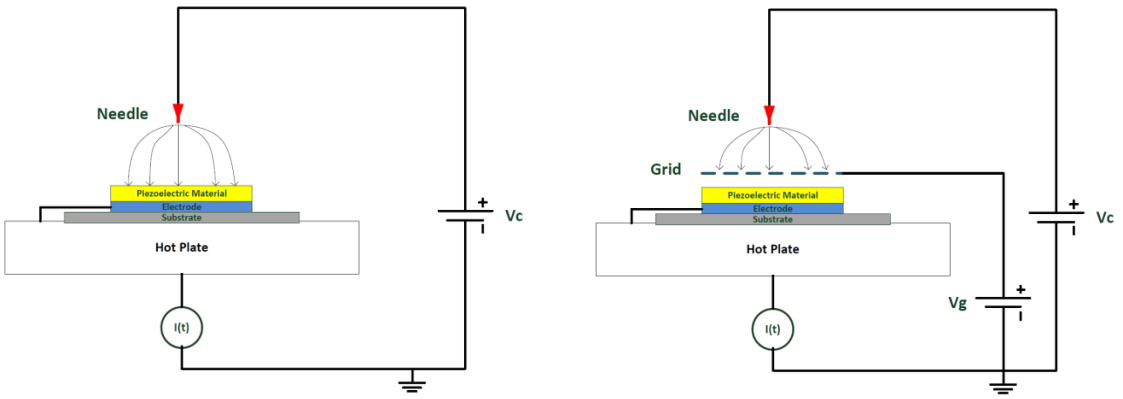

(a) (b)

Figure 2-20: Corona Discharge Poling methods (a) Normal corona poling and (b) Corona triode poling.

2.9.3 Electron-Beam Poling

This technique is dedicated for poling thin fluoropolymer films [121, 122] and piezoelectric nanofibers [123]. The poling principle looks similar to corona discharge, but the process is performed under a vacuum and with an E-beam gun that concentrates the electrons in a specific area [38]. Compared to the corona discharge method, this concentration provides a good penetration of the electric field across the piezoelectric material.

Figure 2-21 shows, schematically, the setup and E-beam poling operation for a piezoelectric element. The general setup of this method can be realised by depositing one side of the

piezoelectric element with a very thin (100 nm) bottom electrode, as proposed by Gross et al. [124]. This electrode is grounded directly and the sample is carefully placed in a Scanning Electron Microscope (SEM) which is then used to generate the electron beam which will be employed for poling the piezoelectric material. The poling is started as soon as the un-electroded front surface of the piezoelectric material is irradiated by electrons supplied by SEM [124]. A space-charge layer is generated in the sample as the electrons accumulated on the surface of the piezoelectric material and an electric field is then created across it. Similar to corona and contact poling, this field orientates the piezoelectric material's dipoles. This causes an increasing negative potential at the surface of the sample. Accordingly, the electron energy is reduced. Furthermore, the emission of the secondary and backscattering electrons causes a reduction of the electron beam current.

If mass-production is an important factor, this method is slow compared to other methods. The samples have to be placed in a vacuum which can severely limit the speed of mass-production. Electron penetration and the poling area are important factors in poling the piezoelectric element. The E-beam gun probe diameter and distance can specify the intensity and the distribution of the accumulated electrons. Compared to other methods, the accumulation of the electrons may be comparable with the Direct-content poling and Corona discharge poling, being that it can be achieved in vacuum. However, the distribution is so limited because the diameter of the E-beam gun probe. The lack of good mass production options and limited distribution of electrons make this type of poling challenging for piezoelectric elements compared to other methods and is therefore not considered further in this thesis.

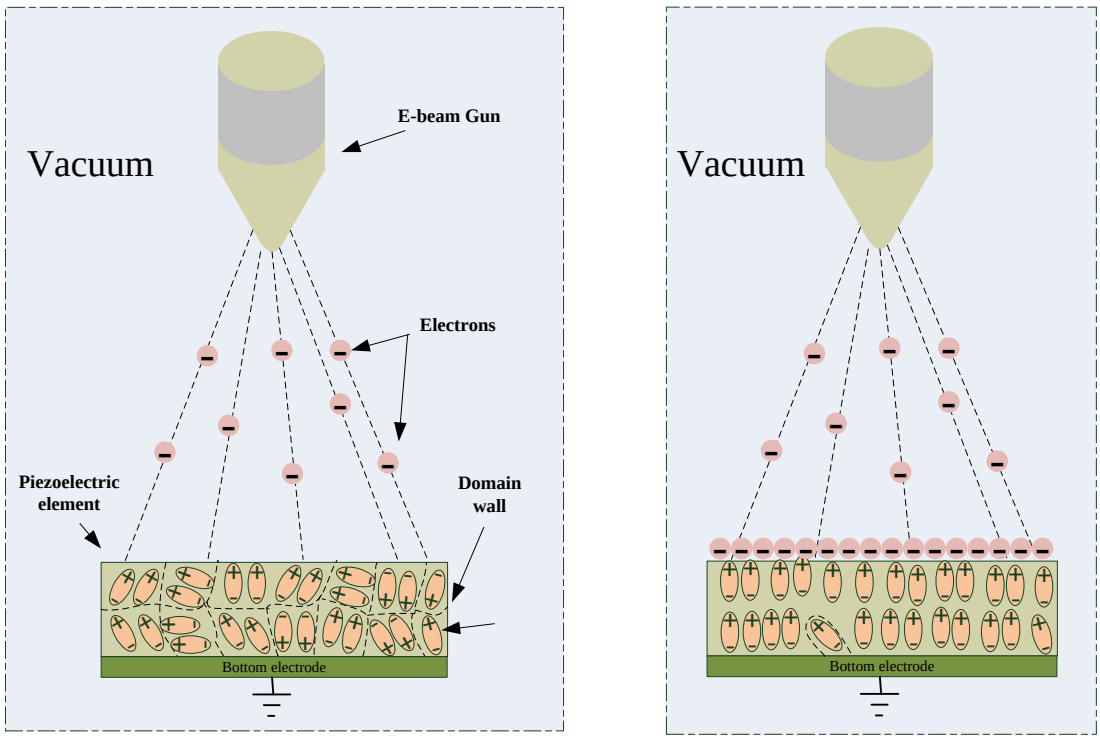

(a) (b)

Figure 2-21: Schematic of the E-beam poling. (a) Stream of electrons is emitted from the E-beam gun. (b) The electrons are accumulated on the surface of the sample

2.10 Conclusions

This chapter has defined the piezoelectric effect and given a summary of piezoelectric theory. In addition, it has classified the piezoelectric materials and compared them for the selection of the suitable material that can be used on smart-fabric and e-textile applications. This chapter has reviewed single-phases and composite piezoelectric materials. Single-phase piezoelectric polymers (PVDF and its copolymers) can be used for harvesting kinetic energy from textiles. Ferroelectret foams can also be employed but fabrication of closed voids is very challenging (no contribution found in the literature for screen printed ferroelectret foams. This is because of the incompatibility of screen printing and creating closed voids within the polymer). However, piezoelectric composites can compete with piezoelectric polymers in desired properties such as low temperature curing, high d_{33} values and flexibility. From this chapter the following conclusions are made to define the next stages of research presented in this thesis:

- Amongst the piezoelectric composites, the 0-3 connectivity composites were found to be easier to formulate and easier to scale up to mass production than some other composites. Importantly, these are the most suitable composite type for screen-printing deposition.

- As the 0-3 connectivity type piezoelectric composite has two main constituents (piezoelectric ceramic and a polymeric binder), the soft piezoelectric ceramic PZT-5H is selected because it can provide higher dielectric constants and piezoelectric coefficients d_{33} compared to its counterparts. It is also the most common piezoelectric ceramic in energy harvesting applications.
- Increasing the particle size of the piezoceramic material (e.g. PZT) in piezoceramic-polymer composites increases the piezoelectric properties of the materials.
- The type of polymer binder mixed with the ceramic in the composite affects the piezoelectric properties. Most of the contributions in the literature have used piezoelectric polymers, such as PVDF and its copolymers, to be mixed with PZT ceramic. However, the opposite polarity of d_{33} between piezoceramic and piezoelectric polymer can reduce the final d_{33} value of the whole composite material. This made the poling process of such composites challenging and require more poling cycles to effectively pole both the piezoceramic and piezopolymer phases in the film. Therefore, we have suggested using non-piezoelectric polymer to be mixed with the piezoceramic.
- We explored the contributions proposed for wearable, smart fabric and flexible piezoelectric applications. The complexity, poor scale up potential and lack of information concerning, for example, the dielectric, piezoelectric and mechanical properties, make it difficult to fully assess their capability.
- Printing techniques can be used to fabricate piezoelectric energy harvesters on fabric because of their simplicity. The screen printing technique is the most used and most compatible for the fabric industry. It is considered the most appropriate depositing technique which can combine the suitability of woven-fabrics and micro-electronics production.
- Choosing the poling method is an important factor to maximise the piezoelectric properties of the printed film. E-beam poling cannot be used because of the poor mass production and also the limited area that can be poled which is confined by the diameter of the E-beam gun.
- Corona discharge and direct contact poling was found to overcome these challenges and experimentally investigated in the following chapter.

Chapter 3: Screen-printing and Poling Low-Temperature Piezoelectric Films

3.1 Introduction

The strength of the electric field on the PZT particles inside the polymer depends on the dielectric properties of the composite and the type of poling method. Using the correct type of poling method is essential for maximising the piezoelectric properties. Poling methods have been compared experimentally by considering the d_{33} values of the films, the ease in applying poling, the consistency of poling i.e. poling the whole film homogenously and finally suitability for mass production (number of devices poled in a specific time). A theoretical investigation of poling methods that can be applied for poling the 0–3 connectivity type piezoelectric composite films is not applicable.

This chapter will describe the initial screen-printing, curing and poling processes on a screen-printed piezoelectric composite film. The commercial screen-printed piezoelectric paste used, PiezoPaint, was supplied by Ferroperm (Denmark). The investigation of poling methods included two different poling methods: direct-contact poling (DCP) and corona discharge poling (CDP). In addition, the poling processes being evaluated are optimised before comparison. The methodology for screen-printing process optimisation and evaluation of the poling process is shown in Figure 3-1.

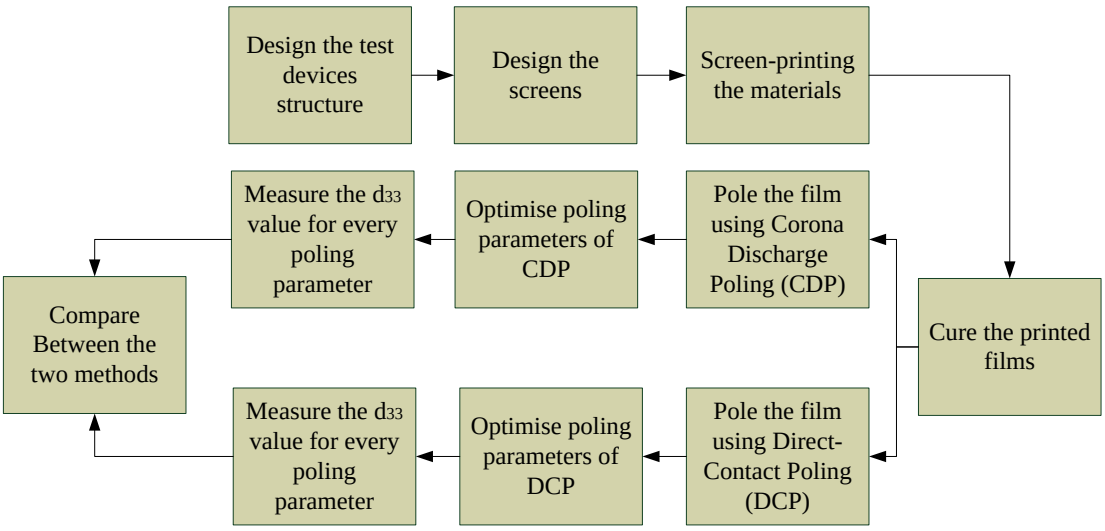

Figure 3-1: Experimental plan of screen-printing and poling method selection

3.2 Test Structure Fabrication

3.2.1 Screen-printed Capacitive Structures

Testing the piezoelectric properties (d_{33}) of the material requires the devices to be in a capacitor structure. As the mechanical force is in the 3-direction, on the top electrode, the charge extraction will be also in the 3-direction and will be collected using the top and bottom electrodes. Such structures are straightforward to print as the number of printed layers is low (3 layers). Figure 3-2 illustrates a schematic of the capacitive structure proposed for designing the screens. It shows the capacitor structure layers (the active piezoelectric layer is sandwiched between the top and bottom layers) that will be printed onto the substrate.

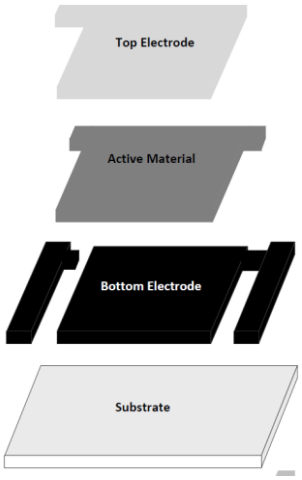

Figure 3-2: Schematic of test capacitor structure

3.2.2 Screen-printed Materials

At this stage of the study, a commercial low temperature piezoelectric composite was used to initially evaluate the quality of the screen-printing process and to provide a benchmark regarding the printability of the paste. This material also enabled an evaluation and comparison between the poling techniques. This material (denoted PiezoPaint, Ferroperm [77]) was brought as it is the only low-temperature screen-printable piezoelectric composite in the market. The material was tested, compared and used as a reference for the screen-printable low temperature piezoelectric composite developed subsequently as part of this work in terms of piezoelectricity and mechanical flexibility.

The test capacitor structure shown in Figure 3-2 requires the piezoelectric material to be sandwiched between two electrode materials. The main two electrode materials that were used in this project are Silver-polymer DuPont 5000 and Silver-polymer ELX 30 from Electra. They are

screen-printable and cured at low temperatures (90–130 °C) and they have a good level of flexibility. When both are printed on alumina (630 µm, Hybrid Laser Tech) and Kapton polyimide (75 µm, KATCO) substrates, they showed good adhesion particularly when applying a scratch test to the surface using a sharp tool.

3.2.3 Screen Designs

Each layer in Figure 3-2 will be printed by its corresponding screen. The printed device layers were drawn in L-Edit on the top of each other as they are, to be printed so the geometry and dimensions can be defined, except for the thickness of the printed layers, which is specified by the actual printing process. The L-Edit layouts were then sent MCI Precision screens Ltd. (screens manufacturer) to be fabricated.

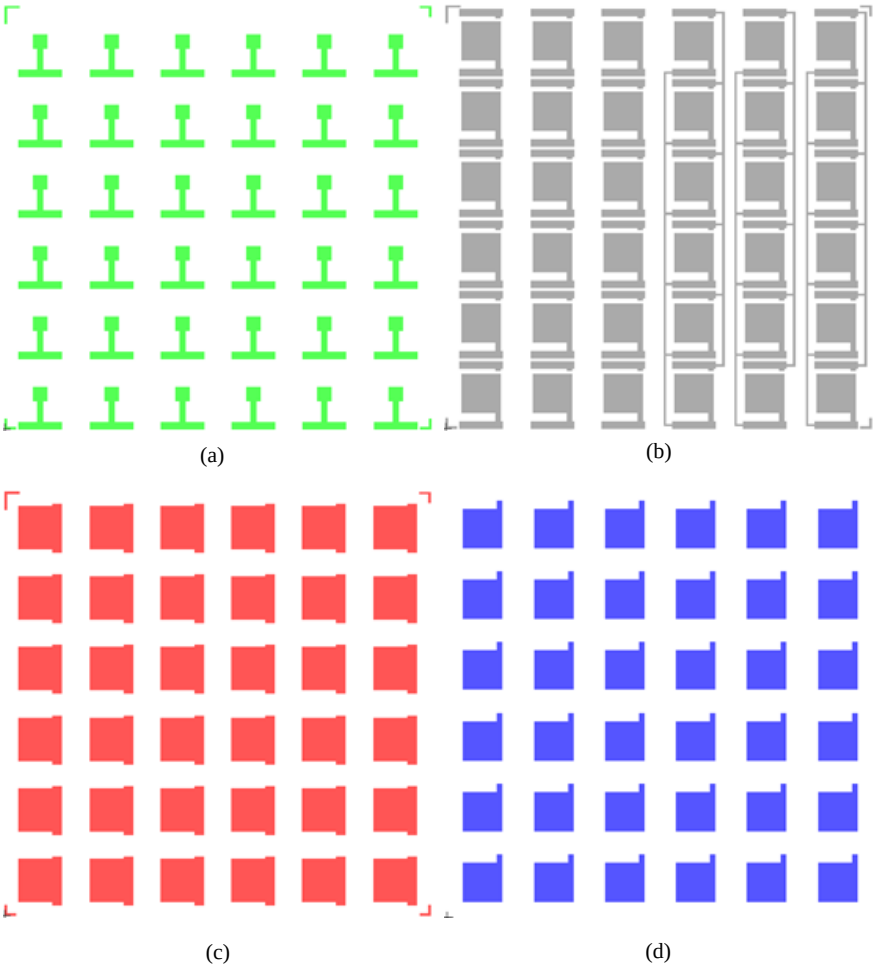

Figure 3-3: L-Edit layout designs for the capacitive devices. (a) Backside electrode layer, (b) bottom electrode layer (b), (c) piezoelectric layer and (d) top electrode layer

The layouts show 36 devices that are fabricated on one substrate. The layers are screen-printed on the top of each other in the same order shown in Figure 3-3. The piezoelectric material

layout has an element size of 1.2 × 1.2 cm^2. However, the bottom and top electrode elements are 1 × 1 cm^2 which should simplify the alignment and prevent short circuits. Before screen-printing the PiezoPaint, its screen-printability and curing conditions was initially tested by hand screen-printing. This procedure was used to minimise waste of the material and also to increase the speed of the evaluation. Figure 3-4 illustrates examples of the semi-automatic and hand printed screens used. Hand screen-printing was used initially when the proposed material formulations are first evaluated.

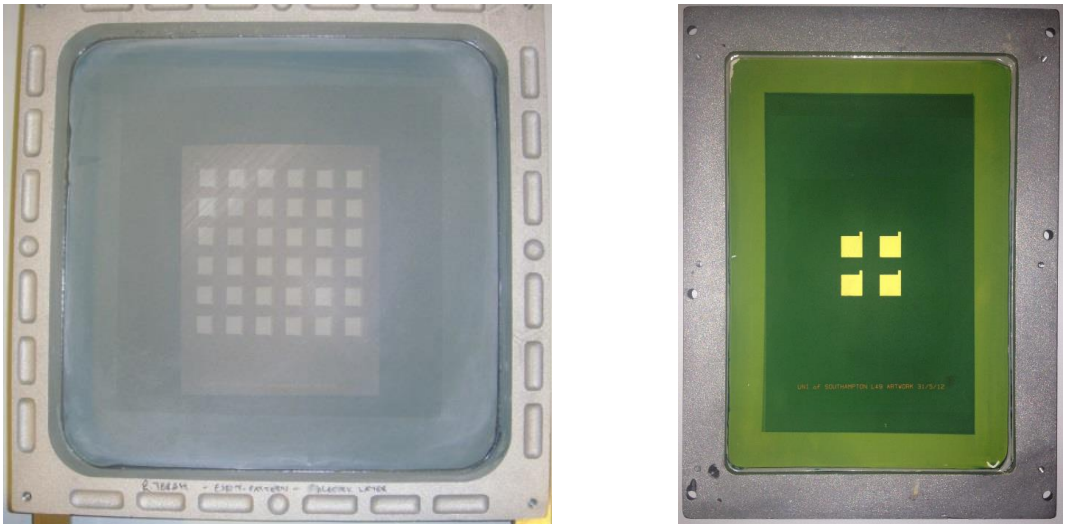

(a) (b)

Figure 3-4: Examples of (a) the 12″×12″ stainless-steel screens for semi-automatic screen-printing and (b) the 6″x8″ polyester screens of the hand screen-printing

Every screen has specifications that differ according to the paste to be printed. Appendix A shows the description of these specifications which define the screen. The screens consist of an aluminium frame that mounts the mesh under tension. Table 3-1 shows the main specifications of the screens that were used for printing the test devices. These specifications define the printed layer in terms of the thickness of the deposit and volume of the paste that passes through every opening. The stainless steel mesh type withstands high squeegee loading and offers a longer life time and a flatter screen during printing compared to its counterparts, such as polyester.

The mesh opening and wire diameter are the most important parameters because they specify the volume that can be transferred. Every mesh opening has its corresponding wire diameter and the screen can be described by these two parameters. The particle size of the printed paste should be taken into consideration before choosing the mesh opening. For example, for the piezoelectric material, the mesh opening is 25 times greater (for the semi-automatic screen-printing) than the average of the main particle size of 2 µm (that will be used later along this study) and 5 times greater than PiezoPaint average particle size (10 µm). The thicker the emulsion on the mesh, the

greater the volume of the paste that is printed on per deposit. However, the thicker emulsions produce less smooth surfaces of the printed layers.

Parameter	**Backside electrode**	**Bottom & top electrodes**		**Piezoelectric material**	
Screen type	Semi-automatic	Hand	Semi-automatic	Hand	Semi-automatic
Description	75/36	55/48	75/36	55/48	50/30
Material type	Stainless steel	Polyeste	Stainless steel	Polyester	Stainless steel
Frame size	12″×12″	6″×8″	12″×12″	6″×8″	12″×12″
Mesh opening (µm)	75	55	75	55	50
Wire diameter (µm)	36	48	36	48	30
Mesh count (n/cm)	230	90	230	90	325
Emulsion Thickness (µm)	15	28	15	28	40

Table 3-1: Main specifications of the printing the hand and semi-automatic screens

3.2.4 Screen-Printer

The machine used for screen-printing is a semi-automatic DEK 248 screen-printer, as shown in Figure 3-5. It consists of many parts that need to be controlled to help either align the substrate to the screen or achieve the screen-printing process. These main parts are summarised as follows:

- *Squeegee:* It is a rubber-edged blade that forces the printed ink to go through the open meshed areas in the screen.
- *Substrate holder:* The substrate holder is located on the substrate table. The holder is the place where the substrate if held firmly in place. The substrate holder can be changed according to the size and geometry of the substrate placed on it.
- *Screen-printing area:* This area is where the screen is fixed and the actual screen-printing process is achieved after the substrate table with the screen holder goes beneath the screen.
- *Control interface:* The control interface is represented by DEK 248 screen-printer software, which controls the alignment and the substrate holder position in the x-y-z axes. In addition, it controls the speed of the squeegee during printing and the number of deposits printed for the printed layer. The control also specifies the limits of the squeegee stroke during printing. The printing gap, which also influences the thickness of the printed device, and the force applied by the squeegee on the screen, can also be adjusted by the control system.
- *Alignment cameras:* These cameras are dedicated to controlling the alignment of the substrates to the screens when needed.

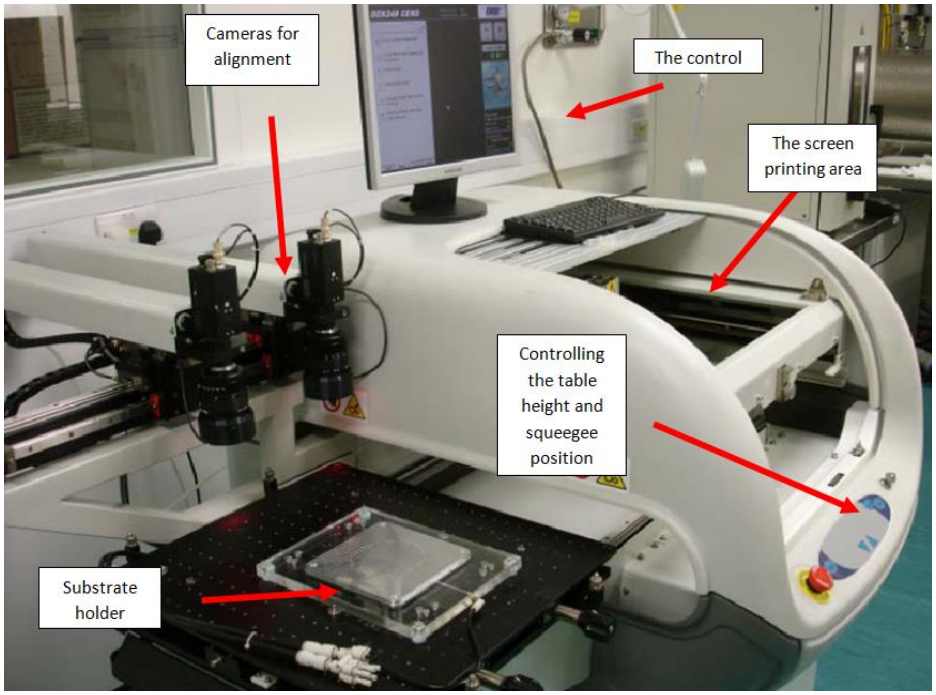

Figure 3-5: DEK 248 semi-automatic screen printer

3.2.4.1 Selectivity and Preparations of Substrates

In order to evaluate the printing and poling processes of the materials, substrate defects (such as the smoothness of the surface) that might affect the results have to be eliminated for making a fair investigation. Screen-printing the piezoelectric material on fabric is the main target of the project. However, the fabric suffers from many problems that affect the devices printed on it such as surface roughness. These problems are investigated and solved later in the following chapters. In order to investigate the poling and curing conditions of the PiezoPaint, it has been printed on ceramic substrates normally used for high temperature pastes. This offers a smooth surface, good adhesion and stability when taking the d_{33} readings and its results will be taken as a reference for the other substrates.

However, there are some alternatives such as Kapton which are flexible, can withstand high temperatures compared to fabric and have a smooth surface. Kapton substrates offer an intermediate step between printing on alumina and fabrics that enables the mechanical flexibility of the materials to be tested. Kapton can withstand temperatures of nearly 350 °C and provides a level of mechanical flexibility that can be comparable to fabrics. The three types of substrate used in this work, alumina, Kapton and fabric, are shown in Table 3-2, which summarises the main challenges for each substrate. These challenges are studied and discussed for the proposed piezoelectric composite materials along this study.

Challenges	Alumina	Kapton	Fabric
Temperature Endurance	High	Moderate	Depends on the type of fabric
Smoothness of the Surface	High	High	Needs surface Treatment
Adhesion	High	Moderate	Needs surface treatment
Flexibility	Inflexible	Flexible	Flexible
Clamping effect	High	Moderate	Low

Table 3-2: Technical challenges of the substrates

3.2.5 Screen-printing and Curing Processes

The screen-printing process differs from device to device. For example, printing a unimorph piezoelectric energy harvester is different from printing a bimorph in terms of the number of the layers printed and the printing side of the substrate. Therefore, the screen-printing process should be planned, particularly if different pastes are printed in many/different substrates, otherwise the process will be difficult to control. Each screen-printed layer follows the process illustrated in Figure 3-6.

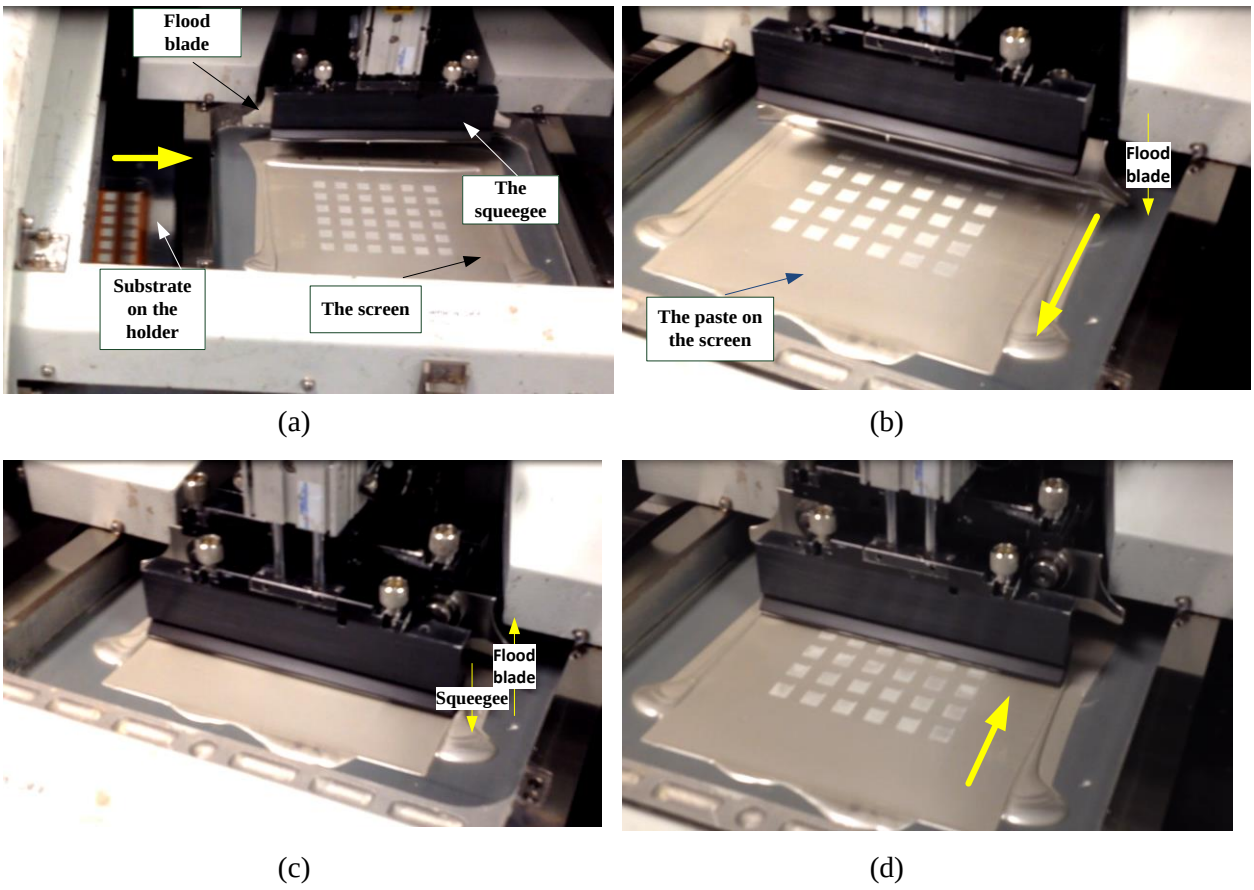

(a) (b)

(c) (d)

Figure 3-6: Screen printing process. (a) The substrate on the holder goes beneath the screen. (b) The spreading blade starts to spread the paste on the screen (Flood stroke). (c) The squeegee starts to push the paste through the screen and the blade lifts up. (d) The squeegee pushed the paste through the mesh opening and lifts up (print stroke)

The screen-printing process for the whole capacitive structure (with more than one substrate at a time) that is used throughout the study is described in detail in the process flow in Figure 3-7. The drying and curing conditions used are given in Table 3-3.

Layer	**Drying Conditions**		**Curing Conditions**	
	Temperature (°C)	**Time (min)**	**Temperature (°C)**	**Time (min)**
Bottom electrode (ElX 30, Electra)	100	12	12	15
Piezoelectric layer (PiezoPaste)	100	8	140	10
Top electrode (ElX 30, Electra)	100	12	120	15

Table 3-3: Drying and curing conditions of the printed materials

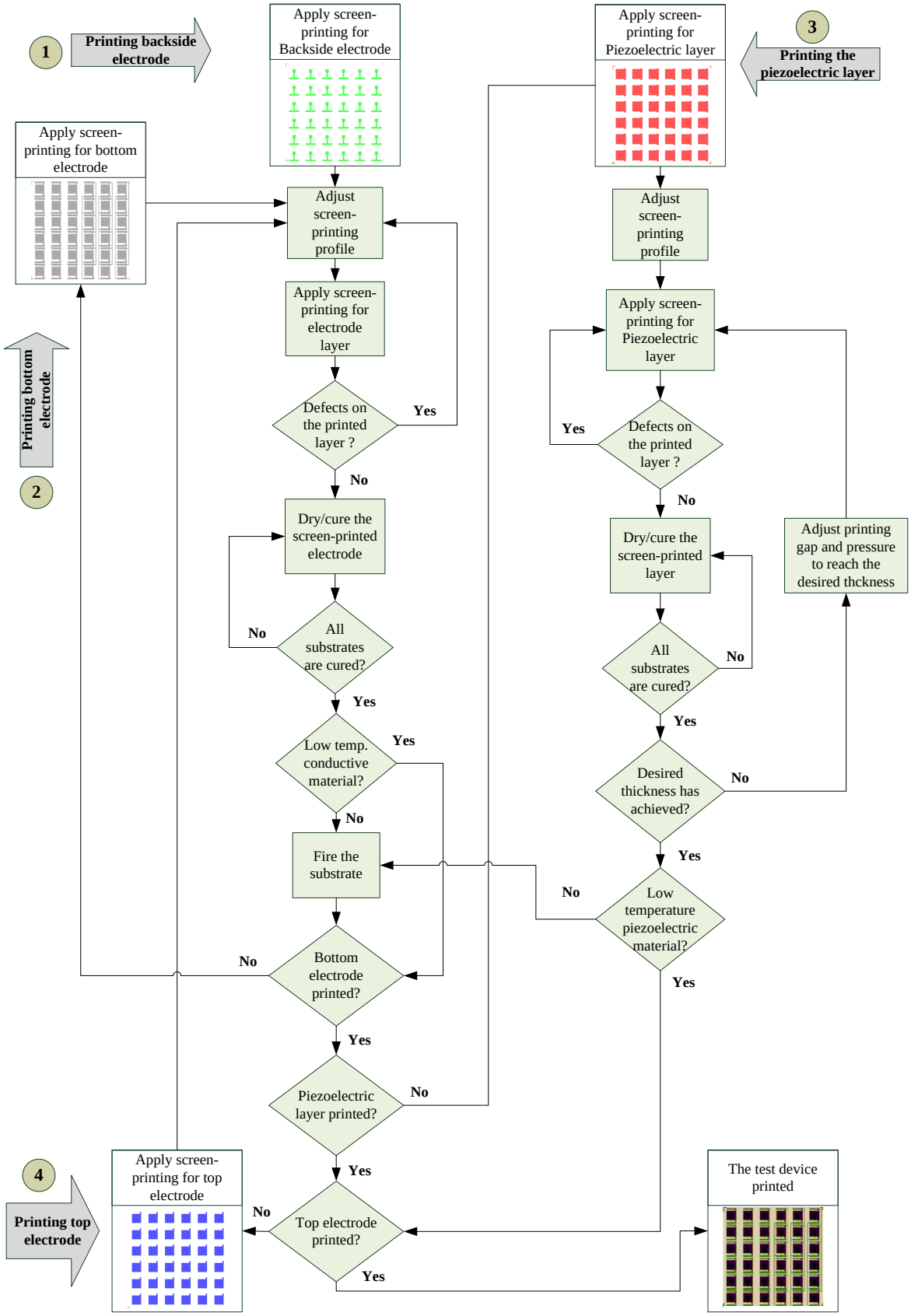

Figure 3-7: General screen-printing process flow of the capacitive test devices

Figure 3-8 shows a scanning electron micrograph of the screen-printed PiezoPaint layer sandwiched between two screen-printed electrodes on a Kapton substrate. The image shows the large piezoelectric ceramic particles (~10 µm).

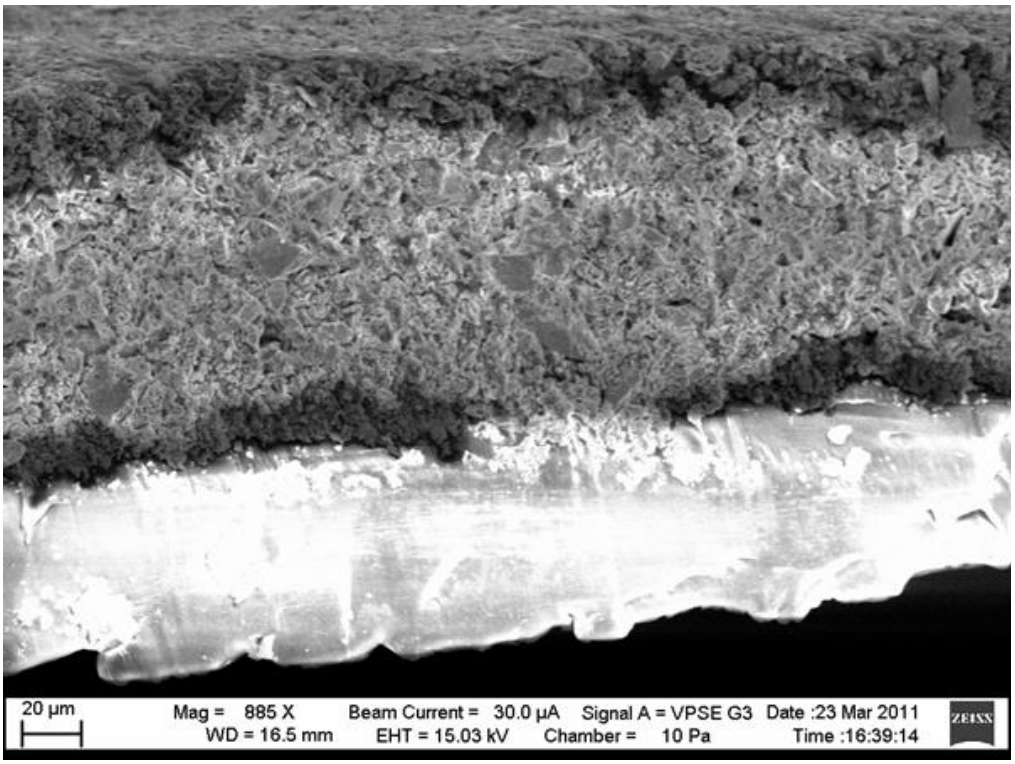

Figure 3-8: Scanning electron micrograph of the screen-printed PiezoPaint layer sandwiched between two conductive electrode layers

3.3 Evaluation of Poling Methods

Polarisation is the key for activating the composite material from being ferroelectric to piezoelectric by aligning the dipole moments with respect to the direction of the electric field. There are many types of poling techniques that can be used to activate piezoelectric films, such as DCP and CDP, as mentioned before. A brief comparison between DCP and CDP methods is shown in Table 3-4.

Method	Advantages	Disadvantages
DCP	• Voltage distribution across the piezoelectric element because of the existence of the electrodes. • It is not dependent on the size of the device. The electric field across the materials is controlled by the area of the electrodes. • Only main three parameters (e.g. poling field, temperature and time) are used. • The applied voltage can be easily estimated by the equation $E = V/d$.	• Both electrodes are required to perform the poling process. • Short-circuiting can occur at any time during poling.
CDP	• Only the bottom electrode is required to perform the poling process. • A high voltage can be applied and short-circuiting is unlikely to happen, compared to DCP.	• Large size devices can be a problem owing to problems homogenously distributing the electric field across the piezoelectric element. • Another poling parameter is used (e.g. needle or grid distance from the sample). • Another power supply is required to control the grid voltage if a grid is used to uniform the field. • The voltage applied on the surface of the sample is not easily estimated and needs an experimental investigation. • d_{33} measurements are not consistent for the far points from the poling cathode (the needle) as the electric field is not uniform.

Table 3-4: Comparison between DCP and CDP with their advantages and disadvantages

Both methods were applied to PiezoPaint (Ferroperm, Denmark) material and the piezoelectric properties will be explored experimentally by measuring the d_{33} values of the piezoelectric film.

3.3.1 d_{33} Measurements using a PIEZOTEST PM300 Piezometer

The PIEZOTEST PM300 Piezometer shown in Figure 3-9(a) was used to characterise the piezoelectric properties of the thick/thin piezoelectric film by measuring the d_{33} coefficient. The PM300 uses a Berlincourt method to obtain the d_{33} measurements. It adopts the dynamic method by applying an oscillating force (0.25 N) to the sample with the aid of a built-in electromagnetic transducer placed at the bottom probe, as shown in Figure 3-9(b). The top probe is only used for clamping the device. The produced charge is estimated with the aid of a differential amplifier to obtain the d_{33} value.

(a)

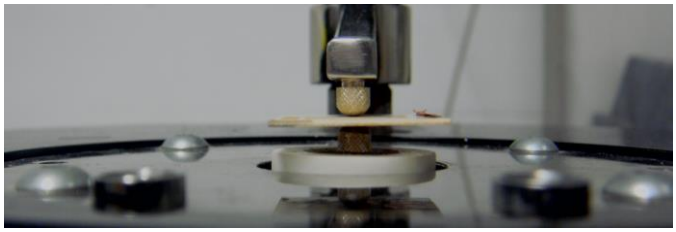

(b)

Figure 3-9: Measurement system used for measuring piezoelectric coefficient d_{33}. (a) PIEZOTEST PM300 used for measuring d_{33} values. (b) The sample as it was clamped in the system

A 5% measurement error has been confirmed when the sample is over or under-constricted [125]. Five positions were used for measuring the d_{33} coefficient values of all the testing devices used in this project, as shown in Figure 3-10. The probe for the d_{33} meter was put at these places and d_{33} measurements were taken. Therefore, for each device tested, an average of five measurements was taken. The maximum and minimum value is included for every d_{33} measurement in the graphs.

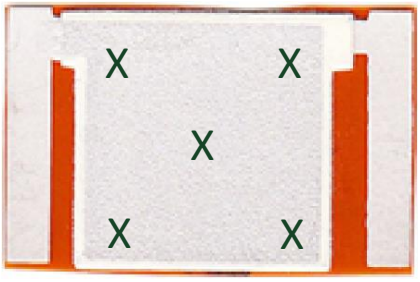

Figure 3-10: The d_{33} measurements positions on the final screen-printed test device printed on Kapton

3.3.2 Experimental Plan of Poling Process Optimisation

The DCP and CDP have three and four main poling parameters, respectively, that require optimisation to maximise the d_{33} values. The experimental plan that was followed to maximise the piezoelectric coefficient d_{33} for each poling method is shown in Figure 3-11. To optimise each

parameter, the other poling parameters should be constant, to isolate the change in d_{33}. As each parameter is optimised, it is fixed for the next poling parameter investigated, and so on, as shown in Figure 3-11.

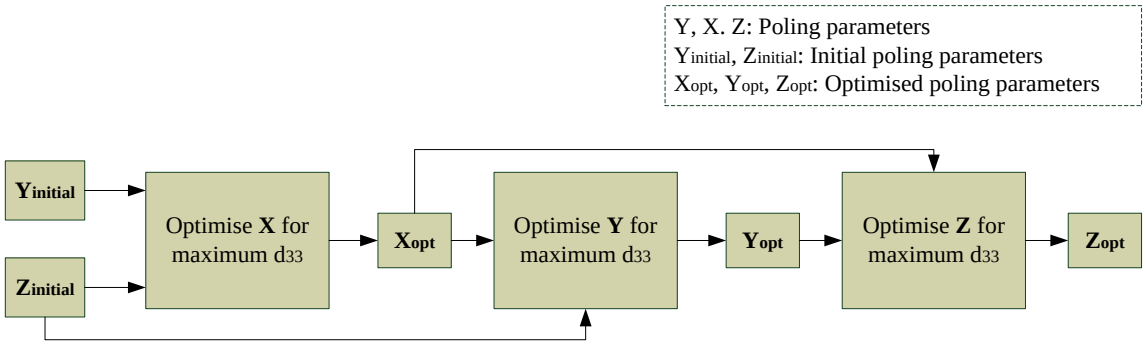

Figure 3-11: The experimental plan for optimising the poling conditions to maximise the d_{33} values of the printed film

The optimisation process does not depend on any parameter to begin with or the order of optimisation. For example, parameter X can be poling temperature or electric field. In Figure 3-11 only three parameters are shown; however, the number of the parameters can be increased under the same principle.

3.3.3 UoS Direct Contact Poling (DCP)

DCP is a straightforward method to pole a piezoelectric material. The electric field penetrates through the piezoelectric material when a voltage difference is applied between the bottom and the top electrodes that sandwich the piezoelectric film. The electric field is equally distributed across the whole area between both electrodes which is the effective poling area. It realigns the dipole moments within the piezoelectric material, as schematically illustrated in Figure 2-1 on page 9.

Figure 3-12 shows the UoS DCP apparatus, which consists of a polarisation box, a hot plate used for heating up the sample, a power supply and a multimeter. A thermocouple was required to measure the temperature on the surface of the hot plate so that it can be adjusted as required. The top and bottom electrodes of the devices are connected to the power supply and the electric field was adjusted according to the applied voltage and the thickness of the device given by $E = V/t_p$, where, E, V and t_p are the applied electric field, the poling voltage and the thickness of the printed piezoelectric film, respectively. The voltage was applied to the samples under an elevating temperature up to a certain point and left for a certain time (called the poling time).

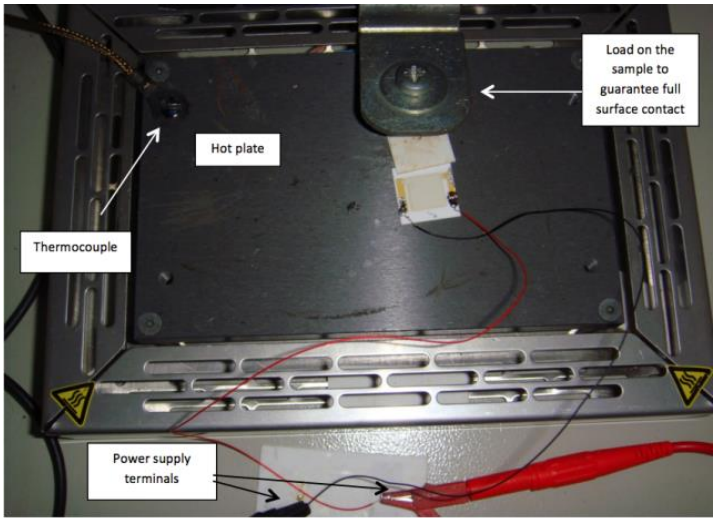

Figure 3-12: Example of a device as it is placed in the direct-contact poling rig during poling

The electric field was first investigated with initial poling conditions of T = 220 °C and t = 30 min. Four devices were used for optimising the poling conditions and five measurements were obtained from each device. Figure 3-13 shows that the d_{33} increased with increasing electric field and reached 48 pC/N at an electric field of 4 MV/m. Beyond this, the PiezoPaint would short-circuit during the poling process. This was an indication that the piezoelectric film cannot withstand higher electric fields.

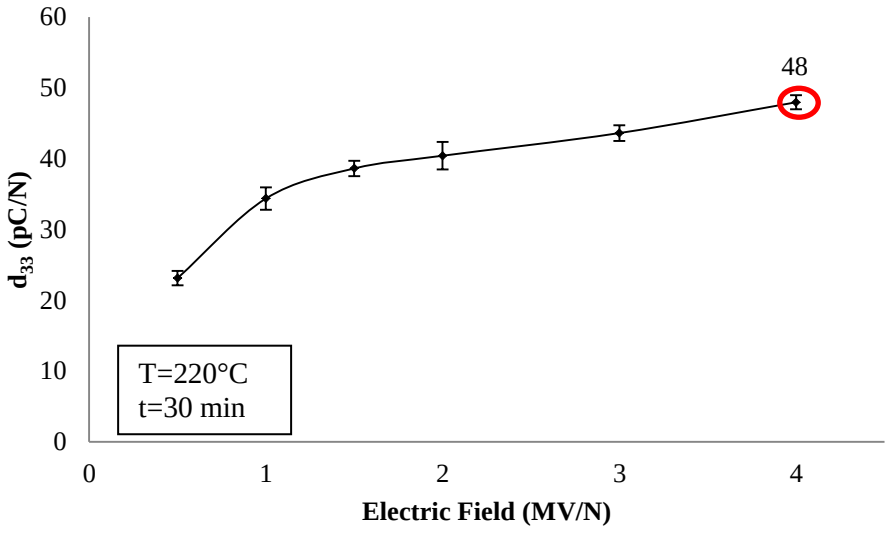

Figure 3-13: Optimising poling field for the piezoelectric coefficient d_{33}

Figure 3-14 shows the poling temperature optimisation for d_{33} at updated poling conditions (E = 4 MV/m and t = 30 min). The results show that d_{33} increases as the poling temperature rises. The maximum d_{33} value of 48 pC/N was reached at a poling temperature of 220 °C. After this temperature at 250 °C, the d_{33} decreased to 47 pC/N. When the devices are poled at an even higher temperature, they short-circuited during poling. The poling temperature can be chosen

according to the application and the type of the substrate that the piezoelectric material is printed on.

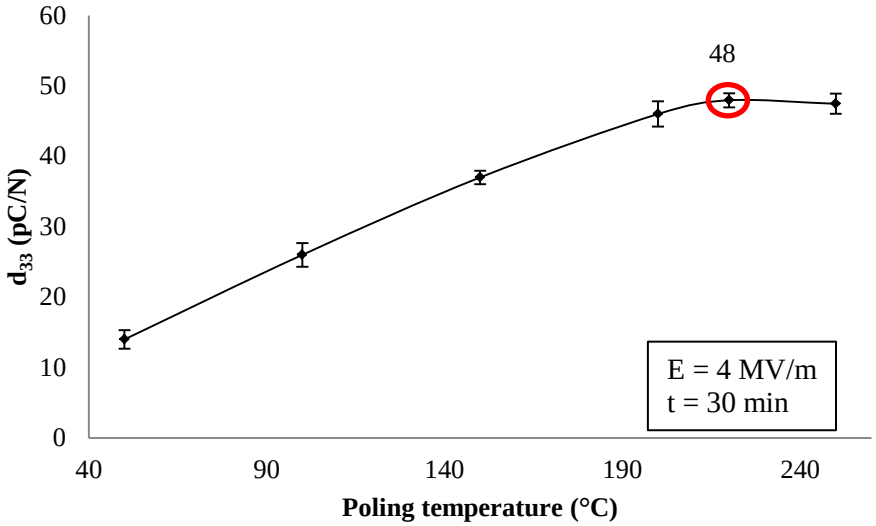

Figure 3-14: Optimising poling temperature of the piezoelectric coefficient d_{33}

The poling time was then investigated with the optimum electric field of 4 MV/m and a poling temperature of a 220 °C. From Figure 3-15, 5 minutes of poling a d_{33} of 48 pC/N. After 5 minutes of poling, there was no further significant change in the d_{33} values. The poling time of 5 minutes was considered the optimum as it gave the highest d_{33} value of 48 pC/N in the shortest time.

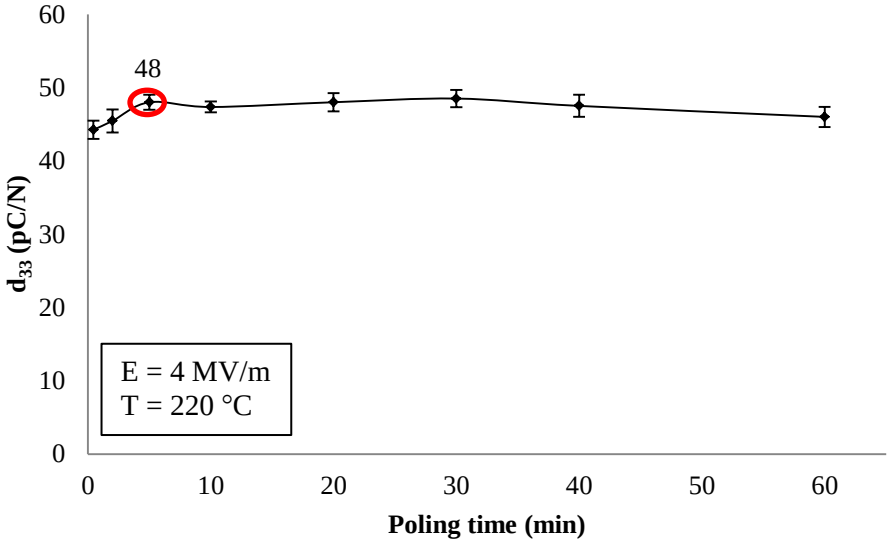

Figure 3-15: Optimising poling time for the piezoelectric coefficient d_{33}

3.3.4 Poling Optimisation using CDP

For corona discharge poling, the fourth parameter that has been added is the needle distance (d_n). Applying higher voltages can create a complete or part short-circuit in the poled devices. In addition, applying lower voltages generates a lower electric field that is not capable of fully penetrating and activating the piezoelectric element. Therefore, optimisation of the needle voltage and distance is essential.

The first parameter investigated is the applied needle voltage with fixed poling conditions of T = 220 °C, t = 30 min and d_n = 1 cm. Six poling voltages were separately explored: 3, 3.5, 4, 4.5, 5 and 5.5. Five samples were used for each investigating needle voltage. As shown in Figure 3-16, the mean average d_{33} values increased from 28 to 47 pC/N when the needle voltage was increased from 3 to 5 kV. There was no further significant change in the d_{33} values above 5 kV with the same poling conditions. The devices were short-circuited above 5.5 kV.

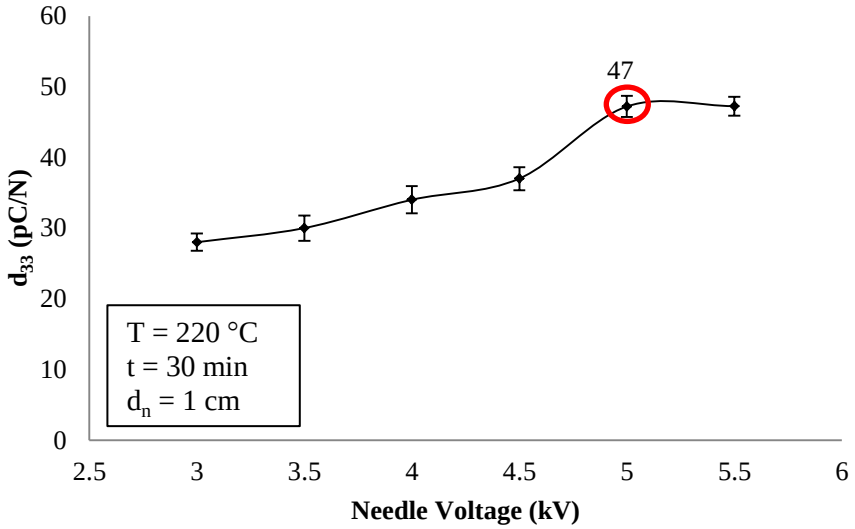

Figure 3-16: Optimising needle voltage of the piezoelectric coefficient d_{33}

After optimising the applied needle voltage, the poling temperature was investigated. The maximum d_{33} value achieved was 47 pC/N at poling temperature of 220°C and other fixed poling conditions shown in Figure 3-17. Above this temperature, the poling process was unstable (sparks and device short-circuiting occurred during poling), which caused a reduction in the d_{33} values.

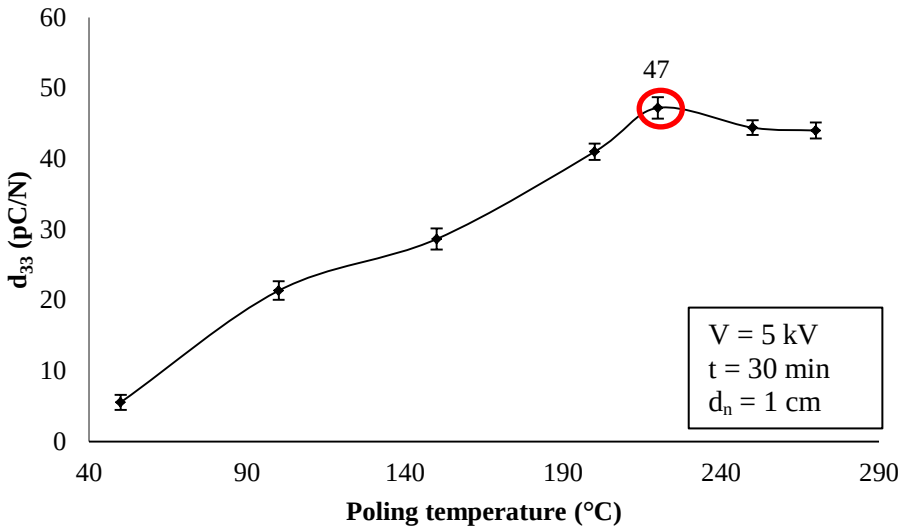

Figure 3-17: Optimising poling temperature for piezoelectric coefficient d_{33}

Poling time was then investigated with the updated needle voltage and temperature. As shown in Figure 3-18, the d_{33} values are consistent over time with a slight reduction after 5 minutes of poling. The 5 minutes poling time provided a maximum d_{33} of 46.6 pC/N. A slight reduction in the d_{33} values was observed after 5 minutes of poling time.

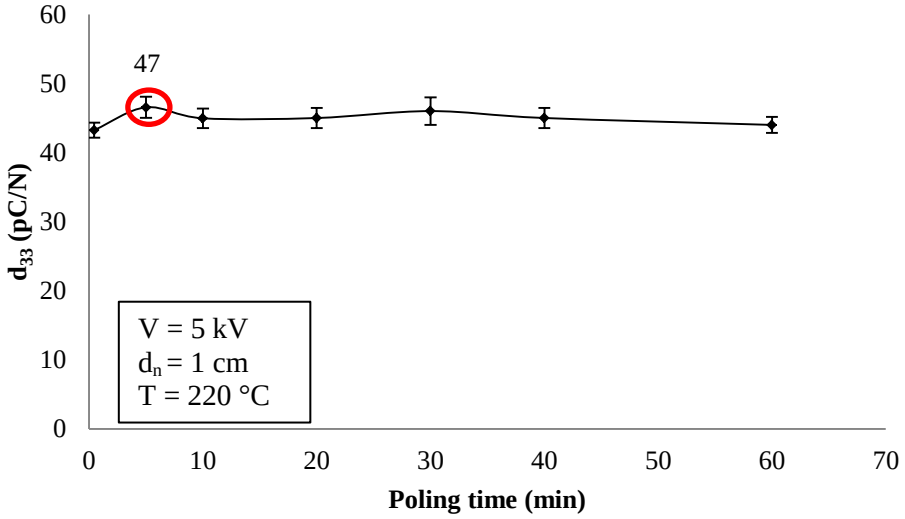

Figure 3-18: Optimising poling time for piezoelectric coefficient d_{33}

The distance between the needle and the sample, d_n, can be adjusted enabling the effects of both the distribution and the intensity of the charge generated by the voltage difference between the needle and the surface of the sample to be investigated. The charge that succeeds in reaching the surface generates another voltage difference between the piezoelectric element and the bottom electrode, which was earthed.

Four needle distances were investigated with the other poling parameter fixed, as shown in Figure 3-19.The optimum d_n, which provided the maximum d_{33} of 47 pC/N, was 1 cm. This value will be applied for the final investigation into poling condition. At greater distances the d_{33} value fell to 36 pC/N because the corona completely burned the surface of the sample.

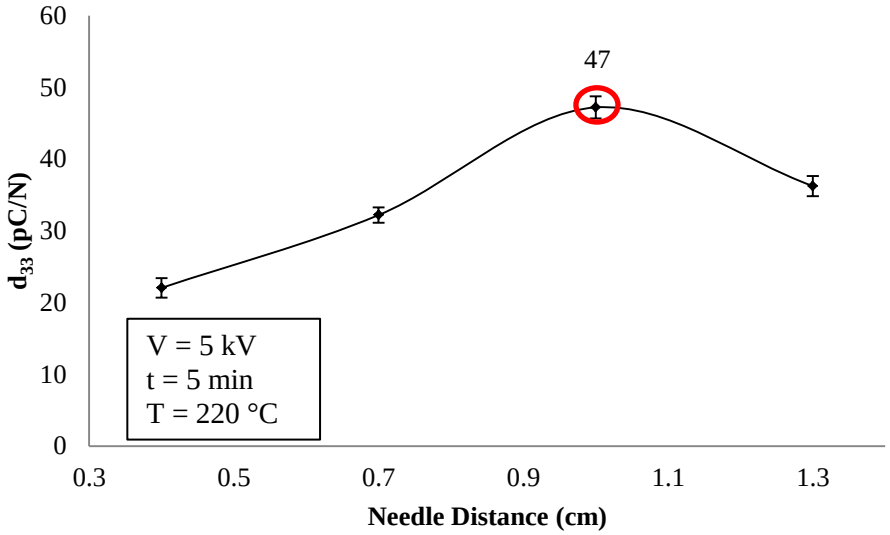

Figure 3-19: Optimising needle distance from the sample for piezoelectric coefficient d_{33}

3.3.5 Evaluation of the Poling Methods

Optimising the poling conditions of the PiezoPaint film increased the d_{33} values either for DCP or CDP. The optimum poling conditions that maximised the d_{33} values for DCP and CDP are summarised in Table 3-5. The DCP showed a slight improvement in the d_{33} value compared to CDP with the same poling temperature and time. Adding the advantages of DCP given in Table 3-4 on page 59 to the improved d_{33} listed in Table 3-5, DCP can be considered the most suitable method for poling the low-temperature screen-printed piezoelectric films.

Poling Parameter	DCP	CDP
Electric field (MV/m)	4	-
Needle voltage (V)	-	5k
Temperature (°C)	220	220
Needle distance (cm)	-	1
Time (min)	5	5
Optimum d_{33} value (pC/N)	48	47

Table 3-5: Summary of the optimum poling conditions and their d_{33} values of DCP and CDP

When measuring the d_{33} values of the samples poled by CDP, they were only obtained at the spot where the corona discharge hit the sample, which was only 0.3 × 0.3 cm on the surface.

Beyond this area, there was no piezoelectric activity. The optimum poling temperature of PiezoPaint is 220°C showing a 20 °C increase compared with the target temperature 200 °C.

Next, the flexibility of the PiezoPaint film printed on Kapton was tested by bending the material around the target 9 mm radius of curvature former. The printed film showed clear cracks and even with greater radius of curvature of 20 mm. This lack of flexibility makes the PiezoPaint unsuitable for the target application.

3.4 Conclusions

In this chapter, the screen-printing process of low temperature piezoelectric composites was discussed. All the procedures followed for screen-printing the piezoelectric devices and testing the d_{33} properties described in this chapter will be adopted for the devices covered in the remainder of this thesis.

The evaluation of poling processes found that DCP and CDP provide almost the same piezoelectric coefficient d_{33} at the same poling temperature and time of 220 °C and 5 min, respectively. However, DCP can provide a reasonable distribution of electric field unlike CDP which is confined to the area of the corona. Given this fundamental weakness in CDP and the relative ease of the DCP process, DCP was identified as the poling process for the remainder of the thesis. The mechanical flexibility of the PiezoPaint film was tested when printed on Kapton. The film did not satisfy the bending specification and cracks were observed at a radius of curvature of 20 mm. The film was considered inflexible for our applications.

Chapter 4: Evaluation of the Binder on the 0-3 Connectivity Type Piezoelectric Composite

4.1 Introduction

The first phase of this investigation focuses on the type of the binder (polymer mixed with a solvent) that was mixed with the piezoelectric ceramic powder and its effect on the d_{33} values of the printed films. The piezoelectric ceramic powder used in this investigation was PZT-5H (PZ29, Ferroperm, Denmark) as it provides the highest d_{33} and dielectric constant values, as mentioned previously. The investigated binders were mostly low-temperature cured. This chapter also provides the mixing, screen-printing and curing processes for the printed films. The binder selection will be based on: its mixing properties and whether it can achieve a suitable-printable paste, the adhesion of the printed film and the initial d_{33} measurements identifying the piezoelectric activity of the film. The mixing properties and adhesion of the material are also dependent on the PZT-binder weight ratio of the composite. This investigation will provide the best PZT-binder weight ratio to achieve a screen-printable film which is suitably bonded to the substrate and produces good piezoelectric activity.

Initial d_{33} measurements were taken for every printed film and the results were compared. After selecting the optimum binder that when mixed with PZT produces the best piezoelectric composites, the PZT to polymeric-binder weight ratio was investigated. PZT content increases the dielectric properties and piezoelectric activity, but only to a certain level. However, increasing the PZT content reduces the flexibility of the printed film. Therefore, finding the suitable PZT weight content in the composite is the important second phase in this investigation. The experimental plan is summarised in Figure 4-1.

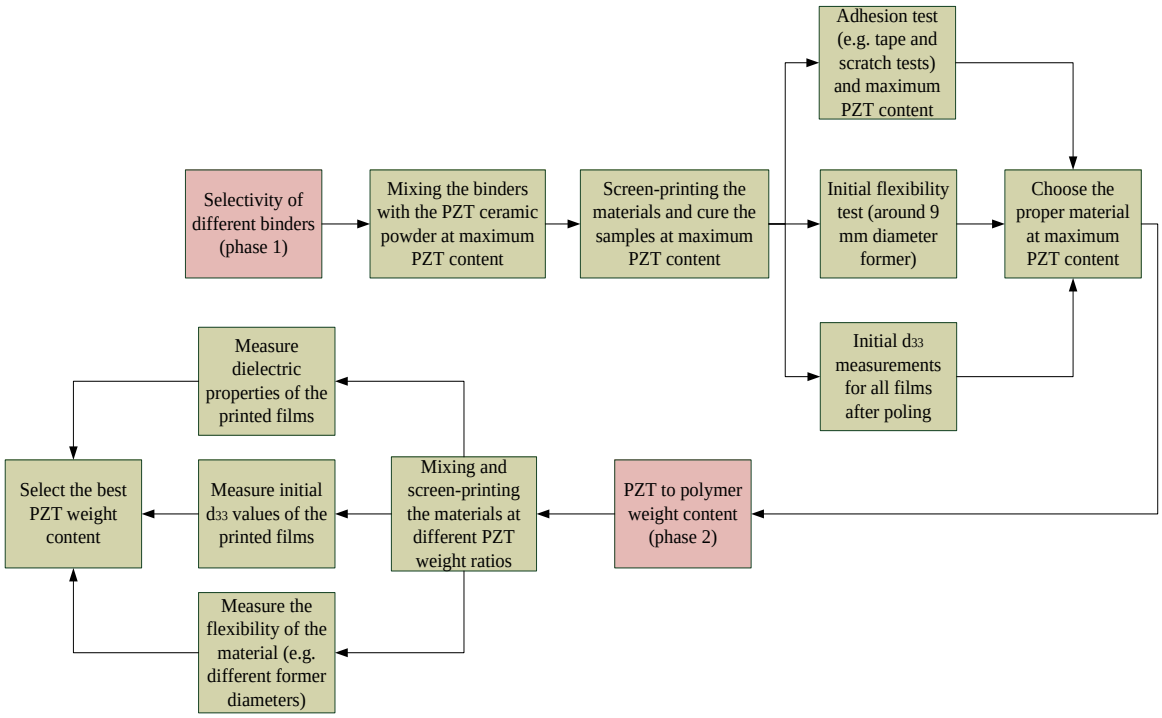

Figure 4-1: Experimental plan for selecting the best PZT-binder and PZT weight percentage that provides maximum d_{33} with suitable flexibility

4.2 Proposed Binding Systems

The binder that is mixed with the PZT-5H powder ideally should provide the following features:

- **Screen-printable:** The viscosity can be modified by a solvent without affecting its properties after curing. Smooth printing is required for good quality printed film. Smooth screen-printing should meet the screen specifications listed in Table 3-1 on page 53. For example, the PZT particles should be small enough not to block the mesh openings. This is best investigated experimentally by applying screen-printing to the pastes.
- **Low-temperature cured:** the curing temperature of the binder specifies the curing conditions of the overall composite, and ideally has a lower processing temperature than PZT. This temperature has to be below 200 °C, which the chosen fabrics can withstand.
- **Good bond to PZT particles**: This feature is evaluated when applying bending and compressive force, and no cracking or wrinkles appear on the surface of the printed layer.

- **Good adhesion on the substrate and silver/polymer layer**: This property is evaluated by withstanding a tape and scratch test after being mixed with PZT and bending around a 9 mm radius of curvature former [126].
- **High dielectric constant**: A high dielectric constant of the polymer will allow an increased effective electric field on the PZT particles dispersed in the polymer matrix [127, 128].

The proposed piezoelectric composites were first denoted PZT-polymers however, it is not only the polymer mixed with the PZT; PZT is mixed with the binder which is a mixture of the polymer and the solvent. Therefore to avoid confusion, the proposed composites will be denoted PZT-binder instead of PZT-polymers; especially before curing the printed film where the solvent phase still exists in the material.

Table 4-1 lists the binders and their viscosities that were used for mixing with PZT powders. The first three polymeric binders, ECS-Poly 1, 2 and 3, were commercially-sourced and provided in a liquid form. ECS-poly 4 is an epoxy which was provided in two parts, resin (A) and hardener (B), which can be mixed in a weight ratio of 2:3. The manufacturer's recommended curing temperature is 120 °C for 2-3 hours. ECS-Poly 5 is a fluoropolymer paste (PVDF-based) denoted Solvene (Solvay Solexis). This paste was supplied in a liquid form, which consists of the fluoropolymer (30% by weight) and a cyclopentanone solvent (70% by weight). The solvent was used to dissolve the polymer into a liquid form and also to control viscosity.

ECS-Poly 6 is a thermoplastic polymer (denoted CR-V) that was provided in a solid form. γ-Butyrolactone solvent was used to dissolve the polymer into a liquid form. When mixing 95% of PZT by weight with the produced polymer-solvent solution, the mixture was coated on a Kapton substrate, and the film was initially subjected to bending force and the adhesive tape test. This was required to choose the best polymeric binder to solvent weight ratio that would show no cracks and have good adhesion to the surface of the substrate. The polymer–solvent mixture had been mixed and left for two days at room temperature until the polymer was completely dissolved.

ECS-Poly 7 is another commercial epoxy that was provided in two parts, A and B, and mixed in a weight ratio of 10:1. The curing temperature recommended by the manufacturer was 150 °C for 1 hour. Finally, ECS-Poly UV is a polyurethane-based UV curable elastomer developed at the University of Southampton's Electronic and Computer Science (ECS) laboratories. The curing conditions are to expose the printed layer to UV light.

Name	Polymer/Epoxy	Initial Viscosity (cPs)
ECS-Poly 1	R2070613D2 Resin Binder (Gwent)	150-330*
ECS-Poly 2	DuPont 8153 LuxPrint	10,000-20,000*
ECS-Poly 3	PH-745 (Conductive Compounds)	6,500*
ECS-Poly 4	Epoxy 280 3M Two Parts (A:B)	A: 12,500 * B: 2,500*
ECS-Poly5	SOLVENE 250, Solvay Solexis	-
ECS-Poly 6	Cyanoethyl Polyvinyl Alcohol (CR-V), Shin-Etsu Chemical Co, Ltd	240-360*
ECS-Poly7	Epo Tek 353ND, EPOXY Technology, Inc.	3,000-5,000*
ECS-Poly UV	UV-Curable Fabink-IF-UK 1004 (Microflex)	5,760-6,000**

* Provided by the manufacturer ** Measured

Table 4-1: Binder used for mixing with PZT and their initial viscosities

4.3 PZT-binder Mixing limits and Adhesion Tests

The paste formulation and subsequent film adhesion are discussed in this section. This procedure was undertaken to obtain the maximum PZT content in the composite that showed proper mixing and good adhesion to the substrate after printing. For the UV-curable polymers, it was very important to obtain the maximum PZT content in the composite and still achieve a fully cured film. Above this PZT content limit, the film is only partly cured because the PZT particles obstruct the UV light penetration thus affecting the polymerisation of the binder.

This maximum achievable PZT content will be used as the basis for investigating the dielectric, piezoelectric and mechanical properties of the films when changing the PZT content in the composite. Also, this maximum limit of PZT content does not only depend on the viscosity of the formulation, but also on the screen-printability, curing conditions and the adhesion of the film. The adhesion problem occurs for two reasons:

- The high content of PZT phase compared to the polymeric binder providing insufficient bond between particles and the subsequent film adhesion to the substrate. If this problem occurs, the amount of PZT phase in the composite is reduced.
- The adhesion of the polymeric binder itself is poor.

The experimental plan is shown in Figure 4-2 to obtain the maximum PZT content in the composite that shows a suitable mixing of the formulations and film adhesion otherwise the problem is the quality of polymer. The minimum PZT content that was involved in this investigation was 50% by weight (or a weight ratio of 1:1). Also, the tape test was performed by applying and peeling tape to/from the surface of the sample five times and looking for any

damage on the surface of the film, or residue (such as PZT particles) on the tape with the aid of the microscope. This process was achieved for five separate printed films.

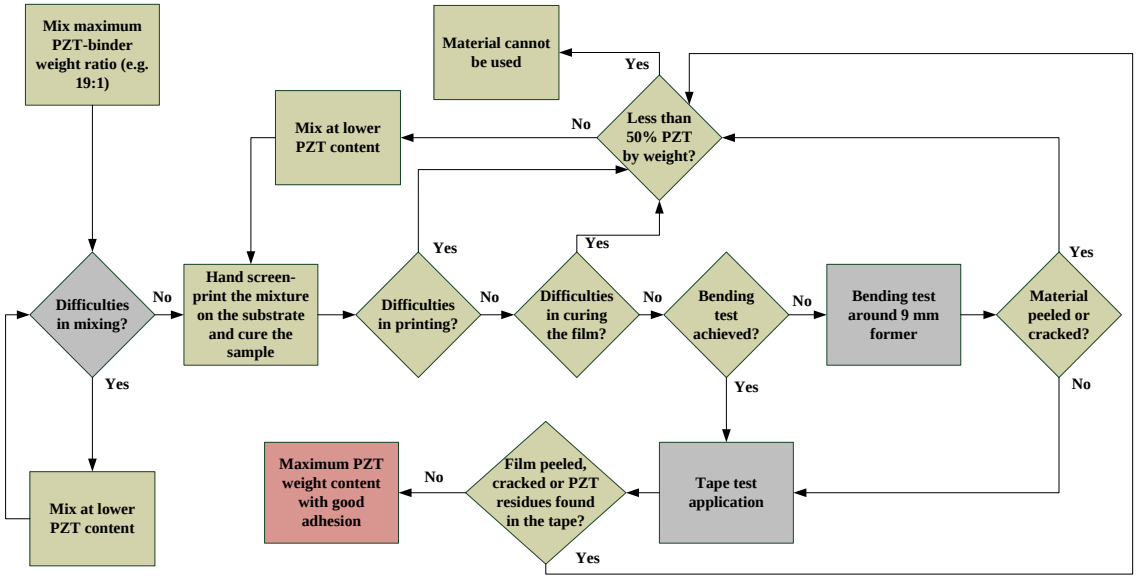

Figure 4-2: Experimental plan of testing the PZT-polymer adhesion of the printed film

4.3.1 Mixing the Formulations

The PZT powder was initially mixed with each binder listed in Table 4-1 with PZT-binder weight ratio of 19:1 (This PZT content at this PZT-binder ratio was considered the maximum starting point in this investigation). The piezoelectric composites that were produced were denoted ECS-PolyPZT 1, 2, 3, 4, 5, 6, 7 and UV. The PZT powder used was a combination of 2 µm and 0.8 µm particles with a weight ratio of 4:1 as suggested by [83, 96, 129]. Figure 4-3 depicts an example of the mixing process used to mix ECS-PolyPZT 6. For commercial binders, such as ECS-poly 1, 2 and 3, applying polymer-solvent mixing was not required, as they were already supplied in a liquid form.

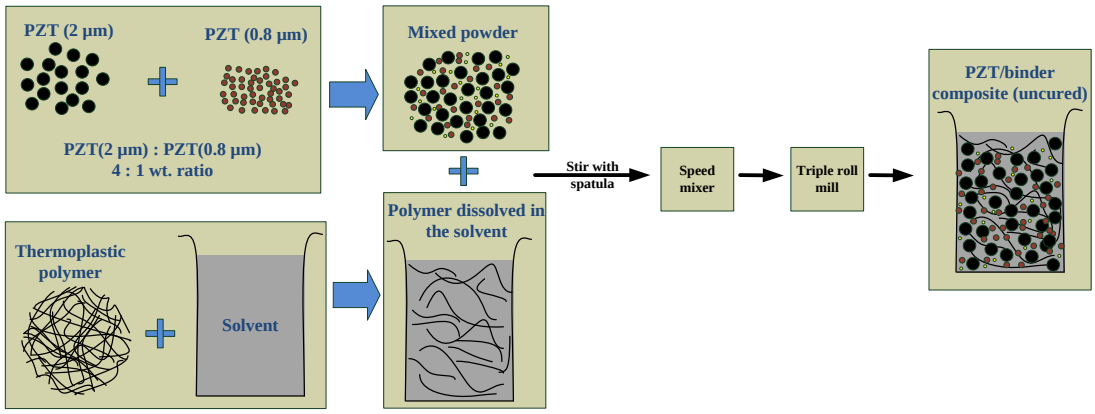

Figure 4-3: A schematic showing the general mixing process of the ECS-PolyPZT 6 composite

The PZT powder was mixed with polymer-solvent mixture (binder) with the aid of a spatula. Then, the blend was mixed again with the DAC 150 Dual Asymmetric Centrifuge mixer (Synergy Device Limited) and then triple-roll milled to homogenously distribute the PZT powder inside the polymeric matrix.

Triple roll milling is an essential process for mixing composites, particularly materials that exist in different forms (e.g. mixing powders in a polymer-solvent binding system). Ideally, the powder has to spread homogenously inside the polymer and this cannot be achieved only by stirring the mixture with a laboratory spatula. The triple roll milling machine consists of three rolls, which are placed horizontal to each other and rotate in opposite directions, as shown in Figure 4-4(a). In order to mill the material, it is put between the feed and the centre rolls. The centre roll transfers the material and the dispersion occurs because of the shear forces between the rolls. High shear can be applied when the distance between the rolls is decreased. The material is taken off from the apron roll using a knife [130]. To enhance the material particle dispersion and homogeneity of the ingredients, the triple roll mill cycle can be repeated until homogeneity of the composite is visually guaranteed. After these mixing steps, a screen-printed paste was produced.

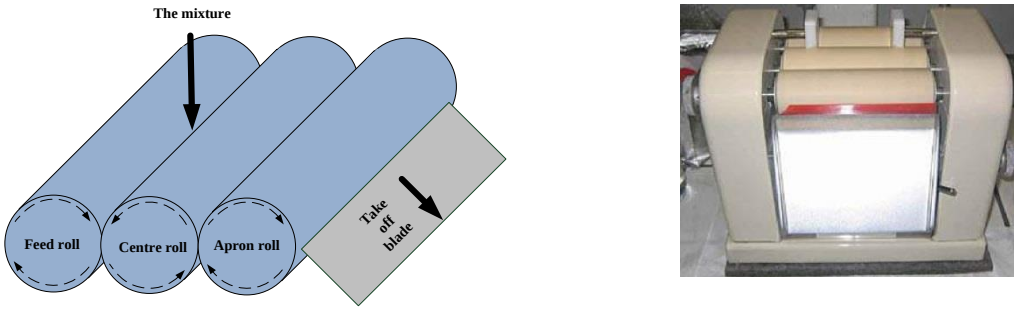

(a) (b)

Figure 4-4: Triple roll mill. (a) Schematic of triple roll milling [130]. (b) Triple roll mill machine [131]

The formulations were mixed as planned in Figure 4-2 by reducing the PZT content inside the composite if the mixing suffered from difficulties (such as powder agglomeration or insufficient binder to cover all the PZT powder). Only for ECS-PolyPZT 6, the polymer to solvent weight ratio was an important factor to control the viscosity (other binders were already provided in a liquid form), screen-printability and the adhesion of the paste at 19:1 weigh ratio of PZT-binder. Therefore, in ECS-PolyPZT 6, the polymer-solvent ratio will be changed with respect to 19:1 PZT-binder weight ratio. When the material was blended at this PZT-binder weight ratio, it was not mixed properly. The binder was not enough to cover all the PZT powder. Therefore, it was decided to reduce the amount of PZT powder until a suitable mix was reached that could cover all the PZT powder. The maximum mixing weight loading of PZT-binder are shown in Table 4-2.

Ratio	**Polymer : solvent**	**PZT: binder**
Value	1 : 4.1	9.2 : 1

Table 4-2: Maximum PZT content in the binding system for ECS-PolyPZT 6

As shown in Figure 4-3, the polymer-solvent binding system was initially mixed at a weight ratio of 1:4.1. This polymer-solvent weight ratio was found to be the suitable starting point for the binding system. The mixing limits (with the maximum PZT weight loading) of PZT-binder of all the proposed composites are listed in Table 4-3. At these mixing limits the materials made homogenous pastes that were ready for screen-printing.

ECS-PolyPZT ref. No	**1**	**2**	**3**	**4**	**5**	**6**	**7**	**UV**
PZT: binder weight ratio	9:1	4:1	9:1	9:1	9:1	9.2 : 1	9:1	4:1
PZT (% by weight)	90	80	90	90	90	90.1	90	80

Table 4-3: Maximum PZT content in every composite for homogenous thixotropic paste

Good mixing of the material at maximum PZT content does not reflect the screen-printability of the material. The screen-printability of the material was explored by detecting material clogging that blocks the mesh opening of the screens, and by visually observing the quality of the print (if there are holes or incompletely-printed areas on the surface of the printed layer).

4.3.2 Screen-printing the Formulations

The same capacitive structure pattern in Figure 3-2 on page 50, and its corresponding screens, were used for screen-printing different formulation films. In addition, the screen-printing process followed the process flow shown in Figure 3-7 on page 57. The proposed materials were printed on both alumina and Kapton. Before screen-printing the proposed materials on the semi-automatic screen-printer, the screen-printability, curing conditions and adhesion were tested with hand screen-printing. This procedure avoids wasting material and reduces setup time. The semi-

automatic screen-printer was used for the final screen-printable materials at maximum PZT content in the PZT-binder composite. For the hand screen-printing, the same procedures were followed as discussed in section 3.2.1 on page 50, except that the squeegee movement and load on the screen were manually applied. The substrate on the holder was placed on a fixed, flat surface, and the screen was placed on the top of them. The paste was put on the screen and it was smeared onto the screen by hand. Note, the squeegee needs to be tilted towards the direction of printing as depicted in Figure 2-15 on page 33.

ECS-PolyPZT 2 and 3 were successfully printed with some difficulties (i.e. the pastes quickly dried on the screen due to the small amount of the binder in the composite). Screen-printing the films with a lower PZT powder content can be a solution to control the viscosity of the blend. However, PZT-PolyPZT 4 blocked the screen mesh while printing. Accordingly, it was decided to reduce the PZT content of the pastes.

For the first screen-printability tests of ECS-PolyPZT 5, it was observed that when the material was smeared on the screen and left for 5 minutes, it dried quickly, which caused the mesh-openings in the screen to be blocked. Accordingly, it was decided that the material should be mixed with a lower content of PZT, with a PZT-binder weight ratio of 4:1. Again, after the first prints of the new ECS-PolyPZT 5 formulation on alumina substrates, large voids and incomplete printed areas were observed on the surface of the deposit. This was because of the rapid drying rate at room temperature, which blocked the screen even at a 2.3:1 PZT-polymer weight ratio. Lower PZT content may solve these problems; however, the piezoelectric activity may be reduced. The PZT content was reduced as planned in Figure 4-2 to produce a good screen-printed film even when screen-printing the ECS-Poly 5 without PZT. It was observed that the material dried quickly on the screen, creating unprinted areas on the surface. Therefore, ECS-PolyPZT 5 was not screen-printable and was not investigated further.

Although ECS-PolyPZT UV paste was produced, the material caused mesh-clogging on the screen. Therefore, a lower PZT content was used to make the screen-printing process of this formulation possible. On the other hand, ECS-PolyPZT 1 and 6 showed good screen-printability at this PZT content. Table 4-4 shows that the updated mixing limits for all ECS-PolyPZT formulations.

ECS-PolyPZT ref. No	**1**	**2**	**3**	**4**	**6**	**7**	**UV**
PZT: binder weight ratio	9:1	2.3:1	9:1	5.3:1	9.2 : 1	9:1	2.3:1
PZT (% by weight)	90	70	90	85	91	90	80

Table 4-4: Maximum PZT content in every composite for homogenous thixotropic paste after screen-printing test

4.3.3 Drying and Curing Processes

The drying and curing processes of the proposed materials are shown in Table 4-5. The drying process was conducted to solidify a printed layer before printing subsequent layers to increase the overall thickness of the printed film. The final printed layer was fully cured using the curing parameters listed in Table 4-5.

Formulation	**Curing**	**Drying**		**Curing**	
		Temperature (°C)	Time (min)	Temperature (°C)	Time (min)
ECS-PolyPZT 1	Thermal	100	5	130	10
ECS-PolyPZT 2	Thermal	100	5	125	10
ECS-PolyPZT 3	Thermal	100	5	130	10
ECS-PolyPZT 4	Thermal	140	5	140	30
ECS-PolyPZT 6	Thermal	90	6	90	8
ECS-PolyPZT 7	Thermal	160	5	170	30
ECS-PolyPZT UV	UV	-	1	-	1

Table 4-5: Drying and curing conditions of the composites

The curing conditions of ECS-PolyPZT 1, 2 and 3 were confined to the curing instructions provided by their manufacturers. Although the polymer phase was less than 10% by weight of the composite, it was discovered (after applying the tape test on the surface) that the same curing conditions have to be followed. However, the curing conditions of the epoxy-based piezoelectric composites ECS-PolyPZT 4 and 7 were different from the curing conditions suggested by their manufacturers. The curing time was reduced to decrease the production time of the devices. The reduced time was compensated by increasing the curing temperature. For example, the suggested curing conditions provided by the manufacturer for ECS-Poly 4 was 120 °C for 2 hours. However, ECS-PolyPZT 4 was cured at 140 °C for 30 min. The 30 minutes curing time was chosen constant with varying the temperature between 120-150 °C. At each temperature, the device was tested using the experimental plan shown in Figure 4-2.

The ECS-PolyPZT 6 material was fully cured at 90 °C for 8 minutes because the PZT powder made up 90% by weight of the film (more binder requires more curing temperature and time). The curing conditions of ECS-PolyPZT 6 were optimised with respect to its piezoelectric activity, which will be discussed later in the poling optimisation of material. There was an attempt to produce a UV-curable PZT-binder composite with ECS-PolyPZT UV. However, the printed layer was not fully cured using the curing conditions shown in Table 4-5. This is because the quantity of PZT particles inside the composite did not allow UV light to penetrate through the film sufficiently to fully cure the UV-curable polyurethane constituent underneath. The PZT content

was reduced to 50% by weight (which is the minimum limit to be mixed with the polymer as shown in Figure 4-2) and the material was not fully cured. Therefore, ECS-PolyPZT UV was not screen-printable and was not investigated further.

ECS-PolyPZT ref. No	**1**	**2**	**3**	**4**	**6**	**7**
PZT: binder weight	9:1	2.3:1	9:1	5.3:1	9.2 :1	9:1
PZT (% by weight)	90	70	90	85	91	90

Table 4-6: Maximum PZT content in every composite for homogenous thixotropic paste after curing process tests

4.3.4 Adhesion Tests Results

After the materials were mixed according to Table 4-6, the materials were hand screen-printed on Kapton and then adhesion tests were performed as in the process flow in Figure 4-2. The adhesion test started with bending the printed film around a 9-mm diameter former after printing on both silver/polymer printed on Kapton and on Kapton directly. The ECS-PolyPZT 1 and 3 showed poor adhesion at a 9:1 PZT-polymer weight ratio when bending the material printed on Kapton around the former. The piezoelectric film was peeled from the substrate and some cracks were observed as shown in Figure 4-5. The film showed good adhesion after bending and inspecting for cracks under the microscope at a PZT-polymer weight ratio of 8:1.

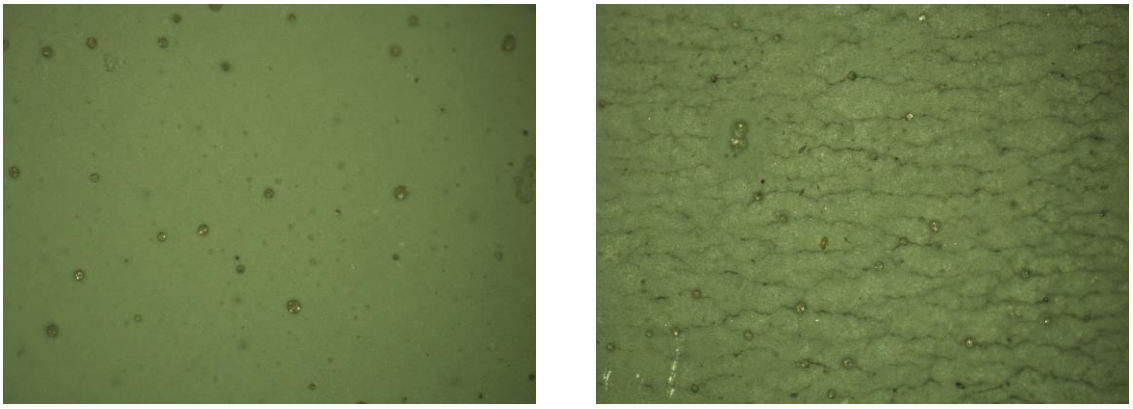

(a) (b)

Figure 4-5: The microscope images (X10) for the ECS-PolyPZT 1 (a) before and (b) after bending around 9 mm diameter former. The surface cracks are obvious after bending

After the bending test, the tape test was conducted for all the materials after changing the mixing ratios for ECS-PolyPZT 1 and 3. All the screen-printed materials showed adhesion without cracks on the surface after applying the tape test, except the ECS-PolyPZT 6 formulations. Some PZT residues were found on the tape after applying the test. The PZT content was slightly reduced in the composite, and the material was screen-printed. The tape test was re-

applied to the surface and the residues were no longer found. The updated mixing ratios of PZT-polymer of all the ECS-PolyPZT screen-printed composites are shown in Table 4-7.

ECS-PolyPZT ref. No	**1**	**2**	**3**	**4**	**6**	**7**
PZT: binder weight ratio	8:1	2.3:1	8:1	5.3:1	2.7:1	9:1
PZT (% by weight)	90	70	90	85	73	90
PZT (% by volume)	48	36	52	44.5	27.5	56.5

Table 4-7: Maximum PZT content in every composite for homogenous thixotropic paste after adhesion tests

The weight and volume ratios of the PZT-binder composites in Table 4-7 are mixing ratios when the binder is still in its liquid phase. These ratios were obtained according to the weight and the volume of the binder phase (which consists of the actual polymer and the liquid phase part mostly represented by the solvent) and the PZT ceramic phase in the mixture. After the evaporation of the solvent part, these weight and volume ratios may change (PZT content is increased) because of the evaporation of the solvent part after curing.

4.4 Initial d_{33} Coefficient Measurements

The piezoelectric composites were initially formulated by separately mixing the PZT-5H ceramic powder and polymeric binders using the PZT-polymer weight ratios shown in Table 4-7. The devices were screen-printed with a semi-automatic screen-printer as discussed in 3.2.5 on page 55. Initial d_{33} values were taken for every printed formulation after the curing process to compare the piezoelectric activity between the composites and then select the best materials that gave the highest d_{33} values at these poling conditions.

As defined previously, the electric field is a key parameter on polarising the piezoelectric material. Maximising the electric field for the test devices gives a comparison of both the maximum dielectric strength of the material and also shows the piezoelectric activity of the material at a poling temperature of 100 °C and a poling time of 10 min. The cured screen-printed piezoelectric composites listed were initially poled using the direct contact method. The d_{33} values were measured using the piezometer.

Figure 4-6 shows the d_{33} values of 25 measurements (5 devices × 5 measurements each) for devices printed on alumina substrates (see the printing process on page 55) after poling the devices with maximum electric field before dielectric failure (maximum dielectric strength). The maximum dielectric strength will vary with changing poling temperature. The results therefore identify the maximum electric field that can be applied at this specific temperature. For example, ECS-PolyPZT 6 was initially poled with a maximum electric field of 3.5 MV/m at a temperature of 100 °C and poling time of 10 minutes. It was observed that when increasing the temperature

over 100 °C, temporary short-circuiting occurred (sparks appeared on the surface of the piezoelectric element) which is an indication of an unstable poling process. The electric field must be applied continuously without interruption during the poling process or net polarisation will not occur.

Figure 4-6 shows the d_{33} values obtained when applying the maximum electric field before breakdown for each composite; a poling temperature and time of 100 °C for 10 minutes, respectively was used. Sufficient poling temperature is essential to increase the internal energy of the dipole inside the PZT materials to improve alignment with respect to the electric field's direction. Furthermore, it was experimentally found that some materials, such as ECS-PolyPZT 2, have a very high dielectric strength (>12 MV/m) when the electric field was applied at room temperature. When the film is printed at the lowest thickness of 100 µm (a lower thickness caused complete short-circuiting), the maximum voltage applied according to $E_{ext}=V/t_p$ will be more than 1,200 V, which is the maximum limit of the power supply used. Therefore, it was also necessary to reduce this dielectric breakdown voltage and observe the d_{33} at the maximum electric field applied by poling the devices at higher temperatures.

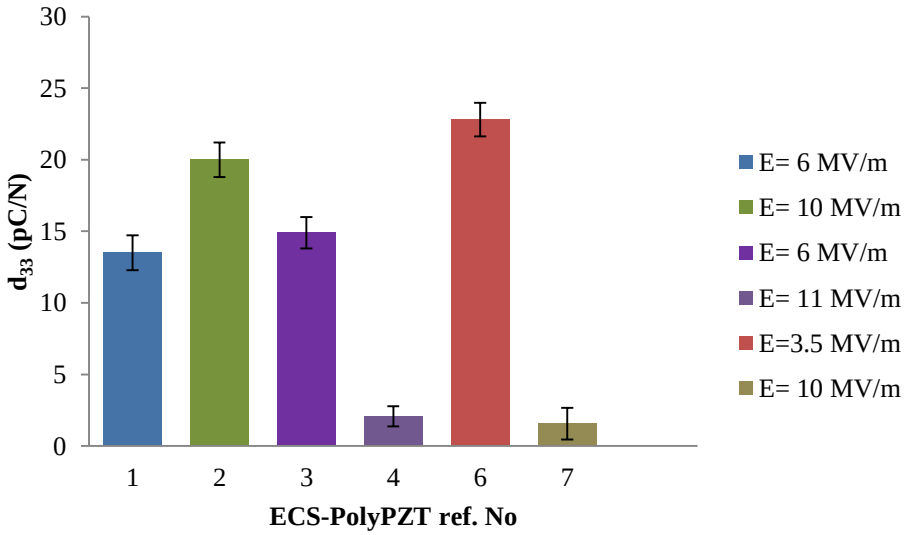

Figure 4-6: Testing the d_{33} values of the composites when initially poled at poling temperature of 100 °C, poling time of 10 minutes and poling electric fields introduced in the graph

Adhesive thermosetting polymer-based piezoelectric composites (ECS-PolyPZT 4 and 7) showed lower piezoelectric properties (d_{33} < 3 pC/N) than their thermoplastic polymer-based counterparts. The d_{33} values for ECS-PolyPZT 1, 2, 3 and 6 were 13.5, 20, 14.9 and 22.8 pC/N, respectively, using the poling conditions shown in Figure 4-6. Therefore, it was decided to focus for further investigations on the thermoplastic polymeric-based piezoelectric composites ECS-PolyPZT 1, 2, 3 and 6. The investigation involved the piezoelectric properties and the mechanical

flexibility of the printed films. Table 4-8 introduces a summary of the maximum PZT content in the composite at every testing stage (such as mixing quality or screen-printability). It also shows the d_{33} values when the printed films were initially poled.

Formulation	Mixing	Screen-printability	Curing conditions	Adhesion	Initial d_{33} (pC/N)	Initial poling conditions*
ECS-PolyPZT 1	9:1	9:1	9:1	8:1	13.5	E= 6 MV/m
ECS-PolyPZT 2	4:1	2.3:1	2.3:1	2.3:1	20	E= 10 MV/m
ECS-PolyPZT 3	9:1	9:1	9:1	8:1	14.9	E= 6 MV/m
ECS-PolyPZT 4	9:1	5.3:1	5.3:1	5.3:1	2	E= 11 MV/m
ECS-PolyPZT 5	9:1	-	-	-	-	-
ECS-PolyPZT 6	9.2:1	9.2:1	9.2:1	2.7:1	22.8	E= 3.5MV/m
ECS-PolyPZT 7	9:1	9:1	9:1	9:1	1.5	E= 10 MV/m
ECS-PolyPZT UV	4:1	2.3:1	-	-	-	-

* Poling temperature and time were 100 °C and 10 minutes, respectively

Table 4-8: A summary shows the maximum PZT content in the proposed piezoelectric composites at every testing stage. Also, it shows the d_{33} values at initial poling conditions

4.5 The Effect of PZT Powder Weight Loading Variations

4.5.1 Proposed PZT-polymer Mixing Ratios

After identifying the maximum PZT loading that can be used in the selected piezoelectric composites, obtaining the PZT weight-loading that provides the highest d_{33} with improved flexibility is essential. The PZT weight-loading has an effect on the dielectric, piezoelectric and mechanical properties of the composite. Selecting the optimum PZT-binder weight ratio can differ from one composite to another. Therefore, it was essential to investigate this effect and explore the optimum weight-loading that gives the highest dielectric constant ε_r, piezoelectric coefficient d_{33} and mechanical performance (represented by mechanical flexibility). Table 4-9 shows the investigated PZT-binder weight ratios for the ECS-PolyPZT 1, 2 and 3 composites. ECS-PolyPZT 1, 2 and 3 were also evaluated together, as they had nearly identical PZT-binder weight ratios (i.e. some of the PZT-binder weight ratios are common such as 3:2 and 2.3:1).

ECS-PolyPZT Ref No.	PZT: binder	PZT (%)	Binder (%)
1	3:2	60	40
	2.3:1	70	30
	4:1	80	20
	8:1	90	10
2	1:2.3	30	70
	2:3	40	60
	1:1	50	50
	3:2	60	40
	2.3:1	70	30
3	3:2	60	40
	2.3:1	70	30
	4:1	80	20
	8:1	90	10

Table 4-9: The investigated PZT-binder mixing ratios for ECS-PolyPZT 1, 2 and 3

ECS-PolyPZT 6 is sensitive in terms of piezoelectric activity small variations of PZT content. The polymer-solvent weight-loading was designed with respect to the PZT powder loading in the composite. Also, it was observed that short-circuiting occurred at PZT-binder ratios lower than 1.77:1 for ECS-PolyPZT 6, even before the poling process, at a film thickness of 130 µm. The solvent phase is usually used to control the viscosity of the mixture, but in ECS-PolyPZT 6, the increase of the solvent was a function of the PZT weight loading to make the mixture thixotropic and screen-printable. Table 4-10 shows the four investigating PZT-binder weight ratios and their corresponding PZT-polymer weight ratios.

PZT: binder	PZT:polymer
1.77: 1	8 : 1
2.17 : 1	10 : 1
2.57 : 1	12 : 1
2.7 : 1	14 : 1

Table 4-10: ECS-PolyPZT 6 with different PZT-binder weight ratios

The materials were printed with the semi-automatic screen-printer and cured according to each formulation. Note, the applicability of the bending test was confined by the minimum radius of curvature of human body (thumb joint = 9 mm) which is considered as the most bendable part. And because all the screen-printed composites satisfied this condition, the optimum PZT-binder weight ratio that gave the highest piezoelectric properties was selected. The flexibility of the materials was later investigated after finding the maximum d_{33} value that could be obtained.

4.5.2 Dielectric Properties and PZT Weight Loading

High dielectric constants of the piezoelectric material lead to good piezoelectric properties of the films. When piezoelectric composite film is exposed to an external electric field, E_{ex}(MV/m) the electric polarisation, P_i (C/m^2) on the PZT particles inside the polymer matrix can be increased if the dielectric constant of both the PZT particles and the polymer are high, as described by equation (4-1) [132], and consequently polarisation, P_i (C/m^2), will increase.

$$P_i = (\varepsilon_{PZT} - \varepsilon_P)E_{eff} = \frac{\varepsilon_{PZT} - \varepsilon_P}{2\varepsilon_P + \varepsilon_{PZT}} 3\varepsilon_P E_{ex} \quad (4\text{-}1)$$

Where; ε_{PZT} and ε_P are the dielectric constants of the PZT ceramic and the polymer, and E_{eff} (MV/m) is the effective electric field on the PZT particles. The higher the remnant polarisation of the piezoelectric material, the higher the piezoelectric properties. The capacitance of the devices was measured using a precision impedance analyser 6500B (Wayne Kerr Electronics). The relative dielectric constant ε_r was calculated with the aid of equation (4-2), where: C_p and t_p are the measured capacitance and thickness of the piezoelectric element, A_e is the effective electrode area, and ε_0 is the permittivity of free space = 8.8541 x 10^{-12} F/m.

$$\varepsilon_r = \frac{C_p . t_p}{\varepsilon_0 . A_e} \quad (4\text{-}2)$$

Figure 4-7 shows that the relative dielectric constant increases with increased PZT powder loading in the composite. The maximum relative dielectric constants (at 1 kHz) 46.6, 135 and 40 were achieved at PZT-binder weight ratios of 4:1, 3:2 and 4:1 for ECS-PolyPZT 1, 2 and 3 films, respectively. However, as shown in Figure 4-8, ECS-PolyPZT 6 provided the maximum relative dielectric constants of 146 and 179 (at frequencies of 1 kHz and 20 Hz) at the optimum PZT-binder weight ratio of 2.57:1. The effect of air-voids appears after these optimum weight ratios (threshold point), which caused a reduction in the dielectric properties of the whole printed film. The air voids can be indirectly identified by the measuring the dielectric constants of the material.

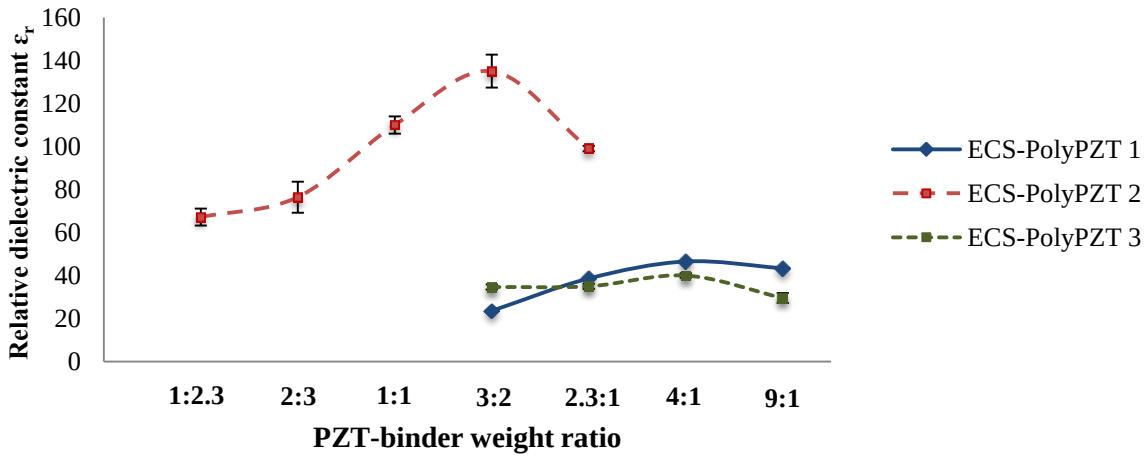

Figure 4-7: Dielectric constant (at 1 kHz) for ECS-PolyPZT 1, 2 and 3 with different PZT-binder weight ratios

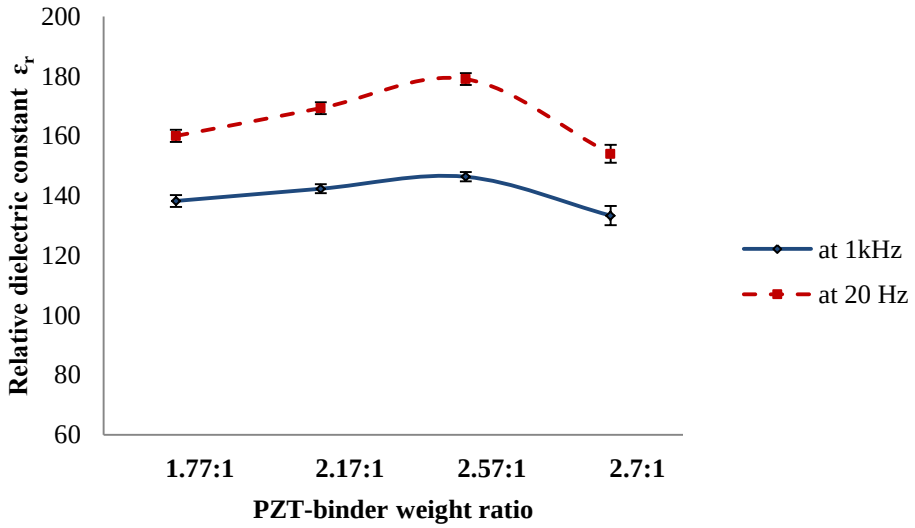

Figure 4-8: Dielectric constant (at1k and 20 Hz) for ECS-PolyPZT 6 with different PZT-binder weight ratios

Air voids exist at low PZT weight-loadings, but they do not significantly affect the dielectric and piezoelectric properties of the composite. However, there is a threshold PZT-binder weight ratio point where these voids begin to negatively affect the dielectric and piezoelectric properties. These air voids exist for two main reasons:

- There is insufficient polymer binder to fill the gaps between the PZT particles. This happens at high PZT weight-loading (particularly when the polymer matrix itself has a high viscosity, which makes it difficult when mixing as the polymer does not penetrate easily between the particles to fill the voids).
- Air bubbles introduced in the mixing and printing processes. They could be trapped inside the polymer at high viscosities.

- The polymer itself creates voids during the curing process, either because when the solvent evaporates it leaves holes and the air is subrogated, or the nature of the polymer creates air voids when exposed to temperature.

Figure 4-9 shows cross-sectional SEM images of ECS-PolyPZT 2 when the PZT weight loading was varied from 45% (1:1.12) to 70% (2.3:1). It shows that a decrease in polymeric phase reduced the bond between PZT particles and increased the number and size of air voids.

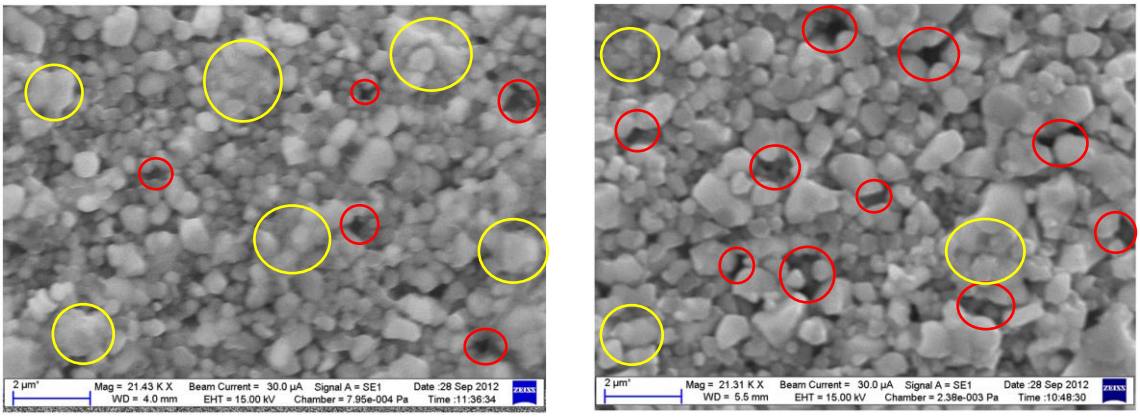

(a) (b)

Figure 4-9: SEM images of ECS-PolyPZT 2 at (a) 1:1.2 and (b) 2.3:1 PZT-binder weight ratios. It shows that the size and the number of air voids increased when increasing PZT weight loading. Examples of PZT particles that are fully covered with polymers (red circles) and also air voids (red circles)

Figure 4-10 shows a cross-sectional image that shows the distribution of the PZT particles with the polymer. Similar to ESC-PolyPZT 2, ECS-PolyPZT 6 suffered from air voids. These air voids introduced a great challenge in optimising the dielectric, piezoelectric and mechanical properties of the printed film.

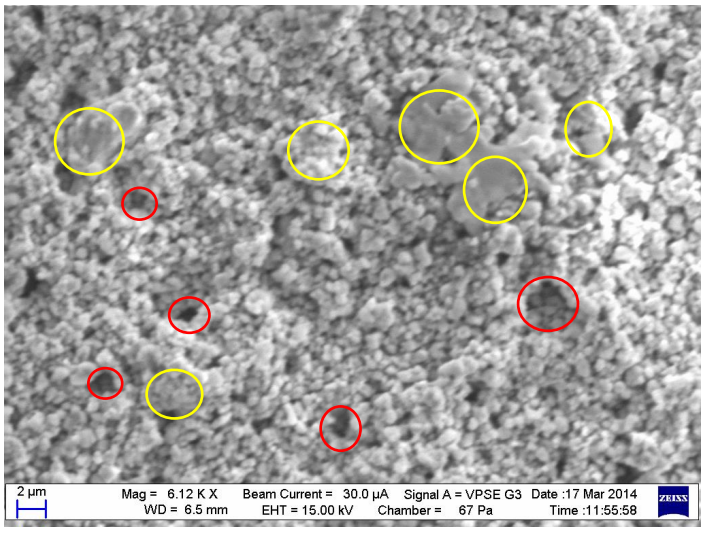

Figure 4-10: A cross-sectional SEM image of ECS-PolyPZT 6 at PZT-binder weight ratio of 2.5:1.

Air voids can be observed by the SEM micrographs as shown in Figure 4-9 and Figure 4-10. However, some other voids cannot be observed because they are very small and difficult to be detected by the SEM micrographs (this is due to the limitations in magnification capabilities of the used SEM micrograph machine). Similarly, some of the PZT particles are covered by only thin layer of polymer which is also difficult to be detected. Therefore, the quality of covering the polymer with PZT can be evaluated by comparing different SEM micrographs. This can be achieved by generally quantifying the number of the observed air voids and observing the size of each of them.

However, quantifying air voids inside a certain piezoelectric film is challenging as it needs further investigation by SEM micrographs and visually counted. Therefore, dielectric constant can be a significant factor to indirectly quantify the air voids in the piezoelectric film as the only third phase that can be incidentally mixed with the mixture is air during mixing or curing process. Therefore, the more air voids in the film, the lower the dielectric constant after a specific point called threshold PZT-binder weight ratio [133] as shown in Figure 4-7 and Figure 4-8 . This is because the dielectric constant of air (1) is mostly lower than the dielectric constant of PZT and the polymer phases.

The target of this study was to discover the optimum PZT-binder weight ratio that provides the best piezoelectric properties. Therefore, the different formulations of every composite were initially poled at the same poling conditions.

4.5.3 Applying Initial Poling Conditions

This stage was essential for selecting the best PZT weight loading that gives the maximum d_{33} properties. Direct contact poling was applied to the materials. The initial poling conditions of E_{ex} = 6 MV/m, T = 160 °C and t = 10 min were applied to ECS-PolyPZT 1, 2 and 3. Similar to the relative dielectric constant results, the d_{33} values increased with the increased PZT phase in the film, as shown in Figure 4-11. The maximum d_{33} achieved by ECS-PolyPZT 1, 2 and 3 screen-printed films were 14.7, 25 and 16.52 pC/N, respectively.

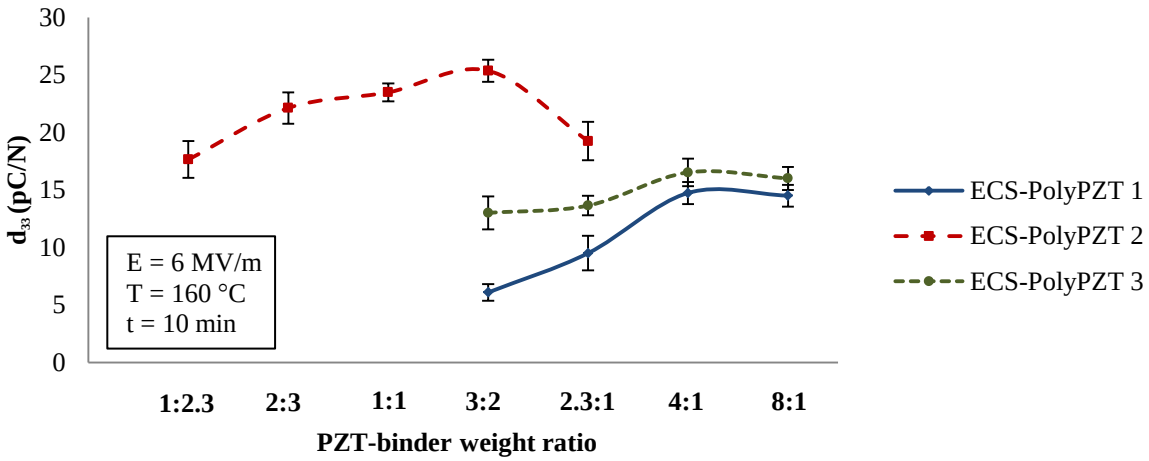

Figure 4-11: The mean d_{33} values of ECS-PolyPZT 1, 2 and 3 films printed on alumina substrate and poled at initial poling conditions

The four PZT-binder formulations shown in Table 4-10 were printed on alumina and Kapton. Because the ECS-PolyPZT 6 had different poling conditions (as discussed in section 4.4 on page 78), it was initially poled at E = 2 MV/m, T = 100 °C and t = 4 min. After poling, the d_{33} was measured for each film using four devices, with five measurements taken from each sample. Figure 4-12 shows the average d_{33} of the 20 measurements. The results show that the maximum d_{33} values achieved were 27 and 29 pC/N at an optimum PZT-binder weight ratio of 2.57:1 for devices printed on alumina and Kapton, respectively. After this PZT loading, the d_{33} values decreased down to 21 pC/N at 2.7:1 weight ratio (threshold PZT weight loading). The difference in the d_{33} values between films printed on alumina and Kapton were because of the clamping effect of the mechanical boundary conditions of the substrate (as discussed in the following chapter).

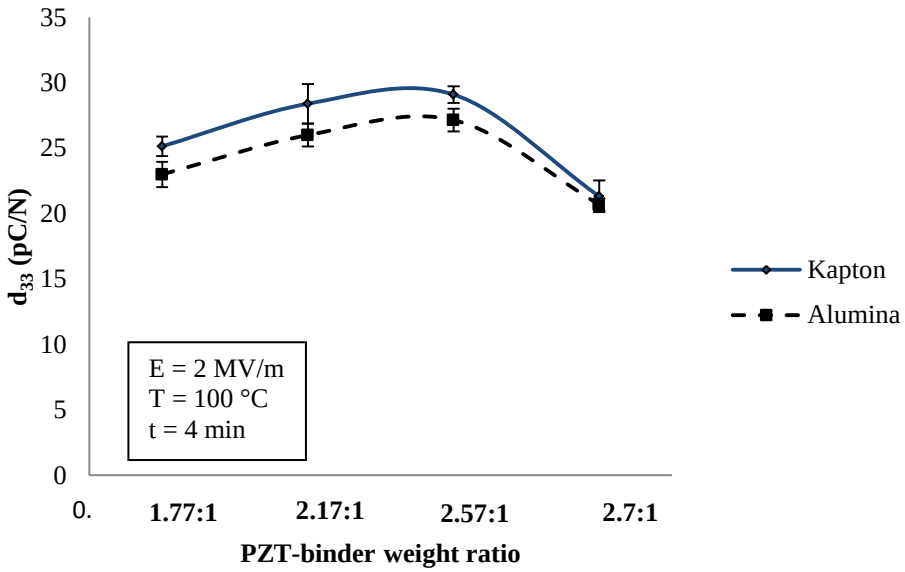

Figure 4-12: The mean d_{33} values for ECS-PolyPZT 6 film printed on alumina and Kapton substrates and poled at initial poling conditions

From the dielectric and piezoelectric results, the change in relative dielectric constant was identical to the change in the d_{33} values of the material when changing the PZT content of the composite. Table 4-11 summarises the maximum d_{33} values and dielectric constant achieved with the corresponding PZT-binder weight ratios. The final investigation in this chapter is to test the flexibility of the devices. These formulations provide the best compromise between increased powder loading but reducing the air voids.

Composite	PZT:binder weigh	ε_r (at 1kHz)	d_{33} (pC/N)	Initial poling conditions
ECS-PolyPZT 1	4:1	46.5	14.7	E= 6MV/m, T= 160 °C, t = 10
ECS-PolyPZT 2	3:2	135	25.36	E= 6MV/m, T= 160 °C, t = 10
ECS-PolyPZT 3	4:1	40	16.52	E= 6MV/m, T= 160 °C, t = 10
ECS-PolyPZT 6	2.57	146	27	E= 2MV/m, T= 100 °C, t = 4 min
		179 at 20Hz	29 on Kapton	

Table 4-11: A summary of the maximum dielectric and piezoelectric properties achieved at the optimum PZT-binder weight ratios for every composite

4.5.4 Testing the Flexibility of the Materials

The bendability of the material can practically reflect the flexibility and the reliability of the internal bonding between PZT particles achieved by the binder, as discussed in section 4.3.4 on page 77. The flexibility of the material was tested in two stages. The first stage bent the samples around different diameter formers and observing the minimum radius of curvature the film could withstand before failure. The film is considered to have failed when cracks or wrinkles are observed on the film's surface using a microscope. The thesis target was to show a film that can

withstand bending with a radius of curvature equal or less than a bent thumb joint. The flexibility of the films was tested after they were printed on Kapton Polyimide substrates. The top electrode was not printed to observe the change on the surface of the piezoelectric film. The experimental procedures of testing the flexibility of the devices is summarised in Figure 4-13.

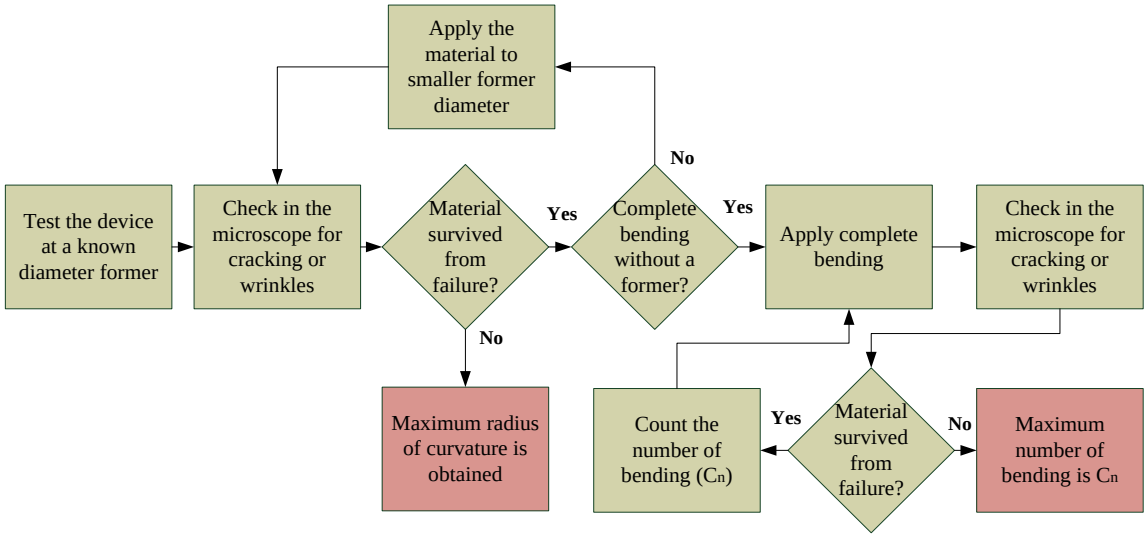

Figure 4-13: The experimental procedures taken for testing the flexibility of the devices

Results show that all the formulations survived at minimum radius of curvature of 9 mm, which showed a measure of flexibility that can be used in human-movement-based energy-harvesting applications. All ECS-PolyPZT 2 and 6 films survived at the minimum radius of curvature former tested (around R_c = 0.95 mm). These films also withstood bending without a former (R_c = 75 µm) i.e folding the Kapton. However, other films survived up to radius of curvature as shown in Figure 4-14. It also shows that the minimum radius of curvature increased with increasing PZT weight loading in the composite.

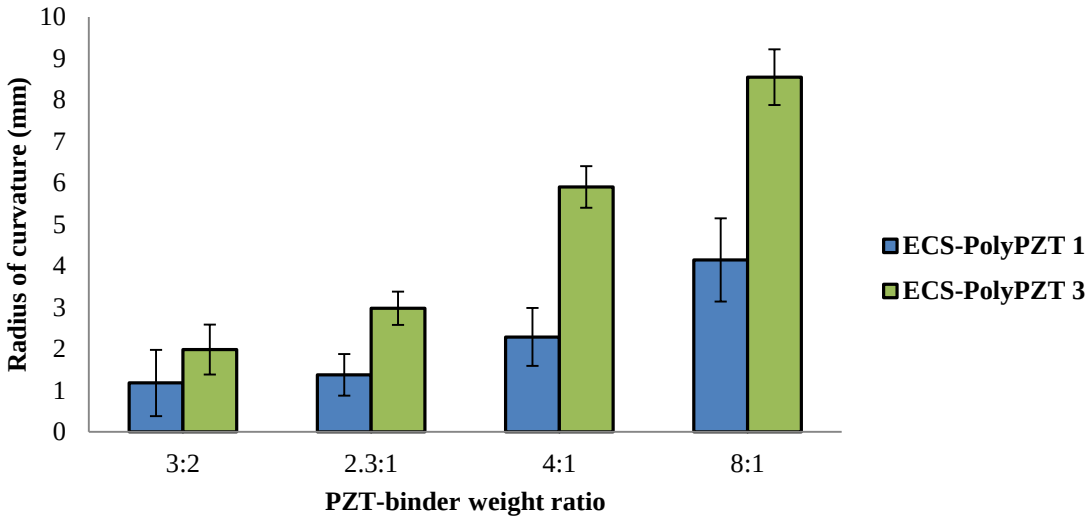

Figure 4-14: Minimum radius of curvature the ECS-PolyPZT 1 and 3 formulations before failure

The second stage was conducted on the most flexible films; ECS-PolyPZT 2 and 6. They were further investigated by observing the number of complete bending cycles without a former as depicted in Figure 4-13. The samples were inspected for cracks under the microscope after each bending cycle. The cycle at which the cracks were observed was called the failure cycle C_f. The maximum number of cycles the films could withstand before C_f was denoted C_n. Figure 4-15 shows the maximum complete bending cycles that ECS-PolyPZT 2 withstood. It also shows the corresponding initial d_{33} values without bending that the material can provide for every PZT weight loading.

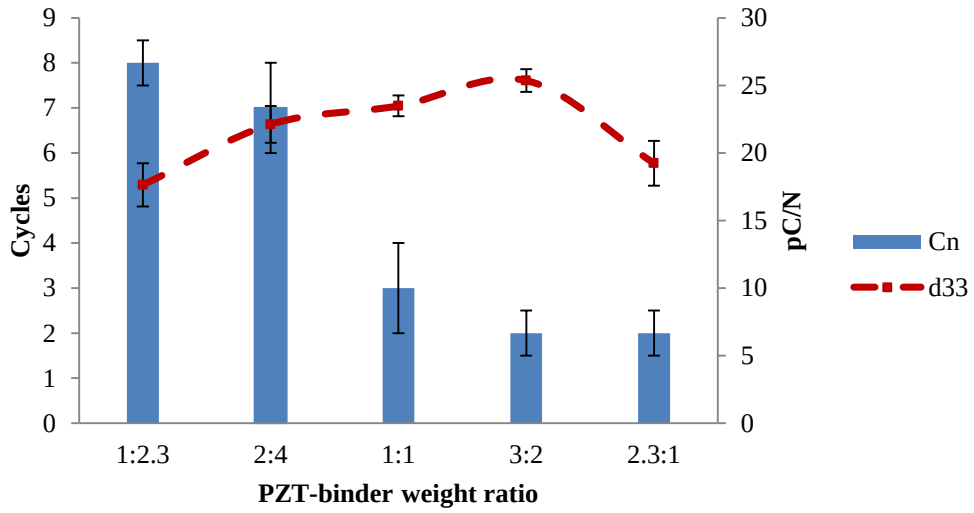

Figure 4-15: Maximum complete bending cycles and initial d_{33} values for the ECS-PolyPZT 2 material at different PZT-binder weight ratios

Similarly, Figure 4-16 shows the maximum complete bending and the initial d_{33} values of the films without bending of ECS-PolyPZT 6 at different PZT-polymer weight ratios. Figure 4-17 introduces two microscope images of the ECS-PolyPZT 6 printed film before and after being subjected to five complete bends. The cracking on the surface of the material is obvious after five complete bends.

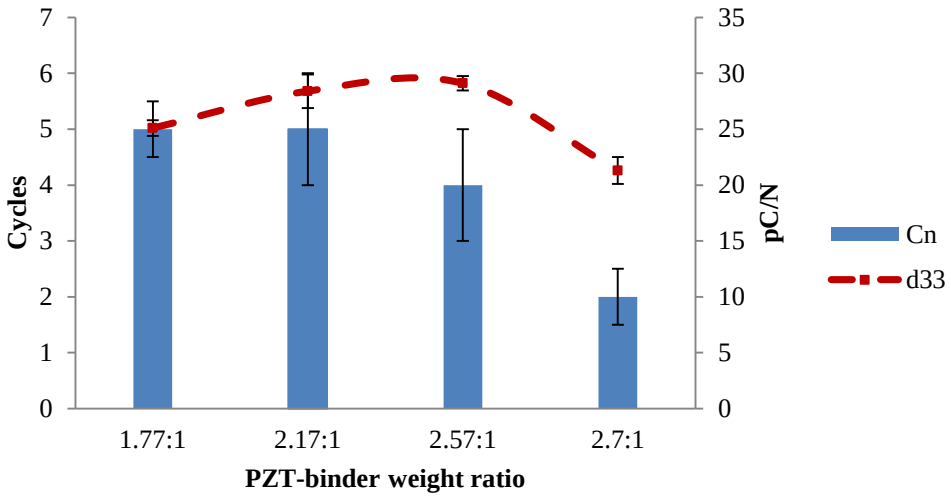

Figure 4-16: Maximum complete bending cycles and initial d_{33} values for the ECS-PolyPZT 6 material at different PZT-binder weight ratios

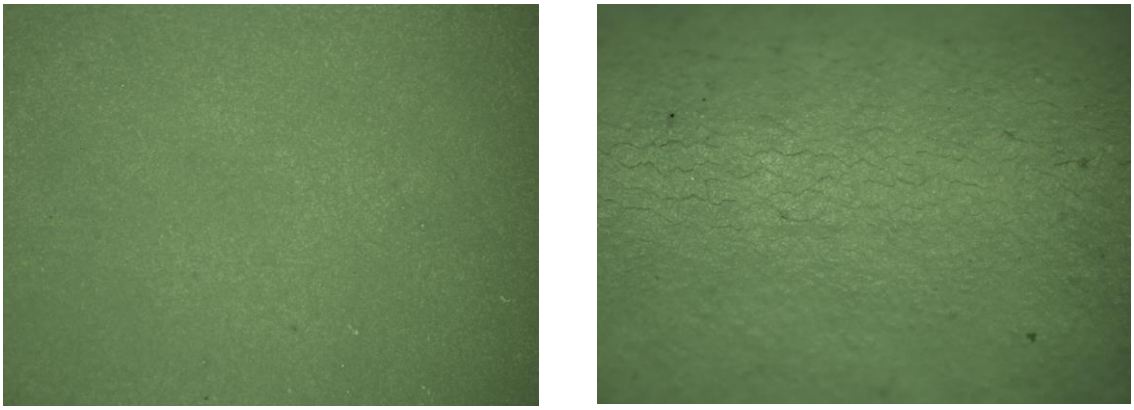

(a) (b)

Figure 4-17: The microscope images (X10) for ECS-PolyPZT 6 with 2.57:1 (a) before and (b) after five complete bends. The surface cracks are obvious after bending

4.6 The Viscosities of the Selected Materials

Viscosity measurements were taken every second for 165 seconds after exposing the materials to air at room temperature. This is to observe the rapidity of drying, and its effect on viscosity over time. Pastes which dry quickly may block the mesh holes and accordingly affect the quality of the printed film. The results show an increase in the viscosity of 54 % and 65% for ECS-PolyPZT 2 and 3, respectively, in the first 90 seconds of exposure to air, after which the viscosity stabilised. ECS-PolyPZT 3 dried at a faster rate before stabilising than all the other materials. However, ECS-PolyPZT 1 and 6 showed stable viscosity values over the 165 seconds.

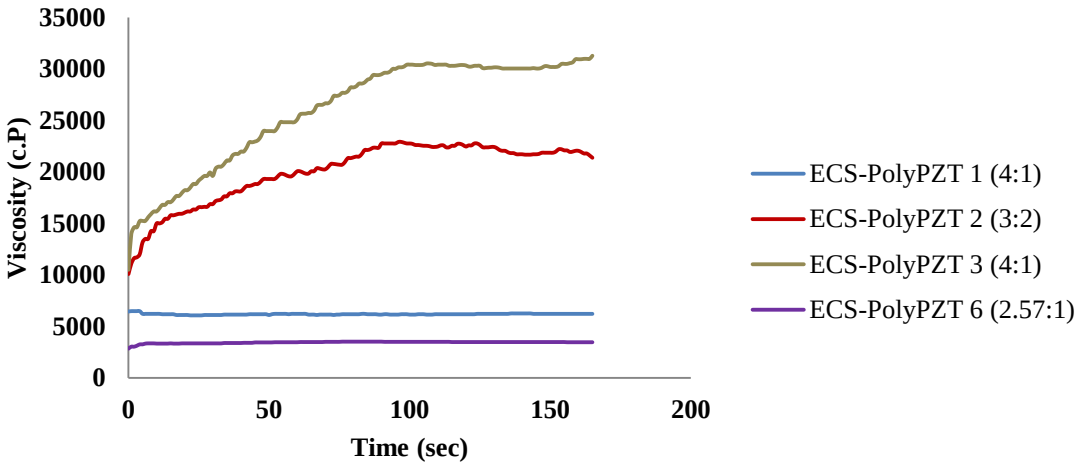

Figure 4-18: The viscosities of the selected materials over time after exposure

Table 4-12 shows the average viscosity of the materials after the corresponding stabilisation time of each paste. Smoother printing was obtained from ECS-PolyPZT 1 and 6 because of their stabilised viscosities over time; however, some difficulties during printing were experienced for ECS-PolyPZT 2 and 3, such as screen blockage. Also, it was difficult to achieve a thinner prints per deposit (<30 µm) for those pastes because of their higher viscosities.

Materials	PZT-binder weight ratio	Viscosity (c.P)
ECS-PolyPZT 1	3:2	6194
ECS-PolyPZT 2	4:1	22273
ECS-PolyPZT 3	3:2	30282
ECS-PolyPZT 6	2.57:1	3447

Table 4-12: The average viscosity of the selected materials after stabilisation

4.7 Selectivity of the Composites

In both ECS-PolyPZT 2 and 6, there was an optimum d_{33} value the material could achieve; however, the flexibility reduced when increasing the PZT weight loading in the film. Although the flexibility target was to bend the film around a 9-mm-radius former, ECS-PolyPZT 2 and 6 not only achieved that but even survived complete folding of the film. The target was to choose first the formulation that gave the best compromise of piezoelectric activity and flexibility, therefore, 3:2 and 2.57:1 PZT-polymer weight ratios were selected for ECS-PolyPZT 2 and 6, respectively. These formulations gave the highest d_{33} values at a reasonable flexibility. All the materials show a certain level of flexibility, which is application-dependent, but the PZT-binder weight ratios listed in Table 4-13 showed the best dielectric and piezoelectric properties combined with flexibility.

Materials	PZT-binder weight ratio	Updated Formulation Name
ECS-PolyPZT 2	3:2	ECS-PolyPZT 2a
ECS-PolyPZT 6	2.57:1	ECS-PolyPZT 6a

Table 4-13: Updated names for the optimum formulations

4.8 Conclusions

Eight types of binding systems were investigated after mixing with PZT powder. The PZT weight loading can have a significant effect on the mixing process, screen-printability, curing conditions and the adhesion of the printed film. Identifying the maximum PZT content that can be mixed with the binder and produce a screen-printed film with suitable adhesion were the key aims of this chapter. These mixing limits differed from one binder to another. They depended on the viscosity and the adhesion strength of the binder. The PZT-binder weight ratios for ECS-PolyPZT 1, 2, 3, 4, 6 and 7 at maximum PZT weight loading are 8:1, 2.3:1, 8:1, 5.3:1, 2.7:1 and 9:1, respectively. All the materials were cured at a range of temperatures (90-130 °C). Furthermore, the adhesion tests proved that all materials at these PZT-binder weight ratios survived bending around a 9-mm former, which was also one of the targets for this study.

Thermoplastic polymeric-based binders showed higher piezoelectric coefficients when mixed with PZT than adhesive thermosetting polymeric-based binders. ECS-PolyPZT 1, 2, 3 and 6 gave 13.5, 20, 14.9 and 22.8 pC/N, respectively, at the maximum electric field. Maximising the piezoelectric property (d_{33}) and improving the mechanical flexibility were essential when adjusting the PZT content in the composite. After applying poling process to the materials printed on alumina, ECS-PolyPZT 2 and 6 showed d_{33} values of 25 and 27 pC/N at threshold PZT-binder weight ratios of 3:2 and 2.57:1, respectively. At the same PZT-binder weight ratios they showed a dielectric constant of 135 and 146, respectively. After these threshold weight ratios the effect of air voids appears and d_{33} and dielectric constant values are reduced as a consequence. This confirms the effect of the dielectric constant on the polarisation and overall d_{33} measurement of the materials.

All ECS-PolyPZT 2 and 6 films survived the lower radius of curvature (Rc = 75 µm). Other films, such as ECS-PolyPZT 1 and 3, showed a lower R_c of curvature but were not selected because they showed lower dielectric constants and d_{33} compared to ECS-PolyPZT 2 and 6. The second flexibility test was conducted by subjecting all printed ECS-PolyPZT 2 and 6 formulations to a number of complete bending cycles, C_n. ECS-PolyPZT 2 and 6 showed a lower number of bending cycles as PZT-binder weight ratio increased. However, ECS-PolyPZT 2 and 6 with weight ratios of 3:2 and 2.57:1, respectively, also showed higher piezoelectric and dielectric

properties as discussed earlier. These two formulations were selected and defined thereafter as ECS-PolyPZT 2a and 6a, respectively.

The effect of the PZT weight loading on the viscosities of the formulations can affect the screen-printability of the selected pastes. ECS-PolyPZT 6a is lower viscosity than ECS-PolyPZT 2a which gives the advantage of smooth screen-printing and the ability to print thinner layers. Also, ECS-PolyPZT 2a showed rapid drying when exposed to air, increasing the viscosity of the material by up to 65% within 2 minutes of exposure. Neither non-smooth-printing nor screen-blockage was experienced with ECS-PolyPZT 6.

Chapter 5: Optimisation of Poling Process and Substrates Clamping Effect on the d_{33} Measurements

5.1 Introduction

This chapter describes the optimisation of the contact poling process for the ECS-PolyPZT 6a film printed on three substrates: alumina, Kapton and polyester-cotton. As described in Chapter 4, the difference in the d_{33} values that may occur when the material is printed on different substrate with the same poling conditions was investigated.

In addition, the fact the piezoelectric film is attached to the substrate introduces a clamping effect that reduces the measured d_{33} values [129, 134]. Piezoelectric material performance is ideally influenced by the mechanical boundary conditions that constraint its mechanical movements (such as expansion or contraction) when an external force is applied. Printing on different types substrates will result to a variation in the boundary conditions that will lead to a change in the measured piezoelectric film properties depending upon the substrate. In this chapter, our screen-printed low temperature piezoelectric composite ECS-PolyPZT 6a was printed on three different substrates (alumina, Kapton and polyester-cotton) and the d_{33} measurements were compared. The free-standing d_{33} values were be estimated according to their effective d_{33} measurements taken on their substrates. The general experimental plan of this chapter is summarised in Figure 5-1.

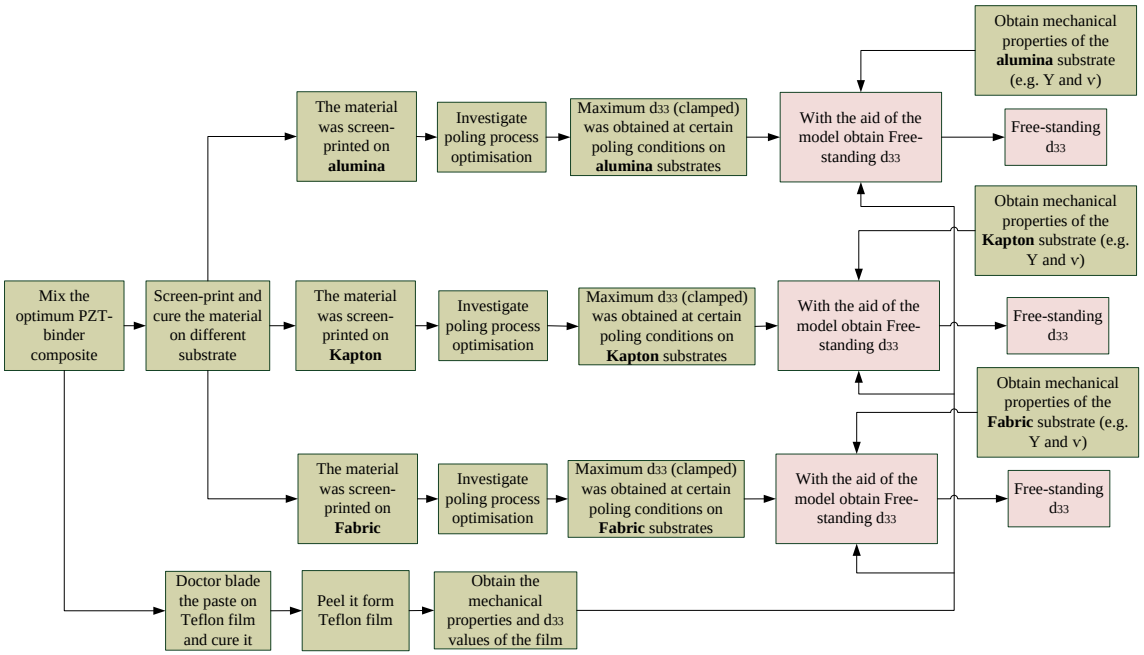

Figure 5-1: Experimental plan of poling process optimisation of the film on alumina, Kapton and woven-fabric. Also, the plan of obtaining the actual d_{33} value for unclamped film (a film without a substrate)

5.2 Experimental Work

The ECS-PolyPZT 6a paste was formulated with the optimum PZT-binder weight ratio 2.57:1 as described in Chapter 4. The capacitive structure and screen-printing process described previously have been used here. The ECS-PolyPZT 6a was screen-printed on alumina, Kapton and a woven-fabric substrate. The woven-fabric substrate used in this study was Polyester-cotton.

The fabric surface is very rough compared with typical smooth substrate and this affects the quality and thickness of the printed layers which makes poling the ECS-PolyPZT 6 unreliable. Therefore, an additional planarising film, or interface layer was required on the surface of the fabric on the side where the capacitive structure is printed. The interface layer, a polyurethane-based paste (Fabink-IF-UV 1039) is printed in order to fill the pores between the yarns. Typically, 6 prints of the interface layer, UV cured for 60 seconds after each deposit, was required to sufficiently smooth the fabric. However, before printing the interface layer, the fabric itself was ironed and then glued to a solid surface to guarantee a flat surface while printing. Figure 5-2 shows the screen-printing process for the test device on woven polyester-cotton. Steps 1 and 2 are the printing of the interface layer. Steps 3, 4 and 5 show the screen-printing process for the capacitive structure on the top of the interface layer. A cross section of the assembly is shown in Figure 5-3.

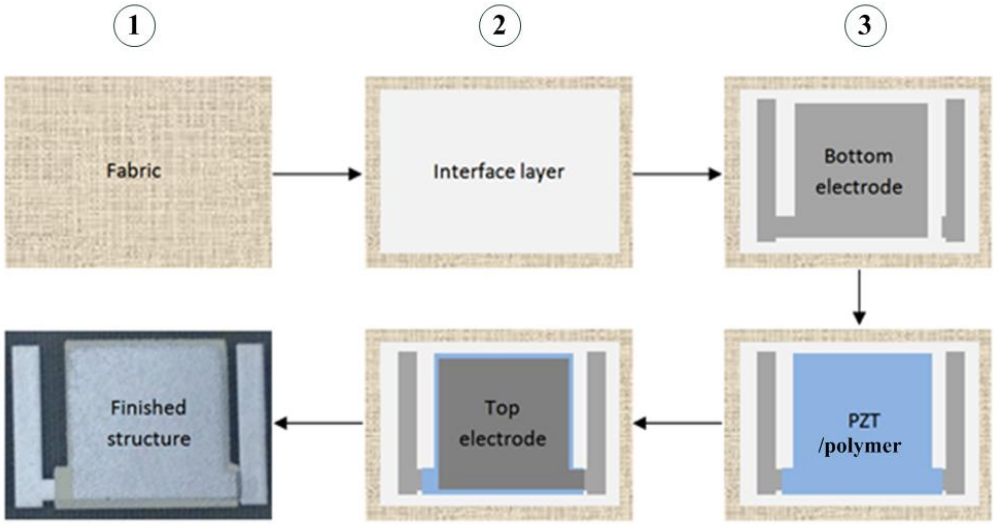

Figure 5-2: Schematic of the printing process of the capacitive structure printed on polyester-cotton. The interface layer is only needed in this type of substrate

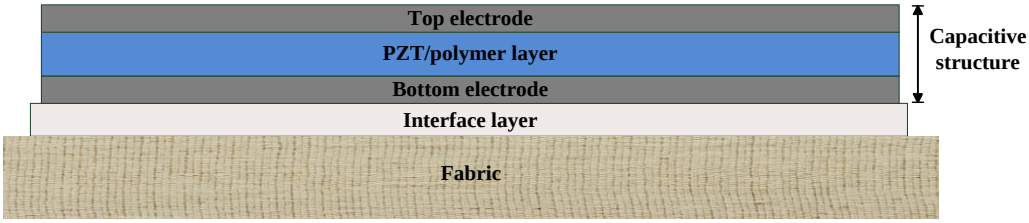

Figure 5-3: A schematic cross-section of the piezoelectric test device printed on Polyester-cotton woven fabric

5.3 Optimising Poling Conditions of the Selected Materials

Maximising the effective electric field on the PZT particles (E_{eff}) was essential to maximise the piezoelectric activity (represented by d_{33} coefficient) of the whole film. This can be only achieved experimentally by optimising the poling parameters; Temperature (T°C), time (t) and electric field (E). The same optimisation process described in Figure 3-11 on page 61 was followed. The investigation was carried out for devices printed alumina, Kapton and Polyester-cotton substrates. The poling temperature was initially explored with fixed electric field E=2 MV/m and poling time t = 4 min.

In Figure 5-4, the d_{33} values improved with the increasing temperature up to 90 °C reaching maximum values of 28, 31 and 53.6 pC/N for devices printed on alumina, Kapton and Polyester-cotton, respectively. For temperatures beyond this point, the devices showed sparks during poling process. This was an indication of dielectric breakdown and the electric field was decreased, hence the reduction in the d_{33} values as illustrated in Figure 5-4.

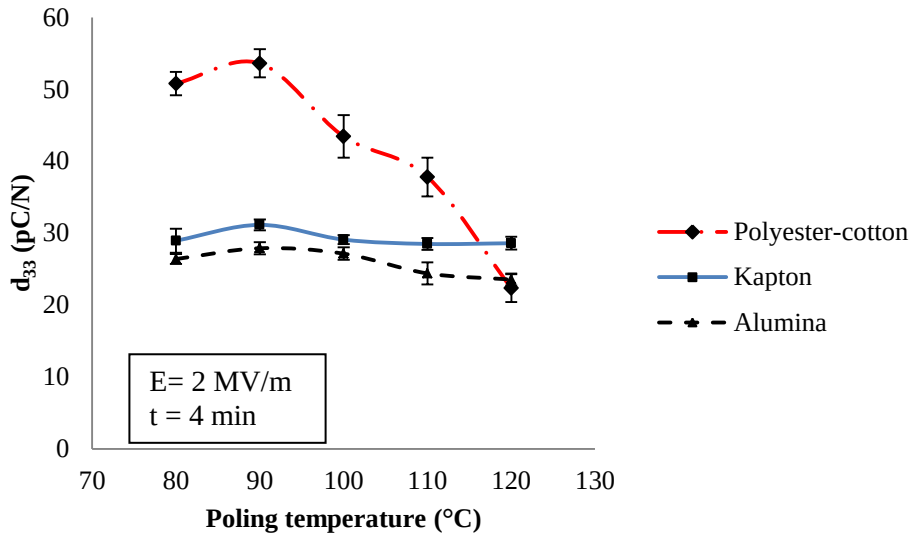

Figure 5-4: Optimisation of the poling temperature for the d_{33} for devices printed on Polyester-cotton, Kapton and alumina

The next parameter to be investigated was poling time. It was optimised with poling field of E_{ex} = 2 MV/m and updated poling temperature of T = 90 °C. Figure 5-5 illustrates that the optimum poling time was 6 minutes that gave a maximum d_{33} values of 30, 33 and 58 pC/N for samples on alumina, Kapton and Polyester-cotton, respectively. Increasing the poling time over 6 minutes resulted in dielectric breakdown during the poling process and accordinly the effective electric field was reduced across the piezoelectric particles in the films. This is beccause of silver migration from the electrodes which its growth is a function of the applied electric field [135]. Silver migrates across the dielectric material under the effect of the applied electric field. Increasing the poling time after 6 minutes, increases the number of these silver migrants across the piezoelectric film causing either sparks or short-circuiting during poling process. This leads to a decrease in the poling efficiency and consequently in the final d_{33} value of the film.

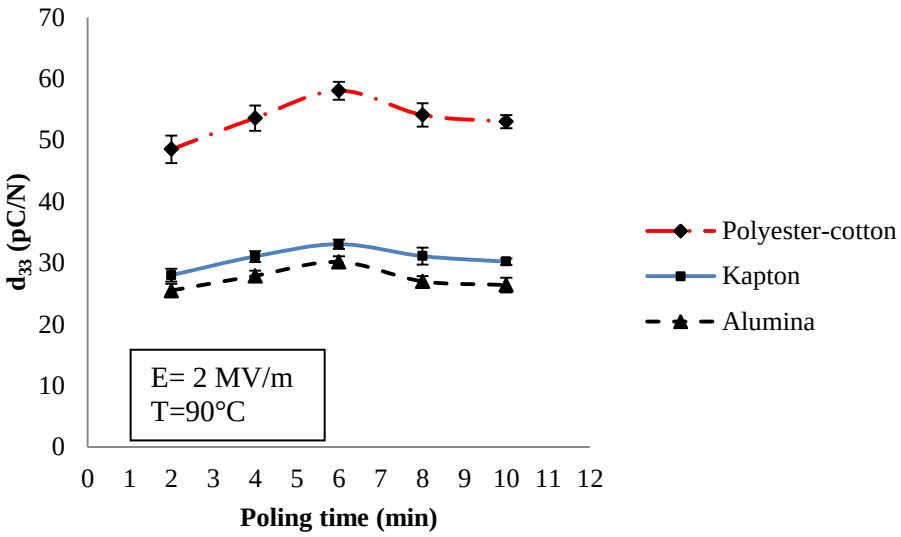

Figure 5-5: Optimisation of the poling time for the d_{33} for devices printed on Polyester-cotton, Kapton and alumina

Finally, the external electric field was optimised at a fixed updated poling time and temperature of 6 minutes and 90 °C, respectively. As shown in Figure 5-6, the d_{33} increased until electic breakdown occurred at around 3.7 MV/m for Kapton and Polyester-cotton, respectively. However, the alumina substrate devices were survived up to 4 MV/m but no further improvements in the measured d_{33} was found. This confirms the maximum external electric field that can be achieved for all the substrates is is 3.7 MV/m giving a d_{33} values of 35.8, 40 and 70 gained for alumina, Kapton and Polyester-cotton substrates, resopectively.

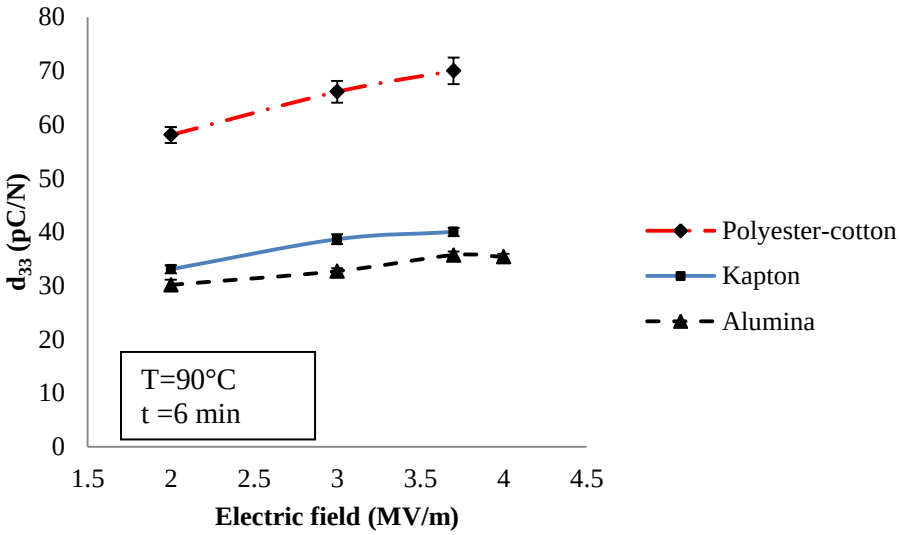

Figure 5-6: Optimisation of the poling field for the d_{33} for devices printed on Polyester-cotton, Kapton and alumina

These results show that the type of substrate material has negligable influence the optimum poling conditions. Table 5-1 shows the optimum poling conditions that give the maximum d_{33} values.

Substrate type	Optimum poling conditions		
	T (°C)	t (min)	E (MV/m)
alumina	90	6	3.7
Kapton	90	6	3.7
Polyester-cotton	90	6	3.7

Table 5-1: The dielectric breakdown and optimum poling parameters of the optimum films on alumina, Kapton and Polyester-cotton

5.4 Clamping Effect and d_{33} Measurements

The d_{33} results taken in the previous section show a difference in the measured values when the ECS-PolyPZT 6a was printed on different substrates. This difference has been observed for all the measurements taken when investigating poling pcoress optimisation. It indicates the clamping of the printed films has an effect on the d_{33} measurements and the magnitude of this effect is dependent on the mechanical properties of the material of the substrates. This section will explore this phenomenon and calculate the actual d_{33} value of the optimum ECS-PoyPZT 6a.

When a compressive force is applied through the thickness of the piezoelectric film, it will cause a lateral expansion in the plane of the substrate due to the Poissons ratio of the material. However, this deformation is confined by the mechanical boundary conditions of the substrate. For such a constrained piezoelectric film, the relationship between the longitudinal measured piezoelectric coefficient d_{33clp} PZT-polymer film which is clamped on the substrate, the freestanding (i.e. without substrate) transverse piezoelectric coefficient d_{31fs} and the longitudinal free-standing piezoelectric d_{33fs} of the film is described in equation (5-1) [129]. Also, it shows the effect of the mechanical properties of the substrate material on the transverse piezoelectric component d_{31fs} and therefore on the measured piezoelectric coefficient of the film.

$$d_{33clp} = d_{33fs} + 2d_{31fs}\left(\frac{-\left(\frac{v_s}{Y_s}\right) - s_{13}^E}{s_{11}^E + s_{12}^E}\right) \tag{5-1}$$

Where, Y_s and v_s are the Young's modulus and the Poisson ratio of the substrate. s_{11}^E, s_{12}^E and s_{13}^E are the mechanical compliances of the PZT-polymer film. For anisotropic piezoelectric materials, the ratio between the transverse and longitudinal piezoelectric coefficients is related by the following ratio [136-138].

$$\frac{d_{31}}{d_{33}} = -\nu_{13} \tag{5-2}$$

Assuming our piezoelectric film is isotropic, from Hooke's law, the ratio between the free-standing transvers piezoelectric coefficient d_{31fs} and longitudinal piezoelectric coefficient d_{33fs} will be as follows

$$\frac{d_{31fs}}{d_{33fs}} = -\nu_p \tag{5-3}$$

And also the mechanical compliance matrix parameters were calculated using the following relationships with the aid of the Young's modulus Y_p and Poisson ratio ν_p of the piezoelectric film.

$$s_{11}^E = \frac{1}{Y_p} \tag{5-4}$$

$$s_{12}^E = s_{13}^E = -\left(\frac{\nu_p}{Y_p}\right) \tag{5-5}$$

Substituting equations (5-3), (5-4) and (5-5) into (5-1) and rearranging it results in

$$d_{33clp} = d_{33fs}.\left[1 - 2.\nu_p\left(\frac{\left(\frac{\nu_p}{Y_p}\right) - \left(\frac{\nu_s}{Y_s}\right)}{\frac{1}{Y_p} - \frac{\nu_p}{Y_p}}\right)\right] \tag{5-6}$$

$$d_{33fs} = \frac{d_{33clp}}{\left[1 - 2.\nu_p.\left(\frac{\left(\frac{\nu_p}{Y_p}\right) - \left(\frac{\nu_s}{Y_s}\right)}{\frac{1}{Y_p} - \frac{\nu_p}{Y_p}}\right)\right]} \tag{5-7}$$

The mechanical properties of the substrates and the piezoelectric film are shown in Table 5-2. Some of these values were provided by the manufacturers and others were measured or calculated. The Young's modulus of the PZT-polymer film and the Polyester-cotton substrate with interface layer were experimentally found.

Material	Y	v
alumina [139]	331 GPa [b]	0.25 [b]
Kapton [140]	2.5 GPa [b]	0.34 [b]
Interface+ Polyester-cotton	0.2 GPa [a]	0.44 [c]
PZT-5H [141]	60 GPa [b]	0.34 [b]
Polymer	0.02 MPa [a]	0.48 [a]
PZT/ polymer	131 MPa [a]	0.40 [c]

[a] measured,[b] provided by the manufacturer and [c] calculated

Table 5-2: Mechanical properties of the substrates and printed film

The Poisson ratio of the piezoelectric film was calculated using formulas developed by [127]. It can be obtained when the Poisson ratio of the two phases of the PZT-polymer are identified with respect to their volume ratio. However, the Poisson ratio of the Polyester-cotton with interface was estimated using equation (5-8).

$$\nu_s = \nu_{fab} V_{fab} + \nu_{intf} V_{intf} \tag{5-8}$$

Where, ν_s, ν_{fab}, ν_{intf} are the Poisson ratios of the whole fabric substrate (Polyester-cotton plus interface layer), average Poisson ratio of the Polyester-cotton fabric (=0.42) [142] and Poisson ratio of the interface layer (=0.47) [143], respectively. V_{fab} and V_{intf} are the volume fractions of Polyester-cotton (=0.58) and the interface (=0.42), respectively.

The longitudinal free-standing piezoelectric coefficient d_{31fs} was obtained for the maximum measured piezoelectric coefficient d_{33clp} shown in Figure 5-6 by using equation (5-7) with mechanical properties values shown in Table 5-2. The reuslts shown in Figure 5-7 illustrate the measured and the corresponding freastanding longitudanl piezoelectric coefficnets of ECS-PolyPZT 6 films on alumina, Kapton and Polyester-cotton substrates. The samples were poled at optimum poling conditions obtained in Figure 5-6. It was found that the calculated free-standing piezoelectric coefficinet d_{33fs} for films printed on Polyester-cotton, Kapton and alumina were 82 pC/N, 81 pC/N and 78 pC/N, respectively. These d_{33fs} values were reasonably consistent with a maximum difference of 4.8% between them, which is because of the variation in d_{33clp} measurements reflected by the standard deviations in the measurements. The average freestanding d_{33fs} value of the three values obtained from the three substrates is 80 pC/N. This average value is 13% , 50% and 55% less than the free-standing piezoelectric coefficient d_{33fs} for films printed on Polyester-cotton plus interface, Kapton and alumina substrates, respectively.

If we assume that all the three substrates are isotropic, the compliance C_s (if a force was longitudinally applied on 3-direction causing a lateral strain at 1, 2-direction) will be $(-\nu_s/Y_s)$

referring to Hooke's law. The compliance of the Polyester-cotton plus interface, Kapton and alumina substrates are -2 × 10^{-9}, -1.3 × 10^{-10} and -7.6 × 10^{-13} m^2/N, respectively. The Kapton substrate is more flexible and shows a compliance which is almost 10^2 times greater than alumina substrates. When substituing these compliances values for every substrates on equation (5-6) and the average d_{33fs} of 80 pC/N, closer clamped d_{33clp} were resulted compared to Polyester-cotton plus interface. This is due to when a substrate shows a compliance ($\leq$ -1x10^{-9} m^2/N), the printed film will show a very small variation in d_{33clp} values. This confirms that the measured d_{33clp} values of the piezoelectric film is only dependent on the compliance C_s of the substrates but not on their flexibility or bendability.

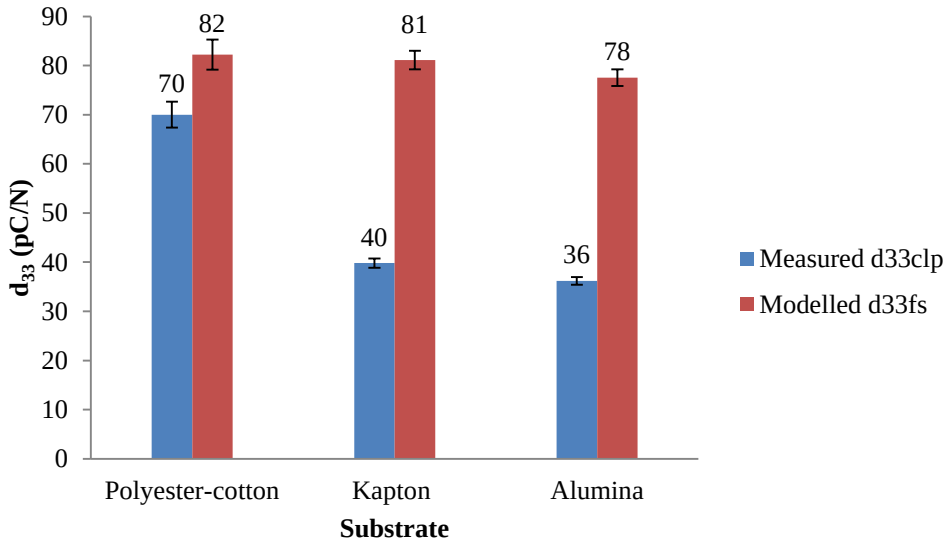

Figure 5-7: d_{33clp} and d_{33fs} for the selected PZT-binder of Polyester-cotton with interface, Kapton and alumina substrates

To confirm the results, free-standing ECS-PolyPZT 6 piezoelectric films were fabricated. The material was doctor bladed on to a Teflon substrate (TEFLON 200A, KATCO), cured and then peeled from the Teflon film creating the free-standing ECS-PolyPZT 6 film. The thickness of the produced film was 500 µm. The DuPont 5000 electrodes were coated and cured on both sides of the film to produce the capacitive structure which is used for testing.

Because of the thickness of the piezoelectric film and the limitation of the maximum voltage that power supply can produce (1000 V), a maximum poling field of E = 1 MV/m was achieved on the free-standing piezoelectric film. These poling conditions were applied to the Polyester-cotton, Kapton and alumina samples to allow comparison with the free-standing structure. The measured and calculated free-standing d_{33fs} values are illustrated in Figure 5-8.

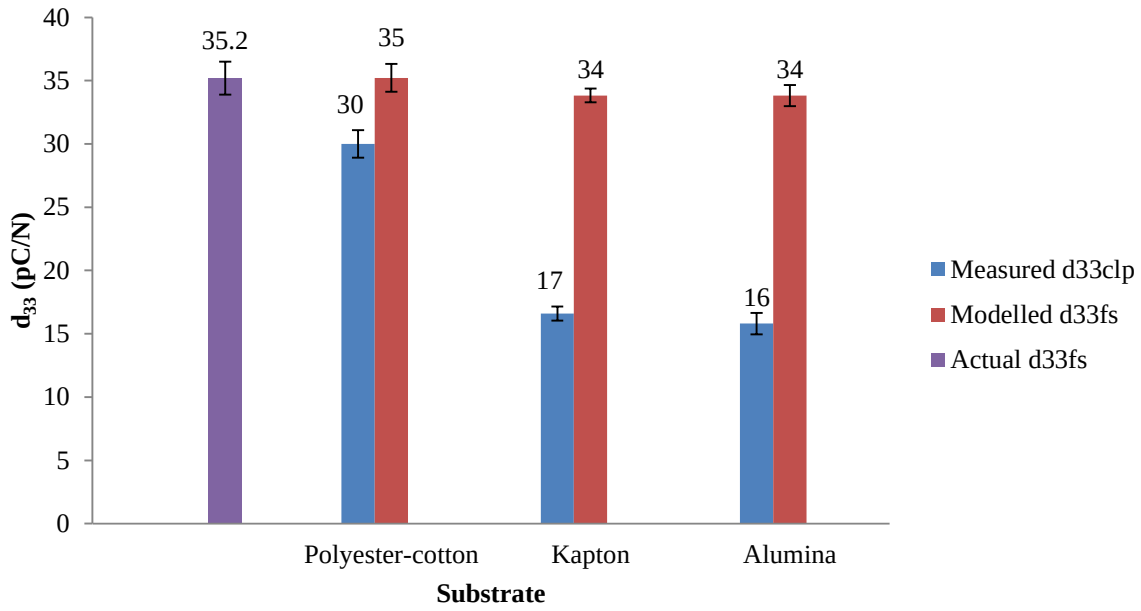

Figure 5-8: Comparisons of measured d_{33fs} of freestanding PZT-polymer film and calculated, d_{33fs} based on measured d_{33clp} of PZT-polymer films on Polyester-cotton with interface layer, Kapton and alumina

The calculated d_{33fs} values of the screen-printed piezoelectric films on the three substrates showed very good agreement with the actual free-standing d_{33fs} values. These results confirm the theoretical analysis and the use of equation (5-7) to calculate the corresponding free-standing d_{33fs}.

5.5 Conclusion

This chapter has presented the optimisation process of the optimum ECS-PolyPZT 6 film of PZT-polymer weight ratio of 12:1. The film exhibited maximum constraint d_{33clp} values of 70, 40 and 36 pC/N at E = 3.7 MV/m, T=90 °C and t=6 minutes, when it was printed on Polyester-cotton, Kapton and alumina, respectively. Optimum poling properties did not change with the change of the substrate. The substrate type has no effect on the optimum poling conditions of the printed piezoelectric film. The variation in the measured d_{33clp} for different types of substrates is caused because of difference in the mechanical boundary conditions of the substrates that clamp the film and then constrain the expansion and contraction of the piezoelectric material when a force is subjected during d_{33} measurement. This is called a clamping effect which causes a decrease in the measured d_{33clp}; however, this decrease differs from one substrate to another depending on its mechanical properties.

It was observed by theoretical and practical explorations confirmed a decrease on the d_{33clp} values by 13%, 50% and 55% for the Polyester-cotton, Kapton and alumina substrates, respectively. The average d_{33fs} value of the freestanding ECS-PolyPZT 6 film was calculated to be almost 80 pC/N. The measured clamped d_{33clp} values on both alumina and Kapton substrates were

found to be almost close although the compliance of Kapton was observed 10^2 times greater than alumina. This is due to the differences in the clamping effect become insignificant below a particular compliance (around -1×10^{-9} m^2/N) and the printed ECS-PolyPZT 6 films only show a small variation in d_{33clp} values. And because the compliance of the polyester-cotton plus interface is bigger than this particular compliance, the measured d_{33clp} is obviously greater.

Chapter 6: Effect of PZT Fillers on the Piezoelectric Properties of the Materials

6.1 Introduction

Powder particle size and distribution of piezoelectric ceramic PZT have an effect on piezoelectric properties as discussed earlier in section 2.4.3.1 on page 26. The piezoelectric properties can be increased by densifying the piezoelectric printed film. Densifying the film can be achieved by using two different PZT particle sizes. The first particle is the large particle which contributes the majority of the piezoelectric properties given by the material. The second particle is smaller and fills the gap between the large particles. This leads to an increase in the film density and improves the mechanical and piezoelectric performance [84]. Large and filler PZT particles have different particle orientations. These orientations specify the size of the filler if we suppose that the large PZT particle size is fixed.

In this chapter, the piezoelectric properties of the improved materials (ECS-PolyPZT 2a and 6a) selected from previous chapters would be investigated when changing the particle size of the filler inside the composite. Also Large PZT particles with and without fillers inside the composite will also be explored. The weight ratios between large particle and fillers will be calculated and then applied according to different suggested large-filler particles arrangements.

6.2 Suggested PZT Particle Distribution

In this work, the large PZT particle size is fixed by the powder manufacturer (e.g. 2 µm) and the filler particle size is calculated based on this. There are three possible PZT particles arrangements as shown in the chart in Figure 6-1. The first arrangement is to mix the large PZT particles powder with the binding system without filler particles. Most of the 0-3 connectivity type composites in the literature are of this type. The second type fills the gap between the large PZT particles with only a single filler particle (SFP) size that fills most of the gap. This type of arrangement was only investigated by Torah et al. [84] for high-temperature screen-printed piezoelectric films. In their work, during the sintering process the binder (glass frit) was melted thus reducing the gaps between the particles. However, in our case the low temperature processing does not allow the PZT to sinter and eliminate these gaps that affect the material. The third possible arrangement is to fill the gap between the large PZT particles by two or more of smaller size PZT filler particles. This type of fillers is called Multi-filler Particle (MFP). The MFP filler should at least as half the size as the lowest SFP filler.

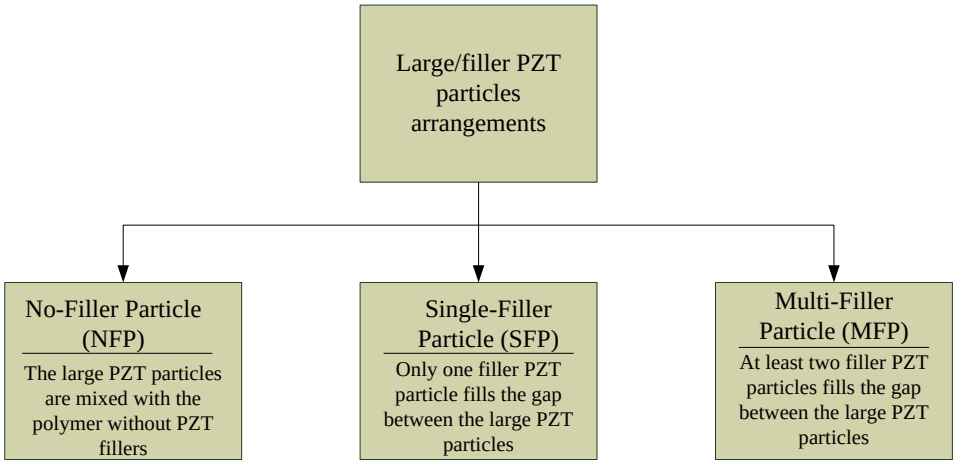

Figure 6-1: The suggested arrangements between large and filler PZT particles

There are two possible large particles to filler particles distributions suggested by [84, 96] as shown in Appendix B. These two distributions will be applied for both SFP and MFP options listed in Figure 6-1. Applying these two distributions requires, firstly predicting the possible size of the filler, secondly the ratio between the number of large particles to filler particles and then finally the weight ratio between both. It is important to know the particle size of the large PZT particles in order to estimate the size of the filler. However, the PZT particles have irregular shapes as shown in Figure 4-9 and the size of the large particle is actually the average diameter of that irregular shape PZT particle as will be discussed latter in section 6.5.1. Estimating the SFP size considering these irregular shapes is challenging. Therefore, this average diameter (size) of large particle can be used to create these two distributions as shown in Appendix B with spherical particles in order to simplify the estimation of the SFP size. If we suppose the difference in average diameter of the irregular and spherical shapes of the large particles is minor. Therefore, the difference between the estimated irregular and spherical shape SFPs is accordingly insignificant. Using this concept, SFP size can be simply estimated and accordingly the weight ratio between the large and SFP powders are calculated.

In this investigation it was decided to use ECS-PolyPZT 2a and 6a with their optimum PZT-binder weight ratios 3:2 and 2.57:1, respectively. The suggested PZT particle distributions assume:

- Large and filler particle sizes can be estimated.
- The polymer content does not introduce any influence on the particles sizes.
- The polymeric binder will fill any remaining gap between the particles.
- The entire polymer will solidify after curing and form a bonding matrix around the mixed PZT particles.

Each of these distributions shown has 2D and 3D representations. In the 2D representation, the calculation of the weight ratios between the large and SFPs considers the particles are in circular shapes. However, in 3D representation, the calculation of the weight ratios between the large and SFPs considers the particles are in spherical shapes. These representations help identify the ideal number of PZT filler particles.

6.3 Experimental Plan

The process flow in Figure 6-2 shows the experimental plan of identifying the optimum large particle to SFP weight ratio that can be mixed with the binder to maximise d_{33}. It starts with the estimation of the particle size according to the type of the PZT particle distribution. The large PZT powder is then attritor-milled to reduce the particle size and produce the SFP powder. These SFP powder will be later mixed with the large PZT particles according to previous calculations which consider the 2- and 3-dimensional representations of the particles as shown in Figure 6-2. The proposed large particle-SFP formulations will then be mixed with the binder according to the calculated optimum ratio.

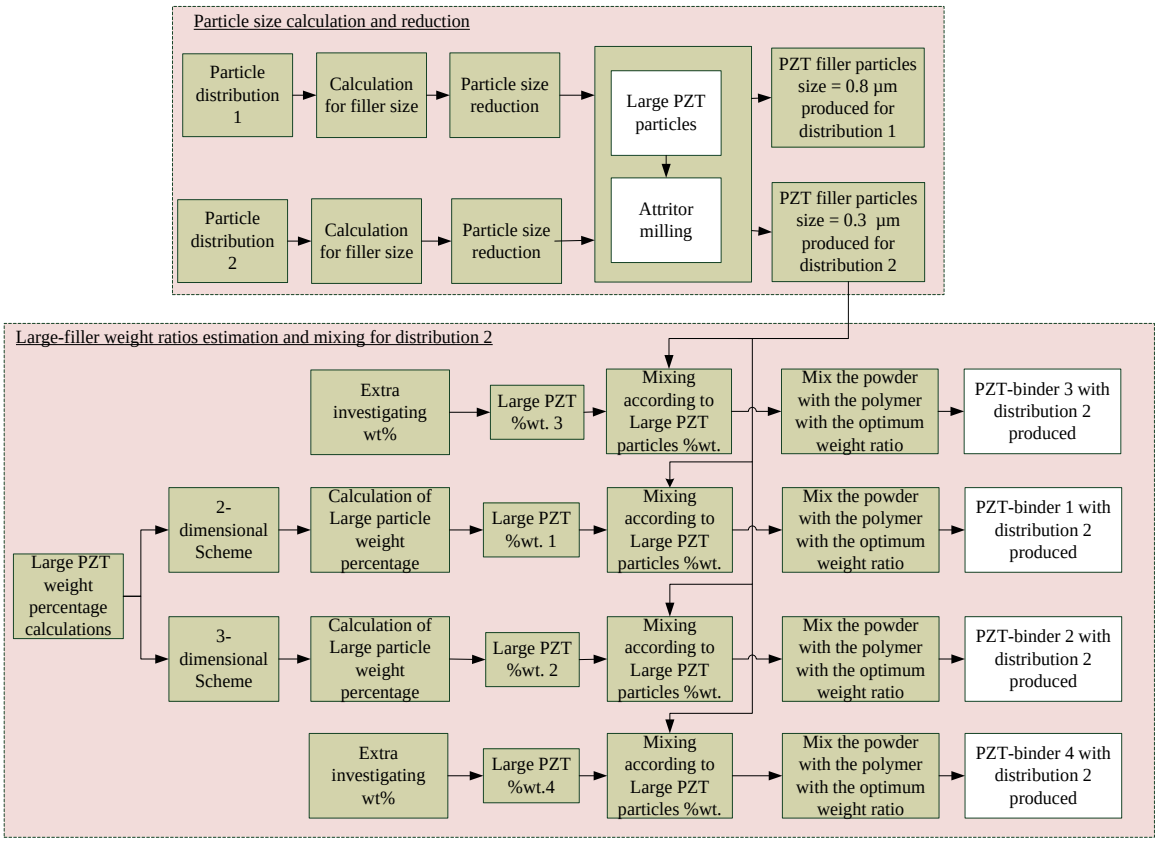

Figure 6-2: Production and investigation process flow of the PZT-binder composites when particles distribution 2 is adapted as an example. The same process flow is followed for distribution 1

6.4 Analysis of the PZT Particle Sizes and Weight Ratios

The difference between the 2- and 3- dimensional representations is that in the calculations of the number of the SFPs that can fill the gap between the large PZT particles, either area (2-dimensional representation) or volume (3-dimensional) is considered in the calculations. However, the 2- dimensional representation does not completely fill the gap around the large particle which means more SFP particles may surround the large PZT particle and increase the weight loading against large PZT particles.

To calculate the weight ratios between the large particle and SFP, the mass of each particle is necessarily obtained. Figure 6-3 shows the procedures taken to calculate the large PZT particles to SFPs weight ratio for any type of distributions with the aid of 2- and 3-dimensional representations. Extrapolation between the ratio of the particle numbers and the masses of each particle ideally present the weight ratios between large particles and SFPs. However, if filling the whole gap between the large particles is desired, this weight ratio is changed. The change only occurs with a factor of R_F (which is the maximum SFPs number that can fill the entire gap between the large particles). This factor is only multiplied by the weight load of the filler, M_{F1}, giving the final weight ratio between large particles and SFPs. The R_F factor can be calculated in terms of the area (2-dimensional representation) or in terms of the volume (3-dimensional representation).

For the 2-dimensional representation, the R_F factor can be calculated with the aid of the outer square A_{seq} or the triangle A_{tri} areas (for distribution 1 and 2, respectively), the area of the large particle A_L and the area of the SFP A_F. However, for the 3-dimensional representation, the R_F factor can be calculated with the aid of the volume of the outer cube V_{cub} or the prism V_{psm} (for distribution 1 and 2, respectively), the volume of the large particle V_L and the volume of the SFP V_F.

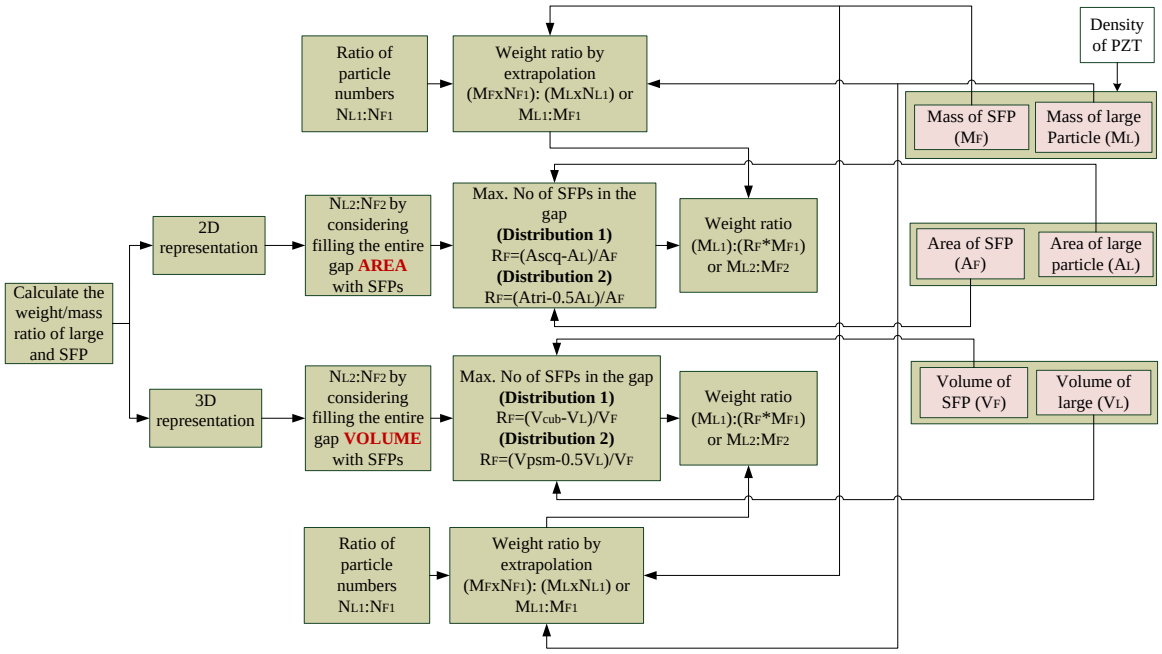

Figure 6-3: Determining the large particle to SFP weight ratio for any type of distributions

Following every step in the process flow in Figure 6-3, the estimated large PZT particles to SFPs weight ratios are obtained for the 2-and 3-dimensional representations. The original ratio only considers the number of the SFPs that surrounds the large particles. However, the updated ratio considers the number of the SFPs that can fully fill the gap between the large particles. The updated ratio is updated by multiplying the R_f factor by the SFP term in the original ratio. Table 6-1 shows the calculations in steps starting from the estimation of the SFPs size to the calculations of the large PZT particles content by weight for all representations and distributions.

Parameter		**Distribution 1**		**Distribution 2**	
Representation		**2D**	**3D**	**2D**	**3D**
Optimum SFP size (µm)	d_{SFP}	0.8		0.3	
Number of SFPs surrounding large particles	N_F	4	6	6	6
Number of large particles surrounding SFP	N_L	4	2	2	2
Ratio of No. Large Particles : SFPs	$N_{L1} : N_{F1}$	1:1	1:1	1:2	1:2
Number of fillers to fully fill the gap	R_F	1.71	14.2	2.28	96.88
Updated Ratio of No. Large Particles : SFPs	$N_{L2} : N_{F2}$	1:1.71	1:14.2	1:4.56	1:193.76
Updated weight ratio Large : Filler	$N_{L2} : N_{F2}$	9:1	1.1:1	65:1	1.52:1
Large PZT particles wt%		90	52	98.6	60.4
SFPs wt%		10	48	1.4	39.4

Table 6-1: Summary of the large PZT particles to SFPs weight ratios calculations

6.5 PZT Powder Milling

Powder milling depends on some variables that control the process. The most important variables are listed in Table 6-2. The type of milling method is mainly dependent on the nature of the milling and quantity of the powder. The filter of the milling machine depends on the size of the particles and the beads which are used to grind the powder. Controlling the milling process speed, and hence the grinding energy, is essential and should be optimised. Higher speeds may cause particle agglomeration as the milling energy is typically transferred to the surface of the particles. This energy occurs via the shear and impact forces and increases the surface energy of the particles, increasing the attraction force between resulting in particle agglomeration. The grinding medium (beads) must have a higher density and be harder than the powder to be milled.

Parameter	Description
Type of the mill	It depends on the type and quantity of the powder, size of milling powder and final shape of the particle.
Milling speed	The higher the speed, the higher the milling energy input due to the impact of the powder and beads.
Milling time	Milling time is carefully controlled otherwise the particles will be milled too much and the desired particle size will not be reached.
Grinding medium	The grinding medium or beads is the key element in the milling process The grinding medium must have a higher density than the powder to be milled.
Bead-to-powder ratio	Suitable range of powder needs to be chosen.

Table 6-2: Most important milling process parameters [144]

Figure 6-4 shows a schematic that depicts the milling process and the specific NETZSCH Microcer bead mill used in this work. The milling process is basically achieved by pouring the powder and the dispersing agent in the container. The mixture is pumped through the pipes to the milling drum where the grinding beads are placed. When the drum is rotated at a certain speed the beads will cause an impact and shear forces on the powders, which produce a reduction in the particle size. The milled particles are pumped out of the drum through the filter, which separate the beads and un-milled powder from the milled powder. The mixture is fed back again into the container completing one milling cycle. This process is continued for as many cycles as necessary until the desired particle size is achieved.

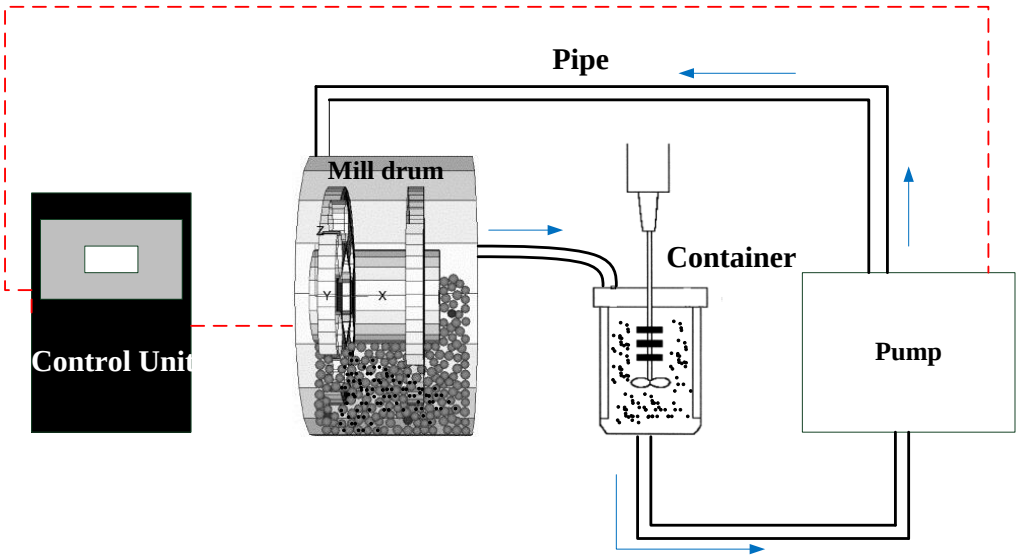

(a)

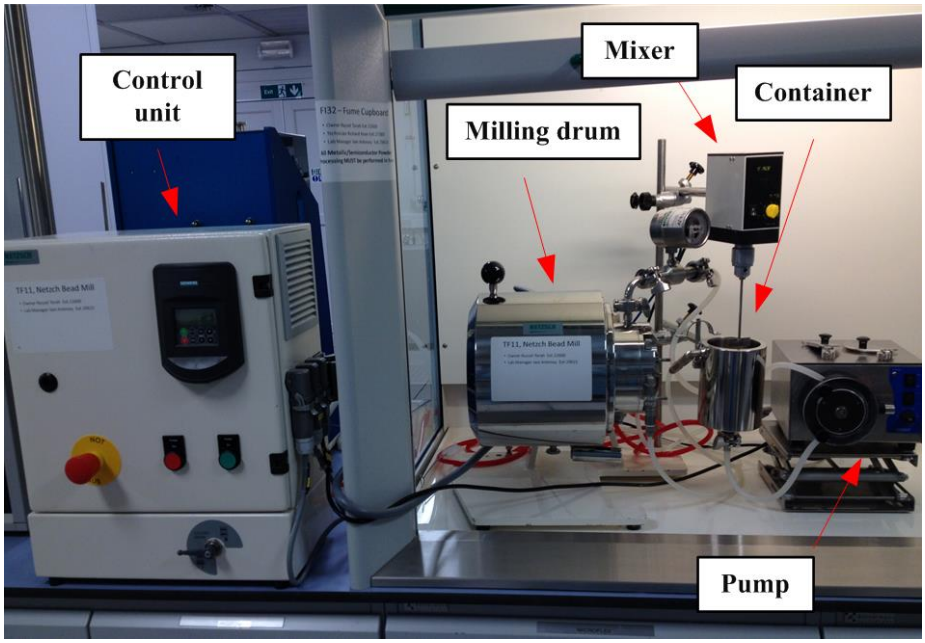

(b)

Figure 6-4: Schematic of attritor mill process. (b) NETZSCH Microcer attritor/bead mill that was used for milling the 2 µm PZT powder into 0.8, 0.3 and 0.15 µm in this work

6.5.1 Milling Process of PZT Powder

For achieving every SFP size (0.8, 0.3 and 0.15 µm), the 2 µm PZT particle size powder was mixed with the deionised water and Ammonium Polyacrylate dispersant agent (DARVAN 821A) with quantities shown in Table 6-3. Adding the dispersant was essential to inhibit the agglomeration and keep the dispersion of the PZT particles homogenous in the mixture during milling process. The mixture was then placed in a beaker inside an ultrasonic bath for 15 minutes

to further aid the PZT powder dispersion in the deionised water-DARVAN mixture. This reduces the blockage of the milling drum filter and helps to ensure that all the particles were milled evenly.

The milling process was prepared by putting 50 ml of beads in the milling drum. Also, the filter was used to separate the milling powder from the beads and was placed at the drum outlet. The powder and the dispersant mixture were poured in the container and the mixer was used to homogenize the mixture during milling. The rotation speeds of the drum and milling time that were used for each particle size are shown in Table 6-3. It was found that increasing the speed of the drum over 2000 rmp, increases the particle size which was a sign of agglomeration. The maximum speed used was 1960 rpm and according to this speed, the milling time was optimised of each particle size. After reaching the desired particle size, the milling process is stopped and the PZT powder plus deionized water-DARVAN mixture was removed from the container. The mixture was left at room temperature for 3 days to evaporate the water and dispersant.

Item	**Parameter**	**SFP size**		
PZT powder	**Particle size (µm)**	**0.8**	**0.3**	**0.15**
	Quantity (g)	175	175	175
Beads	**Type**	Zirconox	Zirconox	Zirconox
	Size (µm)	500	500	500
	Quantity added (ml)	50	50	50
Filter	**Size (µm)**	100	100	100
Milling Machine	**Speed of the drum (rpm)**	1960	1960	1960
	Milling time (min)	10	40	70
Grinding medium	**Mixture**	Deionised water + DARVAN 821 Mixing ratio (49:1 by weight)		
	Quantity (ml)	50		

Table 6-3: Milling process parameter for reducing the particle size from 2µm to 0.8, 0.3 and 0.15µm SFPs

The sizes of the PZT powders (SFP powders) were measured using a Malvern Mastersizer 2000E and Malvern Zetasizer Nano. The 2 µm and 0.8 µm PZT particles were measured with the Mastersizer. However, the 0.3 µm and 0.15 µm PZT particles were measured by using Zetasizer Nano. The Zetasizer was used because it can give more accurate results compared to the Mastersizer with particle sizes below 0.5 µm.

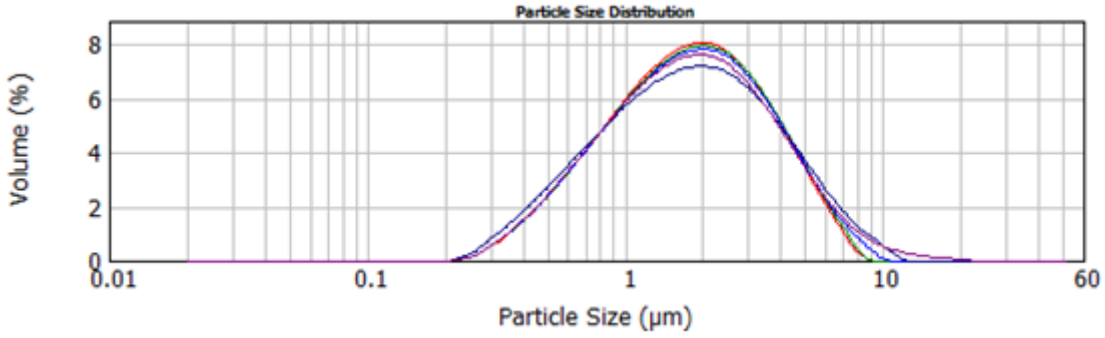

(a)

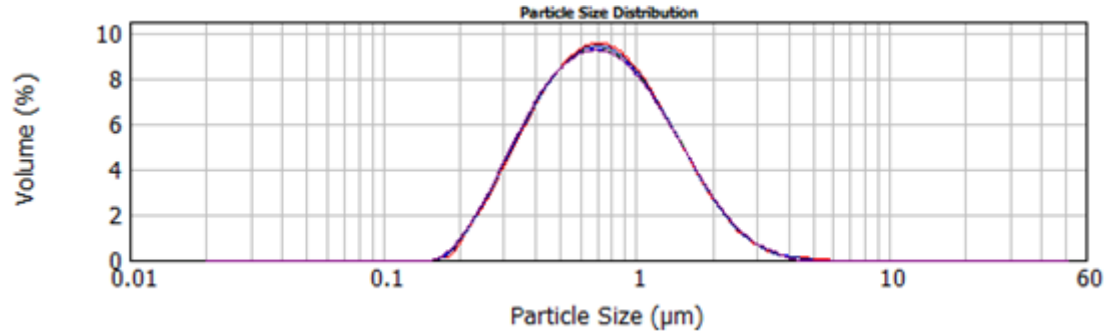

(b)

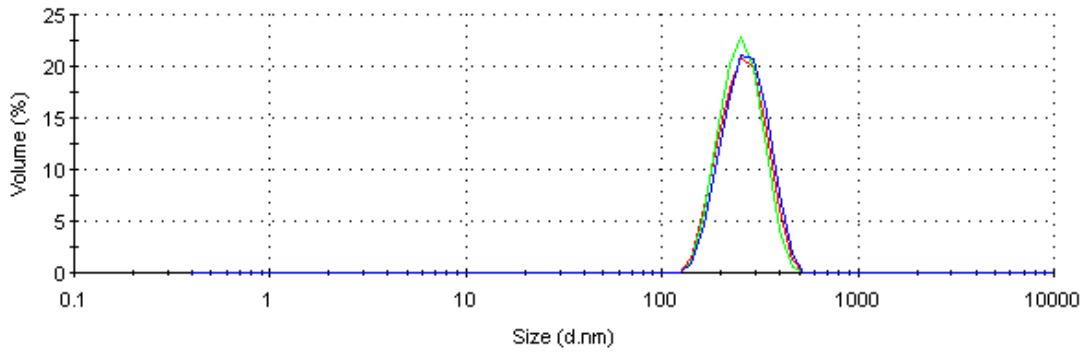

(c)

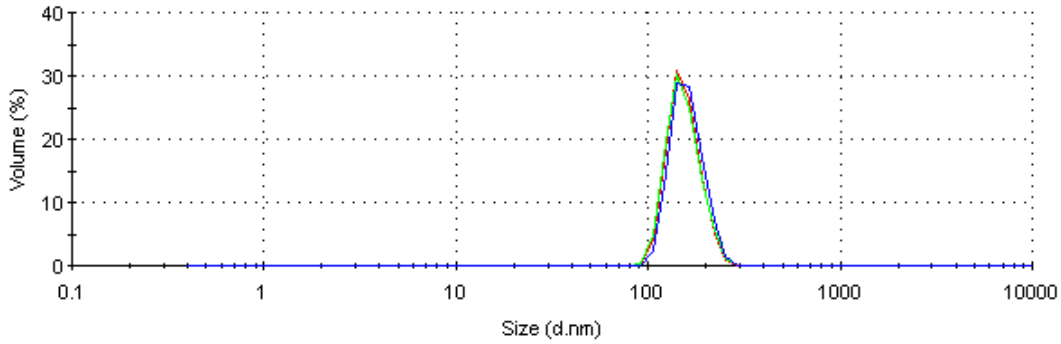

(d)

Figure 6-5: Particle size distribution for (a) the large 2µm particle (b) 0.8 µm (c) 0.3 µm and (d) 0.15 µm SFPs

For distribution 1, Figure 6-5(a) and (b) represent the particle size distributions of the large and SFP particles, respectively. In Figure 6-5(a), the 2 µm PZT particles occupy only 8% of the volume. However, the rest of the particles are either above or below this size with different percentages of volume occupancy. Similarly, from Figure 6-5(b), the 0.8 µm SFP particles occupy only 9% of the volume. Ideally, the large 2 µm PZT particles that occupy 100% of the volume are mixed with the 0.8 µm PZT filler according to the estimated mixing ratio shown in Table 6-1.

However, practically, the actual 0.8 µm particles will fill the gaps of the actual 2 µm which both are the majority when they are properly mixed together in the polymer. However, the larger particles of the SFPs in Figure 6-5(b) (≥ 0.8 µm) will fill the gaps of the larger size particles (≥ 2 µm) observed in Figure 6-5(a). The same concept applies for the lower particle sizes of both Figure 6-5(a) and (b). The lower particles for the SFPs (≤ 0.8 µm) in Figure 6-5(b) will fill the gap between the lower size particles (≤ 2 µm) in Figure 6-5(a).

In this case, the estimated mixing ratio by weight will change according to the particle size distribution of both the large particle (2 µm) and the SFP (0.8 µm). The same concept applies for distribution 2 when using the 2 µm large particle and 0.3 µm SFPs that their particle size distributions shown in Figure 6-5(a) and (c). Therefore, investigating different large PZT to SFP weight ratio is essential to find the suitable weight percentage that improves the density of the film and accordingly improve the piezoelectric properties.

6.6 Experimental

As suggested from the analysis in section 6.4, the large to SFP particles weight ratios were mixed. ECS-PolyPZT 2a and 6a were used in this investigation. The investigation began with milling the 2 µm PZT particle size powder down to the targeting filler sizes (0.8, 0.3 and 0.15 µm). The 0.8 and 0.3 µm represent distributions 1 and 2, respectively. The 0.15 µm was chosen to observe the effect of the piezoelectric properties when filling the gap between dominant large particles with PZT particles smaller than the suggested filler sizes 0.3 and 0.8 µm. Usually, the estimated SFPs weight loading of the 3-dimensional representation is greater than the 2-dimensional one. As the size of each targeting particle is not practically 100% at a fixed size (for the 2 µm large particle and the suggested SFPs 0.8 and 0.3 µm), the estimated large PZT to SFP weight ratio may vary as discussed in section 6.5.1. Accordingly, exploring different SFP loading (by adding additional investigating weight percentages as described in Figure 6-2) is essential to find the improved large PZT particle to SFP weight ratio that improves the overall piezoelectric properties of the film.

After milling each of the powders, the large PZT powder to SFPs was first mixed according to the weight ratios shown in Table 6-4. Each of these mixtures was separately blended according to PZT-binder weight ratios of ECS-PolyPZT 2a and 6a. The blended pastes were separately mixed using a SpeedMixer DAC 150 and then triple roll milled. They were then screen-printed on alumina substrates.

Arrangement type	SFP size (µm)	Large particle wt %	Large particles to SFPs weight ratio
None	-	100	-
SFP	0.8	90	9:1
		82	4.5:1
		75	3:1
		62	1.63:1
	0.3	98.6	65.1
		80	4:1
		60	1.52:1
MFP	0.15	90	9:1
		82	4.5:1
		75	3:1
		62	1.63:1

Table 6-4: The formulations are listed with their references numbers and their corresponding large PZT-filler weight ratios. These reference numbers are common for both ECS-PolyPZT 2a and 6a

6.7 Results and Discussion

Four devices were poled with the optimum poling conditions for each formulation given in section 5.3 on page 96. Five measurements were taken for each device, producing 20 d_{33} readings for each formulation. The results in Figure 6-6 are the average d_{33} measurements that were obtained when mixing the 2 µm with the 0.8 µm SFPs and the polymeric binder. Also, the results show the d_{33} measurements when mixing the 2 µm PZT particles with the polymeric binder without any filler (no-filler arrangement) as shown in Figure 6-1.

Figure 6-6 shows that there is a trend in d_{33} measurements when increasing the SFP weight loading (when mixing the material with 0.8 µm SFPs) in both ECS-PolyPZT 2a and 6a films. The maximum achieved d_{33} value was 36 pC/N for both ECS-PolyPZT 2a and 6a films at large PZT particles to SFPs weight ratio of 4:1. A reduction in the d_{33} values occurred after this weight ratio when decreasing the large dominant PZT particles content. Mixing the large PZT particles to SFPs with weight ratio 4:1 increased the d_{33} by 16.6% compared to no-filler mixture.

There is a specific amount of SFPs that can help increase the density of the material. However, from section 2.4.3.1 on page 26, it was confirmed that reducing the PZT particle size in the piezoelectric film can cause a reduction in the d_{33} values. Therefore, SFPs weight loading can be carefully added into the composite but not on the account of the piezoelectric activity of each PZT particle. Accordingly, the specific SFPs weight loading was explored to increase the density of the film but also to determine if the reduction of the PZT particle size would affect the whole piezoelectric activity of the film.

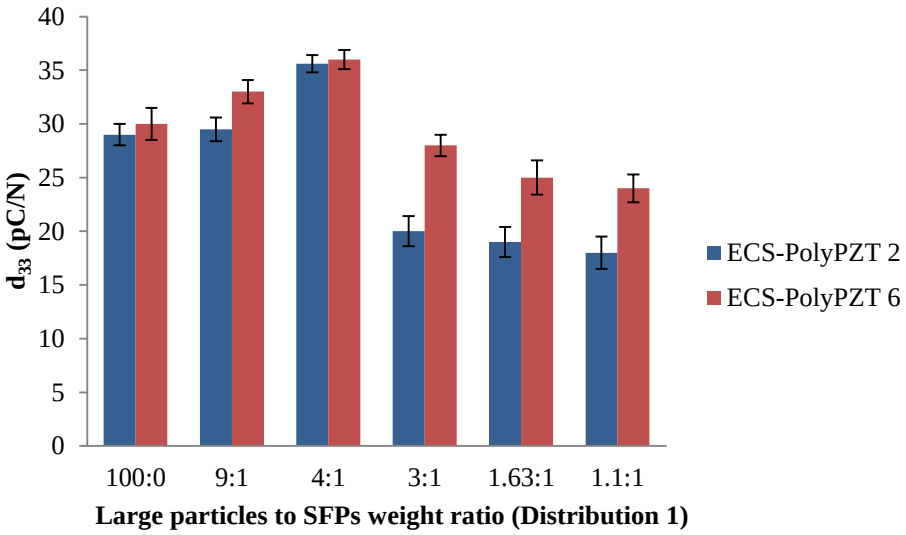

Figure 6-6: d_{33} values of ECS-PolyPZT 2a and 6a when adding SFP powders for distribution 1. Note, the d_{33} measurement were obtained when the films clamped on alumina substrates

Similarly, there was a similar trend in the d_{33} values when mixing the PZT particles with 0.3 µm SFPs. The d_{33} values increased up to 30 and 33 pC/N for ECS-PolyPZT 2a and 6a, respectively, at large particles to SFPs weight ratios of 4:1 as shown in Figure 6-7. The d_{33} measurements were generally reduced compared to the 0.8 µm SFP formulations. However, the d_{33} values were slightly improved compared to no-filler arrangement results (100% large PZT particles by weight). This improvement was for the SFPs weight loading in between the large PZT particles to SFPs weight ratio 4:1 and 65:1.

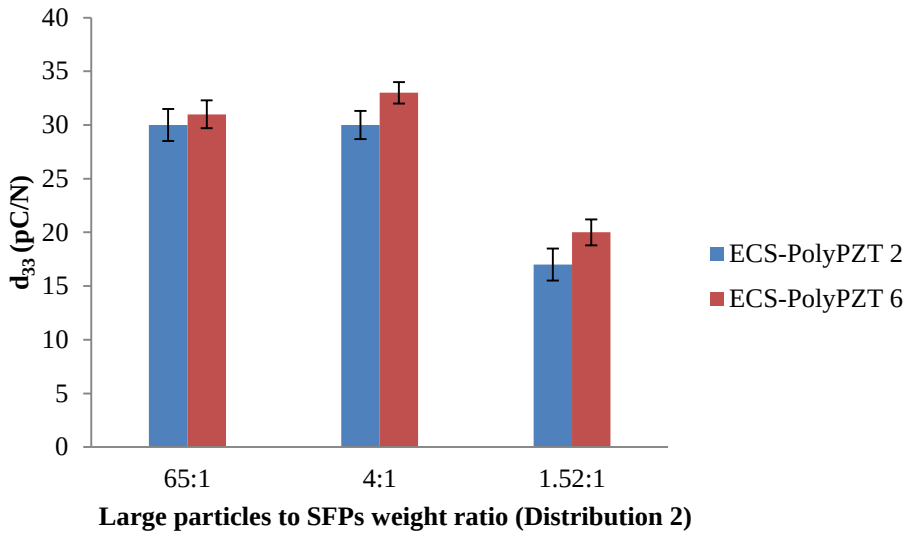

Figure 6-7: d_{33} values of ECS-PolyPZT 2a and 6a when adding SFP powder. The devices printed on alumina substrates. Note, the d_{33} measurement were obtained when the films clamped on alumina substrates

The limitation of the SFP particle size reduction can be confirmed when using MFPs in distribution 1. Instead of filling the gaps between the large particles with 0.8 µm, the multiple 0.15 µm filler particles filled this gap. The result is smaller filler size but with the same large to filler weight ratio. The results in Figure 6-8 showed the same trend as before but with d_{33} values even lower than the no-filler piezoelectric films. This confirms that there is a limit to lowering the filler size or the piezoelectric properties will be worse.

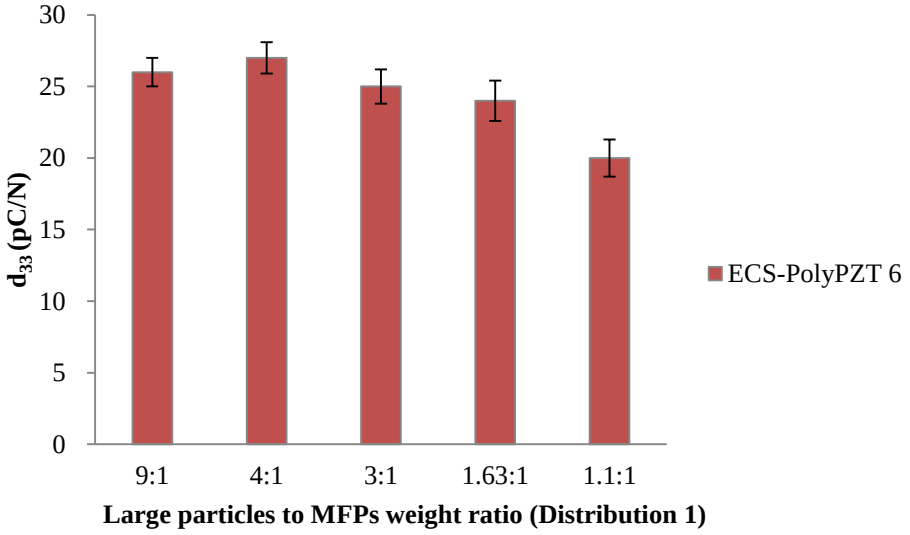

Figure 6-8: d_{33} values of ECS-PolyPZT 6a when adding MFP powder. The devices were printed on alumina substrates. Note, the d_{33} measurement were obtained when the films clamped on alumina substrates

6.8 Conclusions

Using filler particles is essential to improve the piezoelectric properties of screen-printed piezoelectric film. The similar trend in the d_{33} measurements resulted when changing the weight loading of SFPs inside the mixture for both ECS-PolyPZT 2a and 6a confirmed the reliability of the results. The results showed a 16.6% maximum increase in d_{33} at large PZT particles to SFPs weight ratio of 4:1 when distribution 1 was adopted compared with no-filler PZT mixture. The maximum d_{33} achieved at this PZT particle ratio was 36 pC/N for both ECS-PolyPZT 2a and 6a. Distribution 2 showed lower d_{33} values because the filler is smaller (0.3µm particle size). However, a slight improvement was achieved compared to no-filler mixtures for SFP loading between the large PZT particles to SFPs weight ratios 4:1 and 65:1.

When reducing the particle size down to 0.15 µm and using the MFP arrangement, the d_{33} values were reduced below even the no-filler arrangement films. This shows that there is a limit to lowering the filler size and further optimisation is required. Improving the packing density of the film is important and can improve the piezoelectric properties. However, the piezoelectric properties are also defined by another factor which is the overall particle size of the PZT powder (large and filler particles). Increasing the particle size of the powder increases the piezoelectric activity of the material. Therefore, there is a compromise between improving the density by inserting filler and increasing the overall particle size of the PZT powder (for both the large particles and the fillers).

Chapter 7: Effect of Cold Isostatic Pressing on Dielectric and Piezoelectric Properties

7.1 Introduction

Most thick film composites with 0-3 connectivity suffer from porosity which can affect mechanical (e.g. density), dielectric and piezoelectric properties (e.g. dielectric and piezoelectric constants) [145]. Figure 4-10 on page 84 is an example of a printed film that suffers from air-voids. This chapter investigates the effect on the screen-printed piezoelectric composite of the application of a homogenous pressure in order to compress the film matrix and potentially reduce voids. This pressure has been applied using Cold Isostatic Pressing (CIP) and Figure 7-1 shows the experimental plan that was followed.

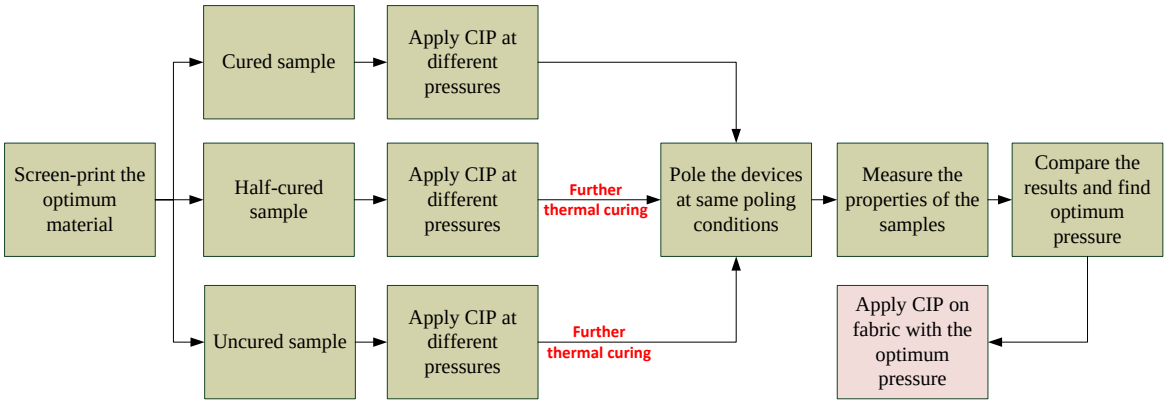

Figure 7-1: Experimental plan of improving the properties of the film using CIP

7.2 Eliminating Air Voids

For piezoelectric composites that have PZT loading over 50% by volume, the number of air voids increases with the increase ceramic weight loading [133]. Applying high pressure on the material can be a solution to improve the material properties which can be achieved by Isostatic Pressing. CIP can be done at room temperature, however, the other types such as warm and hot isostatic pressing are achieved at temperature over 100 °C which may affect our materials properties. CIP increases the density of the printed film by removing the air voids. The CIP process permits complicated shapes structures to be compressed without deformation [146].

Table 7-1 shows the most important contributions of using the CIP process on improving the properties of the piezoelectric materials. One study introduced the effect of CIP process on the

piezoelectric activity of a thick-film high temperature PZT film on alumina substrate [147]. The investigation did consider the dielectric and piezoelectric properties of the printed film. Lakhmi et al., [98] used CIP to improve the sintering process of the screen-printed PZT layers for a cantilever structure. They investigated firing temperature of 850, 900 and 950 °C but did not include the dielectric and piezoelectric properties before and after applying CIP. Lee et al., [148] explored the use of CIP in eliminating the cracks of thin film of 0.5 wt% ZnO-doped 0.2Pb ($Zn_{1/3}Nb_{2/3}$)O_3-0.8Pb ($Zr_{1/2}Ti_{1/2}$)O_3 (PZN-PZT) during sintering. There is no contribution of the effect of the CIP process on the low temperature flexible piezoelectric composite film on flexible substrates such as Kapton and woven-fabrics. Also, the influence of both the curing temperature of the sample and the applied CIP pressure and their effect on the mechanical, dielectric and piezoelectric properties of the materials were not investigated before.

Material	Comments	Ref.
Thick-film PZT film on alumina substrate	• The d_{31} was improved by 32 % • Poling method was not mentioned. • They Used rubber mould to protect the sample from the pressing medium.	[147]
Thick-film free-standing PZT film	• Investigated the improvement of sintering process by applying CIP. • The effect on the d_{33} measurements was not investigated.	[98]
Sol-gel coating of PZN-PZT discs with 2 mm diameter	• They studied the effect of the CIP process on reducing the number of cracks during sintering process. • The effect on the d_{33} measurements was not explored.	[148]

Table 7-1: Contributions of the effect of the CIP process on improving the properties of the high temperature piezoelectric materials

7.3 Description of Cold Isostatic Pressing (CIP) Process

Basically, the CIP machine (CIP-15, MTI Corporation USA) used for reducing the printed film porosity comprised of a pressure vessel for the pressurising medium and a movable die. The die pressurises the oil inside the container as shown schematically in Figure 7-2(a) resulting in the application of a homogenous pressure to the sample that compresses the higher density components (PZT particles and polymer) pushes the lower density bits out the film (e.g. air). Figure 7-2(b) shows the CIP-15, MTI Corporation USA machine used and its specification is given in Table 7-2.

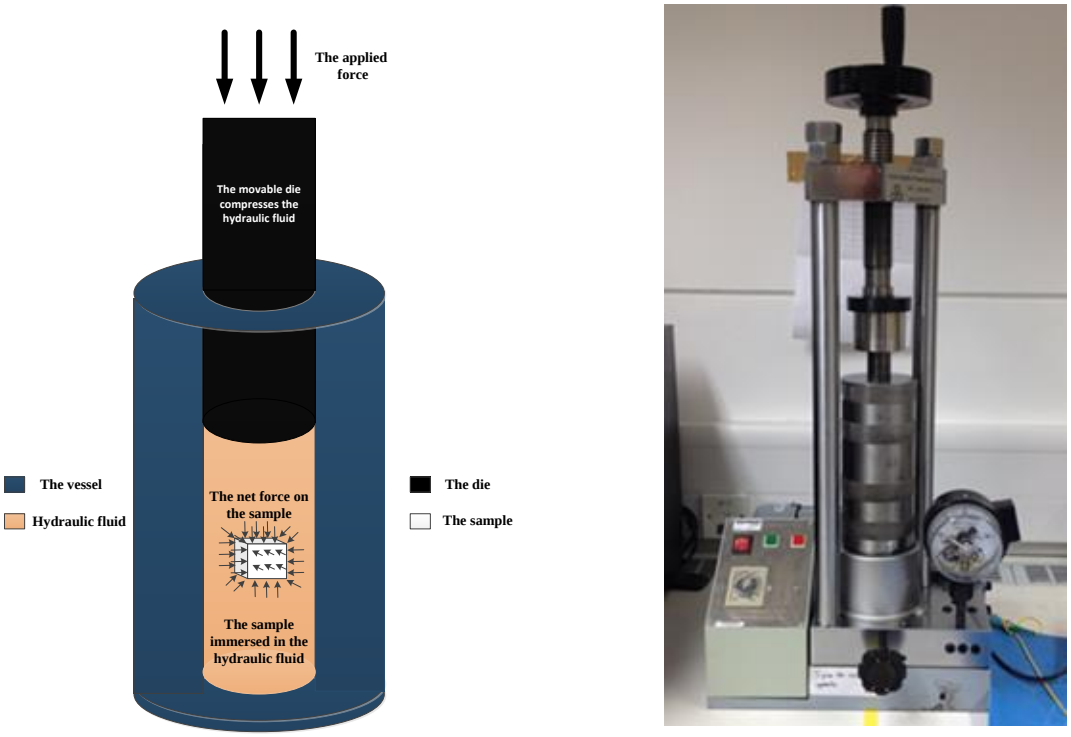

(a) (b)

Figure 7-2: (a) Schematic diagram showing the process of CIP on a sample immersed in a liquid. (b) The CIP-15, MTI Corporation USA machine

The hydraulic oil is placed in the container shown in Figure 7-3(a) and the moveable die inserted. Figure 7-3(b) shows the pressure gauge which is adjusted before applying CIP. The CIP operation can be applied at a temperature range of 10-40 ºC.

Specifications	**Value**
Maximum pressure in the container (MPa)	300
Maximum applied time (min)	5
Container/vessel dimensions	22 mm dia. × 90 mm height
Operation temperature (ºC)	10-40 ºC

Table 7-2: Technical specification of the CIP provided from the supplier

(a) (b)

Figure 7-3: (a) The sample is placed in the vessel that is partly filled with hydraulic oil and the die shown on the right inserted. (b) The pressure gauge is for adjusting and controlling the applied pressure

7.4 Devices Fabrication

The ECS-PolyPZT 6a was printed on Kapton devices and cured for different curing times at 90 °C producing a range of samples denoted fully-cured, half-cured and uncured as shown in Table 7-3. The uncured film is typically more flexible than the fully cured one. Therefore, it was essential to investigate the effect of the CIP under the different curing conditions.

Curing condition	**Curing time (min)**	**Curing Temperature (°C)**
Fully cured	8	90°C
Half-cured	5	
Uncured	2	

Table 7-3: Different curing conditions of the printed films on Kapton

7.5 Preparation of the Sample

Immersing the sample in the hydraulic oil and applying CIP without protection may cause contamination and a change in the film properties. Typically a mould or a protective layer shielding the sample from the pressing medium is used. All the previous investigations of the use of the CIP method to improve the properties of piezoelectric ceramics use rubber bags [149] or spin-coated polymethylmethacrylate (PDMS) [150] to isolate the sample from the hydraulic oil. The protection method should satisfy these criteria:

- It can be deposited and covers the whole sample.
- Simple fabrication method (i.e. applying the protection method on the sample).

- Simply removed from the sample after CIP.
- Do not react with the sample specially the PZT-binder film or cause a shape deformation when applying CIP.
- The protection layer must withstand higher pressure and does not leak.

Rubber bags require the air to be removed and if this is not done properly can negatively affect the distribution of the pressure across the sample. Also, the processing of PDMS on the surface of the sample can affect the sample properties and also may require post-processing for removal. Depositing this material requires an unnecessarily complex process. There are many deposition methods to create a protection layer on the top of the piezoelectric devices such as spray [151], spin-spin coating [152] which requires chemical processing (adding a solvent to the uncured PDMS) to make the PDMS in a liquid form. The solvent phase in the PDMS mixture may react with the printed layers of the piezoelectric device. However, the challenge comes after depositing the PDMS layer particularly when removing this layer. The removal of this layer requires chemical processing and can harm the printed layer underneath. This section suggests and investigates some alternative methods that may be suitable for protecting the sample and satisfy the criteria. These methods have not been used before to protect the flexible piezoelectric material printed on flexible substrates such as Kapton.

The first type of mould was a Teflon substrate (TEFLON 200A, KATCO). The Teflon substrate has a thickness of 50 µm and was placed on the top surface of the sample (i.e. on the side where the capacitive structure was printed). The use of Teflon film was required to prevent sticking to the surface of the sample to the alumina as shown in Figure 7-4(a). Alumina substrates assure the straightness of Teflon film over the sample. The sample, Teflon substrate and alumina substrates were all wrapped in a strong adhesive tape to protect the whole sample from oil leakage into the sample. Another method to protect the sample was to by cover the sample with a polyvinyl chloride PVC film. PVC film with an average thickness of 10 µm was wrapped 4 times around the sample (Figure 7-4(b)). After CIP process, the PVC film was removed easily from the sample.

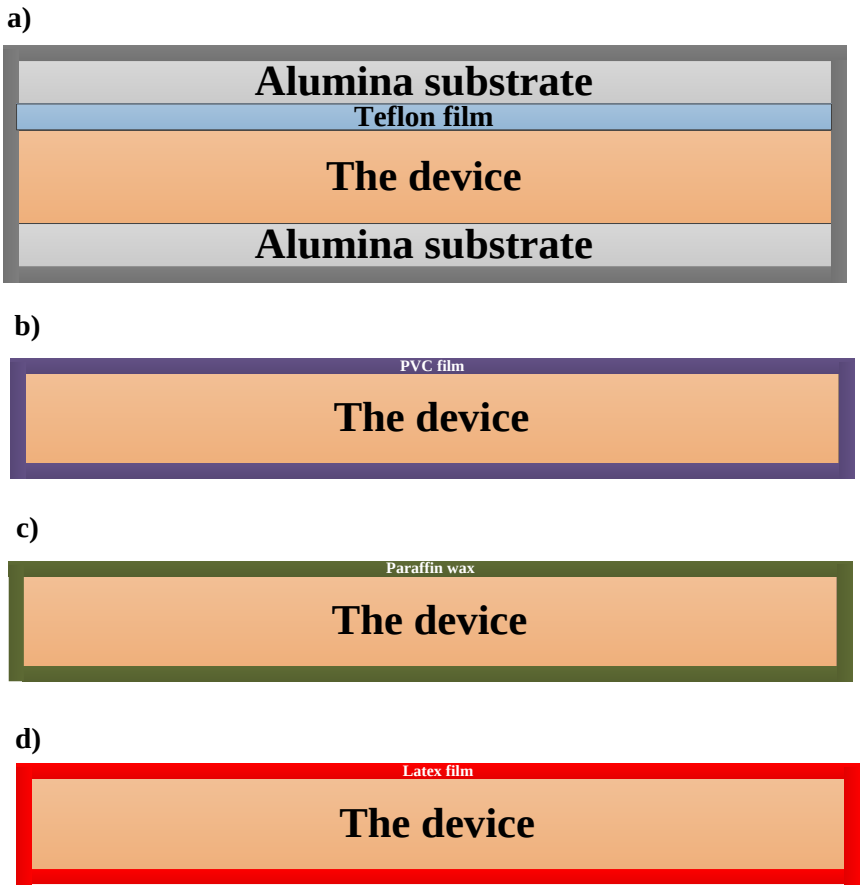

Figure 7-4: Schematics of the four types of molds used for protecting the samples. (a) Teflon film was placed on the top of the sample. The other side of the sample (kapton substrate side) was left without Teflon as Kapton substrate already protects the sample. (b) PVC film wrapped the sample four times for protection. (c) Paraffin wax. (d) Latex film

Protecting the sample by paraffin wax method was also evaluated. Paraffin wax comes in a solid form and requires heating above the melting point (47-65 ºC) to be in a liquid form. Figure 7-5 shows the process flow for covering the sample with paraffin wax. The process is described as follows:

1. The process was started by covering a cylindrical container that has dimensions of (diam.5.5 cm × height.0.8 cm) with aluminium foil. This aluminium foil acted as an interface between the paraffin wax and the container.
2. The container was heated up above the melting point of the wax 70ºC. This temperature is blow the curing temperature of the PZT-binder film and melting points of most of the woven fabrics.
3. Then, a 2 g of paraffin wax was placed in the container and left for 2 minutes until it completely melted.

4. The sample was submersed in the liquid paraffin wax and all covered in wax in 5 seconds.
5. As soon as the sample was covered with the wax, the container was allowed to cool in air dried. A 200 µm layer of wax was created on the top surface of the sample. To make sure that most of the wax was solidified, the sample was cooled down for 3 minutes at 4 ºC.

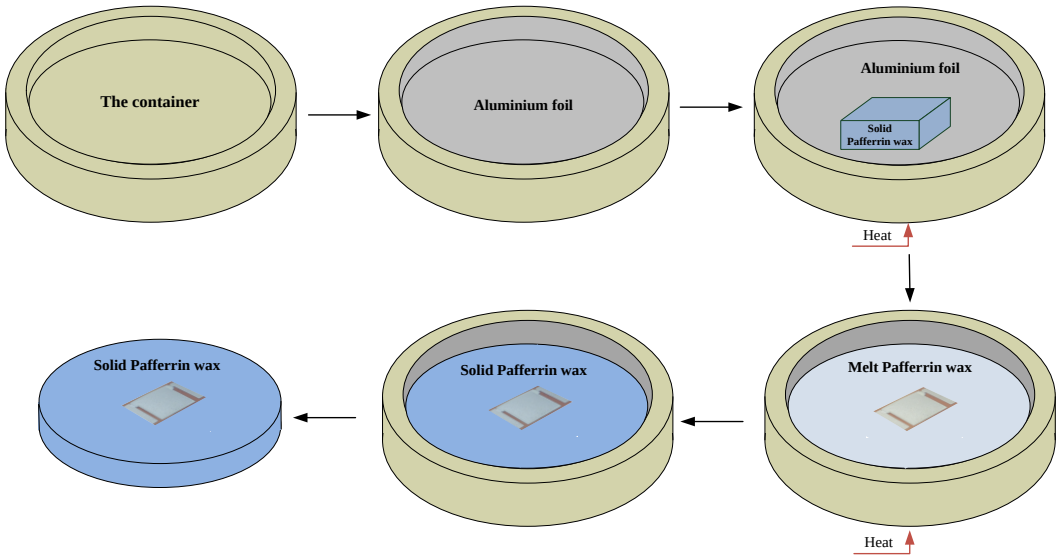

Figure 7-5: A schematic shows the process of covering the device with paraffin wax

Finally, a latex bag was used as an example of rubber bags to demonstrate the negative effect of this approach for protecting of samples during CIP. The latex bag has a feature of expanding under high pressure. The four techniques were evaluated by measuring their effect on the piezoelectric activity and the satisfaction of the criteria given earlier. Table 7-4 generally compares the four techniques. The CIP process was conducted at a pressure of 166 MPa for 2 minutes.

Conditions	**Protection method**			
	Teflon+alumina+tape	**PVC film**	**paraffin wax**	**Latex bag**
Covering the whole sample	Good	Very good	Excellent	Good
Simple application	Very good	Excellent	Excellent	Excellent
Simple removal process	Very good	Excellent	Excellent	Excellent
React with the printed layers	No reaction	No reaction	No reaction	No reaction
Withstanding pressure without leakage	Excellent	Good	Excellent	Very good
Shape deformation	Not observed	Observed	Not observed	Observed

Table 7-4: Comparison between the proposed protection methods with respect to the conditions that has to be satisfied

The best way to cover the whole sample is by using the paraffin wax. When melting the paraffin wax and immerse the sample in it, the liquidised wax covers the whole sample. The other techniques may leave air that may exist between the sample surface and the protection layer. This air may cause shape deformation in the capacitive structure as shown in Figure 7-6.

(a) (b)

Figure 7-6: Shape deformation of the devices after applying CIP at 166 MPa for the devices protected by (a) PVC film and (b) latex bag

This air created spots where the applied pressure was not equal to the container pressure. This difference in pressure in different places on the sample creates the deformation on the sample. Using paraffin wax or the flat Teflon substrate can guarantee a flat continuous contact area between the sample and the hydraulic oil. PVC film, paraffin wax and latex bag methods can be applied and removed easily to the sample compared to Teflon substrate considering the number of layers (or substrates) applied.

The dielectric constant and d_{33} of the sample (poled with DCP at poling conditions E = 3.7 MV/m, T = 90°C and t = 6 min) were measured before and after applying these protection methods. Note, the d_{33} measurements were obtained when the films clamped on Kapton substrates. For the devices with shape deformations as shown in Figure 7-6, the d_{33} measurements were taken from the places that no deformations were found. The average dielectric constant and d_{33} values after paraffin wax removal (without applying CIP) were 143 and 39.2 pC/N respectively. These dielectric constant and d_{33} values are actually close to the original ECS-PolyPZT 6a without CIP-processing.

Also, the sample was put unprotected in the hydraulic oil without applying CIP. The dielectric constant and d_{33} were measured after the sample was the removed from the oil giving 140 and 37 pC/N, respectively. From these results, the oil has a small effect on the dielectric and piezoelectric properties that may increase when applying CIP. The oil in its liquid phase may penetrate the PZT-binder at higher pressure affecting the properties.

The poling process was found to be unstable (i.e. sparks and complete short-circuiting during poling) for devices used paraffin wax and without protection. Decreasing the poling temperature was found to stabilise the poling process after the CIP process. At a temperature of 75°C, a stable

poling process was found. Table 7-5 shows the d_{33} measurements of the samples on Kapton protected with the four methods and without protection after applying a CIP pressure of 166 MPa for 2 minutes.

Protection method	**ε_r**		**d_{33} (pC/N)**		**** Poling temperature**
	Before	After	Before	After	**T (ºC)**
Without protection	146	190	40	42	75
Latex film		*		38	90
PVC film		*		38	90
Alumina		160		40.13	90
Paraffin wax		208		44.88	75

* ε_r measurements were not possible because of shape deformation

** Poling field and time were 3.7 °C and 6 minutes, respectively

Table 7-5: Comparison between the protection methods for dielectric constant and d_{33} values before and after applying CIP at 166 MPa pressure for 2 minutes

The results showed an increase in d_{33} up to 42 and 44 pC/N for devices without protection and those protected with paraffin wax, respectively. Applying CIP for the devices without protection contaminates the samples and substrate (i.e. particularly when dealing with fabric substrates) and therefore paraffin wax was chosen as the best way of protection that can be used for flexible PZT-binder films when CIP is applied. The next stage is to investigate the dielectric and piezoelectric properties when varying the CIP pressure and time.

7.6 Dielectric and Piezoelectric Properties

CIP process conditions are specified by the two main parameters; the pressure inside the container P_{CIP} and the duration time t_{CIP}. These parameters were optimised by measuring the d_{33}, dielectric constant and resistivity of the films. Three devices were used for each pressure and five d_{33} measurements were taken from device giving a reading of 15 measurements for each CIP pressure and curing condition for fully, half and uncured samples.

7.6.1 Investigating the Effect of the Pressure

It was found that there is an inverse correlation between the dielectric constant and resistivity of the material as shown in Figure 7-7 when increasing the CIP pressure of the material. The increase in the dielectric constant was accompanied with a decrease in the resistivity of the material. It was stated by Ho et al., [153] that when air voids increased in a barium titanate ceramic, its dielectric constant decreased but concurrently raised its volume resistivity. In our

case, when reducing the number of air voids inside the composite, the dielectric constant will increase and the volume resistance will decrease as a consequence.

This increase in the dielectric constant consequently led to an increase in the effective electric field applied to the PZT phase inside the PZT-binder film. Also, reducing the resistivity of the material produces an electrical flux that penetrates the piezoelectric element. This current helps increase the effective electric field on the PZT particles [154]. The dielectric constant showed a gradual increase with increasing P_{CIP}. The maximum dielectric constants achieved were 211 and 237 (31% increase from unpressurised samples) at CIP pressure of 250 MPa measured at frequencies of 1 kHz and 20 Hz, respectively. However, a steady decrease was observed in the resistivity of the samples when increasing P_{CIP}. The maximum decrease of 7 GΩ.m was observed at a CIP pressure of 250 MPa. This is a reduction of 41% compared to the unpressurised samples.

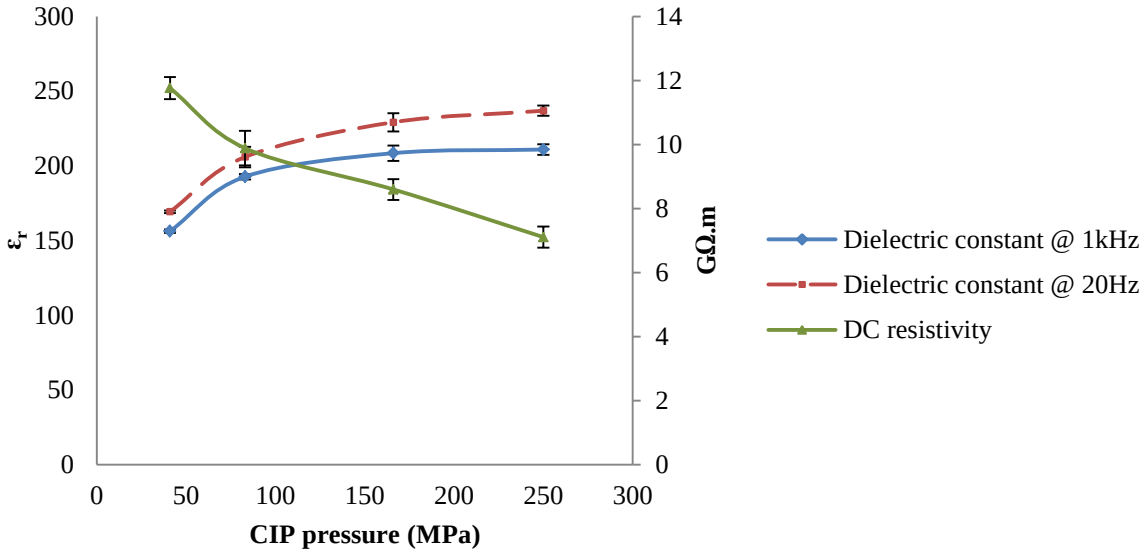

Figure 7-7: The dielectric constant (at 20 Hz and 1 kHz) and DC resistivity as the CIP pressure increased at 2 minutes for the fully cured samples

The half and uncured samples were poled immediately after the CIP process. When completing the curing process after CIP it was found that the dielectric constant and d_{33} values returned to the previous (i.e. unpressed) values. Therefore, it was decided to directly pole and simultaneously cure the samples during poling with the poling temperature. Figure 7-8 shows that the d_{33} values consistently increases with increasing the CIP pressure for all curing conditions. The maximum d_{33} measurement was 45 pC/N, at 250 MPa P_{CIP} for all the curing conditions (i.e. 11% increase from unpressurised samples). The poling temperature was reduced for all the devices to 75°C because of the reduction in the DC resistivity confirmed in Figure 7-7 which caused instability in poling process.

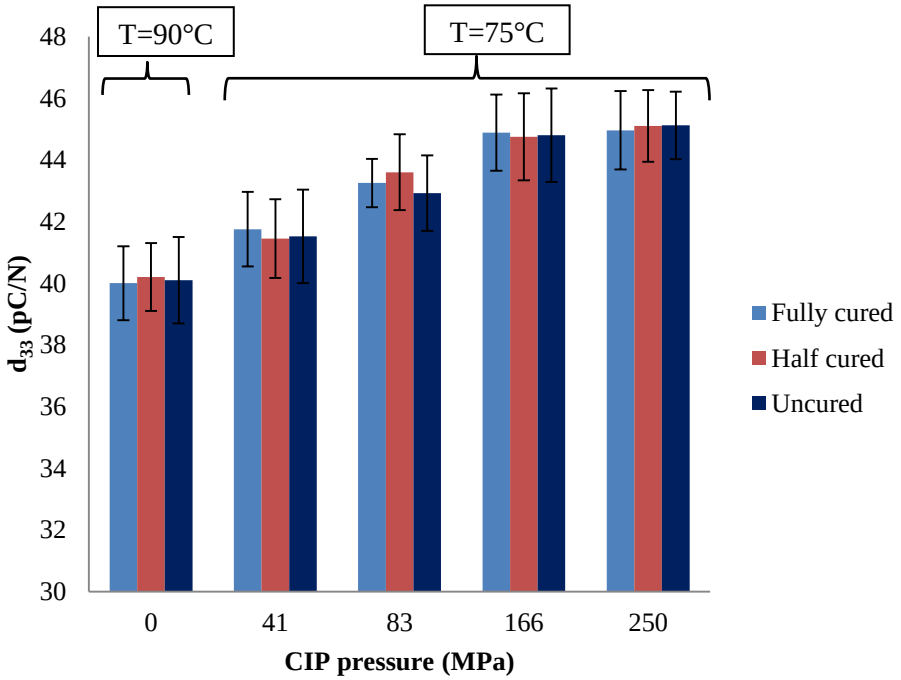

Figure 7-8: The effect of the CIP pressure on the piezoelectric activity for cured, half-cured and uncured samples. Poling temperature was reduced for the pressurised samples. Note, the d_{33} measurements were obtained when the films clamped on Kapton substrates

7.6.2 Investigating the Effect of CIP Time

The maximum CIP time that can be applied is five minutes as instructed by the manufacture. The d_{33} measurements were taken at t_{CIP} = 2, 3, 4 and 5 minutes for 3 samples each. Five d_{33} measurements were used for each sample giving 15 measurements in total. Figure 7-9 shows the negligible effect of the CIP duration time on the piezoelectric properties of the material when applying P_{CIP} = 166 MP. Therefore a lower time period (e.g. 2 minutes) is more efficient for mass-production.

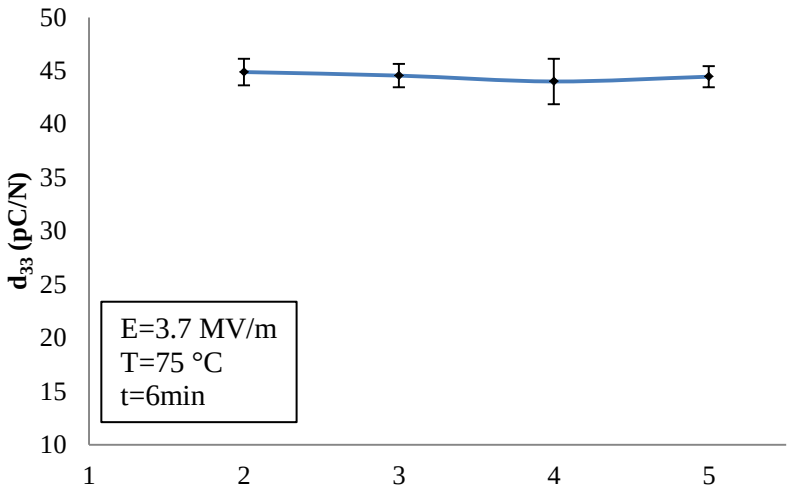

Figure 7-9: Effect of the CIP time on the piezoelectric properties when applying CIP pressure of 166 MPa for the fully cured material

7.7 CIP process for the Materials Printed on Fabric

The suitability of the CIP process for use with fabric substrates was also investigated. The application of CIP to piezoelectric materials printed on textiles substrates has not been reported. Before applying Paraffin wax to the samples, the backside of the sample (i.e. fabric side) was protected with a tape. Similarly, the effect of the CIP process on d_{33} values was investigated when the piezoelectric material printed on Polyester-cotton. The CIP process was conducted at the same range of pressures shown in Figure 7-8. The investigation only involved the fully cured samples.

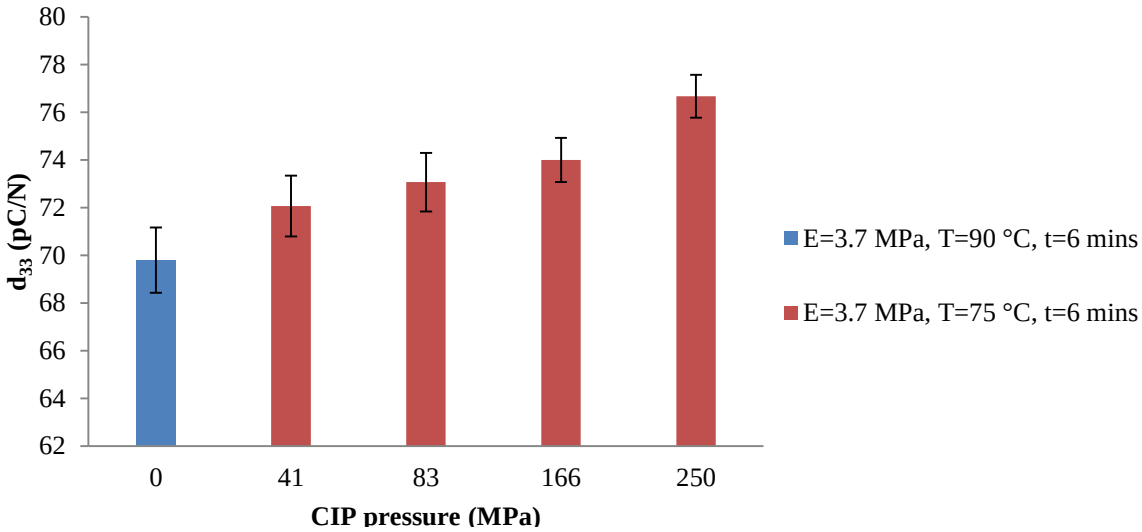

Figure 7-10: The effect of the CIP pressure on the piezoelectric activity for fully cured samples on Polyester-cotton

Figure 7-10 shows that the piezoelectric activity increases with the increasing P_{CIP}. Similar to Kapton substrate results, the optimum P_{CIP} was 250 MPa. At this pressure, a maximum d_{33} of 76.7 pC/N was achieved (an increase of 8.6 % from the unpressurised sample). The new d_{33} values after CIP was put in equation (5-7) and the new free-standing was calculated for devices on Kapton and Polyester-cotton substrates. Figure 7-11 shows the new clamped d_{33clp} and free-standing d_{33fs} values of the samples processed at 250 MPa pressure for 2 minutes. The new average calculated d_{33fs} value is 90 pC/N with an increase of 11% from the value previously obtained.

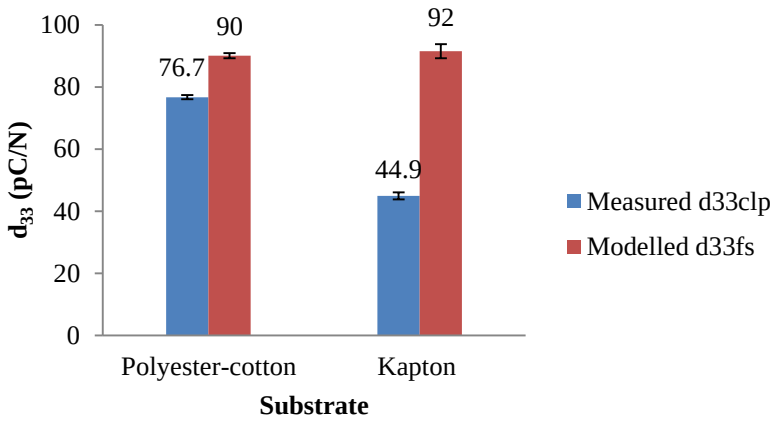

Figure 7-11: Clamping effect of the samples after CIP processed at 250 MPa for 2 minutes for Kapton and Polyester-cotton substrates

7.8 Conclusions

Densifying the screen-printed PZT/polymer film using CIP method has improved the dielectric and piezoelectric properties. The screen-printed PZT/polymer film showed a maximum increase of 31% in the dielectric constant after applying CIP pressure of 250 MPa measured at frequencies 1 kHz and 20 Hz. The effect of resistivity was even more than the dielectric constant with a 43% reduction. This reduction affected the normal poling conditions of the devices even at a P_{CIP} of 41 MPa. Therefore, applying lower poling temperature was essential because it increases the chance of a current passes through the piezoelectric element. The new poling conditions were E=3.7 MV/m, T=75°C and t = 6 minutes. The maximum d_{33} values achieved for devices printed on Kapton and Polyester-cotton were 45 and 77 pC/N, respectively, when the sample CIP-processed at 250 MPa for 2 minutes. This confirms an increase of 11 and 8.6 % from the original values of the devices printed on both Kapton and Polyester-cotton, respectively. The new free standing d_{33fs} value of the printed film was calculated by substituting the new d_{33clp} values obtained for devices printed on Kapton and Polyester-cotton on equation (5-7). The new free-standing d_{33fs} was found to be 90 pC/N showing an 11% increase than the original value 80 pC/N.

Chapter 8: The Effect of Metal Nano-Particles on d_{33} Coefficient of The Piezoelectric Composites

8.1 Introduction

Piezoelectric composites with 0-3 connectivity usually consist of ceramic particles (e.g. PZT) dispersed in a polymer matrix. During poling, the intensity of the effective electric field E_{eff} on the PZT particles is influenced by the surrounding polymeric matrix. This electric field across the PZT particles can be increased by improving the dielectric properties of the polymer. It has also been shown [154] that increasing the current flux through the PZT particles improves E_{eff}. Typically, polymers exhibit low dielectric constants and high resistivity, which leads to the electric field being dispersed within the polymer and E_{eff} is reduced.

This problem can be solved by introducing another polymer matrix with higher dielectric properties or by adding another third phase material that improves the dielectric properties and subsequently E_{eff} on the PZT particles. The current flux that is increased by adding the third phase typically increases the E_{eff} on the PZT particles but the resistivity of the composite as a whole will be reduced. The reduction in resistivity causes instability in the polling process and other poling parameters such as temperature may need to be adjusted to prevent short-circuiting.

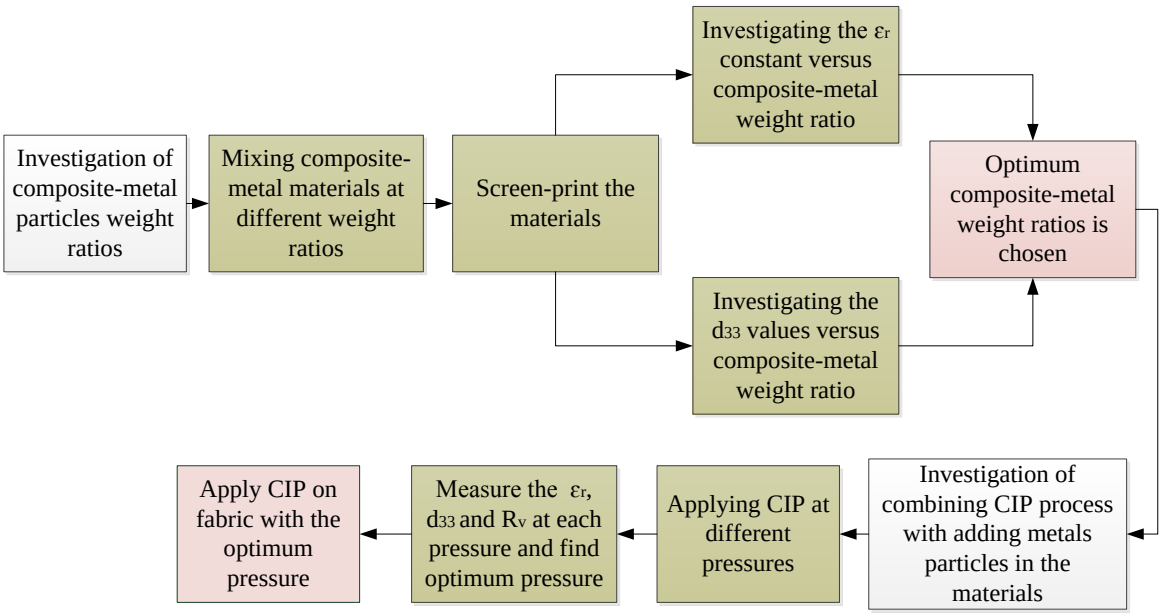

Figure 8-1: Experimental plan of improving the piezoelectric properties of the optimum piezoelectric composite

This chapter reports the influence upon the dielectric and piezoelectric properties of the piezoelectric film with the addition of different percentages of silver nano particles by weight. The effect of the adding silver nano-particles on the poling process is also investigated and optimum poling conditions are obtained. Finally, the CIP process is applied to the optimum PZT/polymer/Ag-nano formulation and the dielectric and piezoelectric properties are investigated with changing pressure.

8.2 Mixing the PZT-Ag-polymer Composite

ECS-PolyPZT 6a was mixed as previously described but with the addition of Silver Ag-nano powder (Sigma-Aldrich) as a third-phase in the composite. The average Ag–nano particle size was 100 nm. The blend was mixed and then triple roll milled as shown in the schematic shown in Figure 8-2.

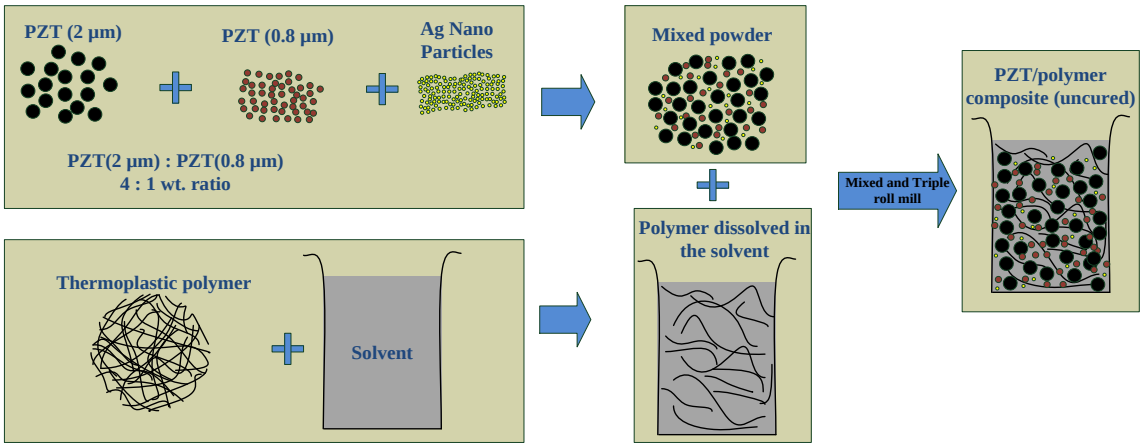

Figure 8-2: Schematic showing the mixing process of the PZT-Ag-polymer composite

Pastes with weight percentages 0.05, 0.1, 0.2, 0.5 and 1% of the Ag-nano powders inside the composite were investigated. The four composites were printed on Kapton substrates and then cured with the same curing conditions listed Table 4-5 on page 76.

8.3 Material Properties versus Ag-nano Particle Weight Content

8.3.1 Dielectric Properties versus Ag-nano Particles Loading

The capacitances of the devices were measured for three devices on Kapton substrates for each Ag-nano particles weight percentage at 1 kHz and the relative dielectric constant was calculated. Figure 8-3 shows that the dielectric constant increases with the increase of the weight content of Ag-nano particles in the composite up to 0.2% which provides a maximum dielectric

constant of 171. This is a 14.6% increase in the dielectric constant compared to samples without Ag-nano particles. After 0.2%, the dielectric constant decreased down to 134, which is lower than the printed material with no Ag-nano particles. This increase in the dielectric constant reflected an improvement in poling conditions by increasing the E_{eff} on the PZT particles.

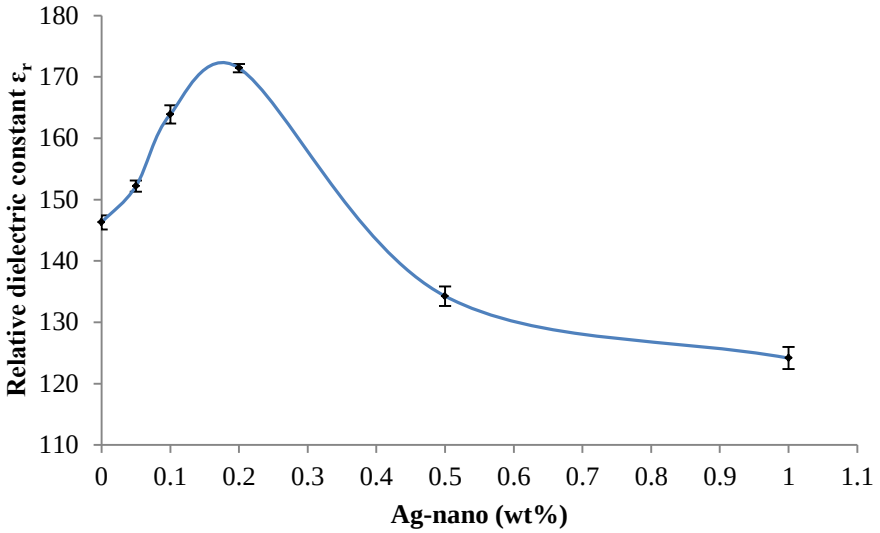

Figure 8-3: Relative dielectric constant of the material as the Ag-nano particles weight percentage varied

8.3.2 Piezoelectric Properties versus Ag-nano Particles Weight Loadings

The corresponding devices of each Ag powder weight percentages were separately poled, using the optimised conditions for ECS-PolyPZT 6a, apart from temperature, and d_{33} measurements were obtained after poling. Adding Ag-nano particles caused difficulties in poling and therefore the poling temperature was lowered with increasing Ag loading. Three devices were used for every Ag weight percentage and 5 measurements were taken from each. Figure 8-4 shows that the d_{33} measurements increased with the increase of Ag content in the printed film. The d_{33} values reached the maximum 43.5 pC/N at 0.2% Ag-nano particles by weight. This shows an increase by 8 % in the d_{33} value compared to ECS-PolyPZT 6a without Ag-nano particles.

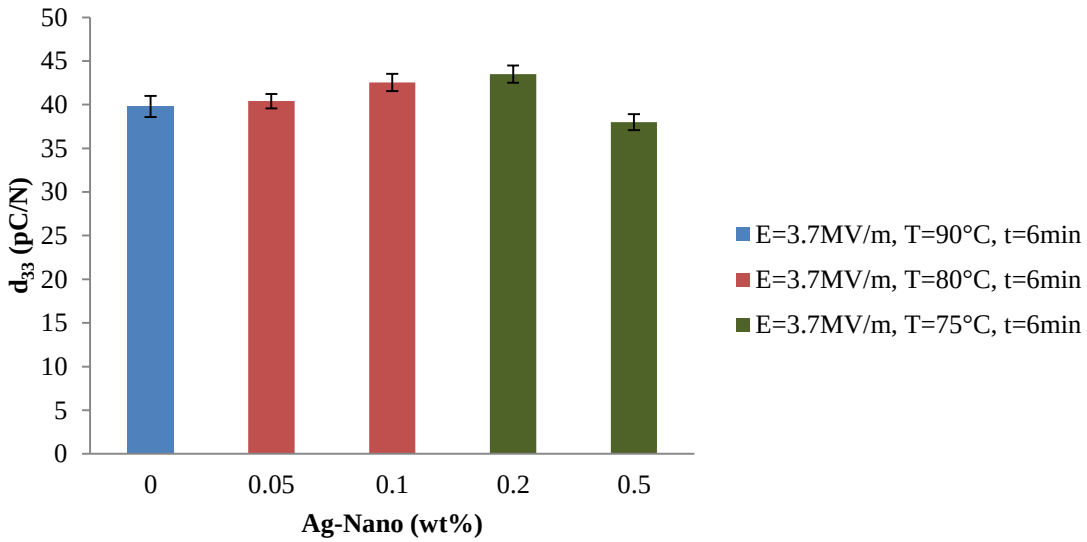

Figure 8-4: The measured d_{33} values of the PZT-Ag-polymer composites with changing the weight percentage of Silver-nano particles. Note, the d_{33} measurements were obtained when the films clamped on Kapton substrates

From the dielectric and piezoelectric properties results, the optimised Ag-nano particles weight ratio is 0.2%. This weight ratio with its new poling conditions will be used along this chapter for the investigation of the effect of the CIP process. When screen-printing the ECS-PolyPZT 6a with 0.2% Ag-nano particles by weight and pole the film with the optimum poling conditions shown in Figure 8-4, the film showed a d_{33} value of 76 pC/N showing a 7.8% increase in the piezoelectric activity from the original ECS-PolyPZT 6a printed on Polyester-cotton.

8.3.3 Effect of CIP Pressure on the Dielectric and Resistive Properties

The dielectric constant (at 20 Hz and 1 kHz) and DC resistivity was measured for the optimum material (ECS-PolyPZT 6a with 0.2% Ag-nano particles by weight) as the CIP pressure was varied. Three devices were used for each pressure. Similar to the results shown in Figure 7-7, the dielectric constant increased with the increase of CIP as demonstrated in Figure 8-5. However, a gradual decrease in the DC resistivity was observed. The results in Figure 8-5 showed a 44.2% increase in the dielectric constant (after applying CIP pressure of 250 MPa for 2 minutes) compared to the original ECS-PolyPZT 6a (146). However, a reduction of 52.8% was observed in the DC resistivity. The effect of Ag-nano particles on the dielectric constant is increased by CIP.

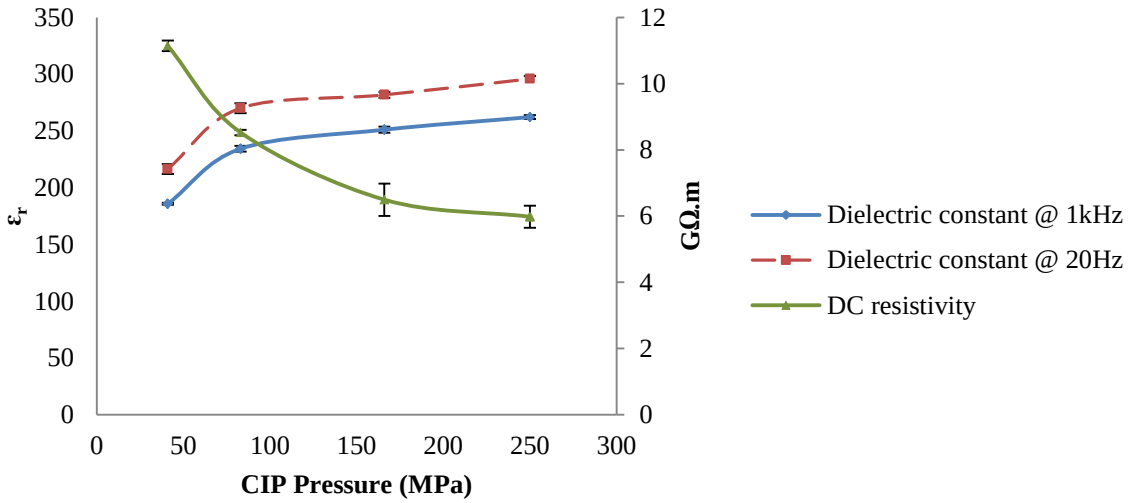

Figure 8-5: Relative dielectric constant (at 20 Hz and 1 kHz) and DC resistivity as the CIP pressure increased at 2 minutes for the fully cured samples of PZT/polymer films with 0.2% Ag-nano particles by weight

The effect of air voids is shown by the DC resistivity of the film. The DC resistivity of the screen-printed film without air-voids should theoretically be 1 GΩ.m. This estimation was done by averaging the volume resistivity of PZT-5H R_{PZT}= 0.1 GΩ.m [155] and the polymer Cyano ethyl PVA R_p= 10 GΩ.m (provided by the manufacturer, Shin Etsu Chemical Co, Ltd). The DC resistivity of the ECS-PolyPZT 6a printed film showed an increase of 91% (Figure 8-6). Applying CIP reduced this percentage to 48% and adding 0.2% Ag-nano particles further decreases the resistivity.

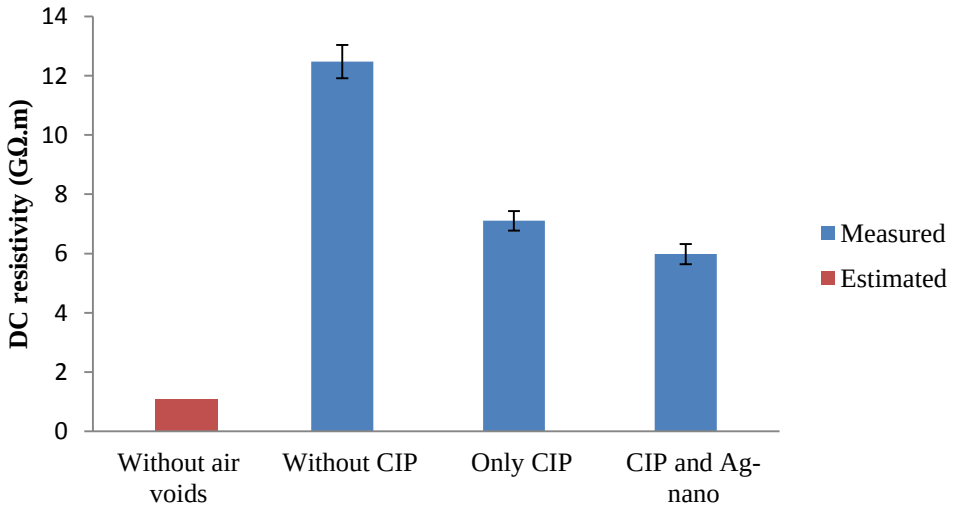

Figure 8-6: An estimation of the effect of the air voids inside the material with the aid of DC resistivity measurements

Assuming a material without air voids is producible, the instability in poling process will be a challenge and poling the material with poling temperature will be difficult. This may lead to a

decrease in the efficiency of poling process and a reduction in d_{33} values. Therefore, it is recommended to reduce the material resistivity to enable an electric flux passes through the piezoelectric element and subsequently improve the poling field across the PZT particles. However, the resistivity should be reduced in a limit that the passing current can be controlled and does not affect the piezoelectric activity.

8.3.4 Effect of CIP Pressure on Piezoelectric Properties

The piezoelectric coefficient was improved by 9% by applying a CIP pressure of 250 MPa for 2 minutes to the Ag-nano particle loaded film. Applying the CIP process at these conditions with the addition of Ag-nano particles also gave an increase in the piezoelectric activity 18.3%. The poling temperature was reduced to 70°C only for samples CIP-processed at 250 MPa for 2 minutes because of the reduction in resistivity up to 5.9 GΩ.m caused instability in poling process.

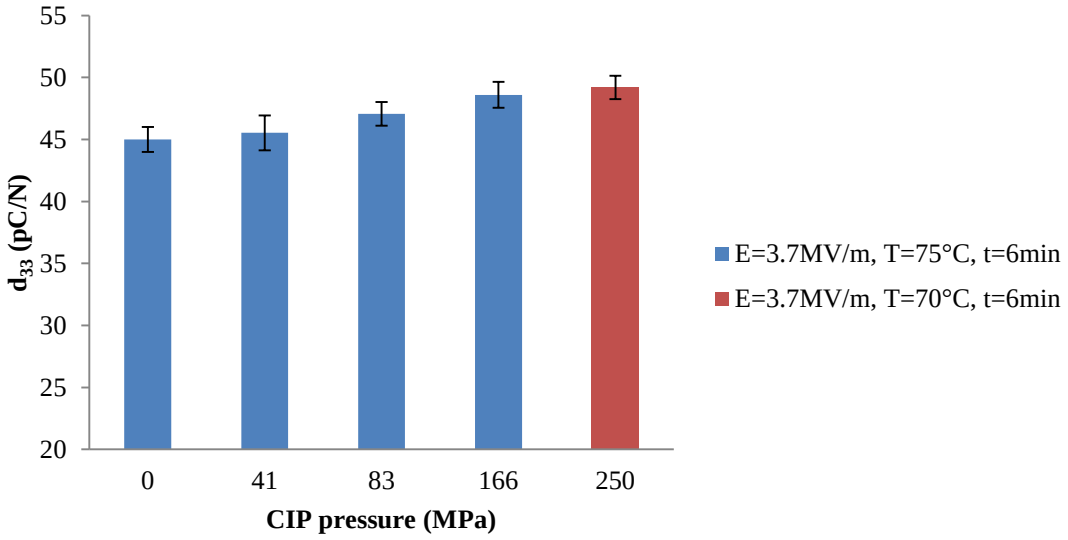

Figure 8-7: The effect of the CIP pressure on the piezoelectric activity for samples with 0.2% Ag-nano particles by weight. Note, the d_{33} measurements were obtained when the films clamped on Kapton substrates

When printing the ECS-PolyPZT 6a with 0.2% Ag-nano particles on Polyester-cotton plus interface layer and applying the CIP process at 250 MPa for 2 minutes, the film showed average d_{33} values of 83 pC/N after poling at E = 3.7 MV/m, T=70°C and t=6 min. This shows an increase of 15.6 % of the original ECS-PolyPZT 6a printed on Polyester-cotton and 8.4% with the material only with 0.2% Ag-nano particles.

The new clamped d_{33clp} values were put in equation (5-7) and the d_{33fs} values obtained are shown in Figure 8-8. The average d_{33fs} calculated from both substrates was 98 pC/N, an increase

of 18.4% compared to the original ECS-PolyPZT 6a without the addition of Ag-nano particles and CIP processing.

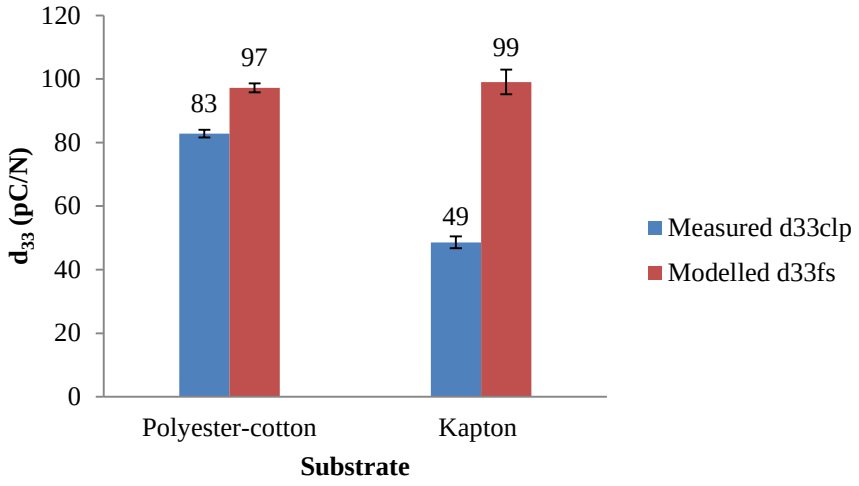

Figure 8-8: Clamping effect of the samples after CIP processed at 250 MPa for 2 minutes for ECS-PolyPZT 6a with 0.2 Ag-nano by weight printed on Kapton and Polyester-cotton plus interface layer substrates

8.4 Summary

Table 8-1 summarises the improvement occurred in the dielectric, resistive and piezoelectric properties for ECS-PolyPZT 6a printed on Kapton and Polyester-cotton and also free-standing films, at each processing type.

Processing type	**Kapton**			**Polyester-cotton**	**Free-standing**
	ε_r (at 1 kHz)	d_{33} (pC/N)	R_v (GΩ.m)	d_{33} (pC/N)	d_{33} (pC/N)
Original	146	40	12.5	70	80
CIP-processed (at 250 MPa)	211 (31[a])	45 (11.1[a])	7.1 (-43[a])	76.6 (8.6 [a])	90 (11.1[a])
Ag-nano particle	171 (14.6[a])	43.5 (8[a])	11.73 (-6.1[a])	76 (7.8[a])	87.5 (8[a])
CIP (at 250 MPa) and 0.2 wt% Ag-nano particles	262 (44.2[a]) (34.5[b])	49 (18.3[a]) (11.1[b])	5.9 (-52.8[a]) (-49.5[b])	83 (15.6 [a]) (8.4[b])	98 (18.4[a]) (10.7[b])

[a] Improvement in percent (%) from original ECS-PolyPZT 6a,

[b] Improvement in percent (%) from ECS-PolyPZT 6a with 0.2 % Ag-nano particles only

Table 8-1: The improvements occurred to the fully cured ECS-PolyPZT 6a at each processing type

8.5 Conclusions

Adding Ag-nano particles to the composite was found to improve both the dielectric and piezoelectric properties of the film. The optimum weight percentage was 0.2% Ag-nano particles by weight gives a dielectric constant of 171 and d_{33} value of 43.5 pC/N when printed on Kapton, showing an improvement of 14.6 and 8%, respectively. Adding Ag-nano particles does affect the film resistivity and therefore the stability of the poling process. In order to prevent short circuits, the material was poled at E=3.7MV/m, T=75°C and t=6 min.

Appling CIP at 250 MPa for 2 minutes to the material with 0.2% Ag-nano particles by weight further improved the dielectric, piezoelectric and resistive properties which were 262, 49 pC/N and 5.9 GΩ.m, respectively. This is a change of 44.2%, 18.3% and -52.8%, respectively compared with the original ECS-PolyPZT 6a without post-processing. When comparing the results with ECS-PolyPZT with 0.2% Ag-nano particles by weight, these values improved by 34.5%, 11.1% and -49.5%, respectively.

Applying the Ag-nano particle composite on Polyester-cotton and applying CIP at 250 MPa for 2 minutes increased the d_{33} value to 83 pC/N when polled at E = 3.7 MV/m, T=70°C and t=6 min. This is an increase of 15.6 % and 8.4% compared to the original ECS-PolyPZT 6 a films and films with only Ag-nano particles with no Ag-nano particles. The maximum free-standing d_{33fs} of the CIP processed Ag-nano particle composite was calculated for Polyester-cotton and Kapton substrates. The average d_{33fs} (98 pC/N) value is 18.4% more than the value of original free-standing ECS-PolyPZT 6a film without the addition of Ag-nano particles and CIP-processing.

Chapter 9: Output Voltage and Power on Different Woven-Fabric Substrates

9.1 Introduction

This chapter shows the experimental results for the optimum output voltage and power produced by the ECS-PolyPZT 6a film. This study will provide a specification for the material which can be used to identify potential applications. Figure 9-1 shows the experimental plan to identify these optimum output levels when the ECS-PolyPZT 6a is printed on three different types of woven fabrics and poled with the same optimum poling conditions. Three different types of force were applied: compression, tensile and bending; these correlated to the human kinetic forces available in typical wearable applications. The three forces were separately applied to the three devices with different fabrics. The output voltage, power and energy were measured, analysed and then compared.

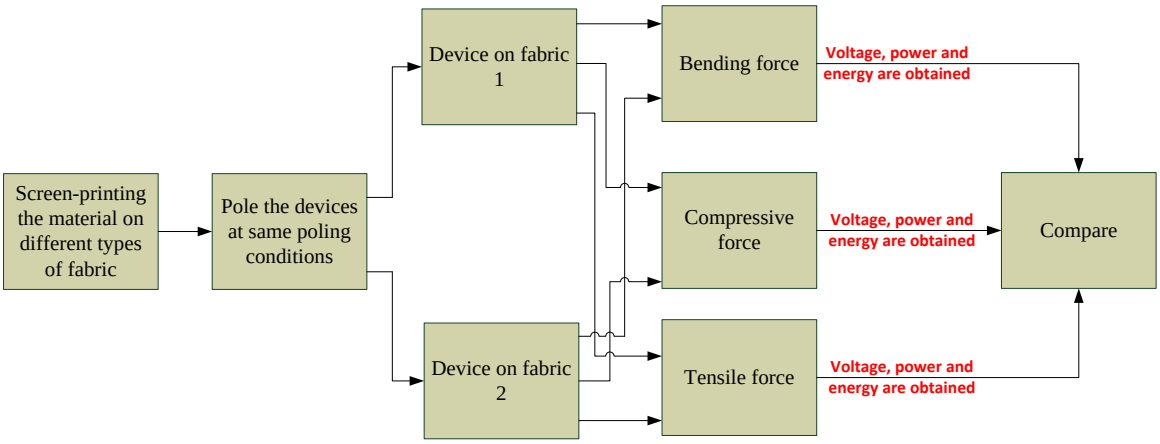

Figure 9-1: Experimental plan of the generated outputs of the material on different types of fabrics

9.2 Screen-Printing and Poling of the Material

The previous capacitive structure pattern was initially used for fabricating the testing device. This device structure can be scaled up or down depending on the application. The ECS-PolyPZT 6a was screen-printed on three different types of fabric: Cotton (Drill Cotton Mercerised white), Polyester-Cotton and Polyimide-imide (Kermel). The same screen-printing process on fabric was used as before (Figure 5-2 on page 96). Also, the same curing conditions were applied to have no negative affect on the fabric properties. Figure 9-2 shows the top view of the screen-printed

capacitive structure on the three woven fabric substrates. Table 9-1 shows the woven fabric substrates thickness without and with the interface layer.

(a) (b) (c)

Figure 9-2: The top view of the capacitive structure as it was printed on (a) Cotton, (b) Polyester-cotton and (c) Kermel

Table 9-1 shows the woven fabric substrates thickness with and without the interface layer. Obviously the Cotton substrate is thicker than Polyester-cotton and Kermel ones.

Substrate	Thickness Before printing the interface (µm)	Thickness after printing the interface (µm)	Interface layer thickness (µm)
Polyester-cotton	300	509	209
Cotton	420	705	285
Kermel	400	650	250

Table 9-1: Thicknesses of the woven fabric substrates without and with the interface layer

The devices were poled using the optimised poling process defined in section 5.3 on page 96. The measured d_{33} values for the devices used for compression, tensile and bending forces tests are shown in Figure 9-3. Again, the difference in the d_{33} measurements was due to the clamping effect of the substrates which is related to their mechanical properties (discussed in section 5.4 on page 99).

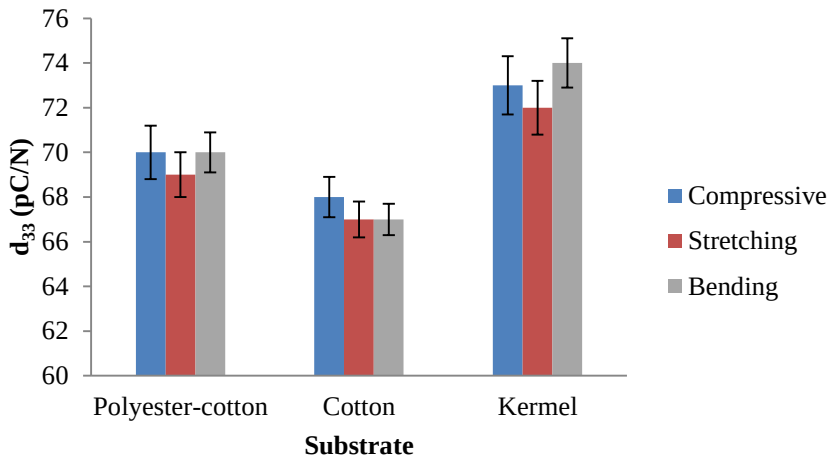

Figure 9-3: The d_{33} measurements of the devices printed on three different woven-fabric substrates used for compressive, tensile and bending force tests

9.3 Compressive Force on the Material

9.3.1 Quantification of the Applied Compressive Force

Compressive force is one the forces that can be applied by the human-body such as heel strike. This force can be applied repeatedly via the human foot during walking or running. The only compressive force that occurs during normal human movement is found at the heels. Heel strike forces can be well-exploited to scavenge energy from human movement by placing piezoelectrics element underneath the heel. The applied compressive force experiment on the devices was designed to mimic the heel strike caused by human walking of an average weight man (80 kg). Typical strike frequency of human walking for one foot ranges from 0.4 to 1.45 strike/second [156]. The compressive force test was applied by using ElectroPuls E1000 from Instron shown in Figure 9-4. It is an electrodynamic test instrument which was produced for static and dynamic experimental works on a range of materials [157]. The output voltage of the devices were observed and saved using an oscilloscope (TDS2014, Tekronix Ltd, UK).

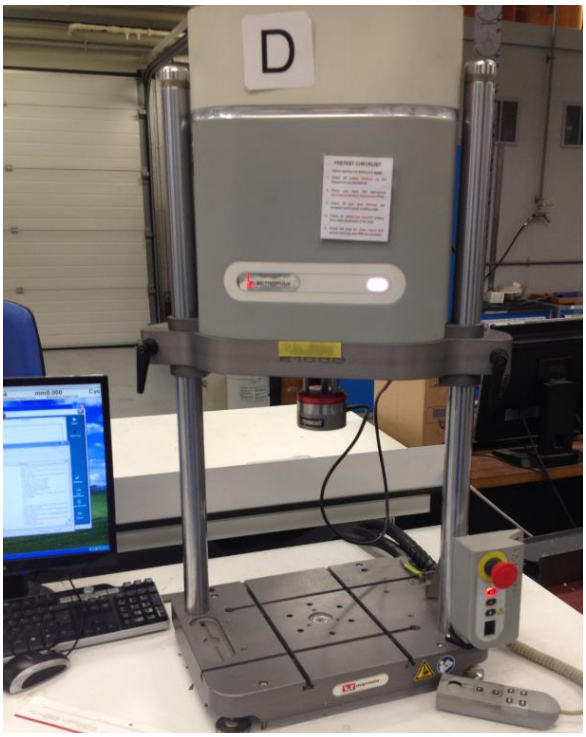

Figure 9-4: The compressive force test was applied by using an ElectroPuls E1000 from Instron

The force time-varying profile shown in Figure 9-5 has been separately applied to the three devices shown in Figure 9-2 creating a maximum pressure of around 8 MPa on the sample. The gait mode has a frequency of 0.8 steps/s with every step held at a maximum force time duration of 0.4 seconds.

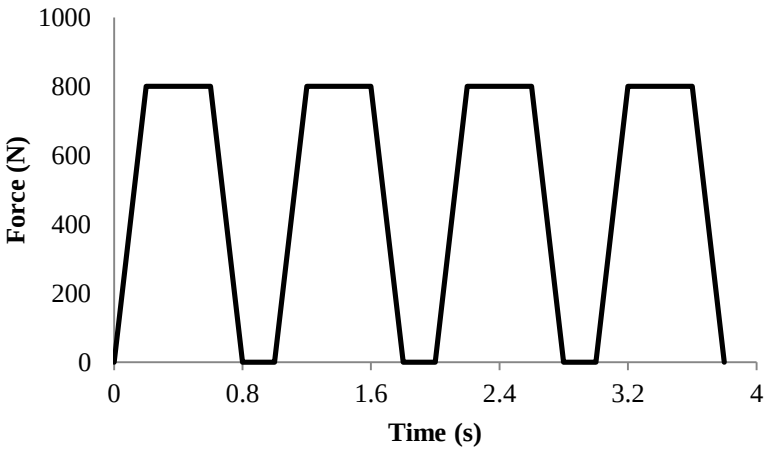

Figure 9-5: The force time profile applied to the devices

The sample was placed on the fixed part as schematically shown in Figure 9-6 and the applied force was applied by the upper part. The bottom and the top electrodes were connected to the oscilloscope using fine aluminium conductive wires to observe the output voltage that when applying the force.

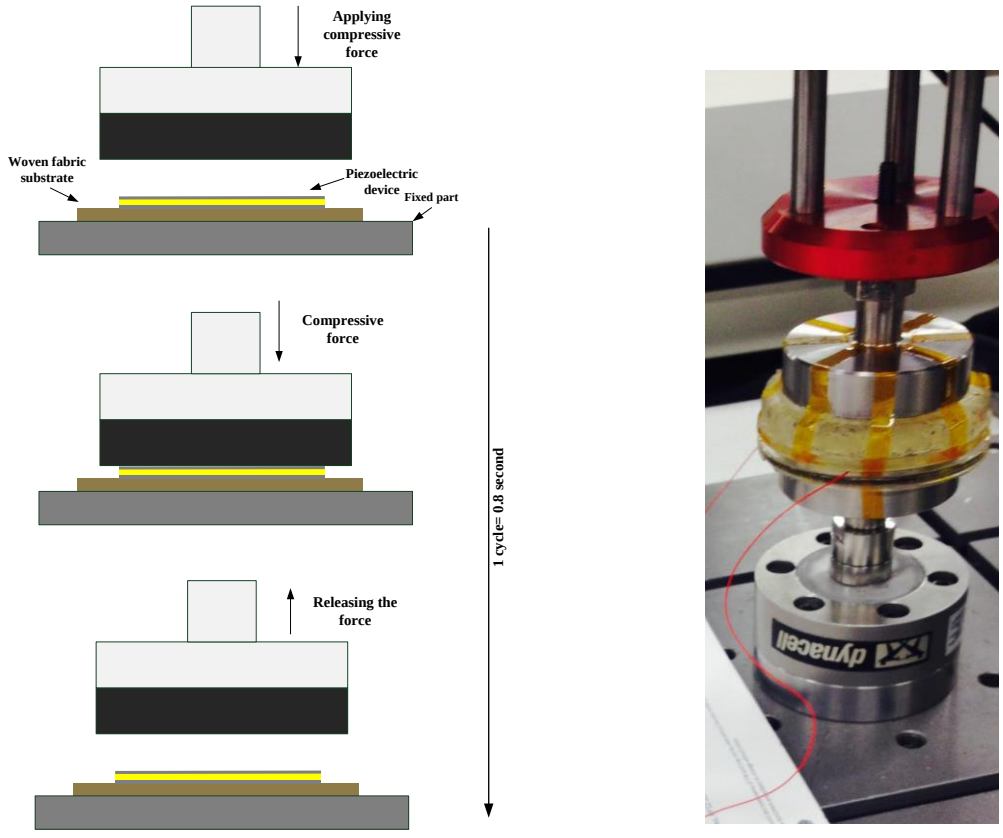

(a) (b)

Figure 9-6: Applied compressive force on the sample. (a) A schematic shows the applied compressive force on the sample. (b) The sample as it was placed between the fixed and movable parts

9.3.2 The Output Power and Energy

For this experiment, the three materials described previously were each subjected to the same compressive force profile shown in Figure 9-5 while separately applying different resistive load (with range 1-80 MΩ).The oscilloscope (TDS2014, Tektronix) was used to record the output voltages. This will identify the optimum load resistance to produce the maximum peak power ($P_{peak} = \frac{V_{peak}^2}{R_L}$) for each of the three fabric piezoelectric devices. The peak voltage and power values shown in Figure 9-7 are the average of three consecutive peak values. As shown in Figure 9-7(a), the peak voltage increases with increasing load resistance. However, the peak power increases up to 10 MΩ load resistance. Maximum power outputs of 6, 4 and 8 μW were produced for devices printed on Polyester-cotton, Cotton and Kermel substrates, respectively.

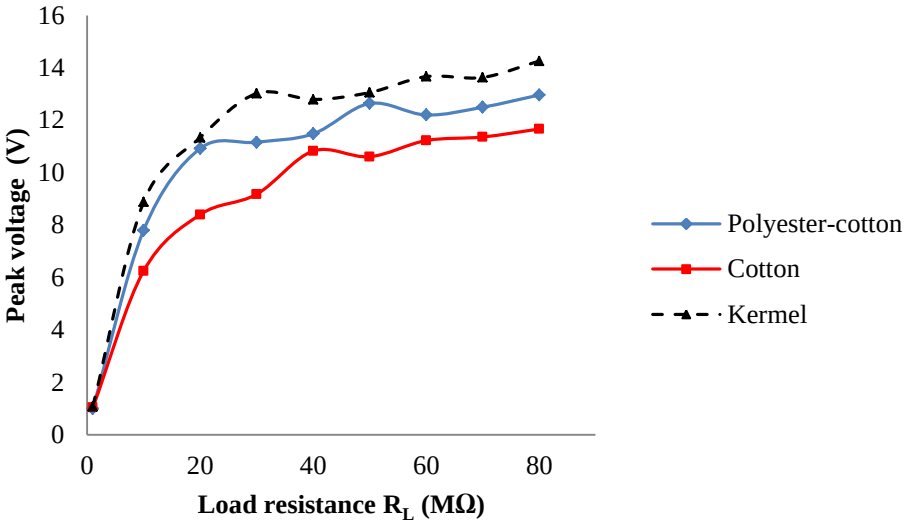

(a)

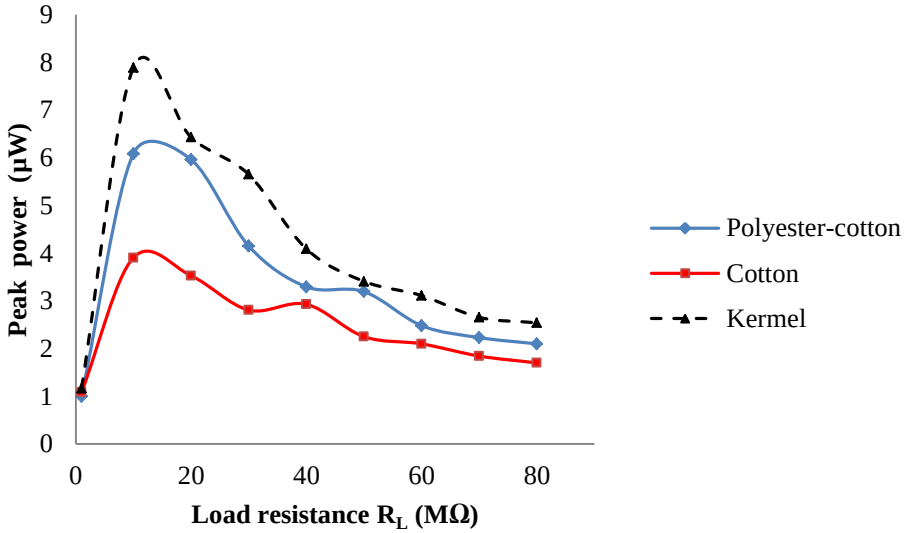

(b)

Figure 9-7: The (a) peak voltage and (b) power when 800 N was applied at different resistive loads for devices printed on Polyester-cotton, Cotton and Kermel

Figure 9-8 shows the output voltage produced per 800 N force cycle at 10 MΩ resistive loads for devices printed on Polyester-cotton, Cotton and Kermel. The results show that Kermel devices showed higher peak voltage and consequently higher peak power.

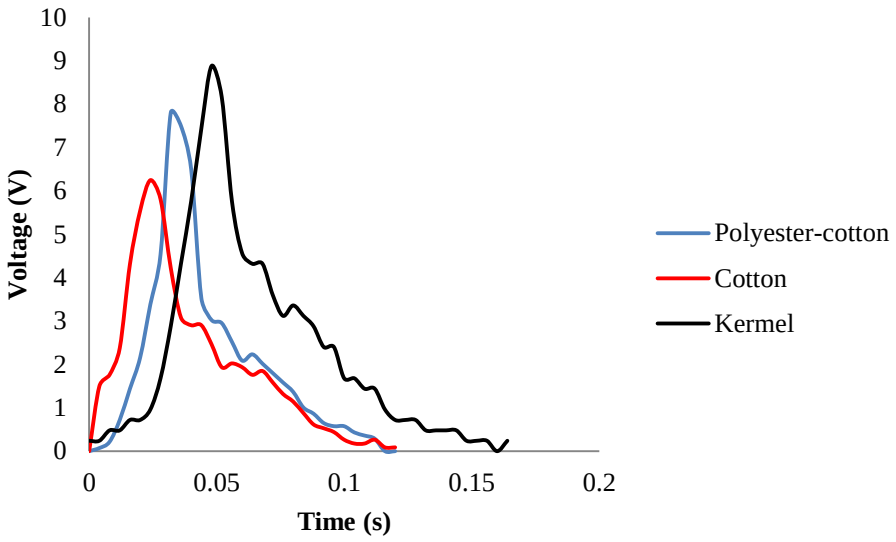

Figure 9-8: The output voltage at 10 MΩ when one force cycle is applied to the devices printed on Polyester-cotton, Cotton and Kermel

Figure 9-9 shows the energy E_c that can be produced in one compressive force cycle for devices printed on Polyester-cotton, Cotton and Kermel. The energy that produced in the active mode region for one cycle; t_1 and t_2 represent the beginning and the end of the active mode. The energy is calculated using equation (9-1) whilst scanning the resistive load in the range 1 M-80 MΩ.

$$E_c = \int_{t_1}^{t_2} \frac{V(t)^2}{R} . dt \qquad (9\text{-}1)$$

The energy increased with increasing load resistance up to 0.17, 0.1 and 0.2 µJ at resistances of 20, 30 and 30 MΩ for Polyester-cotton, Cotton and Kermel, respectively. After these load resistances, the energy per cycle is decreased for each substrate device. Generally, the amount of energy given for every substrate device kept the same order and Kermel is the best substrate for producing more energy.

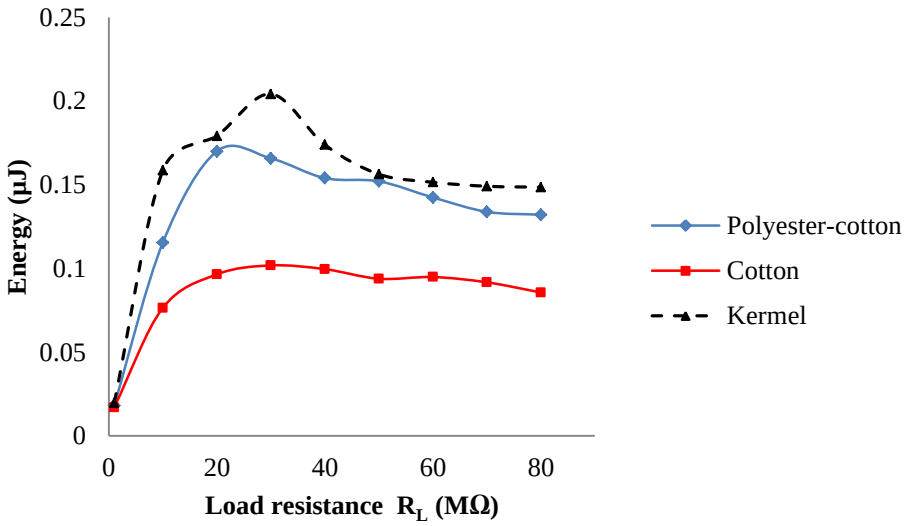

Figure 9-9: The energy at 800 N force cycle was applied at different resistive loads for devices printed on Polyester-cotton, Cotton and Kermel

9.4 Tensile Force on the Material

The tensile force test was performed using an ElectroPlus E100. The device was subjected to tensile force cycle every 1 second as shown in Figure 9-11. The tensile force cycle is identified by the speed and the displacement that the material under test is subjected to. The tensile force was only applied by the upper arm of the machine. There are two different directions that the tensile force was applied as shown in Figure 9-10. The tensile force was only applied to direction 1.

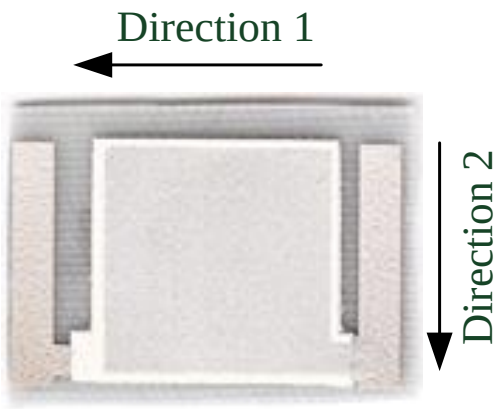

Figure 9-10: Tensile directions applied to all the fabric devices

In tensile, the two factors that may affect the outputs of the piezoelectric film on woven fabric substrate are speed and displacement of tensile. Tensile speed may have an effect on the amplitude of the output voltage. The displacement can have an effect on the duration of the pulse. The test will identify the maximum tensile displacement that can be applied before failure. The displacement factor is investigated first to identify the maximum displacement limit before

investigating the speed factor. In this stage, the investigation has been only applied for Polyester-cotton plus interface layer substrate.

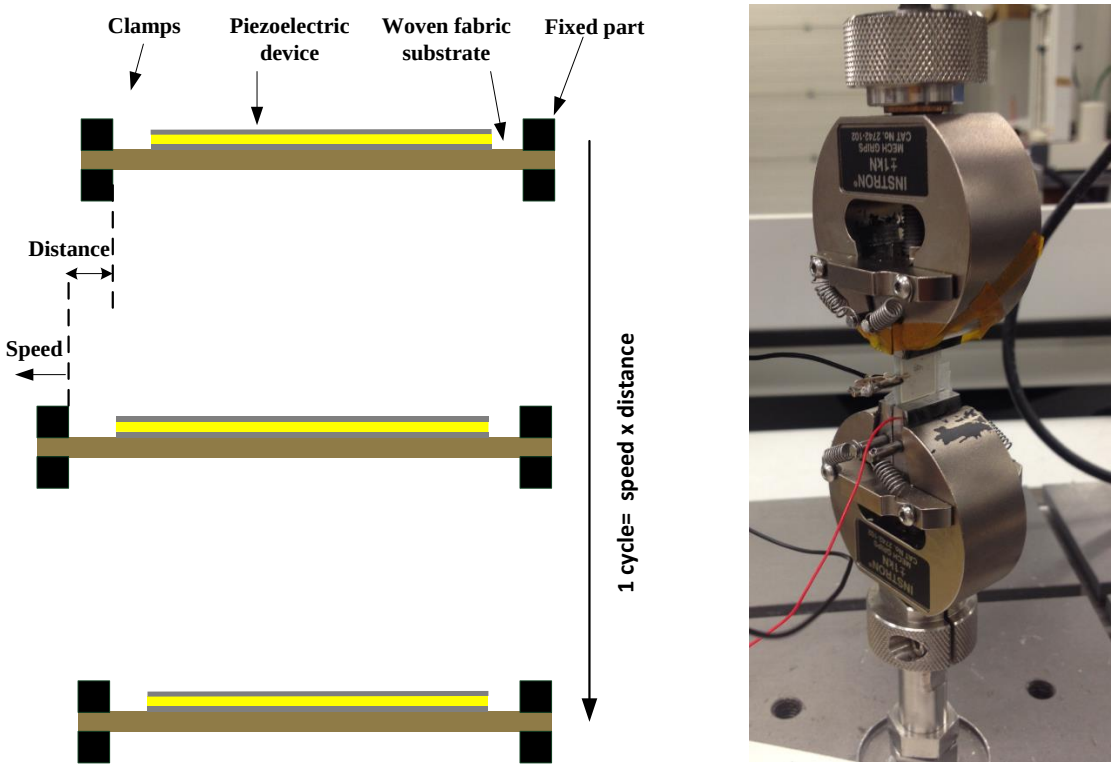

Figure 9-11: Applied tensile force on the sample. (a) A schematic shows the applied tensile force on the sample. (b) The sample as it was stretched using the machine

As shown in Figure 9-12 the peak voltage and power and energy increases with the applying tensile displacement in the range of 0.2-0.7 mm. Cracking was observed at the surface of the piezoelectric film beyond this range. The piezoelectric film on Polyester-cotton provided a maximum peak voltage, peak power and energy of 0.58 V, 0.336 µW and 0.0006 µJ, respectively. The displacement was investigated at a constant speed 0.5 mm/s as the speed will be separately investigated.

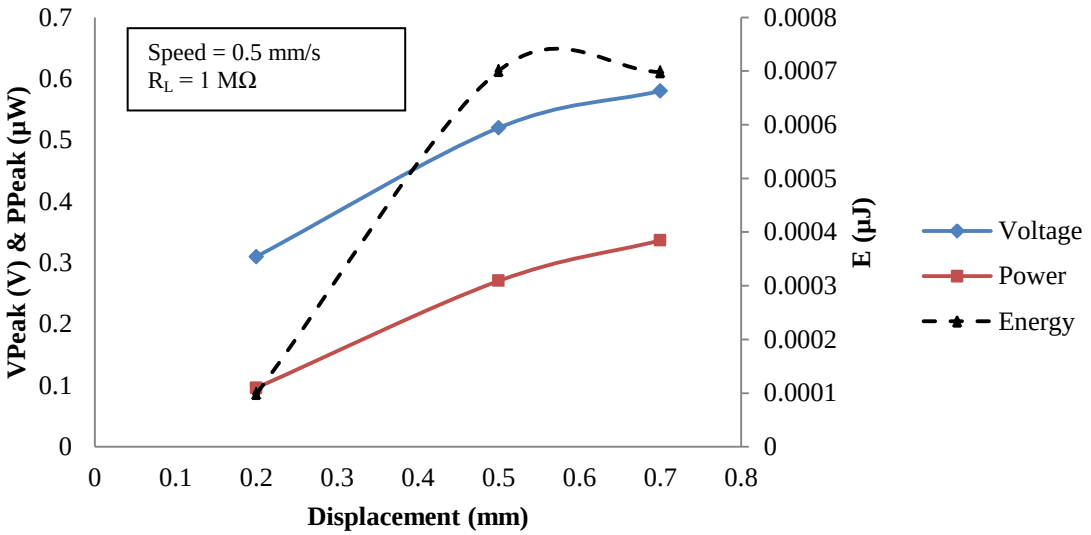

Figure 9-12: Investigating peak voltage and power and energy versus tensile displacement at constant speed 0.5 mm/s for polyester-cotton substrate. The results were taken at 1 MΩ resistive load

The speed of tensile force was also explored with a speed range between 0.01 to 2 mm/s at a constant displacement of 0.7 mm and 1 MΩ resistive load. Similarly, the material showed a gradual increase in peak voltage, peak power and energy with the increasing speed. The maximum speed of 2 mm/s showed maximum peak voltage, peak power and energy of 0.93 V, 0.87 µW and 0.0162 µJ, respectively.

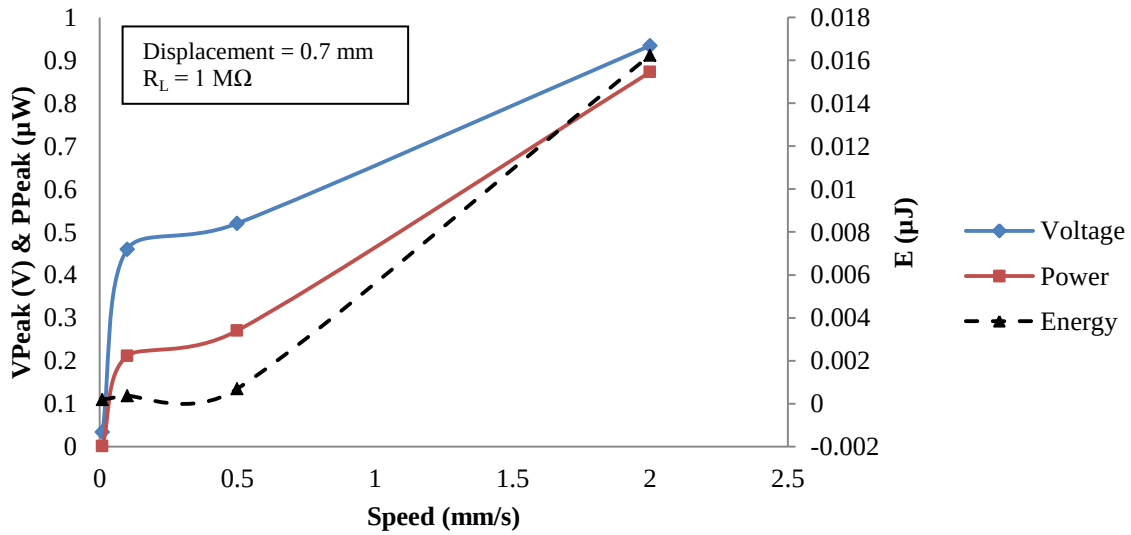

Figure 9-13: Investigating peak voltage and power and energy versus tensile speed at constant displacement 0.7 mm for polyester-cotton substrate. The results were taken at 1 MΩ resistive load

The tensile force was also tested when the material was printed on Polyester-cotton, Cotton and Kermel. Similar to the compressive force results, the piezoelectric film showed higher peak voltage, peak power and energy at every tensile force cycle when the compliance of the substrate is higher (discussed in section 9.6). The Kermel device when stretched at tensile conditions shown

in Figure 9-14 provided a peak voltage, peak power and energy of 1.1 V, 1.23 µW and 0.018 µJ per tensile cycle.

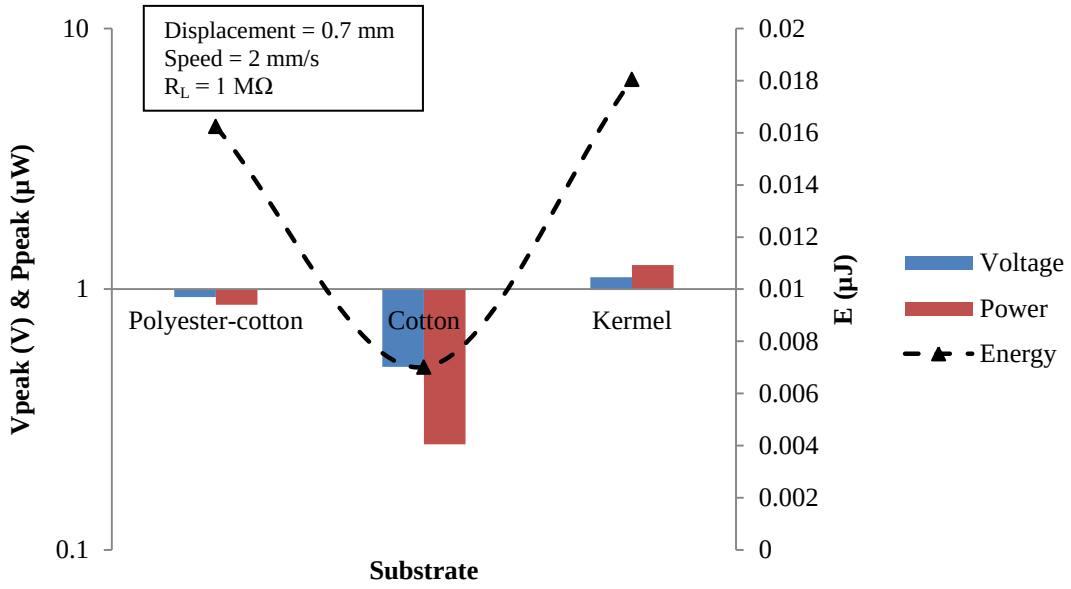

Figure 9-14: Investigating peak voltage and power and energy for polyester-cotton, Cotton and Kermel substrates at constant speed = 2 mm/s and displacement= 0.7 mm. The results were taken at 1 MΩ resistive load

9.5 Bending Force on the Material

The ECS-PolyPZT 6a films were also tested on Polyester-cotton, Cotton and Kermel, when they were subjected to bending force at a frequency of 1 Hz. The force was applied on both sides of the device as shown in Figure 9-16. The bending test system shown in Figure 9-15 was built and then used to apply bending force on the piezoelectric films on woven fabrics. The device was clamped on both ends and the displacement of 5 mm was applied at one end with the other end fixed. This motion subjects the device under test to a 5 mm bending radius of curvature.

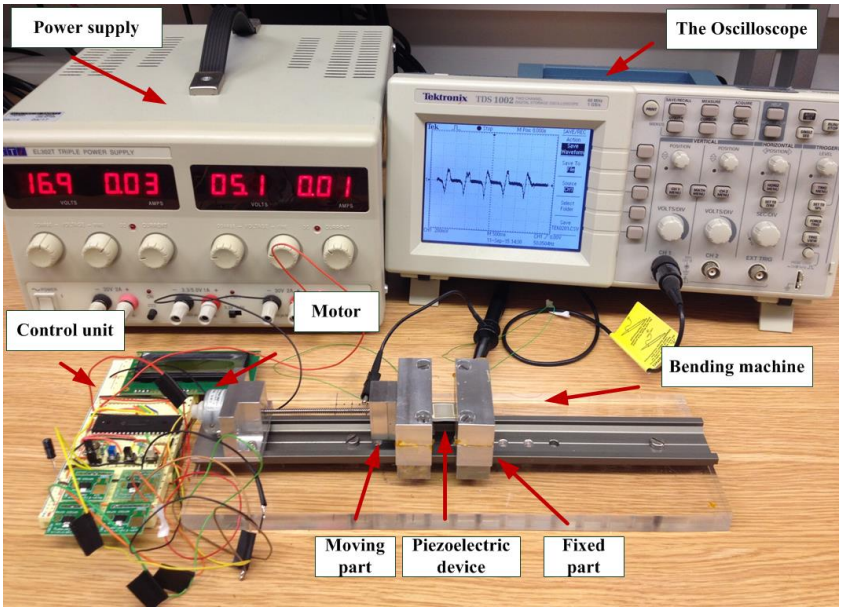

Figure 9-15: The control system used for observing the outputs of the piezoelectric device using the bending machine

The devices were tested using two bending modes. The first mode uses the substrate as the bending element (the substrate is bent at a specific radius of curvature = 5 mm). However, the second mode uses the piezoelectric film as the bending element (the piezoelectric film is bent at a specific radius of curvature = 5 mm). Therefore, bending the piezoelectric material using mode 2 creates more direct stress on the piezoelectric film. This is further described in Figure 9-16 below.

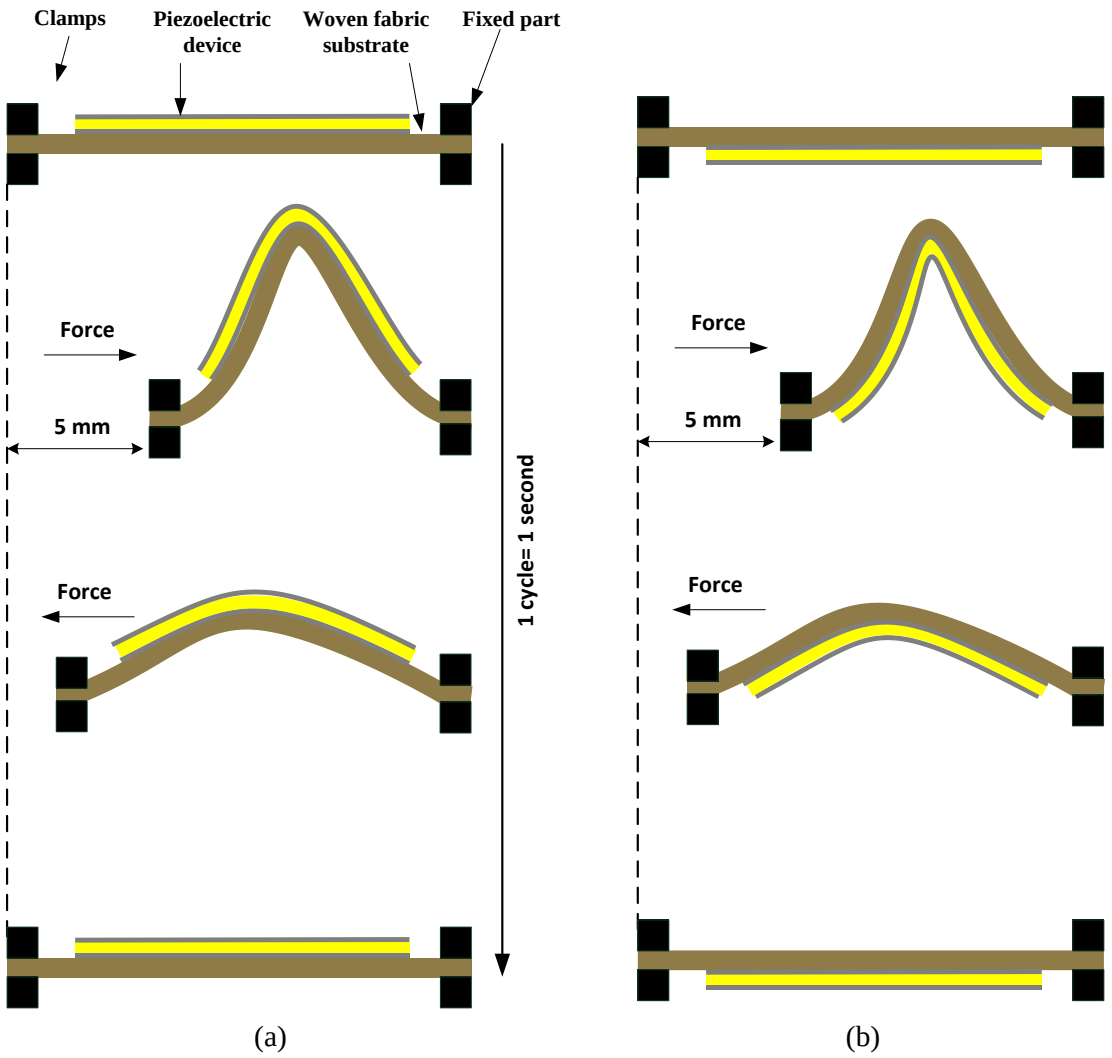

Figure 9-16: Bending force on the sample when the bending force was applied on (a) the substrate side 'mode 1' and (b) the sample side' mode 2'

When applying bending force using the two modes for the three substrates, it was found that mode 2 generates a higher output voltage than mode 1. Figure 9-17 shows the peak voltages while varying the resistive load for devices on Cotton. This difference is because of the effective radius of curvature. The radius of curvature R_c is the inner radius when bending the device. The effective R_c of mode 1 is $R_{ceff}=R_c+t_s$, however, the R_c on the device when bending of mode 2 is $R_{ceff}=R_c=5$ mm. So, in the case of the Cotton substrate the effective radius of curvature is nearly 5.7 mm (for mode 1) if we consider the thickness of the Cotton fabric plus interface layer is 0.7 mm. According to these results, mode 2 will be used in the investigation as it generated a higher output voltage than mode 1.

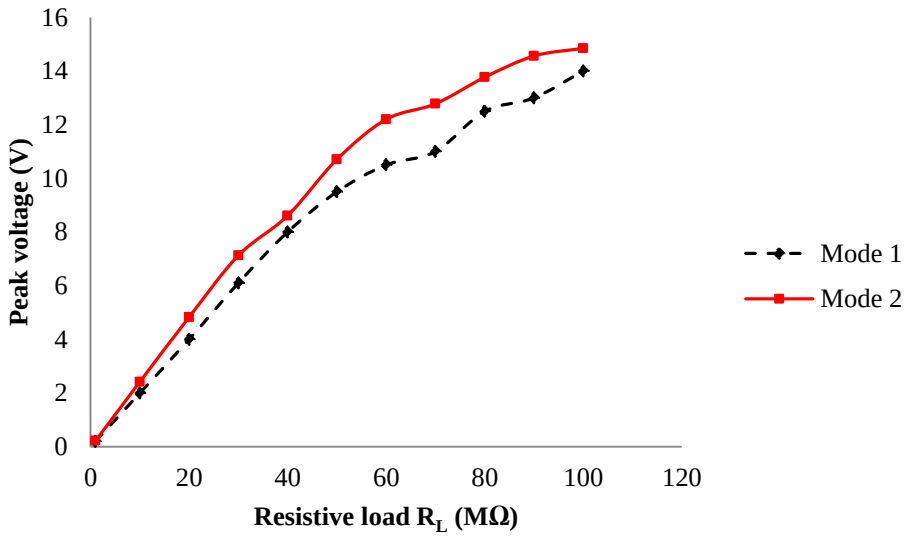

Figure 9-17: The peak voltage when applying bending force using mode 1 and 2 for Cotton devices

When applying a bending force as shown in Figure 9-16(a) for three cycles with mode 2, at different resistive loads the devices produce peak output voltage as shown in Figure 9-18(a). The output voltage increases with increasing resistive load values. The corresponding peak power at each resistance for each device is shown in Figure 9-18(b). Also, the output peak power increases with increasing load resistance up to 50, 60, and 50 MΩ giving maximum peak power of 1, 2.4 and 1.68 μW for Polyester-cotton, Cotton and Kermel devices, respectively. Cotton substrates generate a higher output voltage and power in this case (discussed later in section 9.6).

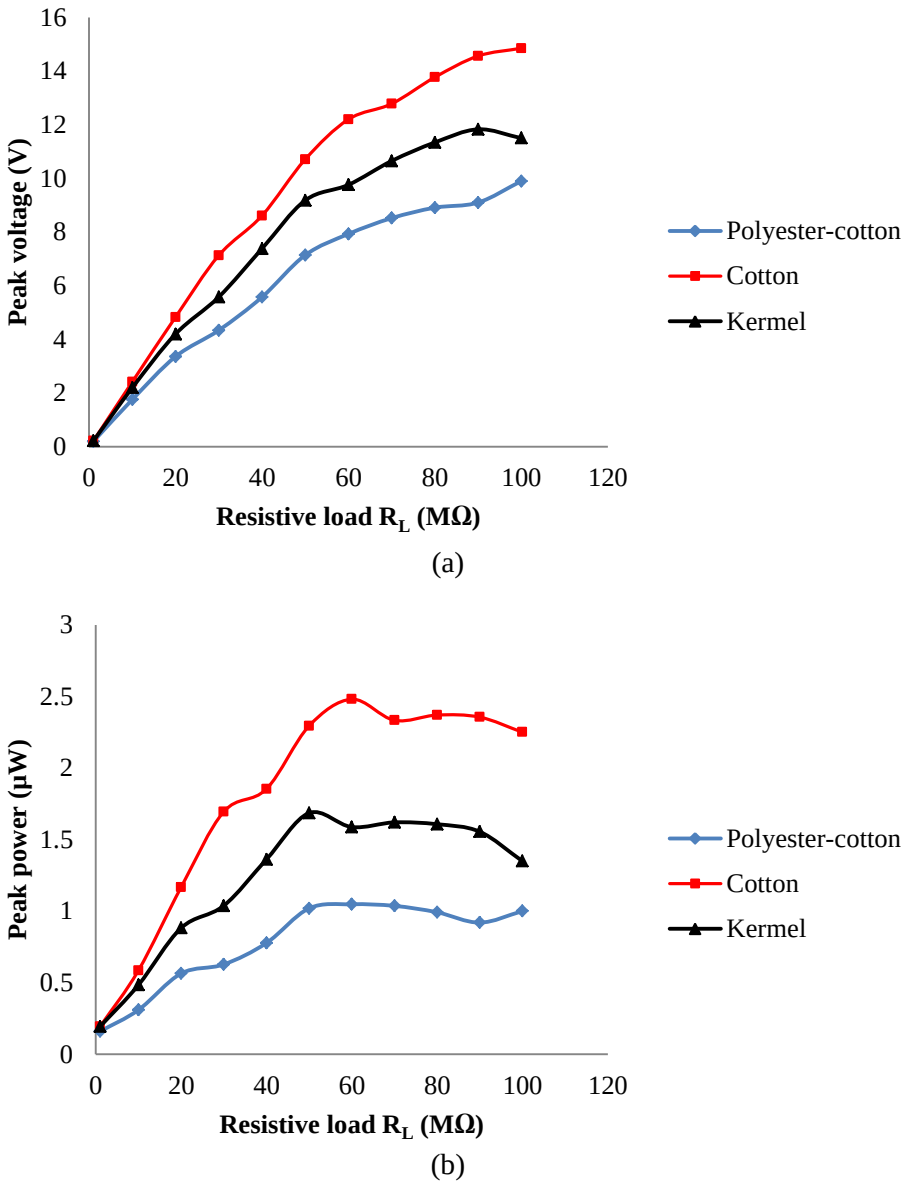

Figure 9-18: The output (a) peak voltage and (b) power when applying different resistive loads for 1 bending cycle

Similar to the results in Figure 9-18, the output energy produced for one bending cycle using mode 2 increases with increasing resistance. However, the maximum output energy for Polyester-cotton, Cotton and Kermel devices are 0.148, 0.19 and 0.16 μJ per cycle at resistive loads of 70, 70 and 80 MΩ, respectively.

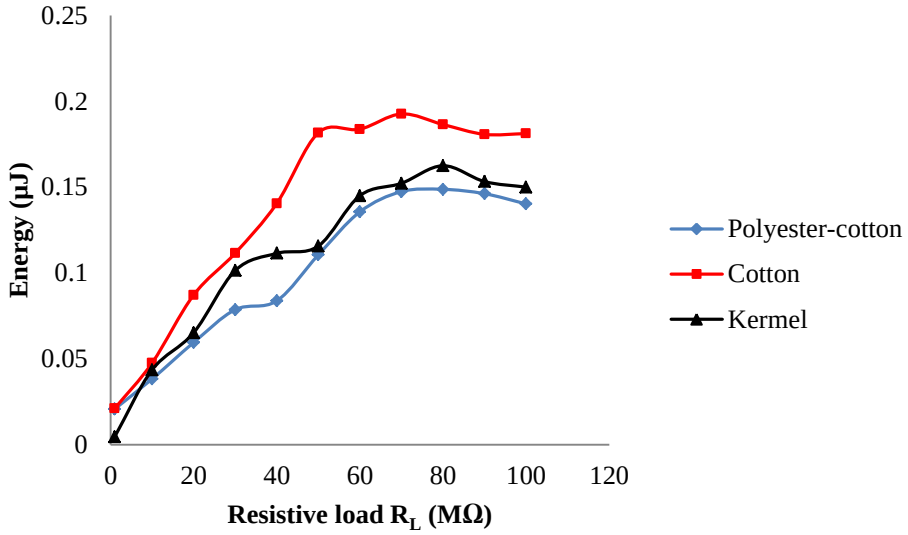

Figure 9-19: The output energy for one bending cycle at different resistive loads

9.6 Discussion

From the previous results, the slight difference in the outputs between the three substrate devices was because of the variations in the mechanical boundary conditions between them. As the d_{33} measurements were affected by the clamping effect of the mechanical boundary conditions of the substrate, the strain S on the piezoelectric film resulting from the applied force was also affected. This effect appears in different forms depending on the type of the substrate. The mechanical boundary conditions, the applied stress and strain depend on the type of force applied to the piezoelectric film on the substrate. Figure 9-20 shows the directions of stress and strain on the piezoelectric film that corresponds to the type of force applied.

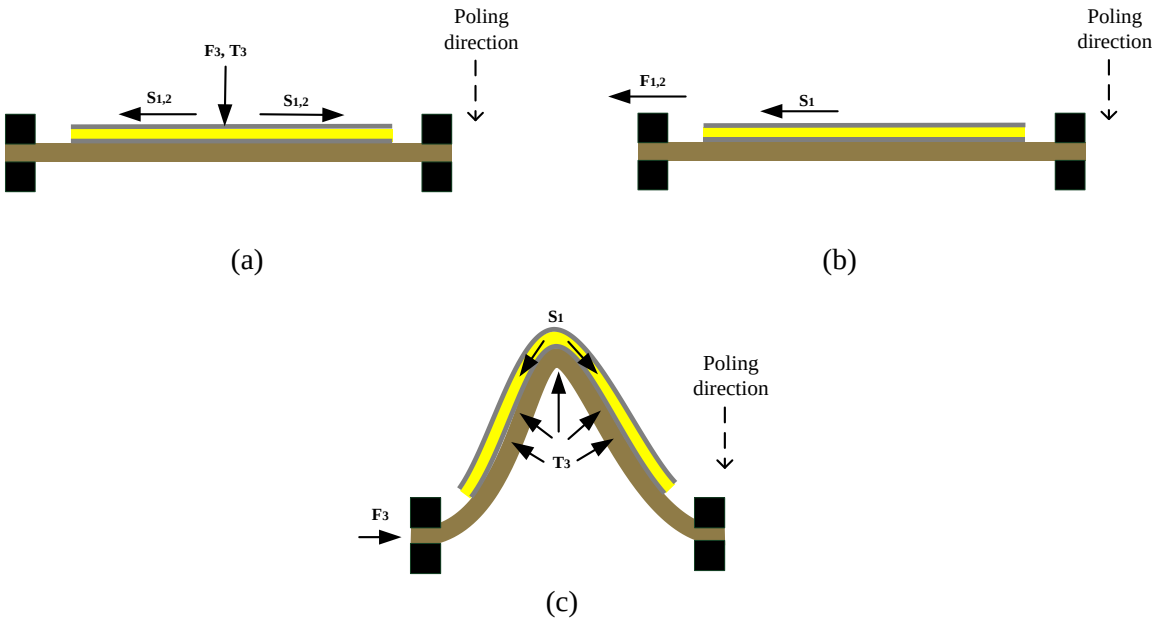

Figure 9-20: A schematics showing the poling, force, stress and strain direction after the applying of (a) compressive, (b) tensile and (c) bending forces to the devices

The mechanical properties of the three fabric substrates are shown in Table 9-2. Some other references confirm that Cotton woven fabrics have a higher Young's modulus [158].

Mechanical property	**Polyester-cotton**	**Cotton**	**Kermel**
Young's modulus Y_s (MPa)	200[a]	220[a]	138[a]
Passion ratio ν	0.44[b]	0.48[b]	0.41[b]
Compliance C_s (m^2/N)	-2.20 x10^{-9}	-2.10 x10^{-9}	-2.80 x10^{-9}

[a] measured, [b] calculated

Table 9-2: Mechanical properties of each woven-fabric plus interface layer substrate

9.6.1 Compressive Force

The strain in the three types of forces applied to the material is different. For the compressive force as mentioned earlier, when the piezoelectric film is subjected to a mechanical stress T in the direction 3, the piezoelectric film will expand and contract along the 1-2 plane. This deformation is dominated by the substrate that was assumed isotropic. At this point, the mechanical strain S is dominated by the mechanical properties of the substrate and the applied stress according to Hooke's law is $S = S_1 = S_2 = C_s T_3$. Where, C_s is the compliance of the substrate and the applied stress $T_3=F_3/A_e$ which is the same for all devices. In this case, the more compliant the substrate, the more strain and accordingly the more output voltage obtained. This hypothesis is confirmed by the small variations between the three substrates.

Comparing our results with other piezoelectric composites contributions that used compressive force in the literature (see Table 2-10 on page 41), our ECS-PolyPZT 6a on Kermel can produce higher voltage 14 V at 80 MΩ resistive load (this value may increase at open-circuit conditions) and optimum power at 7.88 μm at 10 MΩ (Note, optimum power and energy at specific resistance were not given for the proposed flexible piezoelectric devices used in the literature). Printing such materials on higher compliance substrates may improve outputs under the same applied stress conditions.

9.6.2 Tensile Force

For a tensile force, the strain is also dependent on the compliance of the substrate and the mechanical stress. Although the force direction is on the 1-2 plane, the stress and the strain also follow the same direction when the force is applied as shown in Figure 9-20. There are two types of strains caused by this type of force; longitudinal S_3 and transverse $S_{1,2}$. S_3 strain occurs when the force is applied in the 1-2 plane and a deformation is produced in the 3-direction because of Poisson's ratio which is related to the compliance of the material. However, the $S_{1,2}$ is related to the displacement that is applied to the substrate due to tensile. There is not contribution in the literature for exploring the outputs of the piezoelectric composite material when tensile force is applied to piezoelectric composite films. This work has investigated the effect of the mechanical properties of substrates on the outputs of the flexible piezoelectric material when tensile force is applied.

9.6.3 Bending Force

The directions of the stress and the strain are typically similar to those of the compressive force. The stress is directed across the thickness of the film and the resulting strain is transferred along the film area. This stress is due to the lateral applied force in the 1-2 plane. When bending the piezoelectric material on the substrate, the stress on the piezoelectric material is related to the substrate mechanical boundary conditions, the thickness of the substrate t_s and piezoelectric film t_{pc} and finally to the radius of curvature R_c [159].

Bending force results for Cotton substrates can be compared to the contributions in the literature. Note, optimum power and energy at specific resistance were not given for the proposed flexible piezoelectric devices used in the literature (see Table 2-10). Cotton substrate devices (1×1 cm^2 size), show higher voltages 14 V at 100 MΩ and power 2.5 μW at 60 MΩ. These outputs can be increased if the geometry of the device is redesigned and lower compliance woven fabric substrate is employed, under the same axial force conditions. Also, higher output voltages are generated particularly if the substrate is thicker, such as Cotton (705 μm).

9.7 Improved Material Power Impact on Wearable Electronics Systems

The results shown in the previous section for the three types of forces fundamentally show the impact of the improved piezoelectric material in terms of its output energy per 1 Hz strike, bending and stretching considering resistance matching. The investigation of the resistance was important to show the maximum output energy that can be supplied by the piezoelectric element when a specific load is applied. This specific load is application dependent.

The output power of most of the low power piezoelectric energy harvester is small compared to the power consumption of most of the electronic devices used for wearable electronics and sensors (see Table 2-11). Similarly, our 1×1 cm^2 piezoelectric film (printed on Kermel woven-fabric) can produce maximum power of nearly 8 μW at optimum resistive load of 10 MΩ when a compressive force of 800 N. This power is lower than most of the systems listed in Table 2-11. Therefore, power management system is essential to wisely consume the power according to the output power produced from the harvester. This cannot be achieved without specifying the application and also knowing the power consumptions conditions of the employed electronic devices.

In the previous section, the fundamental tests represented by applying fundamental compressive, bending and tensile forces on a 1×1 cm^2 woven-fabric piezoelectric device were necessary to give a general overview about the impact of this material and the range of the applications that is suitable for. However, this section is dedicated to give examples of applications with estimate the power/energy consumption of them when this improved ECS-PolyPZT 6a film is used.

9.7.1 Self-powered Piezoelectric Force Mapping Sensor

Placing small piezoelectric elements as sensors on the sole part of shoe-insole can help provide a map of the force distribution of the sole part for healthcare monitoring during movement of a person [160]. This can be achieved when different forces are applied on the piezoelectric elements and different output voltage is produced for each piezoelectric element according to the shape topology of the bottom side of the foot and the weight of the person. Figure 9-21 shows the suggested shoe-insole piezoelectric force-mapping sensor (PFMS). Each output voltage is analysed and a map of stress distribution can be visualised for each foot. These output voltages that introduced form the sensor in the sole part can only be sent wirelessly for analysis because body movements limit the use of wires.

If a 1×1 cm^2 was used and ECS-PolyPZT 6a was screen-printed on a shoe-insole of a size 9, 48 devices (17 on the heel and 31 on the sole parts) will be introduced as shown in Figure 9-21. The proposed energy harvester can be considered when all of these 48 devices are connected creating the shoe-insole energy harvester.

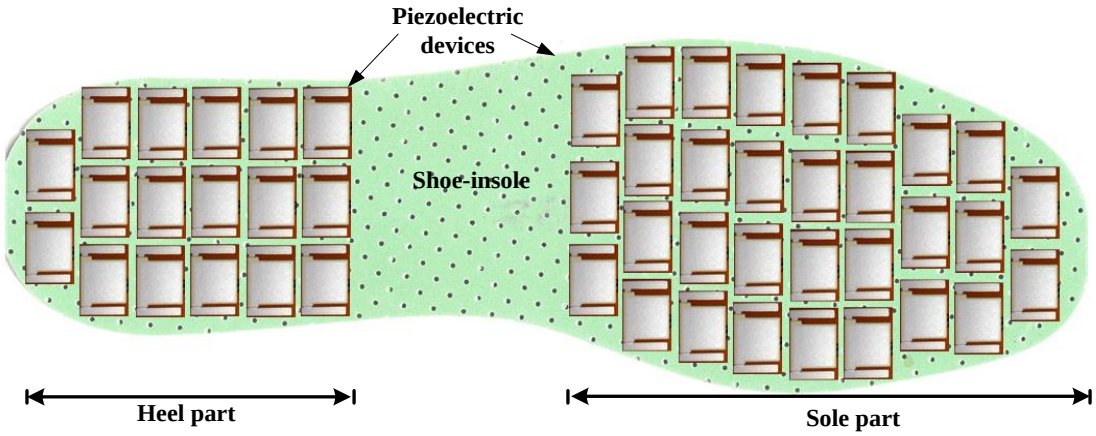

Figure 9-21: Self-powered shoe-insole piezoelectric force mapping sensor PFMS. A schematic of the proposed piezoelectric PFMS device. 17 and 31 of 1×1 cm^2 piezoelectric devices can be printed on the heel and the sole, respectively, of shoe-insole of size 9.

The initial self-powered PFMS system is schematically shown in Figure 9-22 which simply consists of the harvester, the conditioning circuit (e.g. rectifier), the PFMS (the 31 devices placed on sole part) and µ-controller and the transmitter (the output load). The alternating output voltage of the shoe-insole piezoelectric harvesters (48 piezoelectric devices) is conditioned using full-bridge rectifier (that has a typical efficiency of 81%). The whole shoe-insole piezoelectric devices (the heel and sole parts) all together contribute in charging the capacitor. As soon as the capacitor is fully charged the energy required for achieving one duty cycle (i.e. energy required to achieve sensor reading and data management and transmitting) , signals are subsequently obtained from the sole part to the µ-controller (reading state). The microcontroller passes the information to the transmitter to be sent to its final destination for analysis (transmission state).

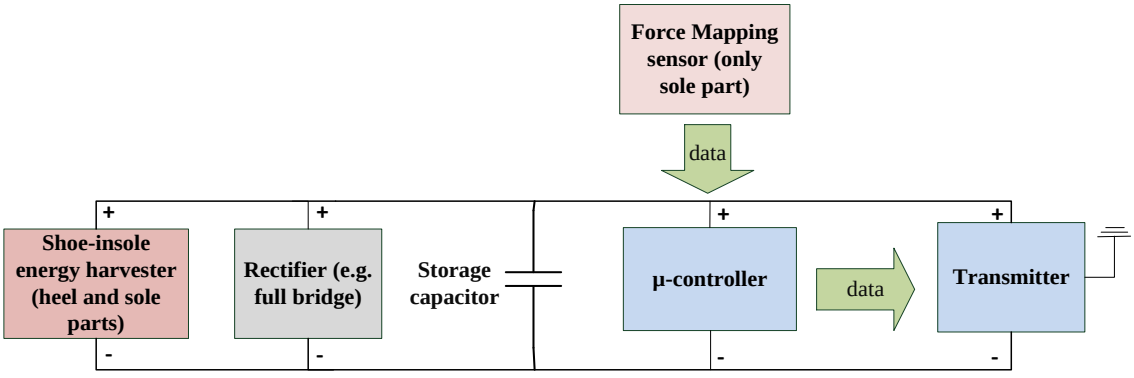

Figure 9-22: Initial design of the self-powered PFMS

The suitable µ-controller and transmitter for this system can be considered from Table 2-11 on page 43. The suggested µ-controller and transmitter for this system are PIC16F676, MICROCHIP and AM-RT4-433 transmitter, respectively, as their power consumption is low compared to other devices. The suggested capacitor that fulfils storing the required energy of one duty cycle is (44 µF). Table 9-3 shows the estimated energy consumption for each processing state according to the power consumption and the time required for processing for each state.

State	Operating devices	Duration	Power	Energy	Comments
Reading data	Only µ-controller	1.03 s	17µW	19.2 µJ	The reading data energy is the energy consumed by the µ-controller during the reading time. The µ-controller obtains the signal from the sensors placed at the sole part when 1 foot strike is achieved.
Transmitting data	µ-controller and transmitter	10 ms	8 mW	88.1µJ	The reading data energy is the combination of energy consumed by the µ-controller and the transmitter during the reading time.

Table 9-3: Estimated energy consumption for each step of the system

The alternating output voltage of the piezoelectric element typically requires a rectifier to convert the alternating output into DC. The output DC power from the rectifier is either stored in a capacitor or a rechargeable battery. Typically, the optimum impedance of the power conditioning circuit (e.g. full bridge rectifier) and the optimum load mentioned in the section 9.3.2 should match to achieve maximum output energy. However, because of the capacity of the storage capacitor, the input impedance of the power conditioning circuit changes with the capacitor voltage [161]. Accordingly, this makes impedance matching more challenging, which needs further experimental investigation and will be a study of future work.

Therefore, it is difficult to predict the optimum resistance across the capacitor that matches the conditioning circuit because it changes during charging. From Figure 9-9, if the optimum matching resistance (30 MΩ) is ideally considered, the output energy will be 0.2 µJ and in this case to charge the 44 µF capacitor to the required energy 107 µJ for achieving one duty cycle typically needs 13.8 seconds. However, if the matching resistance of the capacitor is 1 MΩ, the output energy will be 0.029 µJ and in this case to change the required energy needs 1.6 minutes.

From this, the time required to fully charge the capacitor with the required energy is initially estimated according to the resistive load state of the capacitor at the maximum and minimum energy levels (30 and 1 MΩ, respectively) when 1 or 48 devices are used as shown in Table 9-4. In case of using two devices in the shoe-insole, the range of the time required to fully charge the capacitor t_r with the required energy is ($5.5 \leq t_r \leq 38$ minutes) if the resistive load of the capacitor

is 30 and 1 MΩ, respectively. However in case of using the 48 devices in the insole, the range of time is different (14 seconds$\leq t_r \leq$ 1.58 minutes) when the resistive load of the 1 and 30 MΩ.

Number of devices on the insole	Resistive load (MΩ)	Expected time required to charge the capacitor
2	1	38 minutes
	30	5.5 minutes
48	1	1.58 minutes
	30	14 seconds

Table 9-4: Expected charging time if different number of devices used. Note, these calculations did not consider the current leakage of the capacitor

From these calculations, ECS-PolyPZT 6a film can power the wireless shoe-insole force mapping sensors (µ-controller and transmitter) by transmitting data for analysis every specific time. This specific time was estimated to be in the range of ($5.5 \leq t_r \leq 38$ minutes) or (14 seconds$\leq t_r \leq$1.58 minutes) if one or 48 devices are used, respectively. However, to confirm these calculations an experimental investigation has to be applied. The estimated values may vary if experimental investigation is adopted and also the capacitor leakage current is considered. The output voltage and energy for walking strike (1 Hz) can be improved by:

- Increasing the frequency (≥ 1Hz) of the strike (which will consequently increase the rate of charging when a capacitor is used).
- Increasing the number of the piezoelectric layers per device [95].
- Increasing the number of the 1×1 cm^2.

9.8 Conclusions

The output voltage, power and energy of the piezoelectric film on woven fabric substrates are dependent on the applied strain on the piezoelectric film. This strain is mainly dependent on the mechanical properties of the substrate, which create mechanical constraints on the piezoelectric film, and the type of force applied on the device. When compression or tension is applied to the device, the piezoelectric material is subjected to strain. The strain and the output voltage are only related to the compliance of the substrate with piezoelectric film that has the same geometry for all substrates. The variation in the d_{33} and also the strain on the material is significant with small variations in compliances over -1×10^{-9} m^2/N. When subjected to compressive force of 800 N, Kermel devices produce a maximum peak power and energy of 7.9 µW and 0.2 µJ with a resistive load of 10 and 30 MΩ, respectively. However, when a tensile force is applied, it produces a maximum peak voltage, power and energy of 1.1 V, 1.23 µW and 0.018 at tensile conditions of speed= 2 mm/s and displacement=0.7 mm and a resistive load of 1 MΩ.

However, when bending force is applied, it was found that the Cotton substrate produced greater peak power and energy of 2.5 μW and 0.2 μJ, respectively, at a 5 mm radius of curvature. This is because of the lower compliances and thickness of the Cotton plus interface layer substrates.

Considering area of the film (1×1 cm^2) the simple and high-mass production formulation and screen-printing process of our flexible piezoelectric composite film, the outputs are greater for the three types of forces compared to the contributions in the literature. This study gave an understanding of the relations between the outputs of the piezoelectric composite film and both the mechanical boundary conditions of the substrate and the type of the applied force. This kind of investigation was not provided in the literature.

Chapter 10: Conclusion and Future Work

10.1 Conclusions

In this thesis, low temperature flexible piezoelectric composite films deposited using screen-printing have been explored and developed. Improvements in the piezoelectric properties (described by d_{33} coefficients) of these screen-printed piezoelectric films have been found via the composite formulation and the post material processing. Throughout this study, the piezoelectric coefficient d_{33}, the relative dielectric constant ε_r, the mechanical flexibility (described by bending at maximum radius of curvature before failure) and the observed output energy the film can produce, are considered the main properties to describe the quality and the reliability of the proposed piezoelectric composite materials. This work has led to an improvement in the piezoelectric properties of the screen-printed flexible PZT-non-piezoelectric polymer composite films by 53.4 and 70% from the results obtained at the start of the thesis (22.8 pC/N) and from those obtained in University of Southampton laboratories (15 pC/N) [70], respectively, producing a final maximum d_{33} of 49 and 83 pC/N for films on Kapton and Polyester-cotton, respectively.

10.1.1 Poling Method Selectivity and Optimisation

A polarisation process is required to activate the piezoelectric properties of the ferroelectric materials. Choosing this poling process was an essential stage before developing the piezoelectric material. Amongst a plethora of poling methods, direct-contact poling (DCP) and corona discharge poling (CDP) were studied and compared. The poling process was optimised for both methods and achieved via the interrelated poling parameters of each method. After the optimisation process, the maximum d_{33} achieved for the film was obtained for each method (47 pC/N). The screen-printed PiezoPaint film showed visual cracks on the surface at radius of curvature of 20 mm when the flexibility was tested.

It was found that DCP and CDP provide comparable d_{33} coefficients using the same poling temperature and time of 220 °C and 5 min, respectively. Also, CDP gave a reasonable electric field distribution because of the existence of the bottom and top electrodes while the existence of the electric field is only confined by the area surrounded by the poling needle and field intensity. Three parameters were optimised for DCP: Poling field, temperature and time, whilst four are required for CDP: poling field, temperature, time and needle distance. In addition, applying the top electrode after the poling process for CDP will reduce the piezoelectric activity of the devices because heating the material will result in some depolarisation of the piezoelectric film.

Therefore, DCP which does not have these problems was selected as the poling process for this work.

10.1.2 Developing the Proposed Piezoelectric Material

The choice of binder in the PZT-polymer composite will affect the properties of the piezoelectric film. Two types of binders were used; Thermoplastic polymeric-based and adhesive thermosetting polymeric-based binders. Thermoplastic polymeric-based binders showed better piezoelectric properties than adhesive thermosetting polymeric-based ones. Thermoplastic polymeric-based binders ECS-PolyPZT 1, 2, 3 and 6 showed initial d_{33} values of 13.5, 20, 14.9 and 22.8 pC/N at maximum electric field when printed on alumina, at PZT-binder weight ratios of 8:1, 2.3:1, 8:1 and 2.71:1. These optimum weight ratios were found to provide the best compromise between maximum PZT weight loading, good mixing, good screen-printability, good bonding to the substrate and good flexibility (survived when bent around a 9 mm radius of curvature).

However, when further testing the properties of the films, the PZT-binder weight ratio was varied for the four films. The dielectric, piezoelectric properties and mechanical flexibility of the film were observed. ECS-PolyPZT 2a and 6a with PZT-binder weight ratios of 3:2 and 2.57:1, respectively, produced the best results. They showed dielectric constants (at 1 kHz) of 135 and 146, respectively. At these PZT-binder weight ratio, ECS-PolyPZT 2a and 6a films can even survive 2 and 4 complete bending cycles. The two materials produce d_{33} values of 25 and 27 pC/N, respectively, when printed on alumina substrates. These d_{33} values are further increased if the poling conditions of the materials were optimised.

10.1.3 The Substrate Clamping Effect on the d_{33} Measurements

Screen-printing ECS-PolyPZT 6a on fabric required treatment printed interface layer to overcome the roughness of the fabric. Without this, subsequent printed layers will be uneven and can lead to problems such as short-circuiting of the devices. After optimising the ECS-PolyPZT 6a poling process, it produced maximum constrained d_{33} values of 70, 40 and 36 when printed on Polyester-Cotton plus interface layer, Kapton and alumina, respectively. The optimum poling conditions were the same for each substrate (E = 3.7 MV/m, T = 90 °C and t = 6 minutes). The difference in the measured d_{33} values for different types of substrates is due to the mechanical boundary conditions which clamp and then constrain the expansion and contraction of the piezoelectric material on the 1-2 plane when the material is subjected to a mechanical force in direction 3.

From theoretical and practical investigations, it was confirmed that a reduction on the d_{33} values by 13%, 50% and 55% for Polyester-cotton plus interface, Kapton and alumina substrates, respectively. The average free-standing (without a substrate) d_{33} values for the composite were calculated to be 80 pC/N. The measured clamped d_{33} values on both alumina and Kapton substrates were very similar although the compliance of Kapton was 10^2 larger than alumina. This is because the variations in the clamping effect become minor below a specific compliance (around -1 x 10^{-9} m^2/N) as identified in section 5.4. The measured d_{33} value of the polyester-cotton plus interface is greater because its compliance is larger than this specific compliance.

10.1.4 Large-filler Particle Size Optimisation in the Composite Formulation

Large PZT particles are desirable in the piezoelectric composite films to enhance piezoelectric activity. However, the gaps between these particles reduce the overall density of the film and subsequently the piezoelectric activity. Large 2 µm PZT particle size powder was mixed with filler particles of 0.15, 0.3 and 0.8 µm diameter at calculated weight ratios. When mixing the optimum ECS-PolyPZT 2a and 6a with large (2 µm) and filler (0.8 µm) PZT particles at optimum weight ratios of 4:1, the d_{33} value for both materials printed on alumina when poled at optimum poling conditions is 36 pC/N. This produces a 16.6% improvement in piezoelectric performance compared to PZT formulations with only large particles. Reducing the filler size did not help increase the d_{33} values of the material. The reduction of the filler size can improve the density of the piezoelectric material but does not improve the piezoelectric activity. This result shows there is a compromise between improving the film density whilst also maintaining suitably large particles to provide the highest piezoelectric properties.

10.1.5 Applying Cold Isostatic Pressing (CIP) to Improve Film Density

Most of the piezoelectric composite films contain air voids which can reduce their dielectric and piezoelectric properties. These air voids can be reduced by applying high pressure to the piezoelectric film. After applying the CIP process to a sample of ECS-PolyPZT 6a at a maximum pressure of 250 MPa for 2 minutes, the dielectric constant and resistivity of the material become 211 and 7.1 GΩ.m, respectively. This shows an increase in the dielectric constant by 31% and a reduction in the resistivity by 43%. This reduction in resistivity increases the current through the piezoelectric element which increases the effective electric field on the PZT particles during the poling process. However, this increased current produced dielectric breakdown during poling if the same poling temperature (90°C) was used. Therefore, the poling temperature was reduced to 75°C. After poling the CIP-processed piezoelectric on Kapton and Polyester-cotton plus interface layer, the measured d_{33} values became 45 and 76.6 pC/N, respectively. This shows an increase of

11 and 8.6% from the original ECS-PolyPZT 6a film. The estimated free-standing d_{33} from this improvement was found to be 90 pC/N. This shows an increase of 11% from the previous free-standing value.

10.1.6 Applying Silver Nano-particles

Inserting 0.2% by weight silver nano-particles into ECS-PolyPZT 6a improved the dielectric constant and the d_{33} value by 14.6% and 8%, respectively, for the devices printed on Kapton. The material also showed a d_{33} value of 76 pC/N when printed on Polyester-cotton showing an increase of 8.6% compared to the original ECS-PolyPZT 6a.

When combining the effect of adding silver nano-particles in the film and the applications of CIP, the film showed a dielectric constant and resistivity of 262 and 5.9 GΩ.m, respectively, when the material printed on Kapton substrate. This shows an increase in the dielectric constant by 44.2% and a reduction in the resistivity by 52.8% compared to the original ECS-PolyPZT 6a film. The d_{33} value of the film was also improved to 49 pC/N showing an increase of 18.3% compared to the original material. Applying CIP process on the ECS-PolyPZT 6a film with 0.2% silver nano-particles by weight printed on Polyester-cotton substrate, increased the d_{33} value to 83 pC/N showing an increase by 15.6% and 8.4% compared to ECS-PolyPZT 6a without both the addition of silver nano-particles and CIP and the material only with 0.2% silver nano particles, respectively.

From these improvements, the new d_{33} free-standing value of the ECS-PolyPZT 6a with the addition of 0.2% silver nano-particles and CIP-processing was calculated as 98 pC/N. This value shows an 18.4% increase in the piezoelectric activity of original free-standing ECS-PolyPZT 6a film without the addition of silver nano-particles and CIP processing.

10.1.7 The Output Energy of Materials Printed on Woven-Fabrics

The d_{33} value is linked to the mechanical properties of the substrate and the compressive force applied in the 3-direction. Therefore, the output voltage, power and energy are also related to the mechanical properties of the substrates and the type of force that is applied to the piezoelectric film on the substrate.

For compressive and bending forces, the strain is mainly related to the compliance of the substrate. For substrates with compliances greater than (around -1×10^{-9} m^2/N), the change in the d_{33} and also the output voltage becomes significant. However, for bending force, the strain is highly related to the compliance of the substrate and the stress applied (which is highly dependent

on the radius of curvature of bending, and thickness of both the piezoelectric film and the substrate). From the results, it was found that woven-fabrics with higher compliances provided higher output voltage, power and energy when applying compressive and tensile forces. However, thicker woven-fabrics substrates that have less compliance provide lower outputs when applying bending force. The results have shown the mechanical properties of the substrate and the type of force applied play a significant role in the final energy output. Therefore, when designing a sensor, actuator or energy harvester for use on woven-fabrics, it is important to select these materials carefully to suit the application.

10.2 Summary

Figure 10-1 summarises three major studies that have been covered in this thesis; screen-printing and poling methods, improving the piezoelectric activity of screen-printed flexible low-temperature piezoelectric films and exploring such films on woven fabrics in terms of the d_{33} measurements and the output energy.

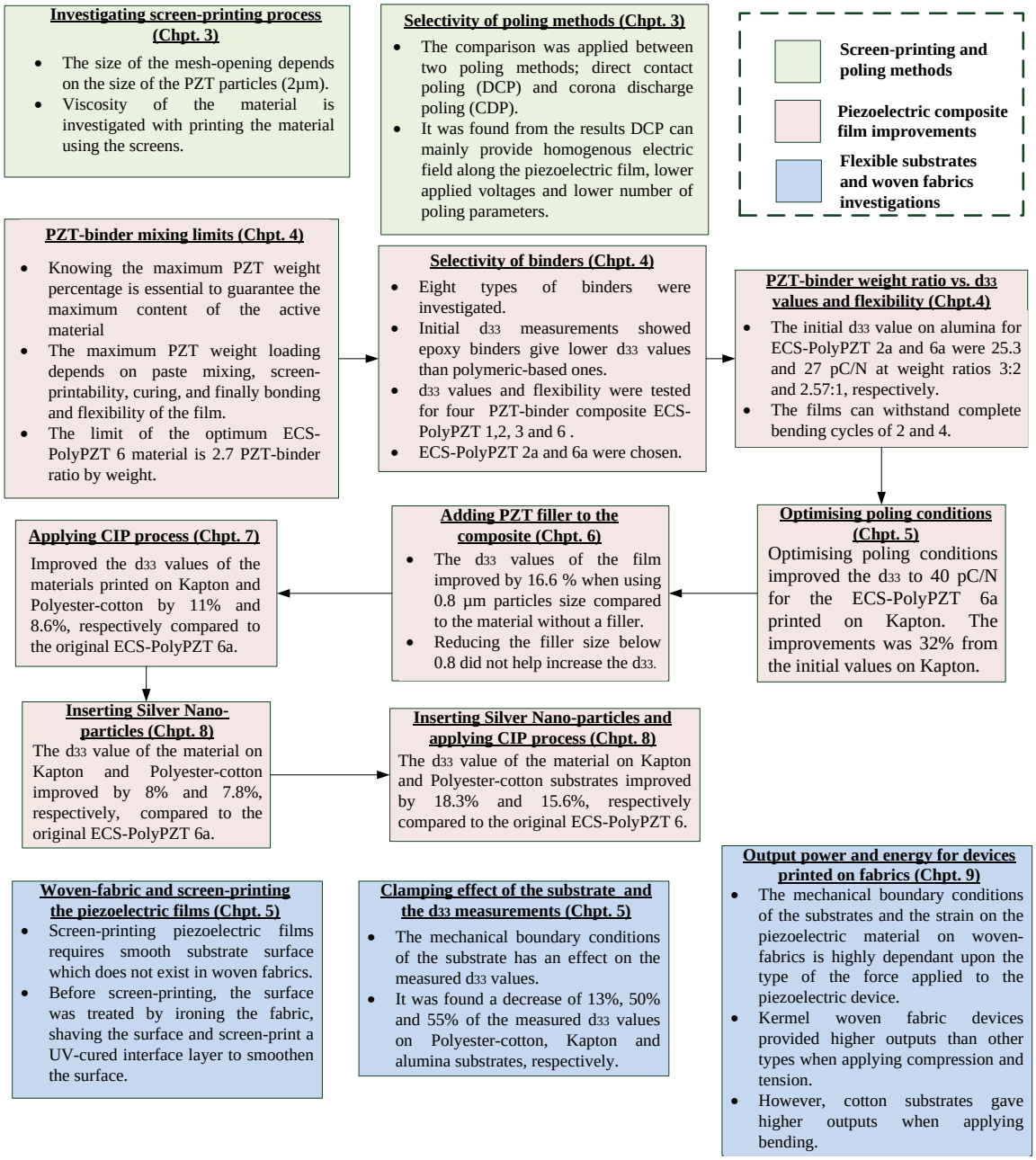

Figure 10-1: The summary of the screen-printability and poling process, material improvement and the investigation of the optimum material on woven-fabrics in terms of d_{33} measurements and output energy

Figure 10-2 summarises the improvement occurred in our optimum piezoelectric composite film ECS-PolyPZT 6 at each stage of the study and comparing them with the maximum d_{33} value of the flexible PZT-non-piezoelectric polymer composite films achieved at University of Southampton laboratories (15 pC/N) [70]. The maximum d_{33} values achieved in the study are 49 and 83 pC/N for devices printed on Kapton and Polyester-cotton. These values are greater than the results when started this thesis and the results in [70] by 53.4 and 70% , respectively, if only ECS-PolyPZT 6 printed on Kapton are compared. If ECS-PolyPZT 6 film on Polyester-cotton is considered, the results are greater by 72.5 and 82%, respectively.

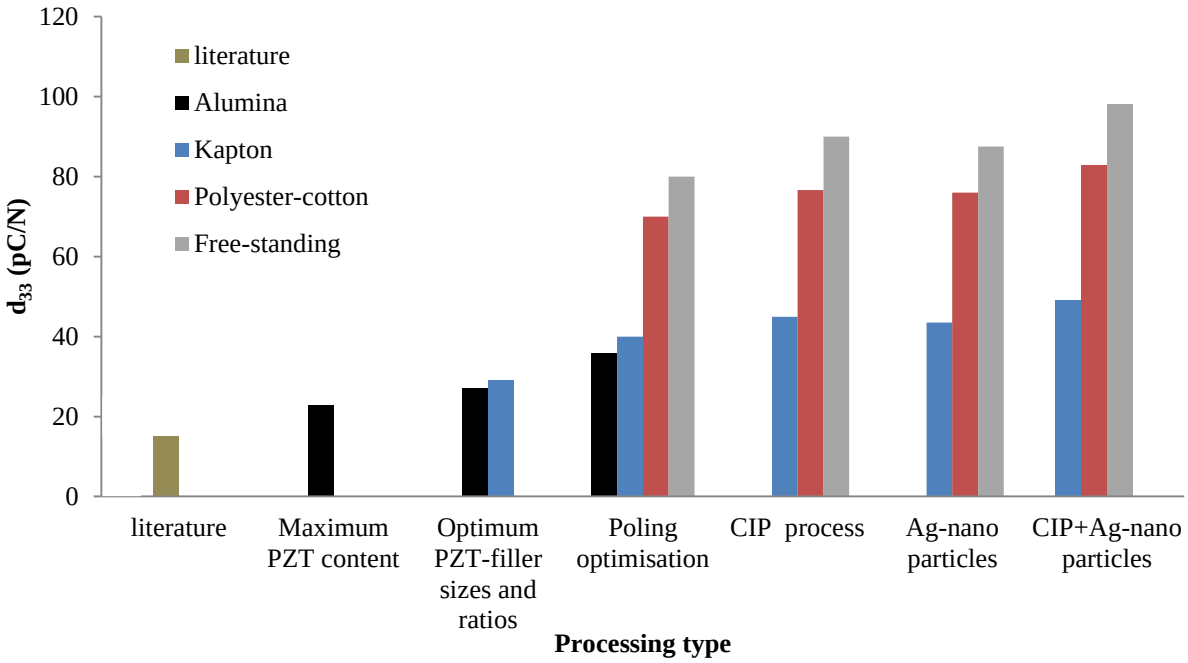

Figure 10-2: Summary showing the improvement of the piezoelectric activity of the ECS-PolyPZT 6 at each stage for the chosen material films printed on alumina, Kapton, Polyester-cotton substrate as well as the free-standing films

10.3 Future Work

10.3.1 Material Improvements

- Investigating the piezoelectric, dielectric and mechanical properties of the piezoelectric film when increasing the main PZT particle size (e.g. 3 or 4 µm) and its corresponding filler. Increasing the size of the PZT particle may increase the piezoelectric properties of the material but this may degrade its mechanical flexibility.

10.3.2 Design and Packaging of the Piezoelectric Device

- The effect on the output of the piezoelectric device on fabric may be investigated when increasing the size of the piezoelectric film (greater than 1 × 1 cm^2).
- Screen-printing multi-layer piezoelectric device and test the outputs of the film when applying the three types of forces. The mechanical flexibility limitations could be investigated with the respect to the number of the layers.
- Investigating the output voltage, energy and power after screen-printing the UV-curable encapsulation layer on the top of the piezoelectric device on fabric. The

compressive and tensile and bending forces can be included in the investigation. Printing the encapsulation layer on the top of the piezoelectric device may improve the durability of the device and also protect the piezoelectric device from damage.

10.3.3 Potential Applications for the Piezo-Composite Films

10.3.3.1 Piezoelectric Shoe-Insole Energy Harvester

- An additional area of investigation would be more enhancement of the piezoelectric shoe-insole energy harvester developed by [2] at University of Southampton. This energy harvesting system greatly depends on the piezoelectric activity (d_{33}) of the printed piezoelectric film. Screen-printing the improved ECS-PolyPZT 6a with 0.2% Ag-nano particles by weight will improve the output voltage, power and energy of the device.
- Screen-print the encapsulation layer and observe the outputs of the devices comparing them with a device without encapsulation layer.
- For protecting the device from being damaged and the foot from being harmed by the printed materials of the capacitive structure an encapsulation layer can be printed. An additional area of study would be testing the output voltage, power and energy with and without this layer. This is an additional mechanical constraint to the piezoelectric film when applying an external force.

10.3.3.2 Self-powered Wireless Shoe-Insole Force-Mapping Sensor

Force mapping sensor that developed by [2] was an initial design for screen-printed piezoelectric version on an insole. The sensor does not need energy to operate as it can be only activated when a force is applied at the piezoelectric elements. The data of the sensor is actually an output voltage with different amplitude at every piezoelectric element. These data can be extracted using an interface circuit, interpreted and transmitted using a microcontroller and low-power transmitter. The microcontroller and the transmitters can be powered with management by the heel device placed at the rear side of the insole. The sensor could be validated by testing it for different people.

10.3.3.3 Finger-joint Piezoelectric Energy Harvester

This kind of energy harvesters exploits the bending force at maximum bending radius of curvature of 9 mm. The device can be screen-printed on woven-fabric gloves. Electric energy is generated when completing one cycle of bending.

Appendix A Technical Definitions

Screen Type Technical Definitions

As mentioned in the literature, the screens consist of mesh and a frame that hold and fix the mesh with tension. Tension is required to guarantee that the surface of the material is levelled and even. The mesh consists of the screen fabric with opening between threads and emulsion that blocks these openings when defining the aiming pattern of the screen. The screen specifications are defined by these basic parameters. These parameters define the final screen that needs to order. They depend upon the type and viscosity of the paste, aiming thickness, smoothness and resolution of the printed layer. These parameters are summarised and defined as follows [162, 163]:

- *Mesh-opening (w):* is the distance between two threads. It is very important parameter that mainly specifies the volume and the intensity of the paste that goes through the screen. Also, the maximum diameter of the particles inside the composites has to be small enough (e.g. at least 10 times smaller than the mesh-opening) to easily pass through and also not to block these opening and consequently block the screen. The larger the mesh-opening, the higher the volume of the printed paste and thicker the deposited layer. However, increasing the mesh-opening leads to uneven surface of the printed layer. Viscous materials require smaller mesh openings otherwise it will chaotically spread over the substrate.

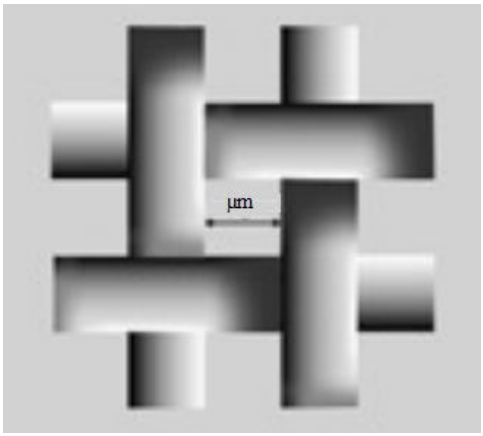

Figure A- 1: Schematic showing the diameter of the mesh opening

- *Thread Diameter (d):* It has an effect on the smoothness of the surface and also controls the diameter of the mesh opening. The larger the diameter of the thread the less smooth and even the surface of the printed material. The circular shape of the threads will also create deformations (e.g. that can be seen by an eye) on the surface of the printed layer.

Therefore, provided the thread diameter is smaller, these deformations caused by the threads will be eliminated.

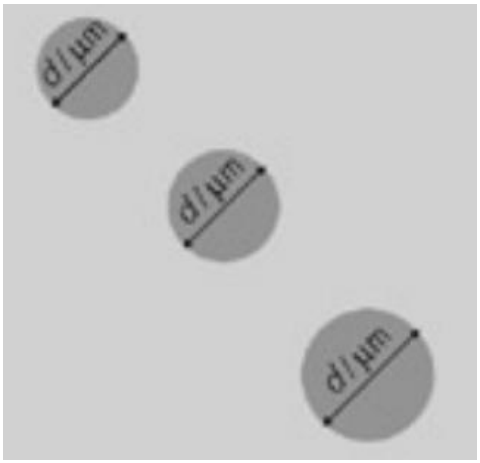

Figure A- 2: Schematic of thread diameter

- *Mesh-count (n):* is the number of threads per centimetre. The mesh opening and the thread diameter can actually control the mesh count of the screen. These three parameters are interrelated. When ordering a new screen only two of them can define a particular screen.

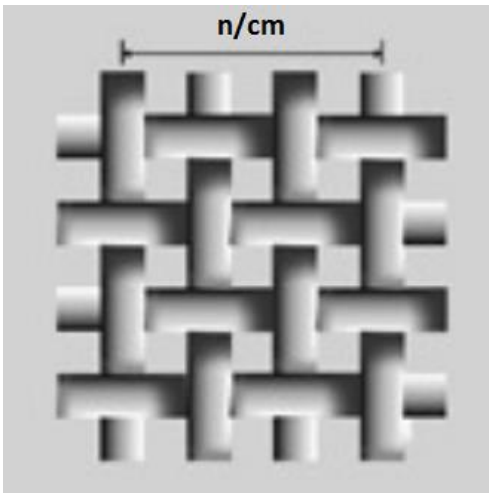

Figure A- 3: Schematic showing the number of threads for each centimetre

- *Percentage of open area:* It reflects the ratio of the mesh-opening relative to the whole screen expressed in %. Increasing the percentage of the open area will lead to increasing the amount of the printed paste. The calculation of the percentage of open-area is as follows.

$$\alpha\,[\%] = \frac{w^2}{(w+d)^2}.100$$

Figure A- 4: Schematic showing the ratio of open area

- *Open-area volume:* This is the mesh-opening area that allows a maximum volume V_{th} of a paste to pass through the screen. This are reflects the amount of paste passes through.

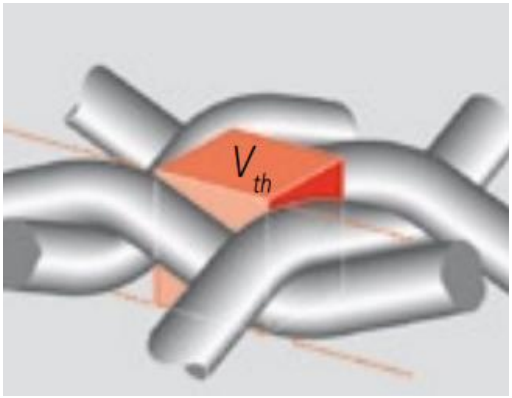

Figure A- 5: Schematic showing the open area volume

Appendix B Filler Particle Size Calculations

Particle Size Distributions

The two distributions that suggested by [84, 96] are shown in Figure B- 1. These two distributions are only assumed to estimate the range of large PZT to SFP weight ratio that could be mixed.

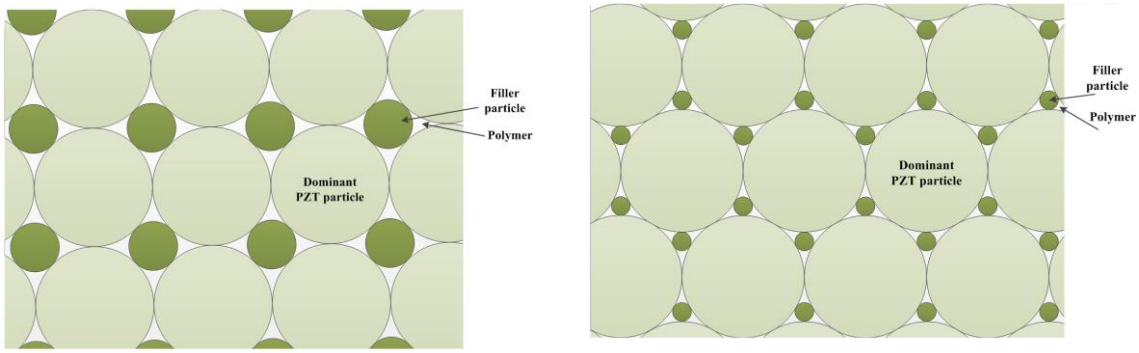

(a) (b)

Figure B- 1: Schematic of two possible large particles to SFP distribution inside polymer matrix. (a) Particle distribution 1. (b) Particle distribution 2

Estimation of the Filler sizes

The large and filler particle sizes of the two distributions shown in Figure B- 1 were calculated. Figure B- 1 shows schematically the calculation diagrams of both particles distributions. The target was to know the sides' lengths of both the inner square and the equiangular triangle which covers their corresponding SFPs in distributions 1 and 2, respectively.

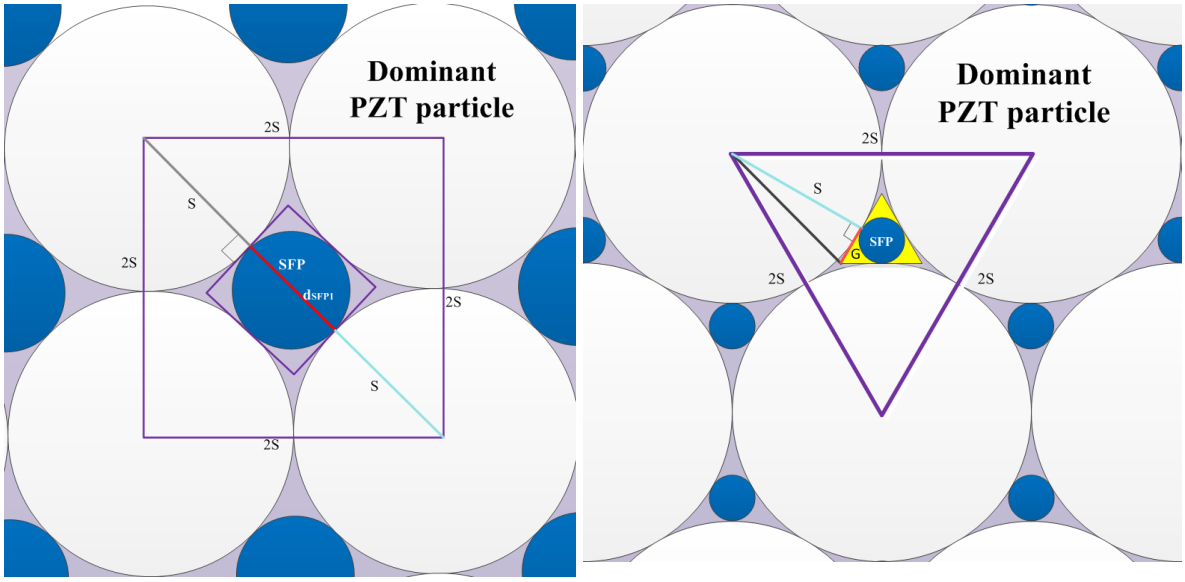

(a) (b)

Figure B- 2: Schematic diagrams for the calculations of method 2 for particle distribution (a) 1 and (b) 2

If these lengths are known, the diameter of the SFP will be equal to the side of the square in distribution 1. The diameter of the SFP of distribution 1 was calculated with the aid of the diagonal of the outer square shown in Figure B- 2(a). The diagonal of the outer square D can be calculated using the following equation.

$$D = \sqrt{2S^2} \tag{10-1}$$

Where, S is the radius of the large particle. Then the diameter of the SFP can be calculated using equation (10-2).

$$d_{SFP1} = D - 2S \tag{10-2}$$

However, the length of the inner equiangular triangle side shown in Figure B- 2(b) can be calculated by the following relationship

$$\cos(90°) = \left|\frac{G}{S}\right| \tag{10-3}$$

Then the side of the inner triangular is double the length of G.

$$U = 2G \tag{10-4}$$

The diameter of circle inside an equiangular tringle can be calculated using equation (10-5)

$$d_{SFP2} = \frac{U^3}{\sqrt{3U^4}} \tag{10-5}$$

If the value of the large particle diameter was substituted in the previous equations, the SFPs sizes of particle distributions 1 and 2 will be 0.8 and 0.3, respectively. The next stage was to calculate for the PZT large particle to SFP weight ratios that can be mixed with the aid 2- and 3-dimentional representations for distribution 1 and 2.

Publications

A. Almusallam, R. N. Torah, K. Yang, J. Tudor, and S. P. Beeby, "Flexible Low Temperature Piezoelectric Films for Harvesting from Textiles," presented at the PowerMEMS 2010, Atalanta, USA, 2012.

A. Almusallam, R. N. Torah, D. Zhu, M. J. Tudor, and S. P. Beeby, "Screen-printed piezoelectric shoe-insole energy harvester using an improved flexible PZT-polymer composites," presented at the PowerMEMS 2013, London, 2013.

A. Almusallam, K. Yang, D. Zhu, R. Torah, J. Tudor , and S. Beeby "Development of a low temperature PZT/polymer paste for screen printed flexible electronics applications," presented at the IEEE Sensors, 2014, Valencia, 2014.

A. Almusallam, K. Yang, Z. Cao, D. Zhu, J. Tudor , and S. P. Beeby, "Improving the dielectric and piezoelectric properties of screen-printed low temperature PZT/polymer composite using cold isostatic pressing," presented at the PowerMEMS 2014, Awaji Island, Hyogo, Japan, 2014.

N. Jamel, D. Zhu, A. Almusallam, R. Torah, K. Yang, S. P. Beeby, *et al.*, "Screen printed free-standing resonator with piezoelectric excitation and detection on flexible substrate," presented at the EUROSENSORS 2014, the 28th European Conference on Solid-State Transducers, Brescia, Italy, 2014.

N. Jamel, A. Almusallam, A. Zhu, R. Torah, K. Yang, J. Tudor, *et al.*, "Screen-printed free-standing piezoelectric devices using low temperature process," presented at the Design, Test, Integration and Packaging of MEMS/MOEMS (DTIP), 2015 Symposium, Montpellier, France, 2015.

A. Almusallam, K. Yang, D. Zhu, R. N. Torah, A. Komolafe, J. Tudor , *et al.*, "Clamping effect on the piezoelectric responses of screen-printed low temperature PZT/polymer films on flexible substrates " *Smart Materials and Structures*, vol. 24, p. 8, 2015.

Bibliography

[1] A. Almusallam, R. N. Torah, K. Yang, J. Tudor, and S. P. Beeby, "Flexible Low Temperature Piezoelectric Films for Harvesting from Textiles," presented at the PowerMEMS 2010, Atalanta, USA, 2012.

[2] A. Almusallam, R. N. Torah, D. Zhu, M. J. Tudor, and S. P. Beeby, "Screen-printed piezoelectric shoe-insole energy harvester using an improved flexible PZT-polymer composites," presented at the PowerMEMS 2013, London, 2013.

[3] A. Almusallam, K. Yang, D. Zhu, R. Torah, J. Tudor , and S. Beeby "Development of a low temperature PZT/polymer paste for screen printed flexible electronics applications," presented at the IEEE Sensors, 2014, Valencia, 2014.

[4] A. Almusallam, K. Yang, Z. Cao, D. Zhu, J. Tudor , and S. P. Beeby, "Improving the dielectric and piezoelectric properties of screen-printed low temperature PZT/polymer composite using cold isostatic pressing," presented at the PowerMEMS 2014, Awaji Island, Hyogo, Japan, 2014.

[5] A. Almusallam, K. Yang, D. Zhu, R. N. Torah, A. Komolafe, J. Tudor , *et al.*, "Clamping effect on the piezoelectric responses of screen-printed low temperature PZT/polymer films on flexible substrates " *Smart Materials and Structures,* vol. 24, p. 8, 2015.

[6] J. Curie and P. Curie, "Development by pressure of polar electricity in hemihedral crystals with inclined faces," *Bulletin de la Société Chimique de France,* vol. 3, p. 90, 1880.

[7] S. Beeby, M. Kraft, and N. White, *MEMS Mechanical Sensors*. Boston: Artch House, Inc., 2004.

[8] C. Jean-Mistral, S. Basrour, and J.-J. Chaillout, "Comparison of electroactive polymers for energy scavenging applications," *IOP Publishing,* vol. 19, p. 14, 2010.

[9] G. Lippmann, "Principe de la conservation de l électricité," *Ann de Chemie e de Physique,* vol. 5, p. 145, 1881.

[10] "Sparkler piezoceramics: General information," Sparkler Ceramics PVT. LTD.

[11] B. Jaffe, W. R. Cook Jr, and H. Jaffe, *Piezoelectric ceramics*: Academic Press in London and New York, 1971.

[12] H. Kawai, "Piezoelectricity of polyvinylidenefluoride," *Japanese Journal of Applied Physics,* vol. 8, pp. 975-976, 1969.

[13] P. Ueberschlag, "PVDF piezoelectric polymer," *Sensor Review,* vol. 21, pp. 118-126, 2001.

[14] Perpetuum. (2015). *Perpetuum vibration energy harvester (VEH)*. Available: http://www.perpetuum.com/products/vibration-energy-harvester.asp

[15] MicroGenSystems.Available: https://www.microgensystems.com/content/MicroGen_BOLT-INDUSTRIAL_Jun2013.pdf

[16] M. Shiozaki, T. Toriyama, S. Sugiyama, H. Ueno, and K. Itoigawa, "Fabrication of flexible thermopile generator sheet," presented at the PowerMEMS Kyoto, Japan, 2004.

[17] D. Damjanovic, "Hysteresis in piezoelectric and ferroelectric materails," in *The science of hysteresis*. vol. 3, G. Bertotti and I. Mayergoyz, Eds., ed: Elsevier Inc., 2005.

[18] S. Rajala and J. Lekkala, "PVDF and EMFi sensor material A comparative study," *Procedia Engineering,* vol. 5, pp. 862-865, 2010.

[19] T. T. Wang, J. M. Herbert, and A. M. Glass, *The applications of ferroelectric polymers*. Glasgow: Blackie and Son Ltd, 1988.

[20] "An American National Standard: IEEE Standard on Pieozelectricity ANSI/IEEE Std 176-1987," 1987.

[21] R. J. Nelmes and W. F. Kuhs, "The crystal structure of tetragonal $PbTiO_3$ at room temperature and at 700K," *Solid State Communications,* vol. 54, 1985.

[22] Z. Huang, Q. Zhang, S. Corkovic, R. Dorey, and R. W. Whatmore, "Comparative measurements of piezoelectric coefficient of PZT films by Berlincourt, interferometer,

and vibrometer methods," *IEEE TRansactions of ultrasonics, ferroelectrics, and frequency control*, vol. 53, 2006.
[23] S. Zerfoss and L. R. Johnson, "Crystal chemical relations in inorganic piezoelectric materials," *Mineralogical Society of America*, pp. 60-67.
[24] P. Guggilla and A. K. Batra, "Novel electroceramic: Polymer composites preperation, properties and applications, Nanocomposites and polymers with analytical methods," in *Nanocomposites and polymers with analytical methods*, J. Cuppoletti, Ed., ed: InTech, 2011.
[25] B. Ando, P. Giannone, S. Graziani, and N. Pitrone, "Characterization of the dielectric and pyroelectric properties," *IEEE Transactions of Instrumentation and Measurement*, vol. 57, pp. 1939-1948, 2008.
[26] J. C. Joshi and A. L. Dawar, "Pyroelectric materials, their properties and applications," *Physica Status solidi (a)*, vol. 70, pp. 353-369, 1982.
[27] J. Li, Y. Liu, Y. Zhang, H.-L. Cai, and R.-G. Xiong, "Molecular ferroelectrics: where electronics meet biology," *Physical Chemistry Chemical Physics*, vol. 15, 2013.
[28] G. Kovacs, *Micromachined Transducers Sourcebook*: McGraw-Hill, 1998.
[29] Almaz Optics. Available: http://www.almazoptics.com/Quartz.htm
[30] J. Chen and R. Panda, "Review: commercialization of piezoelectric single crystals for medical imaging applications," *Ultrasonics Symposium, 2005 IEEE*, vol. 1, pp. 235-240, 18-21 Sept 2005.
[31] M. Sitti, D. Campolo, J. Yan, R. S. Fearing, T. Su, D. Taylor, *et al.*, "Development of PZT and PZT-PT bansed unimorph actuators for micromechanical flapping mechanisms," presented at the IEEE International Conference on Robotics and Automation, 2001, Seoul, Korea, 2001.
[32] L. M. Ewart, E. A. McLaughlin, H. C. Robinson, A. Amin, and J. J. Stace, "Mechanical and Electromechanical Properties of PMN-PT Single Crystals for Naval Sonar Transducers," presented at the Applications of Ferroelectrics, 2007. ISAF 2007. Sixteenth IEEE International Symposium on, Nara, 2007.
[33] B. Neese, Y. Wang, B. Chu, K. Ren, S. Liu, and Q. Zhang, "Piezoelectric responses in poly(vinylidene fluoride/hexafluoropropylene) copolymers," *Applied Institution of Physics: Applied Physics Letters*, vol. 90, 2007.
[34] A. Erturk and D. J. Inman, *Piezoelectric energy harvesting*: John Wiley & Sons, Ltd, 2011.
[35] M. A. Materials, 2015.
[36] Ferroperm. (2014). Available: file:///C:/Users/asa1g09/Desktop/MEGGITT%20(1).pdf
[37] B. Ameduri, "From vinylidene fluoride (VDF) to the applications of VDF-containing polymers and copolymers: Recent developments and future trends," *Chemical Review*, vol. 109, pp. 6632-6686, 2009.
[38] X. Qiu, "Patterned Piez-, Pyro-, and ferroelectricity of poled polymer electrets," *Journal of Applied Physics*, vol. 108, p. 19, 2010.
[39] Y. Bar-Cohen, "Electroactive polymers as artificial muscles-Reality and Challenges," presented at the Structures, Structural Dynamics, and Materials Conference (SDM), Gossamer Spacecraft Forum (GSF), Seattle WA, 2001.
[40] C. Park, Z. Ounaies, K. E. Wise, and J. S. Harrison, "In Situ poling and imidization of amorphous piezoelectric polymides," ICASE: NASA Langley's CSE Center2002.
[41] J. Simpson, Z. Ounaies, and C. Fay, "Polarization and piezoelectric properties of a nitrile substituted polyimide," 1996.
[42] S. Miyata, M. Yoshikawa, S. Tasaka, and M. Ko, "Piezoelectricity revealed in the copolymer of vinylidene cyanide and vinyl acetate," *Polymer Journal*, vol. 12, pp. 857-860, 1980.
[43] J. S. Harrison and Z. Ounaies, "Piezoelectric polymers," *Encyclopedia Of Polymer Science and Technology*, vol. 3, 2002.
[44] J. E. Mark, *Physical Properties of Polymers Handbook*: Springer Science+Business Media, LLC, 2007.

[45] C. Jen, M. Sayer, G. Yi, and J. F. Bussiere, "Fiber-optic piezoelectric devices," United States Patent, 1992.
[46] E. Bihler, K. Holdik, and W. Eisenmenger, "Polarization distribution in isotropic, stretched or annealed PVDF films," *IEEE Transactions on Electrical Insulations*, vol. 24, p. 5, 1989.
[47] A. Omar, "Processing, morphology and product parameters of PVDF filaments for biomedical applications," Universiteit Gent, 2008.
[48] H. R. Gallantree, "Review of transducer applications of polyvinylidene fluoride," in *Solid-State and Electron Devices, IEE Proceedings*, 1983.
[49] K. Ren, S. Liu, M. Lin, Y. Wang, and Q. M. Zhang, "A compact electroactive polymer actuator suitable for refreshable Braille display," *Sensors and Actuators A: Physical*, pp. 335-342, 2008.
[50] C. Li, P. Wu, S. Lee, A. Gorton, M. J. Schulz, and C. H. Ahn, "Flexible dome and bump shape piezoelectric tactile sensors using PVDF-TrFE copolymer," *Journal of Microelectromechanical Systems*, vol. 17, pp. 334-341, 2008.
[51] L. F. Brown, "Design considerations for piezoelectric polymer ultrasound transducers," *IEEE Transactions on Ultrasonics, Ferroelectrics and Frequency Control*, vol. 47, pp. 1377-1396, 2000.
[52] M. Nakayama, Y. Uenaka, S. Kataoka, Y. Oda, K. Yamamoto, and Y. Tajitsu, "Piezoelectricity of Ferroelectret Porous Polyethylene Thin Film," *Japanese Journal of Applied Physics*, vol. 48, 2009.
[53] C. Park, Z. Ounaies, K. E. Wise, and J. S. Harrison, "In situ poling and imidization of amorphous piezoelectric polyimides," *Polymer* vol. 45, pp. 5417-5425, 2002.
[54] M. Zirkl, A. Sawatdee, U. Helbig, M. Krause, G. Scheipl, E. Kraker, *et al.*, "An all-printed ferroelectric active matrix sensor network based on only five functional materials forming a touchless control interface," *Advanced Materials*, vol. 23, pp. 2069-2074, 2011.
[55] J. Y.-H. Kim, A. Cheng, and Y.-C. Tai, "Parylene-C as a piezoelectric material," presented at the Micro Electro Mechanical Systems (MEMS), 2011 IEEE 24th International Conference, Mexico, 23-27 January 2011.
[56] R. Schulze, T. Gessner, M. Schueller, R. Forke, D. Billep, M. Heinrich, *et al.*, "Integration of piezoelectric polymer transducers into microsystems for sensing applications," presented at the Applications of Ferroelectrics held jointly with 2012 European Conference on the Applications of Polar Dielectrics and 2012 International Symp Piezoresponse Force Microscopy and Nanoscale Phenomena in Polar Materials (ISAF/ECAPD/PFM), 2012 Intl Symp, 2012.
[57] A. Decharat, S. Wagle, and F. Melandø, "Effect of polymer electrode thickness on the acoustical properties of all-screen printed piezoelectric PVDF copolymer transducers," *Japanese Journal of Applied Physics*, vol. 53, 2014.
[58] J. Doring, V. Bovtun, M. Gaal, J. Bartusch, A. Erhard, M. Kreutzbruck, *et al.*, "Piezoelectric and electrostrictive effects in ferroelectret ultrasonic transeducers," *Journal of Applied Physics*, vol. 112, 2012.
[59] Z. An, M. Mao, J. Cang, Y. Zhang, and F. Zheng, "Significantly improved piezoelectric thermal stability of cellular polypropylene films by high pressure fluorination and post-treatments," *Journal of Applied Physics*, vol. 111, 2012.
[60] X. Zhang, J. Hillenbrand, G. M. Sessler, S. Haberzettl, and K. Lou, "Fluoroethylenepropylene ferroelectrets with patterned microstructure and high, thermally stable piezoelectricity," *Applied Physics A*, vol. 107, pp. 621–629, 2012.
[61] J.-W. Tsai, J.-J. Wang, and Y.-C. Su, "Piezoelectric rubber films for human physiological monitoring and energy harvesting," presented at the Micro Electro Mechanical Systems (MEMS), 2013 IEEE 26th International Conference 2013.
[62] J. F. Tressler, S. Alkoy, A. Dogan, and R. E. Newnham, "Functional composites for sensors, actuators and transducers," *Composites: Part A*, vol. 30, pp. 477-482, 1999.

[63] H. Shifeng , L. Lingchao, C. Jun, X. Dongyu, L. Futian, and C. Xin, "Influence of ceramic particle size on piezoelectric properties of cement-based piezoelectric composites," *Ferroelectrics,* vol. 332, pp. 187-194, 2006.

[64] H.-G. Lee and H.-G. Kim, "Ceramic particle size dependence of dielectric and piezoelectric properties of piezoelectric ceramicpolymer composites," *Journal of Applied Physics,* vol. 67, pp. 2024-2028, 1990.

[65] W. Supmak, A. Petchsuk, and A. Thanaboonsombut, "Influence of ceramic particle sizes on electrical properties of lead zirconate titanate (PZT)/nylon57 composites," *Journal of Metals, Materials and Minerals,* vol. 18, pp. 147-151, 2008.

[66] Z. Li and H. Gonga, "Effects of particle size on the piezoelectric properties of 0-3 PZT/cement composites," in *AIP Conference*, 2008, pp. 538-543.

[67] G. Rujijanagul, S. Boonyakul, and T. Tunkasiri, "Effect of the particle size of PZT on the microstructure and the piezoelectric properties of 0-3 PZT/polymer composites," *Journal of Material Science Letters,* vol. 20, pp. 1943-1945, 2001.

[68] D. M. Reed, T. T. Srinivasan, Q. C. Xu, and R. Newnham, "Effect of particle size on the dielectric and piezoelectric properties of $PbTiO_3$-polymer composities," presented at the Applications of Ferroelectrics, 1990., IEEE 7th International Symposium, 1990.

[69] B. Ploss, B. Ploss, F. G. Shin, H. L. W. Chan, and C. L. Choy, "Pyroelectric or piezoelectric compensated ferroelectric composites," *Applied Physics Letters,* vol. 76, pp. 2776-2778, 2000.

[70] T. Papakostas and N. White, "Screen printable polymer piezoelectrics," *Sensor Review,* vol. 20, pp. 135-138, 2000.

[71] T. Papakostas, N. R. Harris, S. P. Beeby, and N. M. White, "Piezoelectric thick-film polymer pastes," presented at the Eurosensors XII 13-16 September 1998, 1998.

[72] J. M. Hale, J. R. White, R. Stephenson, and F. Liu, "Development of piezoelectric paint thick-film vibration sensors," *Proceedings of the Institution of Mechanical Engineers, Part C: Journal of Mechanical Engineering Science,* vol. 219, 2005.

[73] M. Dietze and M. Es-Souni, "Structural and functional properties of screen-printed PZT-PVDF-TrFE composites," *Sensors and Actuators,* vol. 143, pp. 329-334, 2008.

[74] Y. H. Son, S. Y. Kweon, S. J. Kim, Y. M. Kim, T. M. Hong, and Y. G. Lee, "Fabrication and electrical properties of PZT-PVDF 0-3 type composite film," *Integrated Ferroelectrics,* vol. 88, pp. 40-50, 2007.

[75] T. Yamada, T. Ueda, and T. Kitayama, "Piezoelectricity of a high-content lead zirconate titanate/polymer composite," *Journal of Applied Physics,* vol. 53, pp. 4328-4332, 1982.

[76] D. A. van den Ende, B. F. Bory, W. A. Groen, and S. van der Zwaag, "Improving the d_{33} and g_{33} properties of 0-3 piezoelectric composites by dielectrophoresis," *Journal of Applied Physics,* vol. 107, 2010.

[77] K. Elkjaer, K. Astafiev, E. Ringgaard, and T. Zawada, "Integrated sensor arrays based on PiezoPaint for SHM applications," presented at the Annual Conference of the Prognostics and Health Management Society, 2013.

[78] K. Prashanthi, N. Miriyala, R. D. Gaikwad, W. Moussa, V. Ramgopal Rao , and T. Thundat, "Vibtrational energy harvesting using photo-patternable piezoelectric nanocomposite cantilevers," *Nano Energy,* vol. 2, pp. 923–932, 2013.

[79] R. N. Torah, S. P. Beeby, M. J. Tudor, and N. White, "Thick-film piezoceramics and devices," *Journal of Electroceram,* vol. 19, pp. 95-110, 2007.

[80] Q. Li, Z.-L. Xu, and L.-Y. Yu, "Effects of mixed solvents and PVDF types on performances of PVDF microporous membrances " *Journal of Applied Polymer Science,* vol. 115, pp. 2277–2287, 2010.

[81] X.-D. Chen, D.-B. Yang, Y.-D. Jiang, Z.-M. Wu, D. Li, F.-J. Gou, *et al.*, "0-3 Piezoelectric composite film with high d_{33} coefficient," *Sensors and Actuators A: Physical,* vol. 65, pp. 194-196, 1998.

[82] D. P. J. Cotton, P. H. Chappell, A. Cranny, and N. White, "A new binderless thick-film piezoelectric paste," *Journal of Materials Science: Materials in Electronics,* vol. 18, pp. 1037-1044, 2007.

[83] R. N. Torah, S. P. Beeby, and N. M. White, "Improving the piezoelectric properties of thick-film PZT: the influence of paste composition, powder milling process and electrode material," *Sensors and Actuators A: Physical*, vol. A 110, pp. 378-384, 2004.
[84] R. N. Torah, S. P. Beeby, and N. M. White, "An improved thick-film piezoelectric material powder blending and enhanced processing parameters," *IEEE transactions on ultrasonics, ferroelectrics, and frequency control*, vol. 52, pp. 10-16, 2005.
[85] http://www.substech.com/dokuwiki/doku.phpid=sinteringofceramics.
[86] W. R. DeHollander and Y. Nivas, "Sintering furnace with hydrogen carbon dioxide atmosphere," United States Patent, 1976.
[87] X. N. Jiang, C. Sun, X. Zhang, B. Xu, and Y. H. Ye, "Microstereolithography of lead zirconate titanate thick film on substrate," *Sensors and Actuators A: Physical*, vol. 87, pp. 72-77, 2000.
[88] C. Decker, "Kinetic study and new applications of UV radiation curing," *Macromolecular Rapid Communications*, vol. 23, pp. 1067-1093, 2002.
[89] S. Priya, J. Ryu, C.-S. Park, J. Oliver, J.-J. Choi, and D.-S. Park, "Piezoelectric and magnetoelectric thick films for fabricating power sources in wireless sensor nodes," *Sensors*, vol. 9, pp. 6361-6384, 2009.
[90] R. N. Torah, "Optimisation of the piezoelectric properties of thick-film piezoceramic devices," PhD, Electronics and Computer Sience, University of Southampton, 2004.
[91] J. Birnstock, J. Blässing, A. Hunze, M. Scheffel, M. Stößel, K. Heuser, *et al.*, "Screen-printed passive matrix displays based on light-emitting polymers," *Journal of Applied Physics*, vol. 78, pp. 3905-3907, 2001.
[92] M. Sauer, S. Meilchen, A. Kalleder, M. Mennig, and H. Schmidt, "Screen printing," in *Sol-Gel technologies for glass producers and users*, M. A. Aegerter and M. Mennig, Eds., ed: Springer Science_Business Media New York, 2004.
[93] N. M. White and J. D. Turner, "Thick-film sensors: past, present and future," *Measurement Science and Technology*, vol. 8, 1997.
[94] P. Glynne-Jones, S. P. Beeby, and N. M. White, "Towards a piezoelectric vibration-powered microgenerator," *IEEE Science measurement and technology*, vol. 148, pp. 68-72, 2001.
[95] D. Zhu, A. Almusallam, S. P. Beeby, J. Tudor , and N. R. Harris, "A Bimorph multi-layer piezoelectric vibration energy harvester," presented at the PowerMEMS 2010, Leuven, Belgium, 2010.
[96] R. N. Torah, S. P. Beeby, and N. W. White, "A study of powder size combinations for improving piezoelectric properties of PZT thick-film devices," presented at the 17th European Conference on Solid State Transducers (Eurosensors XVII), Guimaraes, Portugal, 2003.
[97] S. Wagle, A. Decharat, P. Bodo, and F. Melandsø, "Ultrasonic properties of all-printed piezoelectric polymer transducers," *Applied Physics Letters*, vol. 103, 2013.
[98] R. Lakhmi, H. Debeda, I. Dufour, and C. Lucat, "Study of screen-printed PZT cantilevers both self-actuated and self-read-out," *International Journal of Applied Ceramic Technology*, vol. 11, pp. 311-320, 2014.
[99] Y. Liu and T. Cui, "Polymer-Based rectifying diodes on a glass substrate fabricated by Ink-Jet printing," *Macromolecular Rapid Communications*, vol. 26, pp. 289-292, 2005.
[100] J. Windle and B. Derby, "Ink jet printing of PZT aqueous ceramic suspensions," *Journal of Material Science Letters*, vol. 18, pp. 87-90, 1999.
[101] B.-J. de Gans, P. C. Duineveld, and U. S. Schubert, "Inkjet printing of polymers: State of the art and future developments," *Advanced Materials*, vol. 16, pp. 203-213, 2004.
[102] G. D. Martin, S. D. Hoath, and I. M. Hutchings, "Inkjet printing-the physics of manipulating liquid jets and drops," *Journal of Applied Physics*, vol. 105, 2008.
[103] Q. F. Xiang, J. R. G. Evans, M. J. Edirisinghe , and P. F. Blazdell, "Solid freeforming of ceramics using a drop-on-demand jet printer," *Proceedings of the Institution of Mechanical Engineers, Part B: Journal of Engineering Manufacture*, vol. 211, 1997.

[104] C. E. Slade and J. R. G. Evans, "Freeforming ceramics using a thermal jet printer," *Journal of Science Letters,* vol. 17, pp. 1669-1671, 1998.
[105] D. H. Lee and B. Derby, "Preparation of PZT suspensions for direct ink jet printing," *Journal of the European Ceramic Society,* vol. 24, pp. 1069-1072, 2004.
[106] O. Machida, A. Shimofuku, R. Tashiro, A. Takeuchi, Y. Akiyama, and E. Ohta, "Fabrication of lead zirconate titanate films by inkjet printing," *Japanese Journal of Applied Physics,* vol. 51, 2012.
[107] F. M. Guillot, H. W. Beckham, and J. Leisen, "Piezoelectric Fabrics for Energy Harvesting," National Textile Center2007.
[108] Y. Qin, X. Wang, and Z. L. Wang, "Microfibre-nanowire hybrid structure for energy scavenging," *Nature,* vol. 451, pp. 809-813, 2008.
[109] Y. Qi, N. T. Jafferis, K. Lyons Jr., C. M. Lee, H. Ahmad, and M. C. McAlpine, "Piezoelectric ribbons printed onto rubber for flexible energ conversion," *Nano Letters,* vol. 10, pp. 524-528, 2010.
[110] Y. Qi, P. K. Purohit, and M. C. McAlpine, "Enhanced piezoelectricity and stretchability in energy harvesting devices fabricated from buckled PZT ribbons," *Micro-and Nanotechnology Sensors, systems and Applications,* vol. 8031, 2011.
[111] K.-I. Park, M. Lee, Y. Liu, S. Moon, G.-T. Hwang, G. Zhu, *et al.*, "Flexible nanocomposite generator made of $BaTiO_3$ nanoparticles and graphitic carbons," *Advanced Materials,* vol. 24, pp. 2999–3004, 2012.
[112] S. Xu, Y.-W. Yeh, G. Poirier, M. C. McAlpine, R. A. Register, and N. Yao, "Flexible piezoelectric PMN-PT nanowire-based nanocomposite and device," *Nano Letters,* vol. 13, p. 2393−2398, 2013.
[113] B. K. Yun, Y. K. Park, M. Lee, N. Lee, W. Jo, S. Lee, *et al.*, "Lead-free $LiNbO_3$ nanowire-based nanocomposite for piezoelectric power generation," *Nanoscale Research Letters,* vol. 9, 2014.
[114] H. B. Kang, C. S. Han, J. C. Pyun, W. H. Ryu, C.-Y. Kang, and Y. S. Cho, "$(Na,K)NbO_3$ nanoparticle-embedded piezoelectric nanofiber composites for flexible nanogenerators," *Composites Science and Technology,* vol. 111, pp. 1-8, 2015.
[115] K. Lorincz, C. Bor-rong, G. W. Challen, A. R. Chowdhury, S. Patel, P. Bonato, *et al.*, "Mercury: A wearable sensor network platform for high-fidelity motion analysis," *SenSys,* vol. 9, pp. 183-196, 2009.
[116] S. Park, I. Locher, A. Savvides, and M. B. Srivastava, "Design of a wearable sensor badge for smart kindergarten," in *Wearable Computers. Proceedings. Sixth International Symposium*, 2002, pp. 231 - 238.
[117] E. Casilari, J. M. Cano-García, and G. Campos-Garrido, "Modeling of current consumption in 802.15.4/ZigBee sensor motes," *Sensors,* vol. 10, pp. 5443-5468, 2010.
[118] P. Dargie, R. Sion, J. Atkinson, and N. White, "An investigation of the effect of poling conditions on the characteristics of screen-printed piezoceramics," *Microelectronics International,* vol. 15, pp. 6-10, 1998.
[119] J. A. Giacometti and O. N. Oliveira Jr, "Corona charging polymers," *IEEE Transations on Electrical Insulation,* vol. 27, 1992.
[120] J. A. Giacometti, S. Fedosov, and M. M. costa, "Corona charging of polymers: Rescent advances on constant current charging," *Brazilian Journal of Physics,* vol. 29, pp. 269-279, 1999.
[121] D. Schilling, J. Glatz-Reichenbach, K. Dransfeld, E. Bihler, and W. Eisenmenger, "Polarization profiles of electron-beam polarized VDF-TrFE copolymer films," presented at the Electrical Insulation and Dielectric Phenomena, Pocono Manor, PA, 1990.
[122] D. Schilling, K. Dransfeld, E. Bihler, K. Holdik, and W. Eisenmenger, "Polarization profiles of polyvinylidene fluoride films polarized by a focused electron beam," *Journal of Applied Physics,* vol. 65, pp. 269-275, 1989.
[123] X. Chen, A. Li, N. Yao, and Y. Shi, "Adjustable stiffness of individual piezoelectric nanofibers by electron beam polarization," *Applied Physics Letters,* vol. 99, 2011.

[124] B. Gross, R. Gerhard-Multhaupt, A. Berraissoui, and G. M. Sessler, "Electron-beam poling of piezoelectric polymer electrets," *Journal of Applied Physics,* vol. 62, pp. 1429-1432, 1987.
[125] J. E. Southin, S. A. Wilson, D. Schmitt, and R. W. Whatmore, "e_{31},f determination for PZT films using a conventional 'd_{33}' meter," *Journal of Physics D: Applied Physics,* vol. 34, pp. 1456-1460, 2001.
[126] N. J. Grabham, S. P. Beeby , and N. M. White, "Effects of the binder material on the mechanical properties of thick-film manetostrictive materials," *Sensors and Actuators A: Physical,* vol. 110, pp. 365-370, 2003.
[127] T. Bhimasankaram, S. V. Suryanarayana, and G. Prasad, "Piezoelectric polymer composite materials," *Current Science,* vol. 74, pp. 967-976, 1998.
[128] C. K. Wong, Y. M. Poon, and F. G. Shin, "Explicit formulas for effective piezoelectric coefficients of ferroelectric 0-3 composites," *Journal of Applied Physics,* vol. 90, p. 11, 2001.
[129] R. N. Torah, S. P. Beeby, and N. M. White, "Experimental investigation into the effect of substrate clamping on the piezoelectric behaviour of thick-film PZT elements," *Journal of Applied Physics D: Applied Physics* vol. 37, pp. 1-5, 2003.
[130] J. W. Yi, J. H. Jang, W. Lee, M. K. Um, J. H. Byun, and H. G. Lee, "Mechanical and electrical properties of micro/nanocomposites via CNT dispersed resin film infusion process," in *iccm-central.org*.
[131] Triple Roll Mill. (2010). *Laboratory of Microengineering for Manufacturing*. Available: http://lpm.epfl.ch/page-31733-en.html
[132] A. N. Norris, A. J. Callegari, and P. Sheng, "A generalized differential effective medium theory," *Journal of Mechanics and Physics of Solids,* vol. 33, pp. 525-543, 1985.
[133] M. E. Hossain, S. Y. Liu, S. O'Brien, and J. Li, "Modelling of high-k dielectric nanocomposites," *Acta Mechanica,* vol. 225, pp. 1197–1209, 2014.
[134] M. Al Alhmad, F. Coccetti, and R. Plana, "The effect of substrate clamping on piezoelectric thin-film parameters," presented at the Asia-Pacific Microwave Conference, 2007.
[135] S. J. Krumbein, "Metallic electromigration phenomena," *IEEE Transactions on Components, Hybrids, and Manufacturing Technology,* vol. 11, pp. 5-15, 1988.
[136] M. Kahn, "Acoustic and elastic properties of PZT ceramics with anistropic pores," *Journal of American Ceramic Society,* vol. 68, pp. 623–628, 1985.
[137] V. I. Aleshin and I. P. Raevski, "Negative Poisson's ratio and piezoelectric anisotropy of tetragonal ferroelectric single crystals," *Journal of Applied Physics,* vol. 112, p. 114101, 2012.
[138] T. G. Lupeiko and S. S. Lopatin, "Old and new problems in piezoelectric materials research and materilas with high hydrostatic sensitivity " *Inorganic Materials,* vol. 40, pp. S19–S32, 2004.
[139] Hybrid Laser Tech Ltd. Available: http://www.hlt.co.uk/material
[140] DuPont.Available:http://www.dupont.com/content/dam/assets/products-and-services/membranes-films/assets/DEC-Kapton-summary-of-properties.pdf
[141] Sinocera. Available: http://www.sinocera.net/en/piezo_material.asp
[142] R. W. Williams, "Measuring and modeling the anisotropic, nonlinear and hysteretic behavior of woven fabrics," University of Iowa, 2010.
[143] G. Hayward, J. Benett, and R. Hamilton, "A theoretical study on the influence of some constituents materials properties on the behavior of 1-3 connectivity composite transducers," *Journal of Acoustical Society of America,* vol. 4, pp. 2187-2196, 1995.
[144] C. Suryanarayana, "Mechanical alloying and milling," *Progress in Materials Science,* vol. 46, pp. 1-184, 2001.
[145] S. N. Gwirc and C. A. Negreira, "Evaluation of the effect of porosity and substrate on the piezoelectric behaviour of thick-film PZT elements," *Journal of Physics D: Applied Physics*, vol. 39, 2006.

[146] H. C. Weerasinghe, P. M. Sirimanne, G. P. Simon , and Y.-B. Cheng, "Cold isostatic pressing technique for producing highly efficient flexible dye-sensitised solar cells on plastic substrates," *Progress in Photovoltaics: Research and Applications*, vol. 20, pp. 321–332, 2012.
[147] C. G. Hindrichsen, R. Lou-Møller, K. Hansen, and E. V. Thomsen, "Advantages of PZT thick film for MEMS sensors," *Sensors and Actuators A: Physical*, vol. 163, pp. 9-14, 2010.
[148] S. H. Lee, S. E. Lee, and H. C. Lee, "Application of CIP processing and sol-gel surface coating to PZN-PZT piezoelectric ceramics for use as energy harvesters," *Current Applied Physics*, vol. 11, pp. 6-10, 2011.
[149] P. S. Gaware, O. P. Yadav, and H. H. Kumar, "Manufacturing technology of lead zirconate titanate cylindrical elements for passive transducer arrays," *DEFENCE SCIENCE JOURNAL*, vol. 53, pp. 275-279, 2003.
[150] S. M. Lim, K. Lee, J. W. Chung, H. S. Lee, and J. C. Lee, "Method of forming piezoelectric actuator of inkjet head," ed: Google Patents, 2007.
[151] K. Choonee, R. R. A. Syms, M. M. Ahmad, and H. Zou, "Post processing of microstructures by PDMS spray deposition," *Sensors and Actuators A: Physical*, vol. 155, pp. 253–262, 2009.
[152] J. H. Koschwanez, R. H. Carlson, and D. R. Meldrum, "Thin PDMS films using long spin times or tert-Butyl alcohol as a solvent," *Plos one*, vol. 4, p. 5, 2009.
[153] K. H. Cho and H. Y. Lee, "Pore-dependent dielectric and electrical properties of barium titanate ceramic," in *Applications of Ferroelectrics, 1994.ISAF '94., Proceedings of the Ninth IEEE International Symposium* 1991, pp. 566 - 571.
[154] Z. Ounaies, C. Park, J. Harrison, and P. Lillehei, "Evidence of piezoelectricity in SWNT-Polyimide and SWNT-PZT-Polyimide composites," *Journal of Thermoplastic Composite Materials*, vol. 21, pp. 393-409, 2008.
[155] M. W. Hooker, "Properties of PZT-based piezoelectric ceramics between -150 and 250 °C," NASA Center for AeroSpace Information (CASI)1998.
[156] J. E. A. Bertram, "Constrained optimization in human walking: cost minimization and gait plasticity," *Journal of Experimental Biology*, vol. 208, pp. 979-991, 2005.
[157] Instron Company. *ElectroPuls E1000 All-Electric Test Instrument featuring Linear Motor Technology*. Available: http://www.instron.com/en-gb/products/testing-systems/dynamic-and-fatigue-systems/electropuls/e1000
[158] J. Wu and N. Pan, "Grab and strip tensile strengths for woven fabrics: An experimental verification " *Textile Research Journal*, vol. 75, pp. 789-796, 2005.
[159] B. S. Beery and W. C. Pritchet, "Internal stress and internal friction in thin-layer microelectronic materials," *Journal of Applied Physics*, vol. 67, pp. 3661-3668, 1990.
[160] A. Abdul Razak, A. Aladin Zayegh, R. K. Begg, and Y. Wahab, "Foot plantar pressure measurement system: A review," *Sensor*, vol. 12, pp. 9885-9912, 2012.
[161] D. Zhu, S. P. Beeby, M. J. Tudor, and N. R. Harris, "A credit card sized self powered smart sensor node," *Sensor and Actuators A: Physical*, vol. 169, pp. 317-325, 2011.
[162] Available: file:///C:/Users/asa1g09/Desktop/SEFAR%20PET%201500%20datasheet.PDF
[163] B. SD. *Stainless steel screen printing meshes*. Available: http://www.jdr-websites.co.uk/gallery/images/1431/file/Bopp_SD_Broschure_e_2010.PDF